Sustainable Routes to Multifunctional α-Polylysine for Use in Environmental Remediation and Drug Delivery

XUCHEN JIN

Submitted in accordance with the requirements for the degree of

Doctor of Philosophy

The University of Leeds

School of Chemistry

October, 2025

I confirm that the work submitted is my own and that appropriate credit has been given where reference has been made to the work of others.

Acknowledgements

This project was originally conducted by Xuchen Jin, with valuable contributions from many other researchers.

First and foremost, I would like to express my heartfelt gratitude to my supervisor, Dr Paul Thornton, whose expertise, kindness, and patience have guided me throughout this project, both professionally and personally. His profound knowledge in chemistry provided essential support for this research, and his invaluable assistance in enhancing my English proficiency is deeply appreciated.

I am deeply thankful to Dr Terence Kee, who later joined my PhD journey as a co-supervisor. His extensive expertise in hydrogels materials, significantly contributed to the development of this research. His guidance in providing fundamental knowledge about hydrogels and his insightful analysis and interpretation of NMR spectra were invaluable.

Thanks to Dr Patrick Anthony Wall, Dr Ben Coyne, Dr Anna Morrell, Dr Sui Hung and Dr Huai sheng Chin and other lab-members for their invaluable support in the synthesis of raw materials. Thanks to ChatGPT 4.0 for its support in refining the grammar of this thesis.

I would like to sincerely thank Algy Kazlauciunas for his extensive assistance with SEM and TGA analysis, and Jeanine Williams for support with all aspects of chromatography. My gratitude also goes to Mohammed Asaf for his help with FTIR measurements and to Daniel Baker for providing training on rheology testing. I am equally thankful to Chhaya Patole for MALDI-TOF training and to Benjamin Cooper for his guidance on UV spectroscopy.

I would also like to express my deepest gratitude to my parents, Baozhen Wu and Zhijun Jin, for their unconditional love, unwavering support, and endless encouragement throughout this journey.

Abstract

α-Polylysine (PLys) is a versatile, renewable, and biodegradable polymer with extensive amine functionality and water-solubility, making it an ideal candidate for environmental remediation, biomedical applications and beyond. However, conventional synthesis of linear PLys relies on toxic reagents for preparation of monomer L-lysine N-carboxyanhydride (Lys-NCA) and side-chain deprotection after polymerisation, raising environmental and safety concerns that hinder its commercial scalability and sustainability.

An environmentally friendly method for PLys production was adapted and modified in this study using thermal deprotection of fluorenylmethyloxycarbonyl (Fmoc)-protected PLys, eliminating the need for hazardous deprotection agents and offering a greener and more cost-effective alternative. Homopolymeric PLys and poly(ethylene glycol) -*b*-α-polylysine (PEG-*b*-PLys) block copolymers can be prepared using this method, showcasing their superior performance in removing Pb^{2+} ions from aqueous solutions.

Two types of PLys-based hydrogels, polylysine/glutaraldehyde (Glu) hydrogels (PLys/Glu Gels) and polylysine/genipin hydrogels (PLys/Gen Gels), were prepared by mixing PLys with varying mass ratios of Glu and genipin, respectively. The swelling behaviour, mechanical properties, and maximum uptake capacity of Reactive Black 5 (RB5), a water-soluble azo dye commonly used in the textile industry, were influenced by the degree of crosslinking: a lower crosslinker content resulted in enhanced RB5 adsorption and swelling but reduced mechanical performance. These findings highlight the potential of these PLys-based hydrogels as sustainable adsorbents for effective RB5 removal.

The ring-opening polymerisation of the 2,5-diketopiperazine (DKP) of Lys(cbz) was done as an alternative procedure to NCA ROP to create PLys. Lys(cbz) DKP monomer synthesis was achieved in glycerol, and polymerisation proceeded from hexylamine using an acid-base organocatalyst (MSA /DIPEA) system. Following side group deprotection to form PLys,

genipin was employed as a natural crosslinking agent to yield chemical hydrogels, the mechanical properties of which could be altered by the extent of genipin crosslinking. These hydrogels were able to uptake and withhold diclofenac (DIC, a nonsteroidal anti-inflammatory drug widely used for pain relief and anti-inflammatory treatment), prior to prolonged payload release. PLys synthesis by DKP ROP offers a route to amino acid-based hydrogel materials that have potential as DIC enteric-coated tablets that enhance drug bioavailability.

Overall, the thesis demonstrates sustainable preparation and multifunctionality of PLys-based materials, ranging from synthesis methods with low toxicity, structural design and process optimisation. These applications in chapter 3-5 provide new perspectives for the advancement of PLys-based materials in environmental purification and controlled drug delivery.

Table of Contents

List of Tables

List of Figures

List of Schemes

Abbreviations

$(PEGA)_{30}$-*b*-p$(Lys)_{25}$-*b*-p(His)	Poly(ethylene glycol) methyl ether acrylate-block-poly(L-lysine)-block-poly(L-histidine)
2,5-DKP	2,5-Diketopiperazine
3D	Three dimensional
3-GPS	3-Glycidoxypropyl trimethoxysilane
Alloc	Allyloxycarbonyl
antiNgR	Nogo-66 receptor antibody
APC	Advanced polymer chromatography
ATRP	Atom transfer radical polymerisation
BDD	Boron-doped diamond
BOC	tert-Butyloxycarbonyl
BSA	Bovine serum albumin
Cbz	Carbobenzyloxy
CNTs	Carbon nanotubes
DBA	4-(Decyloxy)benzaldehyde
DBU	1,8-Diazabicyclo[5.4.0]undec-7-ene
DCM	Dichloromethane
DFT	Density functional theory
DHB	2,5-Dihydroxybenzoic acid
DI	Deionized
DIC	Diclofenac
DIPEA	Diisopropylethylamine

DMAP	4-(Dimethylamino)pyridine
DMAP	4-(Dimethylamino)-pyridine
DMF	Dimethylformadime
DMMA	2,3-Dimethylmaleic anhydride
DMSO	Dimethyl sulfoxide
Dox	Doxorubicin
EDC	1-Ethyl-3-(3-dimethylaminopropyl)carbodiimide hydrochloride
EDTA-Na	Ethylenediaminetetraacetic acid disodium salt
Fmoc	9-Fluorenylmethyloxycarbonyl
FTIR	Fourier-transform infrared
G’	Storage modulus
G’’	Loss modulus
GO	Graphene oxide
GPTMS	3-Glycidoxypropyltrimethoxysilane
HA	Hyaluronic acid
HIF-1α	Hypoxia-inducible transcription factor 1α
LC-MS	Liquid chromatography – mass spectrometry
LCST	Lower critical solution temperature
LP-MSNs	Large pore mesoporous silica nano particles
MALDI	Matrix-assisted laser desorption/ionization
MBAA	N,N-methylenebisacrylamide
Mn	Number average molecular weight
MSA	Methanesulfonic acid
Mtt	4-Methyltrityl
Mw	Weight average molecular weight
MWCNTs	Multi-walled carbon nanotubes

N/P	NH_4^+/PO_4^{3-}
NCA	N-carboxyanhydride
NMR	Nuclear magnetic resonance
NSAID	Nonsteroidal anti-inflammatory drug
PBS	Phosphate buffered saline
PEDF	Polymer enhanced diafiltration
PEG	Polyethylene glycol
PEG-*b*-PLys	methoxy-Poly(ethy-leneglycol)–block–poly(l-lysine hydrochloride)
pEGFP	Plasmid DNA
PLLA	Poly(L-lactic acid)
Plys	α-Polylysine
PLys-*b*-P[Asp(DIP)]	[Poly(L-lysine)-b-poly[N-(N', N'-diisopropylaminoethyl)aspartamide]
PLys-g-PMOXA	Polylysine-graft-poly(2-methyl-2-oxazoline)
PMMA	Poly(methyl methacrylate)
PNIPAM	Poly(N-isopropylacrylamide)
PNIPAM-*b*-Plys	Poly(N-isopropylacrylamide)-*b*-Plys
PPy	Polypyrrole
RAFT	Reversible addition−fragmentation transfer
RB	Round bottle
RB5	Reactive Black 5
RIBV	Ribavirin (l-β-D-Ribofuranosyl-1,2,4-triazole-3-carboxamide)
ROP	Ring-opening polymerisation
RSF	Regenerated silk fibroin
RT	Room temperature
SEM	Scanning electron microscopy

SPARC	Secreted protein acidic and rich in cysteine
T3P	n-Propanephosphonic acid anhydride
Tfa	Trifluoroacetyl
TFA	Trifluoroacetic acid
TGA	Thermal gravimetric analysis
THF	Tetrahydrofuran
UV-Vis	Ultra violet – visible
z	Benzyloxycarbonyl

Chapter 1 Literature Review

1.1 Polylysine

Polylysine is a homopolymer composed of numerous lysine residues[1, 2]. It can be categorised into two types based on the bonding position of the amide bond, owing to the presence of two amine groups in lysine[1, 3]. If the amide bond is formed by the α-amine group, α-polylysine (PLys) forms; if the amide bond forms at the ε-amine group (the amine group on the lysine side chain), the polymer is ε-polylysine. The chemical structures of lysine, PLys and ε-PLys are demonstrated in Figure 1-1.

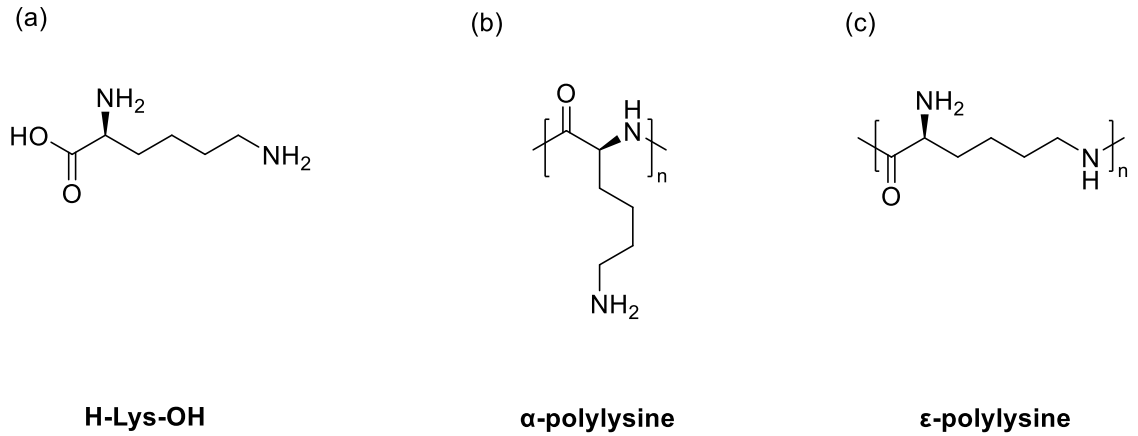

Figure 1-1 Chemical structure of (a) lysine, (b) PLys and (c) ε-PLys.

1.1.1 α-polylysine (PLys)

PLys is a synthetic homopolymer recognised for its biocompatibility and enzymatic degradability into lysine monomers[4]. Its high water-solubility, attributed to the ionisable amine groups, makes it ideal for use in aqueous environments[5]. The positive charge of PLys facilitates electrostatic interactions with negatively charged molecules, such as nucleic acids, anionic proteins, and anionic drugs[6].

As a poly(amino acid), PLys has structural similarity to proteins, for instance the repeat units are linked by amide bonds and the PLys can form secondary structures[7]. The conformation of PLys has been extensively studied using techniques commonly applied in protein research, as these conformational changes significantly influence its efficiency in drug delivery applications[8]. For instance, research has shown that the conformation of PLys transitions from a polyproline II (P_{II})-helix to an α-helical structure as the pH of the external solution increases from 4 to 11.6 (Figure 1-2)[9]. Additionally, temperature variations can induce structural changes, such as the transformation to an aggregated β-sheet structure at elevated temperatures (Figure 1-2)[9]. The solvent environment also impacts its conformation; for example, tetrafluoroethylene and dimethyl sulfoxide promote the α-helical structure, while ethylene glycol and water favour the P_{II}-helix conformation[9]. Such transformations may enable controlled drug release in response to changes in environmental pH or temperature.

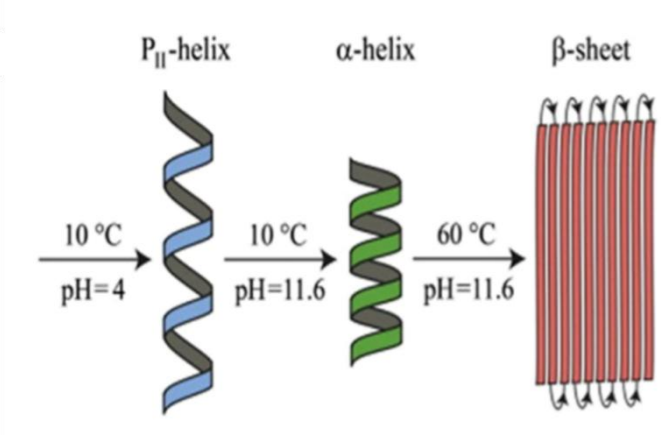

Figure 1-2 Linear polylysine physical structure confirmation[9].

PLys, as an AB_2 type monomer which contains one A functional group (carboxyl group) and two B functional groups (amine groups), where A can react with B, can form as a linear polymer, a hyperbranched polymer, or as a dendrimer, dependent on the synthetic protocol used[10-12] (Figure 1-3). All three polymeric architectures are different, both in preparation and their properties, ensuring the versatility of PLys to create a range of materials. As its name implies, linear PLys presents a simple, long-chain structure, with one free amine group per lysine repeat unit. For linear PLys to form, protecting groups must be present on one of the amines of Lys during polymerisation. If such protecting groups are absent both amine groups can react to form a hyperbranched polymer. The polymeric architectures feature an uncontrolled branched architecture, with branching occurring irregularly throughout the polymer. Dendritic PLys is a highly branched yet symmetrical polymer with a tree-like shape. It is characterised by a well-defined, multi-layered structure in which branches extend radially from a central core, distinguishing it from the irregular branching of hyperbranched PLys. Although dendritic PLys synthesis is challenging due to the requirement that each amine group apart from those on the periphery must react, the polymers produced are identical with a dispersity value of one, and

so highly suited as carriers in controlled release applications[13].

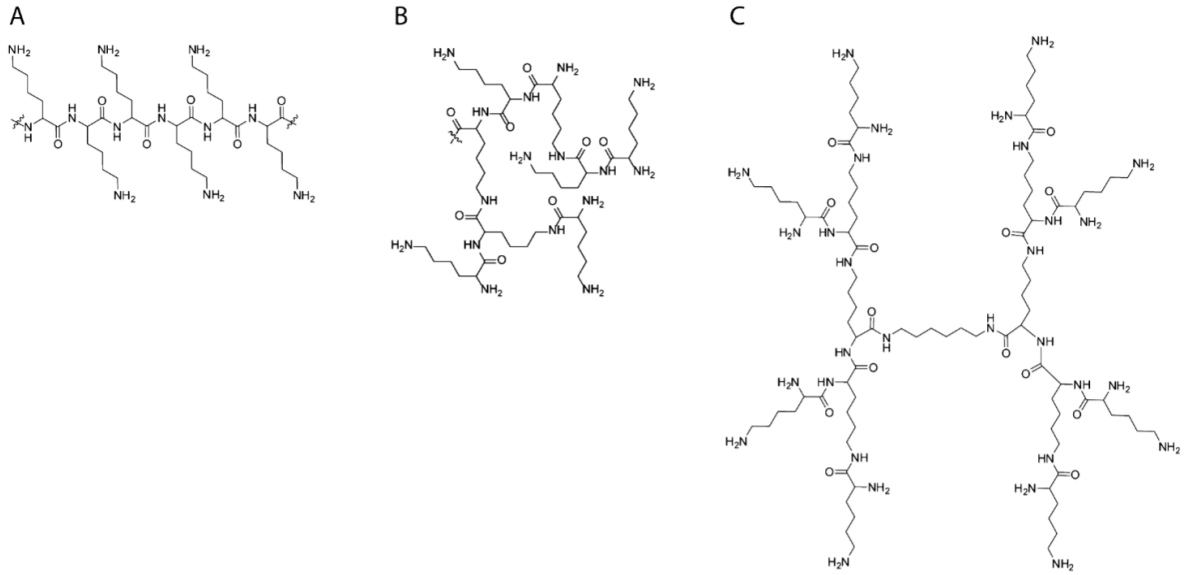

Figure 1-3 Different PLys architectures: (A) linear PLys, (B) hyperbranched PLys, and (C) dendritic PLys[14].

Applications of PLys or PLys derivatives are mainly focused on the biomedical industry. Though high concentrations of PLys are reported to have cytotoxic effects on L929 mouse fibroblasts, the dose control or modification may help to alleviate this toxic side effect, ensuring that the viability of PLys as a biomaterial for use *in vivo*[15]. PLys has been used to promote cell attachment on culture substrates including borosilicate glass and polystyrene culture ware, with polymer modifications done to increase material effectiveness [16]. Grafting polyethylene glycol (PEG) onto PLys can prevent excessive accumulation at the target site by improving the material's biodistribution through adjustments in size and surface charge[17, 18]. Cellular uptake of PLys has generated significant interest in its use for complexing with drugs to enhance intracellular delivery. For instance, certain cancers, including osteosarcoma, breast

and bladder cancer, exhibit resistance to methotrexate due to a deficient methotrexate transport system. However, when methotrexate was conjugated to PLys, the resulting conjugate was efficiently transported into cancer cells, breaking down the drug resistance. Following treatment with the methotrexate–PLys conjugate, the previously required 100-fold difference in the drug concentration necessary to inhibit methotrexate-resistant cells compared to their wild-type counterparts was eliminated [19].

Furthermore, PLys has been used as an intermediary carrier for gene delivery[20, 21]. In addition to adhering to cells, the gene-PLys complex must properly disassemble and subsequently translocate into the cell nucleus upon arrival. Polyelectrolyte exchange reactions enable the release of DNA from PLys complexes, forming the basis for its application as a DNA or RNA carrier[22]. When comparing three different types of PLys-based DNA delivery systems, hyperbranched PLys demonstrated significantly higher transfection efficiency compared to linear and dendritic PLys[23].

1.2 Chemical synthesis of linear PLys

PLys is of critical importance because it bridges the gap between the simple amino acid lysine and the creation of advanced biomaterials. In detail, PLys possesses abundant amine groups, which grant it cationic properties, favourable solubility in water and versatile sites for chemical modification[24]. Creating PLys via a synthetic chemical process affords control to the PLys produced in terms of the architecture, but also the chain length and uniformity of chain lengths. Polymer dispersity impacts performance with high uniformity essential for consistent and

predictable polymer performance in biomedical applications, such as drug delivery. However, for PLys to be widely used within a biomedical context and beyond, scalable, safe, and cost-effective synthesis methods must be devised.

1.2.1 PLys prepared via amino acid N-carboxyanhydride (NCA) ring-opening polymerisation (ROP)

PLys can be synthesised directly by the polycondensation of lysine amino acids. However, this polymerisation is difficult resulting in high dispersity polymers and batch-to-batch variation in molecular weights. Consequently, other synthetic routes have been devised to afford control to the polymerisation process, and consistency to the PLys produced. A common method of poly(amino acid) synthesis, which will be used in this research, features amino acids being converted to cyclic molecules such as NCAs[25]. This polymerisation requires R group amine protection and post-polymerisation deprotection, but PLys can be converted to targeted molecular weight via straightforward nucleophile-initiated ROP[26, 27]. If without protection of R group, branched PLys rather than linear PLys will form.

NCA ROP commences with the conversion of the amino acid to the corresponding NCA. For R-group protected lysine conversion to NCA, triphosgene is commonly used (Scheme 1). While phosgene, a gas, is no longer used in this reaction due to its high toxicity and difficulty in handling, it is created from the decomposition of solid triphosgene during this process[26].

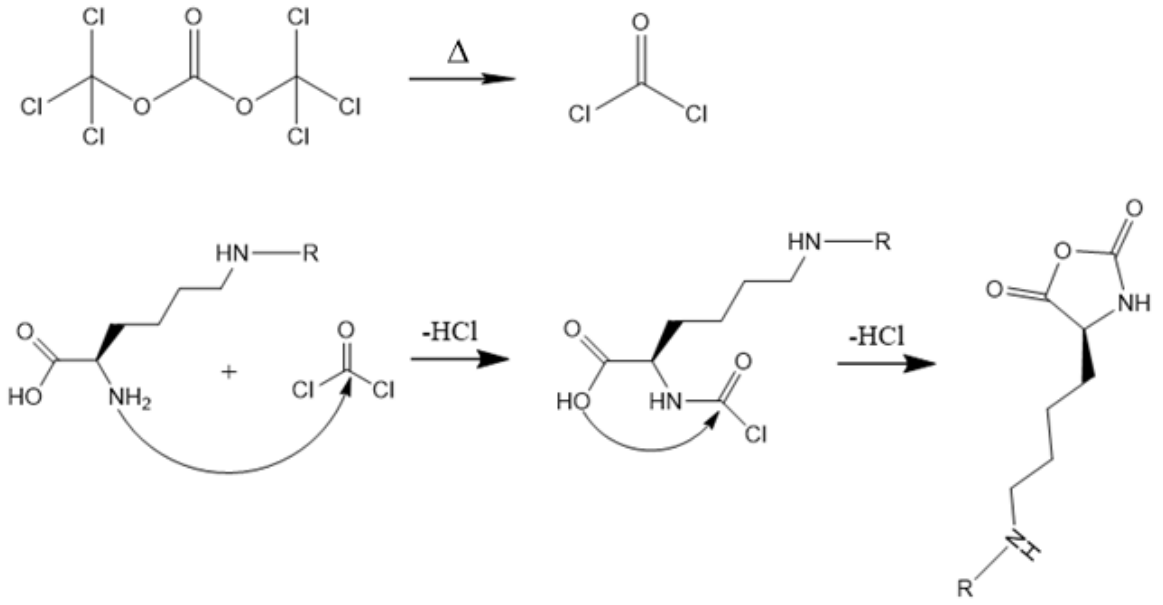

Figure 1-4 Synthesis scheme for Lys-NCA using triphosgene. R represents the various protecting groups that may be used to ensure linear PLys creation.

Two mechanisms for the polymerisation of Lys-NCAs monomers have been reported; the normal amine mechanism and the activated amine mechanism[26]. In the normal amine mechanism, the initiators contain nucleophilic groups such as primary or secondary amines, and alcohols. The carbonyl group that is on the opposite side of the ring from the nitrogen atom is attacked by nucleophilic agents, because it is the most electrophilic position. NCA ring-opening occurs and unstable carbamic acid forms. After the removal of CO_2 from the medium, a new terminal amine group forms that can react with a new NCA molecule in the same way, causing chain propagation and the subsequent formation of PLys. The polymerisation is classed as a 'living' polymerisation due to the absence of chain terminating species and so the molecular weight of the synthesised PLys can match the monomer-to-initiator ratio if the

polymerisation is done in the absence of contaminants.

The activated amine mechanism involves bases, especially tertiary amines, that function as catalysts rather than initiators[28]. They deprotonate the nitrogen in the five-membered ring, increasing the nucleophilicity of the NCA, and thus activating the NCA to form a NCA anion. Analogous to the initiator in the amine mechanism, the activated NCA anion can react as a nucleophile with C5 carbonyl carbon of a new NCA monomer, which is located opposite to the cyclic amide, releasing CO_2 and creating a new activated NCA anion. This propagates the chain extension of PLys. Although PLys with higher molecular weights can be produced through this mechanism, the limited control typically leads to a broader molecular weight distribution of PLys, and thus normal amine mechanism are generally preferred for synthesis of well-defined PLys.[26, 29].

A major drawback of common NCA synthesis is the use of triphosgene as a cyclising agent, used to convert the amino acid to the cyclic NCA structure. Although triphosgene is a solid, it should be handled with the same precautions as phosgene owing to the release phosgene gas upon decomposition. Therefore, meticulous care is essential when using triphosgene to ensure safety. The toxicity of triphosgene has prompted researchers to explore alternative triphosgene-free synthesis methods.

1.2.1.1 NCA formation using n-Propanephosphonic acid anhydride (T3P)

Straightforward phosgene- and halogen-free methods for synthesising α-amino acid NCAs are in-demand. One approach to this involves reacting tert-butyloxycarbonyl (Boc)-protected α-amino acids with T3P, yielding the corresponding NCA derivatives with high purity and yields, while avoiding detectable epimerisation[30]. However, this method imposes strict requirements on the structure of the raw materials; specifically, it necessitates the use of Boc-protected amino acids. The mechanism for NCA formation using this method is illustrated in Figure 1-5. In the presence of T3P (acting as a catalyst) and pyridine (serving as a basic promoter), Boc-protected α-amino acids are activated and react with phosphate groups to form an intermediate characterised by phosphate ester. Pyridine acts as a nucleophilic reagent, attacking the activated phosphate ester, which leads to the removal of T3P. The resulting intermediate then undergoes rearrangement to form a stable NCA product, accompanied by the release of protons from pyridine and isobutene. In the other, thermodynamically driven pathway, the cyclisation reaction occurs following the formation of an intermediate containing a phosphate ester group, ultimately producing NCAs.

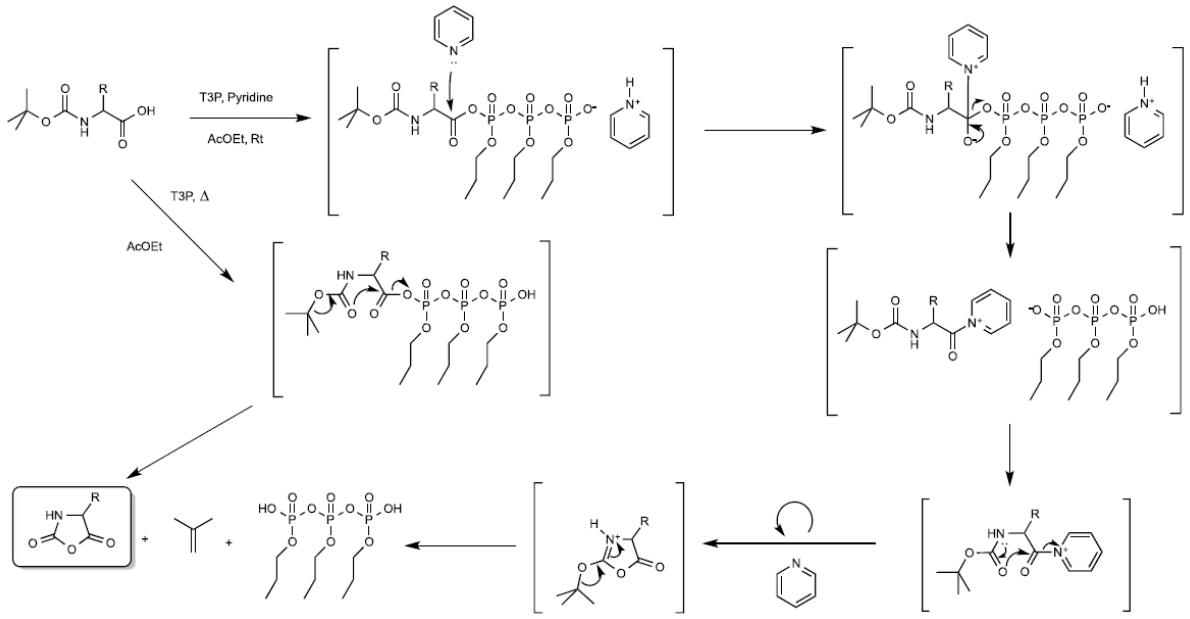

Figure 1-5 Mechanism of formation of NCAs under assistance of T3P[30].

Using this method, (Boc)-NCA was obtained from 10 g of Boc-(L)Lys-(Boc)-OH at an 83% yield, demonstrating the suitability of the process for the production of Lys-NCAs[30].

1.2.2 Poly(amino acids) prepared via 2,5-diketopiperazine (2,5-DKP) ROP

Another class of amino acid-based compound, 2,5-diketopiperazines (2,5-DKPs), has the potential as a monomer for synthesis of PLys. 2,5-DKPs are naturally occurring compounds, often formed as degradation products of polypeptides but also found as components of more complex structures[31]. 2,5-DKPs feature a conformationally constrained, six-membered heterocyclic ring comprising two amide linkages with cis-amide bonds, where the nitrogen atoms and carbonyl groups are positioned on opposite sides of the ring (Figure 1-6). This structure provides two H-bond acceptor sites and two H-bond donor sites and the carbon atoms between the amide linkages are attached to R groups. The R groups differ dependent on the

specific amino acids used to synthesise the 2,5-DKP[31].

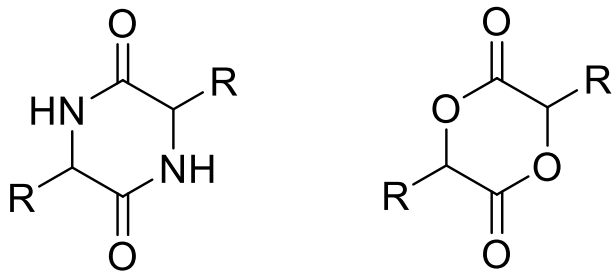

Figure 1-6 General structure of 2,5-DKP (left) and lactide (right).

DKPs can be obtained by the direct condensation of two amino acids in glycerol or ethylene glycol at 170 °C–180 °C. As an eco-friendly alternative, DKPs have the potential to replace NCAs, offering a greener synthesis pathway that avoids the use of harmful and expensive organic solvents and coupling agents. But a significant challenge lies in this developing method is to efficiently open the 2,5-DKP ring for polymerisation.

Research on the ROP of DKP is limited, but a cyclic diester, lactide, has been reported to undergo ROP in different kinds of catalytic system[32-34]. Nonstoichiometric acid−base organocatalyst has been used to promote the ROP of glycolide. A mixture of methanesulfonic acid (MSA) and 4-(dimethylamino)pyridine (DMAP) in a 2:1 ratio has been demonstrated to facilitate the preparation of stereoregular poly(L-lactic acid) (PLLA) via ROP under bulk conditions and elevated temperatures (up to 180°C), producing colourless PLLA with a molecular weight of 40 kg/mol[34].

Under high-temperature conditions, the MSA/DMAP catalyst system cooperatively attacks the carbonyl group at one end of the monomer, initiating an epimerization and ring-opening process, as depicted in the figure 1-7, leading to the synthesis of the desired linear polymer.

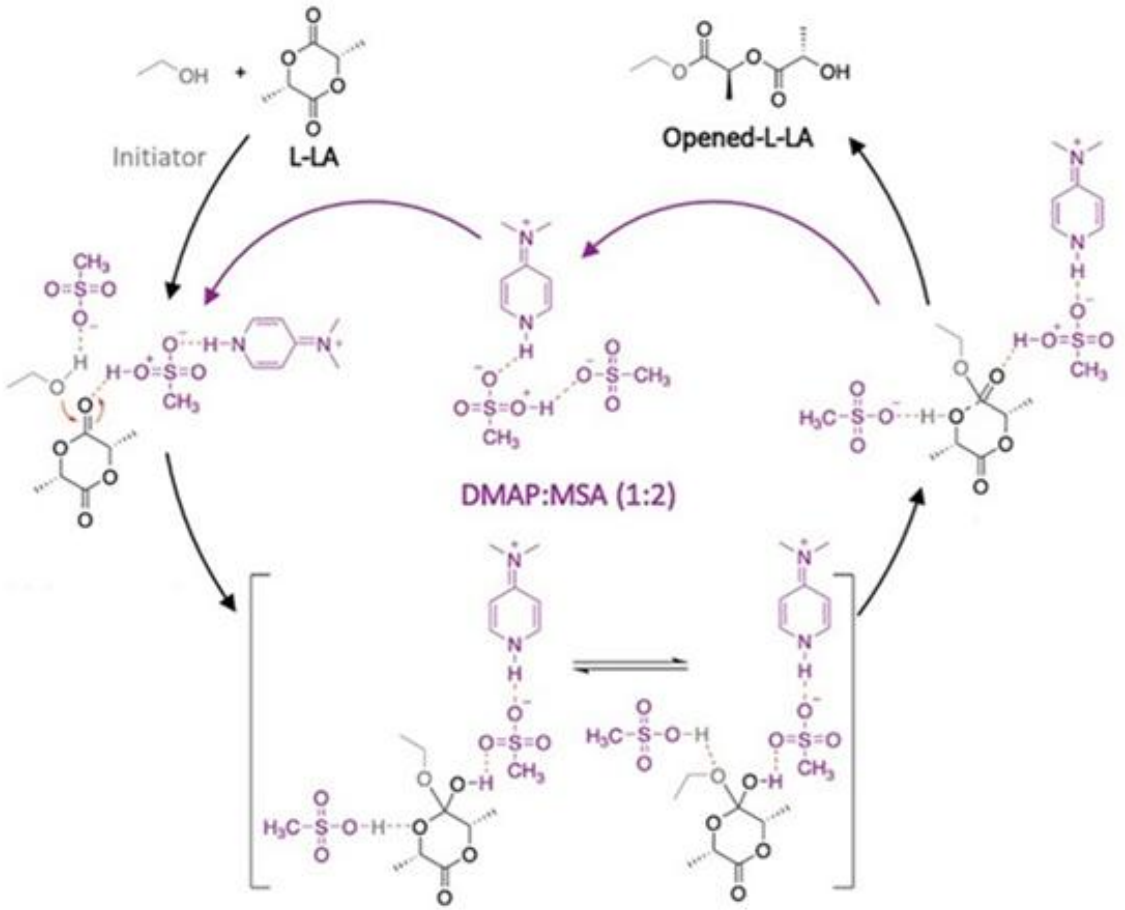

Figure 1-7 Proposed mechanism for ROP of lactide by DMAP:MSA (1:2)[34].

The structural difference between DKP and lactide lies on that the positions of nitrogen atoms in six-member ring (DKP) were occupied by oxygen atoms (Figure 1-6). The carbonyl carbon in an amide exhibits a conjugation effect with the adjacent nitrogen atom, resulting in electron density redistribution. This delocalization reduces the electrophilicity of the carbonyl carbon

compared to the carbonyl carbon in an ester and thus ROP of DKP is more difficult than that of lactide[35]. If using same catalyst system, ROP of DKP may require more intensive reaction conditions or result in polymers with lower molecular weights under the same conditions. However, this remains a speculative comparison.

1.2.3 Deprotection of protected PLys

The polymerisation of PLys typically involves two key steps: (1) the synthesis of intermediate PLys with protecting groups bound to the primary amine of the Lys R groups, and (2) the subsequent removal of these protecting groups. The use of protecting groups in the polymerisation of PLys is crucial for achieving precise structural control, preventing undesired side reactions. Following polymerisation, deprotection restores the native amine functionality, enabling the polymer to meet the requirements of its intended applications.

Common protecting group used in the synthesis of PLys includes: Boc, carbobenzyloxy (Cbz), 9-fluorenylmethyloxycarbonyl (Fmoc), allyloxycarbonyl (Alloc), 4-methyltrityl (Mtt) and Trifluoroacetyl (Tfa) protecting groups. Their structure and common methods how to removed them were summarized in Table 1-1.

The methods presented in the table 1-1 indicates that regardless of the protecting group employed during polymerisation, certain challenges persist in the deprotection process. These include the use of highly corrosive acids, reliance on costly precious metal catalysts, or the

involvement of organic reagents with physiological toxicity.

Table 1-1 Common protecting group for PLys synthesis and corresponding removal method.

Protecting group	Chemical structure (marked in blue colour)	Removal Methods	References
Boc	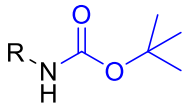	(1) 25-50% Trifluoroacetic acid (TFA)- Dichloromethane (DCM) (2) 1M HCl in EtOAc (3) 2M $MeSO_3H$ in dioxane	[36, 37]
Cbz	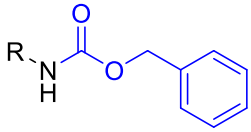	(1) 33%HBr/AcOH solution in TFA (2) H_2-Pd/C	[38, 39]
Fmoc	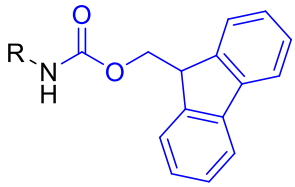	Piperidine or morpholine in organic solvents	[40]
Alloc	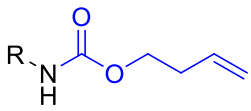	$H_3N{\cdot}BH_3$, $Me_2NH{\cdot}BH_3$ or $PhSiH_3$ in organic solvents	[41]
Mtt	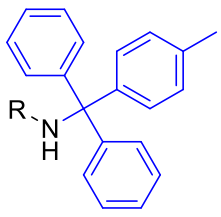	1% TFA-DCM	[42]

To enhance practical application of PLys, future developments in its chemical synthesis should

emphasise cost-effectiveness and simultaneously strive to minimise the use of toxic reagents and environmentally harmful materials.

1.3 Application of PLys

Building on the general overview of PLys provided in Section 1.1, this section will introduce more specific applications of PLys and its derivatives. The chemical preparation process of PLys is relatively complex, resulting in high production cost, which limits its popularity in low value-added fields. Combined with its excellent biocompatibility, functional potential and positive charge characteristics, PLys has become an ideal candidate for high-end biomedical applications, including gene delivery, tissue engineering, wound care and corresponding interdisciplinary area.

Non-viral gene delivery systems, recognised for their safety, ease of handling, and cost-effectiveness compared to viral tools, can be developed using PLys[43]. Due to its positive charge under physiological conditions, PLys efficiently condenses negatively charged DNA. However, unmodified PLys has been observed to increase membrane permeability and cause nanoscale pore formation with considerable cytotoxicity[44]. To mitigate these disadvantages, bioinert polymers or chemicals are grafted onto PLys, effectively masking its cationic charge, reducing aggregation, and improving both cellular uptake and stability[45, 46].

PLys conjugated with various lipids has been shown to effectively function as a gene delivery

system[47]. This strategy has enabled the successful transfer of plasmid DNA (pEGFP) into skin fibroblasts. Lipid-modified PLys with higher lipid substitution levels exhibited greater resistance to dissociation upon heparin treatment, providing enhanced protection of pEGFP from enzymatic degradation. Flow cytometry confirmed efficient protein expression with PLys conjugated to myristic or stearic acid, with stearic acid demonstrating comparatively lower cytotoxicity. Compared to pristine lipids alone, lipid-conjugated PLys achieved higher gene delivery efficiency and supported stable intracellular pEGFP expression for up to seven days.

PEG has been grafted onto the side amine groups of PLys, creating a gene delivery system for the therapeutic candidate gene hypoxia-inducible transcription factor 1α (HIF-1α), which plays a critical role in blood vessel regeneration[48]. Delivery of the HIF-1α gene using this tool has been shown to promote the number of endothelial cells and smooth muscle cell precursors, which are essential for the formation of mature blood vessels during the wound healing process.

Polylysine-graft-poly(2-methyl-2-oxazoline) (PLys-*g*-PMOXA) polymers, featuring varying grafting densities and PMOXA molecular weights, were evaluated for their ability to complex and deliver plasmid DNA[49]. The study revealed that efficient DNA delivery was highly dependent on the PMOXA grafting density and molecular weight, with optimal performance observed at a low grafting density of 7–14% and a moderate NH_4^+/PO_4^{3-} (N/P) charge ratio between 3.125 and 6.25. After transfection, PLys-*g*-PMOXA-DNA condensates were internalized by cells within 2 hours and were observed to localize near the perinuclear region after 6 hours. These condensates, with a hydrodynamic diameter of approximately 100 nm,

exhibited stability in serum and retained their structural integrity even after exposure to 70°C heat treatment. Additionally, they effectively protected DNA from degradation by nucleases.

A novel large pore mesoporous silica nano particles (LP-MSNs) functionalized with PLys were designed as a new carrier material for gene delivery applications, and preparation of this vehicle can be described in the following procedures[50]: (1) 3-glycidoxypropyl trimethoxysilane (3-GPS) grafted onto the silica surface of the spheres through a standard silanoxane coupling mechanism to make LP-MSN-E. (2) PLL was attached to the silica through a nucleophilic addition reaction with the epoxide groups of 3-GPS. This interaction is driven by the nucleophilic attack of the lone electron pair of nitrogen atoms in PLL on the strained acidic carbons of the epoxide ring, leading to the ring opening to obtain LP-MSN-P.

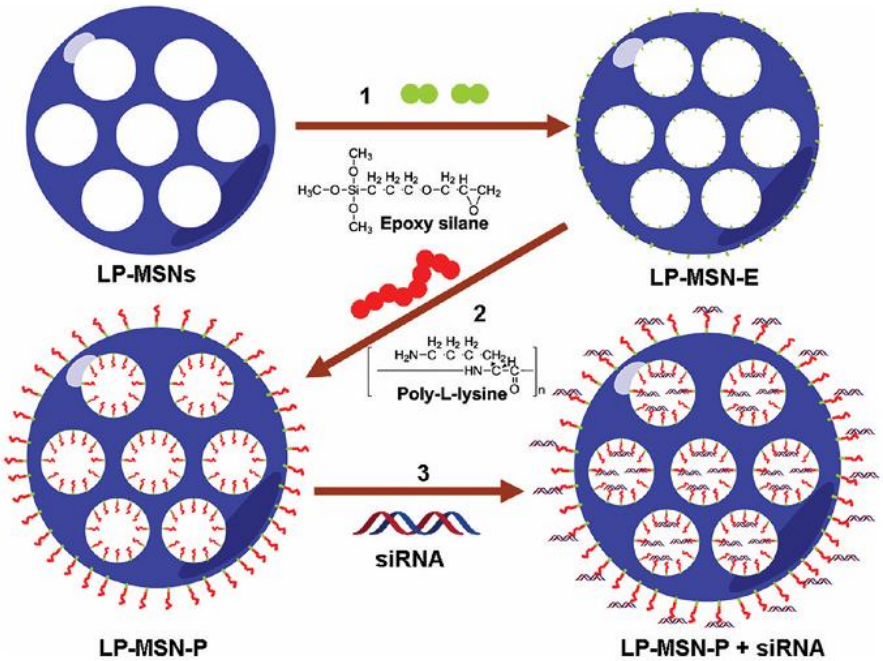

Figure 1-8 Schematic illustration of the steps for the PLys grafting and gene loading into LP-MSN-P[50].

The composites of LP-MSNs and PLys, referred to as LP-MSN-P, were developed as carriers

for DNA or siRNA. The incorporation of PLys significantly enhanced the nanoparticles' binding affinity for oligo-DNAs compared to unmodified silica particles, thereby surpassing native nanoparticles in their efficiency as gene carriers. These functionalized nanoparticles demonstrated low cytotoxicity at concentrations up to 100 μg/mL. Moreover, LP-MSN-Ps effectively delivered siRNA, leading to a significant reduction in the viability of oncogene-expressing cancer cells, highlighting their potential for therapeutic applications[50].

Targeted drug delivery is achieved through stimuli-responsive signals, which may include pH, temperature, enzymes, or other biological triggers that regulate the rate of controlled drug release[2]. PLys-based materials, utilized in forms such as conjugates, block copolymers, or gels, enhance the efficiency of targeted delivery systems[51].

4-(Decyloxy)benzaldehyde (DBA) was conjugated to methoxy-poly(ethy-leneglycol)–block–poly(l-lysine hydrochloride) (PEG-*b*-PLys) to develop a pH-responsive nanoparticle system[52]. Under physiological conditions (pH 7.4), the alkyl groups of DBA interacted with the polylysine segment via benzoic-imine bonds, forming a toothbrush-like structure. Upon exposure to a lower pH, the benzoic-imine bonds broke, causing the super amphiphilic structure to disassemble into hydrophilic components, leading to the release of encapsulated molecules. This disassembly was reversible when the pH was increased (Figure 1-9). Notably, the nanoparticles disassembled at a pH of approximately 6.5, which is close to the extracellular pH of tumour cells. Above pH 7.4, the encapsulated concentration of Nile Red (measured via fluorescence intensity) remained stable at around 0.6 mg/mL. However, at a mildly acidic pH

of 6.5, the encapsulated drug concentration dropped sharply to about 0.05 mg/mL. This pH shift from 7.4 to 6.5 triggered the release of encapsulated Nile Red within 20 minutes, demonstrating the rapid-release capability of the self-assembled system.

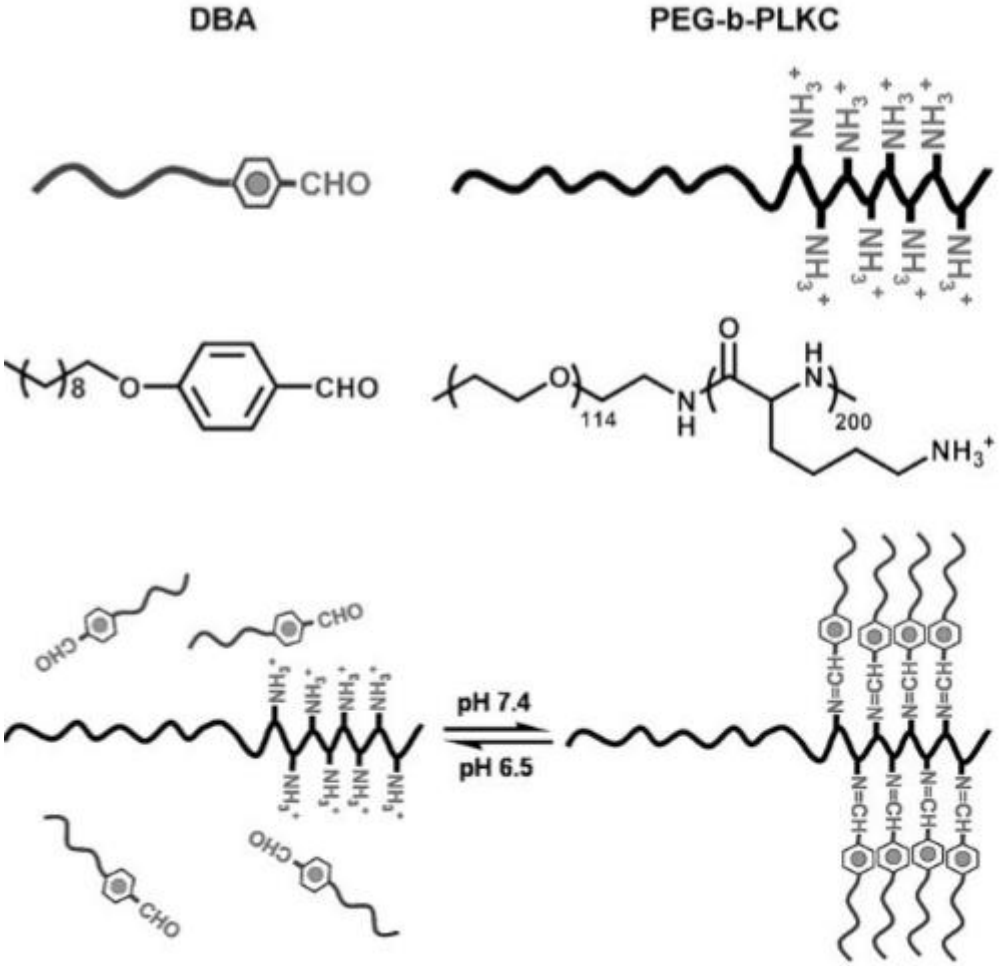

Figure 1-9 Building blocks of the super-amphiphile and the pH-responsive property of the self-assembled aggregates[52].

Biocompatible and pH-responsive vesicles were successfully developed using the triblock copolymer poly(ethylene glycol) methyl ether acrylate-block-poly(L-lysine)-block-poly(L-histidine [$(PEGA)_{30}$-*b*-$p(Lys)_{25}$-*b*-p(His)] synthesized through a combination of reversible addition−fragmentation transfer (RAFT) polymerisation, ROP of lysine-NCAs, and

azide−alkyne click cycloaddition reactions[53]. These stimuli-responsive copolymers were capable of forming hybrid vesicles that effectively internalized into NIH 3T3 and CT26 cells, with cell viability exceeding 94% across a wide vesicle concentration range (0.1−100 μg/mL). Doxorubicin (Dox)-loaded vesicles demonstrated preferential drug release in acidic environments, particularly in CT26 cells. Acidic endosomal pH caused the imidazole ring of the p(His) block to be protonated, and the positively charged imidazole groups repel each other, leading to the pH-induced destabilization of the vesicle bilayer. At pH 7.4, around 30% of Dox remained in the vesicles after 72 h. At pH 5.5, the release rate was much faster; within the first 24 h, beyond 50% of the initial load was released, reaching 80% within 72 h.

To introduce temperature-responsive properties to PLys, it must be conjugated with a polymer that inherently exhibits such characteristics. Among temperature-sensitive polymers, poly(N-isopropylacrylamide) (PNIPAM) is the most well-known, displaying lower critical solution temperature (LCST) behaviour at 32 °C[54].

Rod-coil block copolymers, poly(N-isopropylacrylamide)-*b*-PLys (PNIPAM-*b*-PLys), were obtained using a combination of atom transfer radical polymerisation (ATRP) and ROP[55]. These amphiphilic hybrid rod-coil block copolymers exhibited the capacity to form a variety of morphologies, including spherical micelles, wormlike micelles, and vesicles, through adjustments in copolymer compositions or solvent conditions. In aqueous environments, the block copolymers demonstrated dual stimuli-responsive behaviour, undergoing coil-to-helix and coil-to-globule transitions when subjected to environmental changes, such as a shift from

neutral pH to pH 13 or an increase in temperature from 25°C to 45°C (Figure 1-10). These adaptable self-assembly characteristics emphasise the potential of PNIPAM-*b*-PLys for applications requiring highly tunable and responsive systems. For example, they can be used as "smart" drug or gene carrier, where PLys segment can adhere to membranes of abnormal cells or complex with nucleic acids, while PNIPAM segment can control the release of capsulated contents under thermal stimulation[56-58].

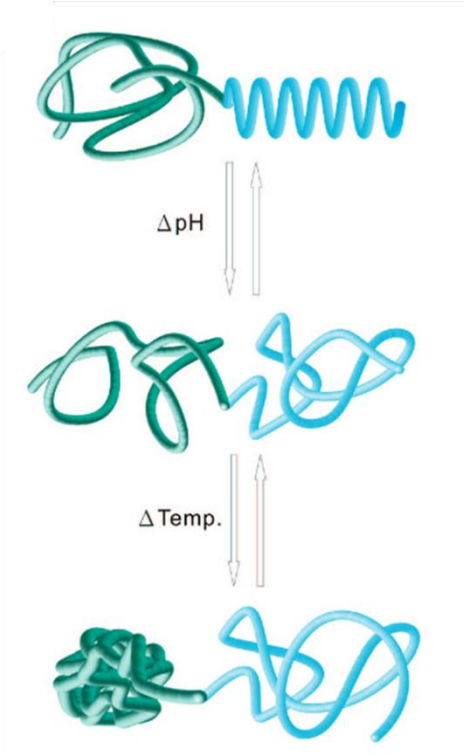

Figure 1-10 Proposed schematic representation of the PNIPAM -b-PLys stimuli-responsive behaviour of the pH-induced coil-to-helix and thermo-induced coil-to-globule transition in aqueous solution, adapted from [55].

Codelivery of genetic material and a small molecule drug proves beneficial. Co-delivery systems can overcome drug resistance and increase the effectiveness of treatment, especially in cancer therapy.

Through complex synthesis procedures, involving ROP, click chemistry, aminolysis, and hydrolysis, [poly(L-lysine)-*b*-poly[N-(N', N'-diisopropylaminoethyl)aspartamide] copolymers (PLys-*b*-P[Asp(DIP)]) can be prepared[59]. Designed pH-responsiveness and self-assembly behaviours can be achieved with varying PLys and PAsp(DIP) block lengths. These copolymers formed stable micelles at pH 7.4, characterised by a partially hydrated PAsp(DIP) core and a PLL corona which could effectively encapsulate DOX in the PAsp(DIP) core, while simultaneously forming complexes with siRNA through interactions with the PLL shells. At pH 5.4, the micelles disassembled due to the further protonation of the tertiary amines in the PAsp(DIP) block, disrupting the micellar structure and facilitating the release of both the encapsulated drug and siRNA.

Due to its polycationic nature, PLys plays an important part in wound care and tissue regeneration fields. Cationic protonated amine groups can electrostatically interact with negative-charged surface of cell membranes or proteins which contributes to tissue repairing[60-62]. Hence, cells adhesion and tissue repairing performance on PLys-based substrates can be promoted at the same time. PLys can form layer by layer assembly polyelectrolytes with hyaluronic acid, a natural biocompatible and biodegradable anionic polysaccharide under the assistance of crosslinker 1-ethyl-3-(3-dimethylaminopropyl)carbodiimide hydrochloride (EDC)[63]. Human adipose-derived stem cells were selected for cultivation on substrates with varying crosslinking densities, which were regulated by the concentration of EDC. Substrates with higher crosslinking density promoted greater cell spreading and enhanced osteogenic differentiation, whereas those with lower

crosslinking density were more favourable for supporting adipogenic differentiation[63]. Richert *et al.* fabricated a multilayered polyelectrolyte film consisting of PLys and poly(glutamic acid) which was capable of modulating cell adhesion performance through pH adjustments during the deposition process[64]. Films prepared at pH 10.4 exhibited enhanced cell adhesion, whereas those formed under acidic conditions (pH 4.4) repelled cells. This variation was linked to the water swelling properties of the films, which were greater under basic conditions and reduced under acidic conditions[65]. Incorporating PLys into composite materials allows for the modulation of mechanical robustness, biodegradability, and bioactivity to suit specific requirements in tissue engineering or wound healing. These composites, particularly in the form of hydrogels, have shown great promise in various applications, including bone, cartilage, and neural tissue regeneration[66]. Discussions on these applications will be provided in the section on PLys-based hydrogel materials.

1.4 Adsorption, adsorbents and PLys-based adsorbents

Pure and uncontaminated water is vital for all living organisms; however, despite covering over 71% of the Earth's surface, less than 1% of available water meets international standards for potable use due to extensive pollution[67]. Among the various pollutants, heavy metal ions and organic dyes are particularly hazardous, as even trace amounts can pose significant risks to human health and contribute to the development of numerous diseases[68].

Eliminating toxic elements and compounds at low concentrations is a challenging task. To

tackle this issue, a range of purification techniques has been taken to remove pollutants such as heavy metals, dyes, insecticides, fertilizers, organic acids, and halogenated and phenolic compounds[69-71]. These methods include precipitation, incineration, flocculation, coagulation, ion exchange, reverse osmosis, membrane filtration, electrochemistry, photo-electrochemistry, advanced oxidation processes, and biological methods, each demonstrating varying levels of remediation efficiency[72].

However, these approaches have suffered from several drawbacks, including limited removal efficiency, excessive sludge generation, high costs and energy consumption, the formation of toxic by-products, and the potential introduction of additional harmful chemicals into the environment. In light of these challenges, adsorption has emerged as one of the most effective and economical water treatment strategies[67]. Recent years have witnessed notable advancements in the design and development of various adsorbents for wastewater purification, These adsorbents, aiming for different pollutants, are illustrated in Figure 1-11[73].

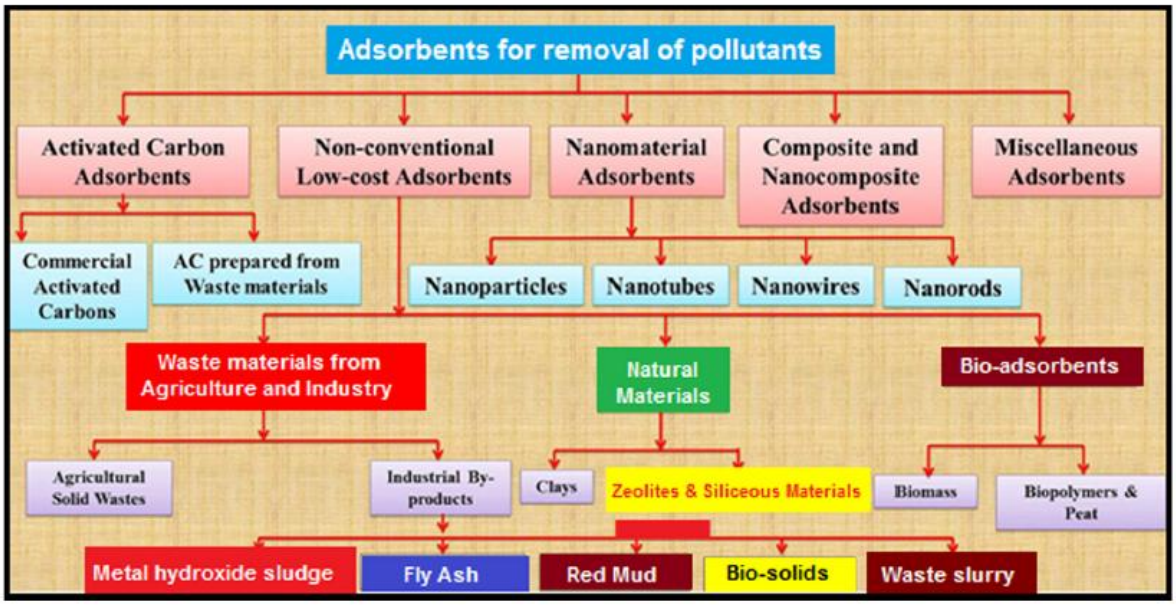

Figure 1-11 Various types of adsorbents for removal of pollutant from water environment[73].

Two key concepts are fundamental to understanding the adsorption process. Adsorbate refers to the substance that is adsorbed onto the surface of an adsorbent[74]. This can include molecules, atoms, or ions present in a gas, liquid, or solution[75]. For instance, in wastewater treatment, pollutants such as heavy metal ions and dye molecules in the solution act as the adsorbate. Adsorbents, on the other hand, are natural or synthetic materials with the ability to adsorb substances[76]. Their surfaces attract and retain the molecules or ions of the adsorbate. Adsorbents typically possess a high surface area and a porous structure, which enhance their adsorption capacity[77]. Adsorption behaviour in aqueous environment can be vividly depicted in Figure 1-12.

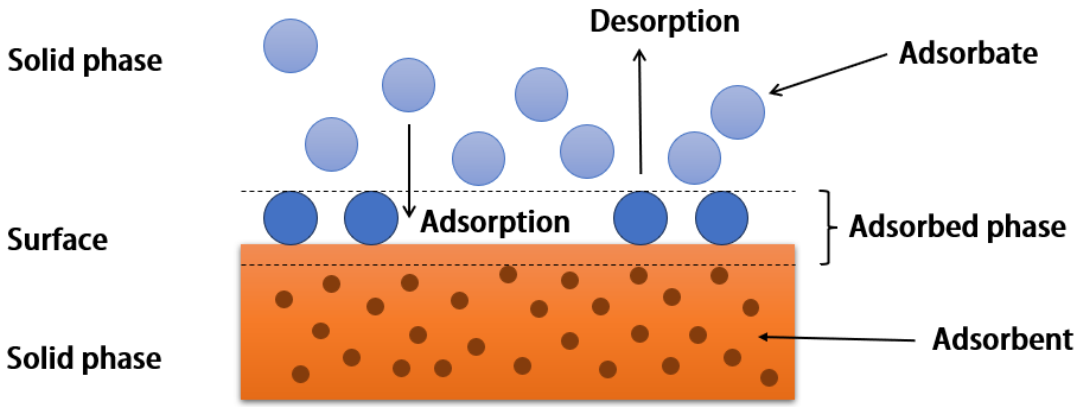

Figure 1-12 Adsorption behaviour in aqueous environment, modified from [78].

The advantages and disadvantages of five types of adsorbents have been summarised in Table 1-2, based on Singh *et al.*'s comprehensive review [67] on adsorbents for water purification.

Bioadsorbents are materials obtained from biological sources, including agricultural byproducts, natural polymers, microorganisms, and waste biomass, which are employed to adsorb and eliminate contaminants[79]. Strictly speaking, the agricultural waste adsorbents mentioned in the above table also fall under the category of bioadsorbents.

Table 1-2 Pros and cons of different type of adsorbents.

Type	Examples	Pros	Cons
Natural	Clay, zeolites, peat	Low cost, eco-friendly, abundant, effective for metals/dyes	Limited capacity, requires modification for complex pollutants.
Biomass (Bioadsorbents)	Chitosan, algae, yeast	Renewable, biodegradable, high selectivity for metals	Stability and preparation costs are concerns.
Industrial Waste	Fly ash, red mud	Cost-effective, reuses waste, high capacity for pollutants	Requires pretreatment, potential secondary pollution.
Agricultural Waste	Rice husk, banana peels, orange peels, coconut shells, wheat straw	Inexpensive, sustainable, good for low-pollutant scenarios	Low durability, needs treatment, limited high-scale use.
Synthetic	Activated carbon, carbon nanotubes (CNTs), graphene oxide, polymer resins	High capacity, selective, reusable	Expensive, potential environmental risks.

Bioadsorbents have gained increasing popularity in recent years due to the following reasons[79]: they are derived from renewable and biodegradable sources, making them an environmentally sustainable option for wastewater treatment. Their production is typically low-cost, as they are often manufactured from inexpensive, readily available materials. Many bioadsorbents contain functional groups, such as hydroxyl, carboxyl, and amino groups, which exhibit strong interactions with contaminants, enabling efficient adsorption. Additionally, bioadsorbents can be chemically tailored or modified to target specific pollutants, enhancing

their adsorption efficiency and selectivity. Furthermore, their preparation and disposal are less prone to causing secondary pollution, further emphasizing their environmental advantages.

Chitin and chitosan, as biomass materials rich in amino and hydroxyl groups, have demonstrated significant potential for adsorbing heavy metal ions and organic dyes[80]. These biopolymers are derived from renewable sources, including crab and shrimp shells, insect exoskeletons, and fungal cell walls[80]. Chitin is a linear polysaccharide composed of N-acetyl-D-glucosamine units linked by β-(1-4) glycosidic bonds. Through a deacetylation process, chitin is converted into chitosan, where some or all of the acetyl groups ($-NHCOCH_3$) in the N-acetyl-D-glucosamine units are removed, yielding D-glucosamine units[80]. This structural modification enhances the solubility and adsorption capabilities of chitosan, making it particularly effective for removing pollutants from aqueous solutions.

Although the artificial synthesis of PLys adds to its cost, it offers several advantages over chitosan, making it superior in many applications. PLys is a homopolymer containing multiple amine groups in its side chains, providing a higher density of positively charged sites than chitosan[81]. These sites allow PLys to chelate effectively with anionic heavy metal ions or electrostatically attract cationic dye molecules. Besides, PLys exhibits superior solubility in water across a broader pH range, while chitosan is poorly soluble in neutral and basic conditions[2, 80]. This enhanced solubility makes PLys-based adsorbents more versatile and effective in a variety of aqueous environments, broadening their applicability in pollutant removal processes.

PLys with a molecular weight exceeding 30,000 kDa was utilized to adsorb chromium ions, achieving a maximum adsorption capacity of approximately 42.2 mg/g (Cr/PLys) at a solution pH of 4.6[82]. The metal uptake performance of PLys was further assessed using a Polymer Enhanced Diafiltration (PEDF) system based on membrane separation technique, in which metal ion was captured by polymer, forming polymer-metal complex. This complex was effectively retained via a tangential flow filtration membrane and further concentrated by continuous diafiltration. In the large-scale adsorption experiment, 0.6 mg of PLys dissolved in 0.2 L of water was introduced into 2 L of a chromium solution with an initial concentration of 30 mg/L. At the end of the process, the chromium concentration in the permeate was reduced to 7.8 mg/L. However, the chromium ion concentration was not fully accounted for in the system analysis, and the recovery of PLys from the adsorption system posed a significant challenge.

A novel magnetic bioadsorbent was synthesised by chemically grafting 3-glycidoxypropyltrimethoxysilane (GPTMS) and PLys onto Fe_3O_4 nanoparticles (Figure 1-12)[83]. The adsorption capacities of this bioadsorbent were assessed using four typical sulfonated organic dyes: methyl blue, orange I, amaranth, and acid red 18. After a 40-minute adsorption process, the uptake capacities for these dyes reached up to 318, 128, 90, and 245 mg/g, respectively. The adsorption mechanism is primarily attributed to electrostatic interactions between the amino groups of PLys and the dye molecules. Notably, even after three adsorption-desorption cycles, the bioadsorbent maintained 80–90% of its initial dye adsorption capacity.

This study offers a comprehensive and systematic exploration of organic dye adsorption using the synthesized bioadsorbent. The magnetic properties of the Fe_3O_4 core facilitate easy recovery of the adsorbent from aqueous solutions. However, it is important to acknowledge that the experiments were conducted at pH 2, which is considerably more acidic than typical industrial wastewater and may restrict the adsorption capacity of the material in practical applications.

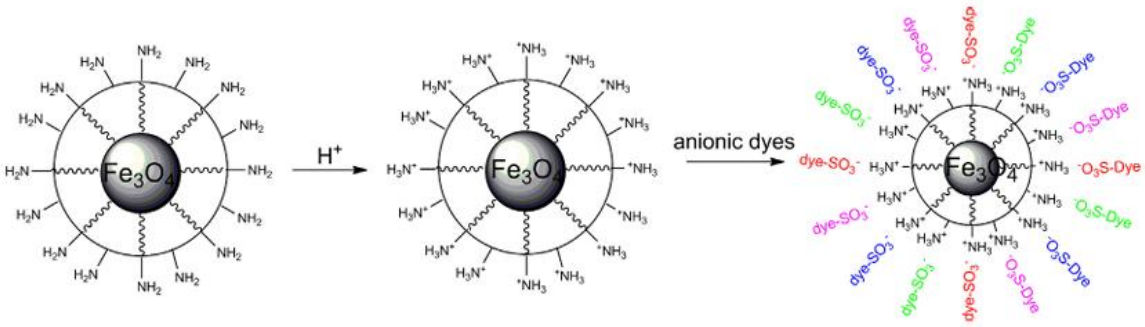

Figure 1-13 Structure of Fe_3O_4-GPTMS-PLys nanoparticle and its mechanism on capturing dyes[83].

A new composite adsorbent was developed through a three-step synthesis process[84]: (1) grafting multi-walled carbon nanotubes (MWCNTs) onto graphene oxide (GO), (2) incorporating magnetic Fe_3O_4 particles into the GO-MWCNTs framework, and (3) modifying the resulting material with PLys to form the final PLys-Fe_3O_4-(GO-MWCNTs) hybrid nanocomposite. This environmentally friendly hybrid composite exhibited excellent adsorption performance for the removal of a dye (tartrazine) and a heavy metal (Pb^{2+}), separately. The adsorption of Pb^{2+} reached equilibrium within 30 minutes, while tartrazine adsorption achieved equilibrium in approximately 60 minutes. Under optimal conditions, the equilibrium adsorption capacities were 1038.42 mg/g for Pb(II) and 775.19 mg/g for tartrazine. Both adsorption

processes followed the Langmuir adsorption model, indicating monolayer adsorption on homogeneous surfaces. Additionally, the adsorption kinetics were best described by the pseudo-second-order kinetic model, reflecting chemisorption as the rate-limiting step. The adsorbent maintained a high adsorption capacity, retaining 80% of its initial adsorption performance even after five adsorption-desorption cycles, highlighting its reusability and durability.

The mechanism for how this nano-sized hybrid capture pollutants from wastewater are illustrated in Figure 1-14[84]. At low pH, the adsorption of Pb^{2+} is primarily attributed to chelation interactions between the amino and hydroxyl groups on the hybrid surface and Pb^{2+}, as well as ion exchange between H^{+} and Pb^{2+}. While the effective adsorption of tartrazine dye can be explained by two key mechanisms. On one hand, electrostatic interactions are enhanced due to the positively charged surface of the hybrid composite at low pH; on the other hand, the presence of various functional groups, such as OH, NH_2, COOH, and C=C, facilitates the formation of covalent bonds, hydrogen bonds, and van der Waals forces with tartrazine, further contributing to its high adsorption efficiency.

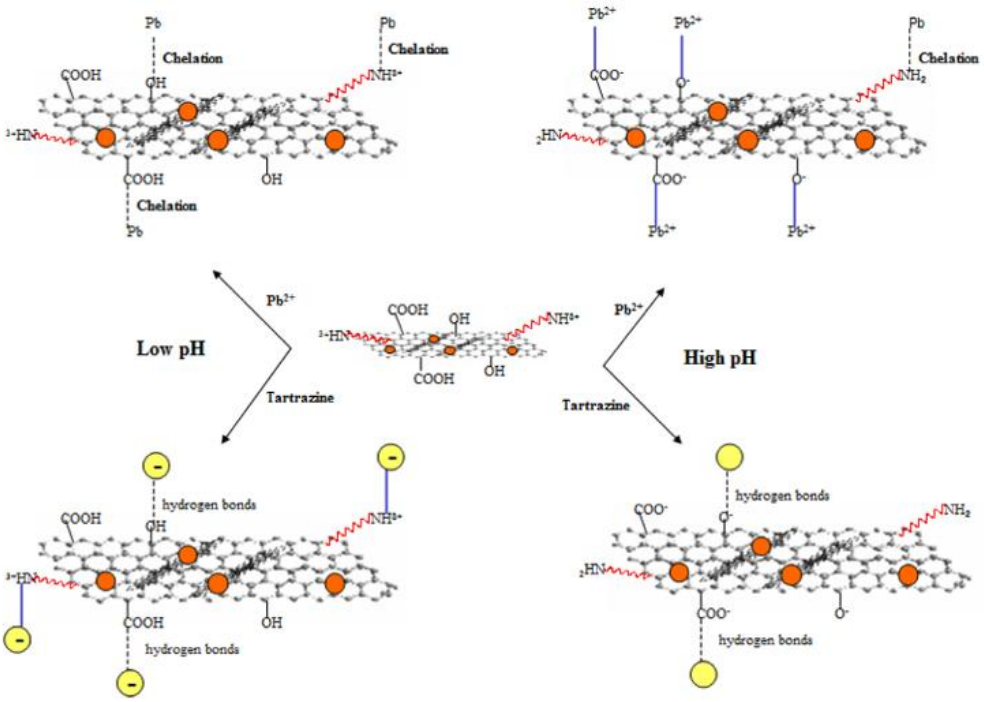

Figure 1-14 Mechanism of Pb^{2+} and tartrazine adsorption onto PLys-Fe_3O_4-(GO-MWCNTs) composite[84].

In a high-pH alkaline environment, the amino groups on the hybrid surface undergo deprotonation, releasing H^+ into the solution and resulting in a negatively charged adsorbent surface. This change facilitates a new electrostatic attraction between the negatively charged hybrid surface and Pb^{2+}, enhancing Pb^{2+} adsorption. However, for dyes such as tartrazine, appearance of negatively charged surface causes electrostatic repulsion with the anionic tartrazine molecules, thereby reducing the adsorption efficiency for the dye.

This composite adsorbent is both highly effective and easily recyclable. The incorporation of carbon nanotubes and graphene enhances the nanoscale pore structure and introduces a variety of functional groups, significantly improving its adsorption efficiency for targeted pollutants.

However, the complex preparation process and the high cost of raw materials may limit its large-scale application.

As demonstrated in the three articles above, the development of PLys as a bioadsorbent represents a gradual, step-by-step process of material enhancement. Starting from the basic use of standalone PLys, advancements have led to the creation of multifunctional PLys-based materials designed to achieve more diverse functionalities, such as improved adsorption capacity and enhanced recovery or recyclability. Throughout evolution of PLy-based bioadsorbents, PLys consistently serves as the core component of the material. However, due to the considerable costs associated with PLys synthesis, it is sometimes incorporated as an auxiliary constituent in adsorptive systems. This emphasises the importance of thoroughly understanding and investigating the adsorption mechanisms of pure PLys for pollutants. Such foundational knowledge is crucial for optimizing the performance of PLys and seamlessly integrating it into advanced adsorptive systems, enabling the design of more efficient and cost-effective materials for pollutant removal.

1.5 Hydrogel and PLys-based hydrogels

The concept of hydrogels was first introduced by Wichterle and Lím in 1960[85]. Hydrogels are three-dimensional (3D) networks of hydrophilic polymers capable of swelling in water and retaining significant amounts of water, while maintaining structural integrity through chemical or physical cross-linking of polymer chains. To be classified as a hydrogel, the material must

contain more than 10% water (by weight or volume), which is essential for its flexibility and functionality. Hydrophilic groups such as amine, carboxyl, hydroxyl, amide, and sulfonic acid groups contribute to the water-absorbing properties of hydrogels.

Hydrogels can be categorised as either physical or chemical, based on their cross-linking mechanisms[86]. Physical hydrogels form through non-covalent interactions and can transition from liquid to gel states in response to environmental changes such as temperature, ionic concentration, pH. Chemical hydrogels, rely on covalent bonding to create a stable network structure. This covalent cross-linking enhances their mechanical strength and resistance to degradation, making them more durable compared to physically cross-linked hydrogels.

The distinction between the two types of hydrogels is effectively illustrated in Figure 1-15, which highlights the various types of cross-linking mechanisms[87]. Hydrogel formation via chemical cross-linking and ionic interactions is a common approach for alginate-based hydrogels[88]: (1) Alginate contains carboxylate groups on its guluronic acid residues. When calcium ions are introduced, they bind to these carboxylate groups, creating "egg-box" junction zones that serve as crosslinking points. (2) Polyacrylamide gels rely on covalent cross-linking between polymer chains, which is achieved using N,N-methylenebisacrylamide (MBAA) as a crosslinking agent. (3) In the alginate-polyacrylamide hybrid gel, the two polymer networks—alginate and polyacrylamide—are integrated covalently cross-linked with MBAA.

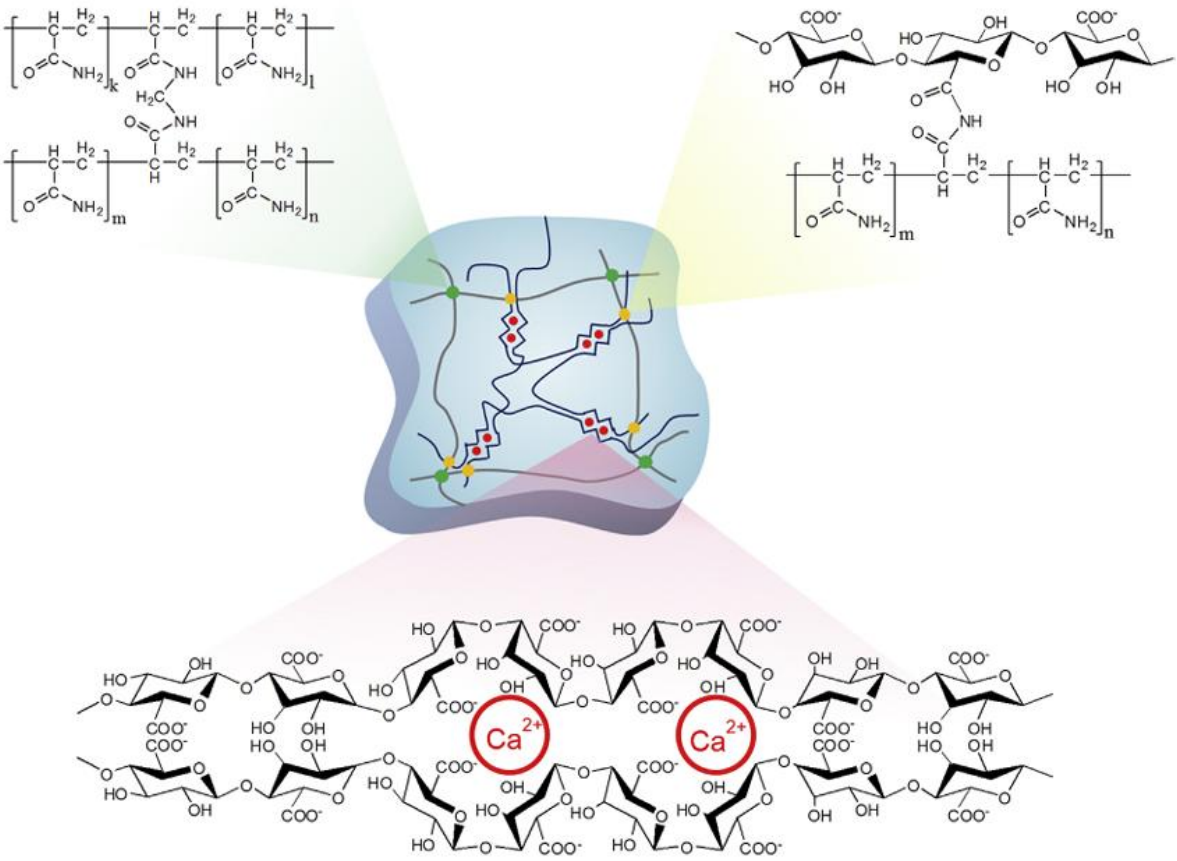

Figure 1-15 Hydrogel formation via chemical cross-linking and ionic interactions[87].

PLys-based hydrogels are hydrogels derived from PLys, inheriting the properties of PLys, such as its biodegradability, and pH- responsive cationic charge due to the protonated amino groups in its side chains. Hence, applications of PLys-based hydrogels are mainly focused on the biomedical fields such as biomaterials in wound healing, delivery systems and tissue engineering[89, 90].

PLys has been reported as a cross-linking agent for hyaluronic acid (HA) hydrogels, facilitated by EDC, to enhance cell affinity[91]. This fabricated hydrogel platform was further functionalised by immobilising nogo-66 receptor antibody (antiNgR), a molecule known to

promote spinal cord regeneration. In a study involving rats subjected to lateral hemisection of the spinal cord, the HA-PLys/antiNgR hydrogel demonstrated significant therapeutic potential. After eight weeks post-implantation, anti-neurofilament-positive axons were observed extending into the hybrid hydrogel. Furthermore, an increased presence of cells and normal myelinated axons was noted within the implanted scaffold.

PLys was employed in the physical cross-linking of a polypyrrole-alginate copolymer to form alginate-polypyrrole/poly-L-lysine hydrogels, with Ca^{2+} acting as the cross-linking agent[92]. This hydrogel integrates the antioxidant properties of polypyrrole (PPy) with the neural differentiation-enhancing ability of PLys. The hydrogel's performance characteristics, such as morphology, porosity, swelling ratio, oxidation resistance, rheological behaviour, and conductivity, could be tailored by adjusting the molar ratios of the three primary components. These hydrogels exhibit excellent cell compatibility for P19 cells, alongside electrical conductivity and antioxidant activity, making them particularly suitable for nerve tissue applications. Moreover, P19 cells cultured within these hydrogel scaffolds successfully differentiated into neurons.

PLys was chemically bonded with chitosan through a coupling reaction and then physically crosslinked with regenerated silk fibroin (RSF) using Ca^{2+} to create a bioadhesive material for wound healing[93]. This material demonstrated excellent adhesion strength, which was high up to 70 kPa on separated pig skin. Besides, it did not trigger immune system irritation, demonstrating good biocompatibility. The significant antibacterial effects of this material were

observed against *Staphylococcus aureus* and *Escherichia coli*, reaching a 100% antibacterial rate after 120 minutes of treatment.

The development of PLys-based hydrogel materials has progressed towards the creation of composite and multifunctional hydrogels. However, PLys with high concentrations and high molecular weights can exhibit physiological toxicity, which is why it is often used as a component in hydrogels rather than independently or is replaced by ε-polylysine in some applications. The toxicity of PLys can be mitigated by strategies such as reducing its molecular weight, lowering its concentration, or chemically modifying its structure to improve biocompatibility. This toxicity is largely attributed to the high cationic charge densities and the flexibility of the polymer, which can cause higher cytotoxic effects compared to materials with lower cationic charge densities[15]. Studies have shown that as the molecular weight of PLys decreases, its toxicity is significantly reduced[15].

Despite these challenges, with substantial room for improvement and further research, PLys has the potential to deliver enhanced performance, reduced side-effects, and broader applications in advanced tissue engineering and wound healing systems.

Reports on PLys-based hydrogels as bioadsorbents or drug delivery materials remain limited. However, the preparation of PLys in hydrogel form significantly enhances its specific surface area and pore structure, making it more effective for the adsorption of target pollutants. Additionally, the hydrogel format addresses the issue caused by PLys's strong water solubility

which previously complicated recovery after adsorption.

When used as a drug carrier, PLys-based hydrogels effectively respond when the pH of their external environment changes, enabling controlled drug release behaviour. PLys-based hydrogels with pH-sensitive swelling behaviour can be fabricated by mixing a PLys solution with the crosslinker genipin[94]. The chemical crosslinking by genipin significantly reduces the cytotoxicity of PLys, while the resulting hydrogel promotes cell adhesion and proliferation. The anticancer drug Dox was employed as a model water-soluble drug to investigate the loading and release capabilities of these hydrogels. Experimental results indicated a mild burst release of Dox, with the drug release properties being effectively adjustable through the degree of crosslinking.

In the third and fourth chapters of this thesis, the common theories of adsorption and drug release will be integrated to address the gap in research on pure PLys-based hydrogels as materials for organic dye adsorption and as drug carriers. This exploration aims to provide a comprehensive understanding of their potential applications in these fields.

1.6 Adsorption theory

Adsorption kinetics models mathematically describe the rate of adsorption between a solute and an adsorbent, along with the controlling steps involved. They are often used to determine the relationship between the target adsorbed substance and adsorption time/amount. By fitting

experimental data to these mathematical models, it can be determined whether the adsorption process is governed by physical diffusion or chemical interactions. This analysis is instrumental in revealing the fundamental mechanisms underlying adsorption. There are a few kinetic adsorption models for the explanation of adsorption processes. These models may play an important role in revealing adsorption mechanisms of organic dyes (chapter. 4).

1.6.1 Pseudo-first-order kinetics

At the end of the 19th century, Lagergren introduced the pseudo-first-order kinetics model to describe adsorption processes[95]. This model is based on the hypothesis: proportionality to unadsorbed adsorbate concentration. Specifically, the adsorption rate is proportional to the concentration of the target adsorbate that has not yet been adsorbed. This model is led by a physical mechanism and can be expressed as equation (1-1):

$$q_t = q_e(1 - e^{-k_1 t}) \tag{1-1}$$

where q_e (mg/g) is the amount of adsorption at the adsorption equilibrium, and qt is the amount of adsorption at time t. k_1 (min^{-1}) represents the kinetic adsorption rate constant in the pseudo-first-order model.

1.6.2 Pseudo-second-order kinetics

Although pseudo-second-order kinetics were first proposed in the late 20th century[96], the

model gained significant popularity after Ho and MacKay applied it to analyse numerous experimental results[97]. This model is based on two key hypotheses: 1) The adsorption sites on the surface of the adsorbent are uniformly distributed, and each site can bind only one molecule of the adsorbate. 2) the adsorption sites on the surface of the adsorbent are uniformly distributed, and each site can bind only one molecule of the adsorbate. This model is dominated by a chemical mechanism, and represented by Equation. (1-2)[98]:

$$q_t = \frac{{q_e}^2 k_2 t}{1 + q_e k_2 t} \tag{1-2}$$

where the q_e and q_t are defined as in Equation. (1-1). k_2 (g/(mg·min)) is the kinetic adsorption rate constant of the pseudo-second-order model.

1.6.3 Elovich kinetic model

An equation based on chemical adsorption was suggested by Zeldowitsch in 1930s[99]. In this model, the energy distribution of surface adsorption sites is considered to be not uniform, and the more activation energy is required for further adsorption increases with time. It is particularly suitable for chemisorption on heterogeneous surfaces. The equation, assuming abt $\gg$ 1, can be expressed as follows (equation 1-3)[100]:

$$q_t = \frac{\ln(ab) + lnt}{b} \tag{1-3}$$

where q_t (mg/g) means the amount of adsorption at time t. a is initial adsorption constant and b is a constant associated with the surface coverage of the adsorption sites. A larger a

corresponds to a faster initial adsorption process. A larger b reflects greater sensitivity of the adsorption rate to the coverage of adsorption sites, meaning the rate decreases more sharply as the sites become occupied.

1.6.4 Avrami kinetic model

Based on pseudo-first-order kinetics, a generalised Kolmogorov-Erofeev-Kazeeva-Avrami-Mampel (KEKAM) equation was developed to describe reactions occurring on the surface active sites of solid supports[101]. Its equation shows as follows (equation 1-4):

$$q_t = q_e(1 - e^{-(kt^n)}) \tag{1-4}$$

where q_e and q_t have the same meanings as in the pseudo-first-order kinetics model, representing the amount of adsorption at equilibrium and at time t, respectively. The parameter k is the Avrami kinetic constant, and n is an index associated with the adsorption mechanism, describing the complexity of the adsorption process. The introduction of n enhances the flexibility of the model by accounting for variations in adsorption behaviour. If n>1, the adsorption process is primarily limited by surface reactions, with adsorbate diffusion occurring rapidly; if n <1, it suggests homogenous distribution of adsorbate on adsorbents with the adsorption rate being more controlled by diffusion; if n =1, the model can be simplified to the pseudo-first-order kinetics model, where the adsorption rate is directly influenced by the concentration of the adsorbate[102].

1.7. Adsorption Isotherm

Adsorption isotherm is an important tool to study the interaction between adsorbate and adsorbent during adsorption. It describes the relationship between the equilibrium concentration of solute and the amount of solute adsorbed by per unit of adsorbents under constant temperature conditions. These isotherms not only reflect the mechanism of adsorption process, but also play an important role in adsorption system design, performance optimisation and material selection.

Adsorption isotherms are essential tools for understanding the interactions between adsorbates and adsorbents during the adsorption process. They depict the relationship between the equilibrium concentration of a solute in the liquid phase and the amount of solute adsorbed per unit mass of the adsorbent at a constant temperature. By providing this relationship, adsorption isotherms offer valuable insights into the adsorption mechanism.

These isotherms are not only fundamental for theoretical studies but also have significant practical implications. They play a crucial role in the design and optimisation of adsorption systems and select appropriate materials for specific applications. Through analysis of adsorption isotherms, the adsorption capacity of materials can be determined, and the adsorption performance of an adsorbent can be predicted under various conditions, thereby allowing adsorption processes to be tailored for maximum efficiency.

1.7.1 Langmuir isotherm

The Langmuir isotherm is one of the classic adsorption models, first proposed by Irving Langmuir in 1916[103]. It describes the equilibrium behaviour of adsorbates forming a monolayer on the surface of an adsorbent. This model is widely applied to analyse adsorption processes occurring on homogeneous surfaces. In the Langmuir model, it is assumed that each adsorption site on the adsorbent surface behaves independently and is not influenced by the occupation of neighbouring sites. Its equation can be expressed as equation 1-5[104]:

$$\frac{1}{q_e} = \frac{1}{q_m b C_e} + \frac{1}{q_m} \tag{1-5}$$

where C_e (mg/L) represents the amount of adsorbed substances in the solution at adsorption equilibrium, q_e (mg/g) represents the equilibrium capacity of the adsorbent, q_m (mg/g) is the maximum adsorption capacity of the adsorbent, and b (L/mg) is the Langmuir isotherm constant, suggesting the affinity between the adsorbent and the adsorbate. Higher this constant, stronger binding ability of adsorbent to adsorbate.

1.7.2 Freundlich isotherm

Different from Langmuir isotherm, Freundlich isotherm was an empirical model suggested by Freundlich in the early 20th century[105]. Besides, the inhomogeneity of the adsorbent surface and the possibility of multilayer adsorption were considered in the overall adsorption process in this model. However, this model did not provide an upper limit of adsorption capacity. Its

equation (equation 1-6) showed as follows[106]:

$$q_e = k_f C_e^{1/n} \tag{1-6}$$

where q_e and C_e are equal to equation 1-5, k_f ($mg^{1-n} \cdot g^{-1} \cdot L^{-n}$) is the constant depicting adsorption capacity and n is the constant describing the adsorption intensity. The value of n generally ranges from 2 to 3, and $n > 1$ is favourable to adsorption, meaning increase of the concentration of adsorbate is good for promotion of adsorption capacity, $n = 1$ is linear adsorption, indicating adsorption capacity is proportional to the concentration of adsorbate, $n < 1$ is detrimental to adsorption, in other words, the adsorption efficiency decreases at high concentration, which may occur due to the saturation of adsorption sites[107].

1.7.3 Dubinin-Radushkevich isotherm

Dubinin-Radushkevich isotherm model was developed to describe adsorption processes based on the mechanism of adsorption with Gaussian energy distribution across heterogeneous surfaces[108]. The core concept of this model is to relate the adsorption process to the energy distribution on the surface and the pore-filling behaviour of the adsorbent[109]. There was an assumption in this model: adsorbate molecules are drawn into the pores through an energy gradient. This model is particularly suitable for describing the adsorption of vapours and gases on microporous adsorbents. Non-linear form of this semiempirical model was showed as follows (equation 1-7)[109]:

$$q_e = q_m e^{-k\varepsilon^2}$$

(1-7)

where q_e and q_m have the same meaning as in equation 1-5. k (mol^2/KJ^2) is constant, related to adsorption energy. ε represents Polanyi potential, which quantifies the energy requirement for adsorption. For adsorption in the vapor phase, it is calculated using the equation $\varepsilon=RT \ln (P_s/P)$, where P_s is the saturation vapor pressure (atm), P is the adsorbate equilibrium pressure (atm), R is gas constant (8.314 J/mol·K) and T is absolute temperature (K)[110]. For adsorption in aqueous phase, ε is modified as: $\varepsilon=RT\ln(1+1/C_e)$, where Ce stands for adsorbate equilibrium concentration(mg/L)[111].

Some factors, such as pH of solvent on surface charge of adsorbents and functional groups of solutes, were not accounted for when this model is used to describe solute adsorption behaviour from solution. As a result, it can hardly distinguish that the adsorption belongs to physical or chemical process[112].

1.7.4 Hill isotherm

The Hill isotherm model is well-suited for describing adsorption processes where cooperative binding occurs on a homogeneous adsorbent surface. In this model, adsorption is treated as a cooperative behaviour, meaning that the binding of solute molecules to active sites on the adsorbent surface influences the binding ability of other active sites. The equation of this model was evolved from non-ideal competitive adsorption isotherm and listed as follows (equation 1-8)[113]:

$$\frac{q_e}{q_m} = \frac{kC_e^n}{1 + kC_e^n} \tag{1-8}$$

where q_e and q_m have the same meaning as described in Equation 1-5, k means the Hill constant representing the affinity of the adsorbate for the adsorbent, C_e is equilibrium concentration of solute in the solution, and n shows Hill coefficient, indicating the nature of cooperative binding. If n > 1, adsorption of one adsorbate molecule enhances adsorption of others, demonstrating positive cooperativity; if n = 1, adsorption is non-cooperative, similar to Langmuir model; if n < 1, negative cooperative behaviour can be observed[109].

1.8 Mathematical models for the drug release

Mathematical models for drug release serve as essential tools for studying the drug release process[114]. They describe the kinetic behaviour of drug molecules as they are released from carriers, such as nanoparticles or hydrogels, to their target location or surrounding environment. These models not only enhance understanding of the underlying mechanisms of drug release but also provide a theoretical foundation for drug design and the optimisation of drug release systems[115]. Several common models for drug release will be discussed, which may theoretically support the DIC release from PLys-based hydrogels (chapter. 5).

1.8.1 Zero-order kinetics

Zero order kinetics describes a drug release mechanism with a constant rate of release, independent of time. Zero order kinetic release is generally considered an ideal release mode, and its equation (equation. 1-9) can be expressed as follows:

$$q_t = kt \tag{1-9}$$

where qt means the amount of released drug at time t and k is constant of drug release rate.

Zero-order kinetic drug release can be achieved in drug suspensions encapsulated within a transdermal system[116]. The active ingredient remains in a saturated state and creates a constant concentration gradient across the reservoir membrane, thus driving a stable diffusion process through the membrane. A steady release rate maintains until the diffusion rate eventually decreases to zero.

1.8.2 First-order kinetics

The first-order kinetics model describes a drug release mechanism in which the release rate is directly proportional to the amount of unreleased drug[117]. In this model, the release rate gradually decreases over time. Release behaviour of buffered aspirin tablets fit well with this model[118]. The integrated form of the equation (Equation 1-10) is expressed as:

$$q_t = q_m(1 - e^{-kt}) \tag{1-10}$$

where q_t and q_m stands for the amount of released drug at time t and the maximum amount of

released drug, respectively. k is first-order kinetic constant.

1.8.3 Higuchi model

The Higuchi model describes the release rate of drugs from matrix systems where drugs are evenly dispersed or anchored within insoluble or swelling polymeric networks [119]. The use of the Higuchi model relies on the following assumptions: 1) Initial drug concentration contained in the matrix far exceeds the solubility of the drug. 2) Drug release occurs from inner part of the vehicle to the external aqueous environment through diffusion. 3) The diffusion coefficient for the drug is constant throughout whole release process. 4) The volume of the drug carrier remains unchanged. Under these conditions, the equation can be simplified as follows (equation 1-11)[115, 120]:

$$q_t = k_H t^{1/2} \tag{1-11}$$

where the meaning of q_t is the same as that in equation 1-10 and k_H ($mg/h^{1/2}$) is the Higuchi release constant, reflecting diffusion rate.

1.8.4 Ritger–Peppas and Korsmeyer–Peppas model (Power law)

The Power Law model is widely employed to describe drug release processes, particularly in cases where the release mechanism is complex or not fully understood. It is especially suitable for drug delivery systems that feature intricate structures, such as hydrogels,

microspheres, and nanoparticles. In this model, an exponential relationship between drug release and time is expressed as (equation 1-12):

$$\frac{q_t}{q_m} = kt^n \tag{1-12}$$

where q_t and q_m have the same meaning as described in equation 1-10. k is the model constant, and n is the release index, which is used to characterise the drug release mechanism.

For drug carriers in the form of thin films, the n-value in the Power Law model indicates the governing drug release mechanism[121]: When $n \leq 0.5$, the model is referred to as the Fickian model. In this case, the relaxation rate of polymer chains is significantly slower than the transport rate of the solvent, indicating that drug release is primarily diffusion-controlled. When $0.5 < n < 1$, the drug release follows a non-Fickian model. The diffusion of the solvent and the swelling or shrinking of the polymer occur at comparable rates, meaning that both mechanisms cooperatively control the drug release process. When n =1, the model is still non-Fickian but is referred to as Case I. This represents an extreme release behaviour and can also be considered a zero-order kinetic model. The mechanism driving drug release is dominated by the swelling or relaxation of polymeric chains. In the jellified region, superfast diffusion dominates, surpassing the relaxation at the gel-vitreous polymeric interface. But in the vitreous region, solvent penetration is minimal or absent, resulting in a nearly zero drug concentration. When n >1, it is referred to as Super Case II. During the sorption process, the diffusion of solvents occurs at an exceptionally fast rate, accelerating the movement of solvents into the vitreous region of the carrier. However, the expansion of the vitreous region

is constrained by the surrounding jellified region, resulting in compression tension within the polymer. This tension leads to stress and ultimately causes the polymer to undergo breaking.

Besides, the division of regions with distinct release mechanisms, as mentioned above, is influenced by the values of n, which vary depending on the shape of the drug carriers. These variations are illustrated in Figure 1-16[121]. As the shape of the matrices approaches a spherical form, the critical n-value for distinguishing different release mechanisms decreases.

Table 1-3 Interpretation of power low models from polymeric matrices with different geometries[121].

Release mechanism model	**Geometry**	**Release exponent (n)**	**Time in function of n**
Fickian diffusion	Planar (thin films)	0.50	$t^{0.50}$
	Cylinders	0.45	$t^{0.45}$
	Spheres	0.43	$t^{0.43}$
Anomalous transport	Planar (thin films)	$0.50 < n < 1.0$	$t^{0.50<n<1.0}$
	Cylinders	$0.45 < n < 0.89$	$t^{0.45<n<0.89}$
	Spheres	$0.43 < n < 0.85$	$t^{0.43<n<0.85}$
Case I transport	Planar (thin films)	1.0	t([a])
	Cylinders	0.89	$t^{0.89}$
	Spheres	0.85	$t^{0.85}$
Super Case II transport	Planar (thin films)	$n > 1$	$t^{n>1}$
	Cylinders	$n > 0.89$	$t^{n>0.89}$
	Spheres	$n > 0.85$	$t^{n>0.85}$

[a] Zero-order release.

Chapter 2 Characterisation and chemical inventory

2.1 Nuclear magnetic resonance (NMR) spectroscopy

^{1}H NMR spectra were tested by a Bruker AV3HD 400MHz NMR spectrometer equipped with a 5 mm BBO Probe. Chemical shifts (ppm) were calibrated using trimethylsilane (TMS), the chemical shift of which is 0 ppm. XR-55 NMR tubes (Norell) were used. NMR spectra were analysed using MestreNova x64. Abbreviations used in ^{1}H NMR analysis are: singlet (s), doublet (d), triplet (t), multiplet (m), doublet of doublets (dd). $CDCl_3$ and DMSO-d_6 were used as deuterated solvents.

2.2 Fourier-transform infrared (FTIR) spectroscopy

All samples were stored under vacuum oven at 55 °C for at least 1 day prior to FTIR analysis. All spectra were recorded via Perkin Elmer Spectrum One equipped with Bruker OPUS 7.0 software and a Specac Golden Gate Attenuated Total Reflection (ATR) diamond top plate. 100 scans were collected in the range of 4000-400 cm^{-1} at a resolution of 4 cm^{-1}.

2.3 Advanced polymer chromatography (APC)

Average polymer molecular weight was determined by APC, a form of size exclusion chromatography. Specifically, an ACQUITY APC system, equipped with an ACQUITY refractive index (ACQ-RI) detector was used. The column temperature was maintained at 40 °C and the flow rate at 0.5 mL/minute. System calibration was carried out using PEG standards and data processed using Empower 3 software. DMF containing 1 g/L LiBr was used as the mobile phase on an ACQUITY APC AQ column packed with bridged ethylene

hybrid (BEH) particles (200Å, 2.5 μm).

2.4 Thermal gravimetric analysis (TGA)

The polymers and polymer-Pb^{2+} complexes were analysed by TGA (TA Instruments TGA Q50 model) to determine the adsorbed Pb^{2+} content. The apparatus was continually flushed with nitrogen and temperature increased from RT to 700 °C at a rate of 10 °C/min.

2.5 Zeta (ζ) potential measurements

20 mg samples were totally dissolved in the 10 mL NaCl solution (concentration:10 mM) firstly. Then the pHs of the solutions were adjusted to the desired values with 0.05 M HCl or 0.05 M NaOH. ζ potential measurement was conducted using a Malvern Zetasizer Nano ZSP instrument (Malvern Panalytical Ltd, Malvern, UK). Every data point was collected from 5 measurements by the software.

2.6 Centrifugation, sample-drying and lyophilisation

Samples within appropriate centrifuge tubes were placed in a HERMLE Z 326K centrifuge and centrifuged at 0 °C and 4500 rpm for 5–15 minutes. After centrifugation, the samples were dried overnight in a Fistreem vacuum oven. Samples requiring lyophilisation were frozen using liquid nitrogen and then freeze-dried for a minimum of 2 days using a Thermo Scientific Heto PowerDry LLI500 freeze-dryer.

2.7 Matrix-assisted laser desorption/ionization (MALDI) mass spectrometry

MALDI mass spectrometry was conducted using an Axima Performance instrument (Shimadzu Biotech Inc, Japan). The matrix, 2,5-dihydroxybenzoic acid (DHB), was prepared by dissolving it in methanol. For sample preparation, 30 mg of PLys was dissolved in 300 µL of methanol. A mixture of DHB solution, sample solution, and DHB solution (1:1:1 by volume) was spotted sequentially onto a target sample plate and air-dried to form a matrix-polymer-matrix sandwich structure. Desorption and ionization of the samples were achieved using a 337 nm nitrogen laser. The accelerating voltage was set to 15.0 kV in linear mode, with 200 profiles collected and 5 laser shots per profile.

2.8 Liquid chromatography – mass spectrometry (LC-MS)

LC-MS analysis was conducted using a Thermo Scientific Ultimate 3000 HPLC system (Thermo Fisher Scientific, Waltham, MA, USA) coupled with a mass spectrometer equipped with an electrospray ionization (ESI) source operated in positive mode (Bruker amaZon Speed, Bruker Daltonik GmbH, Billerica, MA, USA). Chromatographic separations were performed on a Kinetex C18 column (2.1 × 50 mm, 2.6 µm particle size; Phenomenex, Torrance, CA, USA) at a column temperature of 40 °C. The mobile phases consisted of (A) 0.1% formic acid in water and (B) 0.1% formic acid in acetonitrile. A gradient elution was applied, starting with 98% A and 2% B over 1.2 minutes and ending with 2% A and 98% B, at a flow rate of 1.3 mL/min. The concentration of Lys(cbz)DKP in acetonitrile solutions for the LC-MS analysis was 1 mg/mL.

2.9 Preparation of phosphate buffered saline (PBS)

A PBS tablet was dissolved in 200 mL of deionised water under vigorous stirring to prepare a

PBS buffer solution with a pH of 7.4.

2.10 Rheology test of PLys-based hydrogels

The rheological properties of PLys-based hydrogels were assessed using an Anton Paar MCR 502 stress-controlled rheometer (Anton Paar GmbH, Austria). Hydrogel samples were first cut into discs with an 8 mm diameter, and the measurements were performed using a titanium parallel-plate setup. A strain sweep was initially conducted at an angular frequency of 6.28 rad/s for each hydrogel to establish suitable parameters for subsequent frequency sweep tests within the viscoelastic range. Frequency sweeps from 0.1 to 100 Hz were performed at room temperature with a strain of 0.5% to measure the storage modulus (G') and loss modulus (G'') of the hydrogels. The reported values represent the average of three independent rheological measurements for each hydrogel.

2.11 Scanning electron microscopy (SEM)

SEM analyses were conducted to observe internal structure of hydrogels. Small fragments of the freeze-dried hydrogels were affixed to SEM stubs using conductive tape. The morphological characteristics of the hydrogels were examined with a JEOL JSM-6610LV Scanning Electron Microscope, operated at adjustable accelerating voltages between 5 kV and 15 kV, with an average working distance of 11 mm.

2.12 Ultra violet – visible (UV-Vis) spectrophotometry

For the measurements of concentration of Reactive Black 5 (RB5) and Diclofenac (DIC), absorbances at 598 nm and at 276 nm were recorded separately using a dual-beam Varian

Cary 50 UV0902M112 UV-Vis spectrophotometer (Agilent Technologies), equipped with a xenon pulse lamp and Varian Cary WinUV 3.0 software. The liquid samples containing RB5 were loaded into 10 mL poly(methyl methacrylate) (PMMA) cuvettes, while the liquid samples with DIC were loaded into 10 mL quartz cuvettes. Each absorbance measurement was taken at least three times for accuracy.

The standard curve for RB5 was generated by linearly fitting the absorbance to RB5 solutions of varying concentrations (5 ppm, 10 ppm, 15 ppm, 20 ppm, 25 ppm and 30 ppm). The resulting equation was $y=0.0268x$ ($R^2=0.993$), where y represents the UV absorbance of the DIC solutions, and x is the concentration of the DIC solution (ppm).

The calibration curve for DIC was generated by linearly fitting the absorbance to DIC solutions of varying concentrations (1 ppm, 5 ppm, 10 ppm, 15 ppm, and 20 ppm). The resulting equation was $y=0.0345x+0.0369$ ($R^2=1$), where y represents the UV absorbance of the DIC solutions, and x is the concentration of the DIC solution (ppm).

2.13 Materials inventory

The chemicals used in the research featured in this chapter three to five are listed in Table 2-1.

Table 2-1 Inventory of chemicals used.

Chemical	Supplier
Fmoc-Lys-OH	Flurochem
H-Lys(cbz)-OH	Flurochem
Dimethyl sulfoxide (DMSO)	Fisher Chemical
Triphosgene 98%	Sigma-Aldrich
(-)-α-Pinene	Sigma-Aldrich
Poly(ethylene glycol) (PEG) amine (Mn=5000 g/mol)	Sigma-Aldrich
Acetone	Sigma-Aldrich
DMSO-d_6 (99.8 atom % D)	Eurisotop
$CDCl_3$	Sigma-Aldrich
Hexane 97%	Sigma-Aldrich
Methanesulfonic acid 98%	Alfa Aesar
Diethyl ether 99.5%	Fisher Chemical
TFA	Sigma-Aldrich
Methanol	Fluorochem
Hydrogen bromide, pure 33wt.% sol. in glacial acetic acid	AcroSeal
Acetonitrile	Sigma-Aldrich
Glycerol	Fisher Scientific
PBS tablets	Sigma-Aldrich
HCl (1 M)	Fluorochem

Continued Table 2-1. Inventory of chemicals used

Chemicals	Supplier
RB5	ChemCruz
DIC	ChemCruz
Lead (II) chloride	Fisher Chemical
Hexylamine 99%	ACROS
Diisopropylethylamine (DIPEA)	Fluorochem
Genipin	BioServ
Dimethylformadime (DMF) 99.5%	Fisher Chemical

Chapter 3 Thermal Deprotection: A Sustainable and Efficient Strategy for Synthesising α-Polylysine Adsorbents

3.1 Introduction

Poly(amino acids) are a class of bio-renewable and biodegradable polymers that derive their versatile functionalities from amino acid repeat units[122-124]. With 20 proteogenic amino acids available, these polymers can host diverse functional groups, such as amino, thiol, and carboxyl[125]. This inherent chemical diversity enables applications in drug delivery[126-128], tissue engineering[129-131], and biosensing[132-134]. Additionally, poly(amino acids) that possess alkene and alkyne functionalities have been produced and allow straightforward and effective polymer modification via click chemistry, further broadening their potential uses[135]. These properties, combined with their environmental compatibility, position poly(amino acids) as promising alternatives to non-biodegradable, petroleum-derived polymers, provided that sustainable methods of polymer synthesis are employed.

Among poly(amino acids), α-polylysine (PLys) has emerged as a particularly promising candidate due to its unique combination of water solubility, biodegradability, and rich primary amine functionality[2]. These attributes make PLys highly versatile, with applications ranging from antimicrobial coatings and protein release systems to heavy metal adsorption [136, 137]. PLys has also shown great promise in advanced biomedical applications. For instance, research by the Heise group demonstrated the creation of high molecular weight (MW = 765,000 Da) PLys star polymers, capable of encapsulating and delivering plasmid DNA for gene therapy[138]. Additionally, PLys-based materials have been effectively used to adsorb heavy metal ions such as CrO_4^{2-} and Cu^{2+} from aqueous solutions, a property attributed to the strong chelation interactions between the primary amine groups of PLys and the target metal ions[139].

Heavy metal contamination, particularly lead (Pb^{2+}), represents a pressing environmental

challenge. Lead, commonly found in industrial effluents such as those from lead-acid batteries, poses severe risks even at low concentrations[140, 141]. It has been linked to significant ecological damage and human health problems, including cognitive impairment, kidney damage, and increased cancer risks[142, 143]. Various methods for Pb^{2+} removal from wastewater have been developed, including chemical precipitation, ion exchange, flocculation, membrane filtration, electrochemical treatments, and bio-adsorption[144]. Among these, bio-adsorption stands out for its simplicity, cost-effectiveness, and ability to operate efficiently across a wide pH range[145, 146]. Polymers such as PLys, with abundant pendant primary amine groups, are particularly well-suited for this application due to their strong metal-binding capabilities.

Despite its potential for widespread application, the commercial viability of PLys is hindered by challenges associated with its synthesis. The conventional production method for PLys relies on NCA ROP, which proceeds in three main steps: (1) the synthesis of an NCA monomer from side-chain protected lysine, (2) polymerisation of the NCA monomer to yield side-chain protected PLys, and (3) deprotection of the side-chain groups to liberate the amino functionality[147]. While this method is more efficient than solid-phase synthesis and more controlled than polycondensation, it requires side-chain protection to prevent premature NCA ring-opening, and all methods require side-chain protection to prevent the formation of branched polymers.

The final PLys deprotection step is particularly problematic as it conventionally involves highly toxic reagents [148]. For instance, benzyloxycarbonyl (z) protecting groups are commonly used for Lys NCA synthesis, but PLys(z) deprotection requires hazardous reagents such as hydrogen bromide in strongly acidic solutions for cleavage, leading to safety risks [36]. Alternative protecting groups such as Boc and Fmoc may also be used, but they still require strong acidic or basic agents for their removal[36]. Even efforts to use less toxic reagents, such as piperazine with 2% 1,8-diazabicyclo[5.4.0]undec-7-ene (DBU) for Fmoc deprotection, face economic and environmental barriers that limit scalability[149]. The Boc group may also be

prematurely cleaved during conventional NCA synthesis by the HCl produced, causing premature polymerisation in the monomer synthesis step[150].

To address these limitations, we explored the use of thermal deprotection as a sustainable alternative. This approach eliminates the need for hazardous reagents, relying instead on heat to remove Fmoc groups from PLys in DMSO, which could be readily recovered by simple distillation. The method not only simplifies PLys synthesis but also aligns with the principles of green chemistry, reducing the environmental impact and improving the safety and scalability of the process. The use of piperidine is eliminated and DMF is replaced with DMSO which, whilst not a completely green solvent, has lower relative toxicity in comparison to DMF[150].

We report the synthesis and characterisation of both homopolymeric PLys and α-polylysine-*b*-poly(ethylene glycol) (PEG-*b*-PLys) block copolymers produced using thermal deprotection. The efficacy of these polymers for adsorbing Pb^{2+} ions from aqueous solutions was assessed to determine their potential as efficient and sustainable materials for wastewater treatment. By addressing the dual challenges of hazardous deprotection in PLys synthesis and the need for effective heavy metal remediation, this work underscores the feasibility of thermally driven PLys production as a safer, greener, and more cost-effective pathway for developing high-performance bio-based polymers.

3.2 Experimental

3.2.1 Preparation of Lys(Fmoc)-NCA

As a general procedure, 16 mmol of Fmoc-Lys-OH was added into a three-necked round bottom (RB) flask connected a condenser, nitrogen supply, and a dropping funnel. The flask with this amino acid was maintained under vacuum for an hour to eliminate water from the system, and then 70 mL of anhydrous tetrahydrofuran (THF) and alpha-pinene (32 mL, 32

mmol) were added to the RB flask under a steady flow of nitrogen. 10 g (33mmol) triphosgene dissolved in 20 mL anhydrous THF was added to the reaction mixture dropwise through the dropping funnel until the heated mixture began to reflux. The reaction was complete when the mixture became clear and transparent solution, which demonstrates the generation of Lys(Fmoc)-NCA that is soluble in THF. The whole reaction last 6 h. If reaction mixture remained cloudy, the clear liquid was collected by filtration. The clear solution created was rotary evaporated to ~20 mL before precipitation into hexane yielded the NCA (hexane: THF ratio = 8:1, v/v). This was stored in a freezer overnight to facilitate further NCA precipitation. The crude product was collected by vacuum filtration and washed with cold THF to remove the unreacted reagents. The final product was obtained under vacuum at room temperature (RT) after at least twice recrystallisation processes. ^{1}H NMR (400 MHz, DMSO-d_6): δ 9.10 (s, 1H), 7.94-7.31 (m, 8H), 7.31-7.26 (m, 1H), 4.47-4.39 (m, 1H), 4.334.26 (m, 2H), 4,25-4.18 (m, 1H), 3.03-2.94 (m, 2H), 1.78-1.59 (m, 2H), 1.49-1.10 (m, 4H); FTIR: Vmax/cm^{-1} (solid): 3341 (N-H), 3066 (C-H from phenyl), 1842 (C=O), 1780 (C=O), 1690 (C=O from acylamino), 757 and 735 (benzyl ring). Yield:63.8%

3.2.2 Preparation of PLys(Fmoc)

Lys(Fmoc)-NCA was added to an oven dried Schlenk tube that was purged with nitrogen for an hour. Anhydrous DMF was added and the solution underwent mixing prior to a solution of hexylamine dissolved in DMF being added by syringe. Anhydrous conditions were maintained during four days of polymerisation conducted at room temperature. Polymer recovery was achieved by adding the reaction solution dropwise to stirred, ice cold, diethyl ether, prompting polymer precipitation. The solid polymer was then isolated from the liquid by centrifugation. This process was repeated twice before the final polymer product was washed several times with diethyl ether and dried in the vacuum oven at 55 ℃ overnight. ^{1}H NMR (400 MHz, DMSO-d_6): 7.93-7.17 (m, 8H), 4.40-4.15 (m, 2H), 1.80-1.04 (m, 6H), 0.90-0.74 (t, 3H). Yield: 70.1%

3.2.3 Preparation of PEG-*b*-PLys(Fmoc)

Synthesis of the amphiphilic block copolymer PEG-*b*-PLys(Fmoc) was conducted in a comparable manner to the synthesis of PLys(Fmoc), but with the hexylamine initiator being replaced with a PEG5000 macroinitiator, where 5,000 denotes the polymer number average molecular weight. Lys(Fmoc)-NCA (300 mg, 0.79 mmol) was dissolved in DMF (3 mL) and added to an oven dried Schlenk tube. The macroinitiator, methoxyPEG-amine (65 mg, 0.013 mmol) was dissolved in 3 mL DMF with the aid of sonication (5 minutes) and added to Schlenk tube. Polymerisation was undertaken under nitrogen at room temperature for four days. Polymer recovery was achieved by adding the reaction solution dropwise to stirred, ice cold, diethyl ether, prompting polymer precipitation. The solid polymer was then isolated from the liquid by centrifugation. This process was repeated twice before the final polymer product was washed several times with diethyl ether and dried in the vacuum oven at 55 ℃ overnight. ^{1}H NMR (400 MHz, DMSO-d_6): 7.98-7.15(m, 8H), 4.38-4.03 (m, 2H), 3.56-3.42 (m, PEG), 3.24 (s, 3H, PEG),1.80-1.12 (m, 6H). Yield: 72.4%

3.2.4 Thermal deprotection of PEG-*b*-PLys(Fmoc) and PLys(Fmoc)

The Fmoc protected (block co-)polymer (200 mg) was dissolved in DMSO (6 mL), and the solution stirred at 120 °C. To monitor the deprotection kinetics, 1 mL aliquot was retrieved from the solution every 15 minutes by syringe, and the polymer recovered by precipitation into ice cold diethyl ether. Polymer isolation from solvent was done by centrifugation, with the retrieved solid washed several times with ice cold diethyl ether before being dried overnight in a vacuum oven at 55 °C. Larger samples used for Pb^{2+} adsorption were created over 1 h but without the intermittent sampling.

3.2.5 Water solubility of PEG-*b*-PLys and PLys with different deprotection degree

20 mg PEG-b-PLys and PLys samples with different deprotection degree (0 min, 30 min and 60 min thermal deprotection time) were mixed with 10 mL and 20 mL distilled water, respectively. The resulting solutions were visually inspected for differences in solubility and turbidity.

3.2.6 Pb^{2+} Adsorption by PEG-*b*-PLys and PLys

50 mg $PbCl_2$ was dissolved in DI water (10 mL). 20 mg of PEG-*b*-PLys or PLys was mixed with Pb^{2+} solutions at pH 3.5, 4 and 4.5. The polymer under investigation was added (20 mg) to the solution and the mixture was maintained for 1 day at room temperature. Following this, each sample underwent dialysis against deionised water for two days with frequent water changes to remove non-adsorbed Pb^{2+}. The remaining material was recovered by freeze drying.

3.3 Results and Discussion

The commonly used z protecting group can be used to produce both Lys(z) NCA and PLy(z) by NCA ROP effectively. However, the z group is thermally stable and thus unsuitable for deprotection in the absence of harsh, acidic, chemicals[151]. In contrast, the thermal deprotection of Fmoc groups in dimethyl sulfoxide (DMSO) at 120 °C has been reported to achieve over 96% cleavage from FmocProOH and FmocLys(Boc)OH [152], prompting the question: can this methodology be extended to macromolecular poly(amino acid) deprotection? If successful, this would eliminate the need for toxic reagents, significantly enhancing the environmental sustainability and cost-effectiveness of PLys production, enabling its enhanced application for instance as a scavenger for metal ions.

The synthetic pathway employed in this study consisted of three steps (Scheme. 3-1): (1) synthesis of Lys(Fmoc)-NCA, (2) polymerisation of Lys(Fmoc)-NCA to yield PLys(Fmoc),

and (3) thermal deprotection of PLys(Fmoc) to produce PLys. Additionally, a block copolymer, PEG-*b*-PLys, was targeted to determine the versatility of thermal deprotection for Fmoc cleavage from larger amphiphilic block copolymers. The inclusion of a PEG block was expected to improve polymer solubility or dispersion in aqueous environments, particularly when high levels of Lys-metal coordination occurred in the target application of Pb^{2+} adsorption.

3.3.1 Synthesis and Characterisation

Lys(Fmoc)-NCA was produced as an off-white powder[153]. ^{1}H NMR spectroscopy analysis confirmed successful synthesis[154]; the peak at 9.10 ppm corresponds to the NH group within the five-membered ring, peaks in the range of 7.94–7.31 ppm are associated with the aromatic protons of the Fmoc protecting groups, the CH_2 protons in the Fmoc structure are represented by a peak at 4.47–4.39 ppm, and the peak between 1.78–1.10 ppm is attributed to the protons of the CH_2 groups on the side chain. (Figure. S3-1). FTIR spectroscopy further confirmed successful NCA synthesis[155] (Figure. 3-1), with the spectrum featuring peaks at 1842 cm^{-1} and 1780 cm^{-1} that represent the C=O bonds of the NCA. The peaks at approximately 757 cm^{-1} and 735 cm^{-1} (bend vibrations of O-disubstituted benzyl ring), combined with the peak at 1690 cm^{-1} (C=O from acylamino), corresponded to the Fmoc protecting groups. While for PLys(Fmoc), an additional peak appears at ~1700 cm^{-1}, which is attributed to C=O stretching of carbonyl group bonded to NH group on hexyl amine side chain.

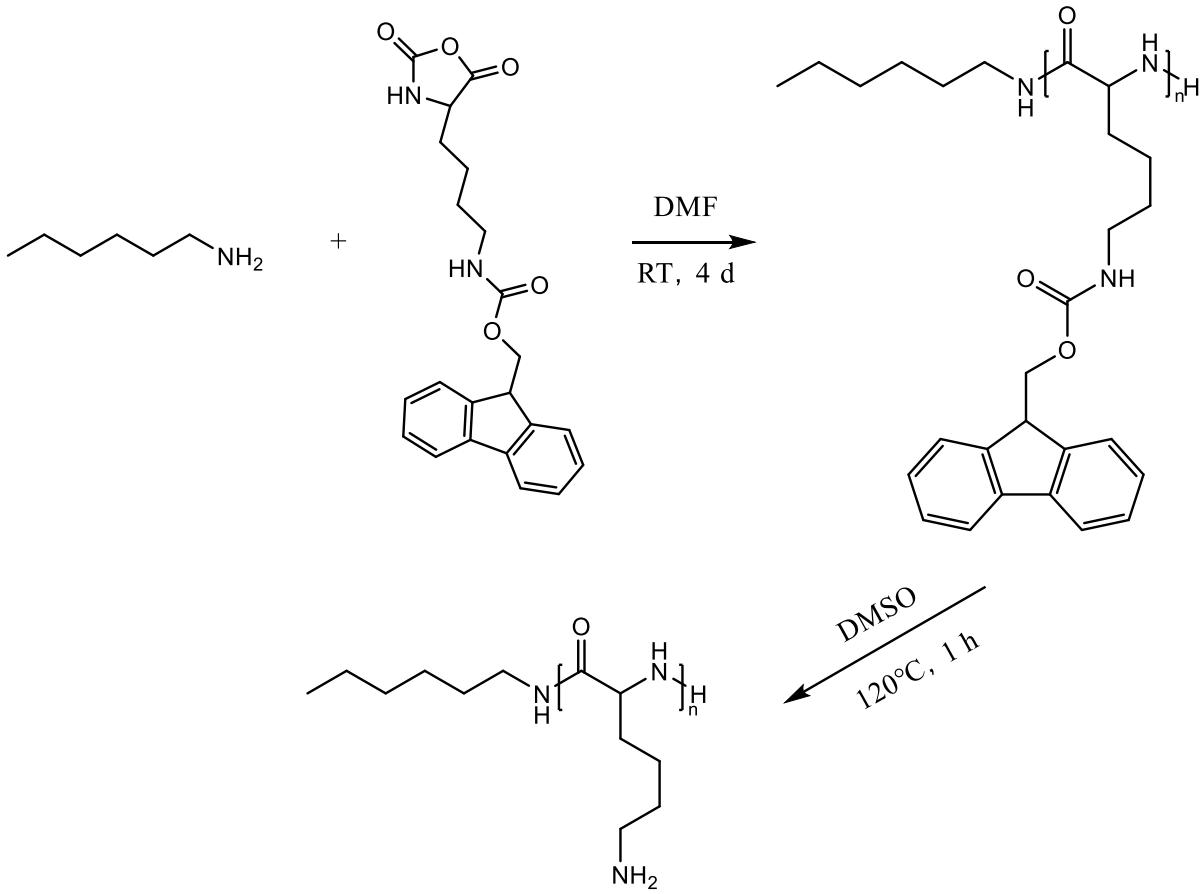

Scheme 3-1 The synthesis of PLys(Fmoc).

Hexylamine was chosen as the initiator for Lys(Fmoc) NCA polymerisation due to its easily identifiable alkyl chain which allows precise quantification of the degree of polymerisation by ^{1}H NMR spectroscopy (Scheme 3-1). The corresponding ^{1}H NMR spectrum revealed a peak at 0.87 ppm that represents the terminal methyl group of hexylamine[156] (Figure S3-2). The peaks between 7.00 – 8.00 ppm represent the aromatic protons of the Fmoc group. Comparison of the integrals representative of both groups provides a strong indication of the average degree of polymerisation as one group (hexylamine methyl protons) is provided by the initiator whilst the other group is provided by the polymer repeat unit (Fmoc aromatic protons). Complete NCA ring-opening was confirmed by the disappearance of anhydride stretches at 1842 cm^{-1} and 1780 cm^{-1} in the FTIR spectrum (Figure 3-1). Advanced Polymer Chromatography (APC) analysis of the PLys(Fmoc) produced indicated a number average molecular weight (M_n) of 16,000 Da and a polydispersity index (PDI) of 1.06, corresponding

to a monodisperse polymer of 47 repeat units on average. These results confirm that both Lys(Fmoc) NCA and PLys(Fmoc) syntheses are efficient and provide a viable route to PLys.

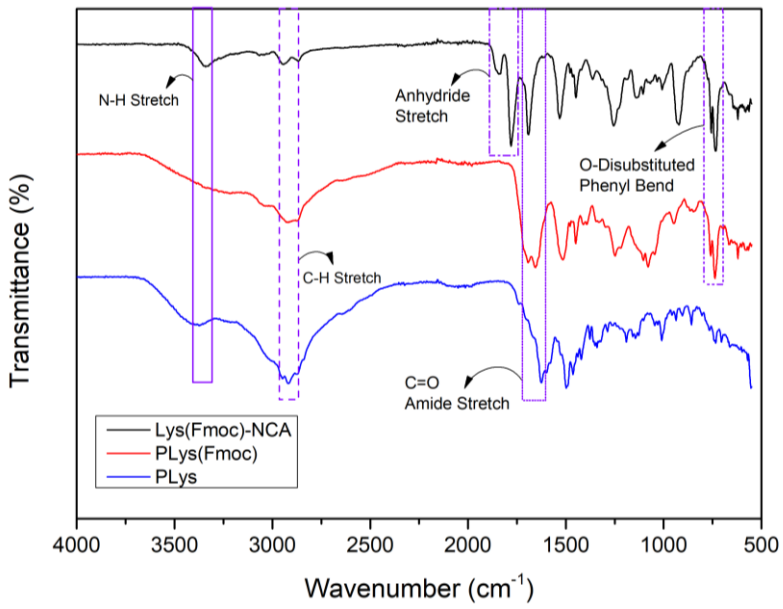

Figure 3-1 FTIR spectrum corresponding to Lys(Fmoc)-NCA, PLys(Fmoc), and PLys.

PLys is an excellent candidate to be used for heavy metal adsorption. However, metal binding to the primary amine sites of the polymer may reduce polymer solubility in aqueous solutions, potentially leading to aggregation and reduced activity. To ensure that PLys remains soluble, or at least dispersed, in aqueous solution, the diblock copolymer methoxyPEG -*b*-PLys (PEG-*b*-PLys) was created. The intended role of the PEG block is to ensure polymer solubility even at large levels of Lys-metal coordination as it is not anticipated to participate in metal binding. PEG-amine has proven to be a very effective initiator for the creation of amphiphilic PEG-*b*-poly(amino acid) block copolymers that are highly promising for controlled release applications, including their potential use as drug delivery vehicles[157]. Although PEG-*b*-PLys(Fmoc) is an amphiphilic block copolymer that may be suited for nanoparticle formation and controlled release applications, the focus of this research is on the creation of polymers for Pb^{2+} adsorption and so the doubly hydrophilic block copolymer PEG-*b*-PLys was created (Scheme 3-2)

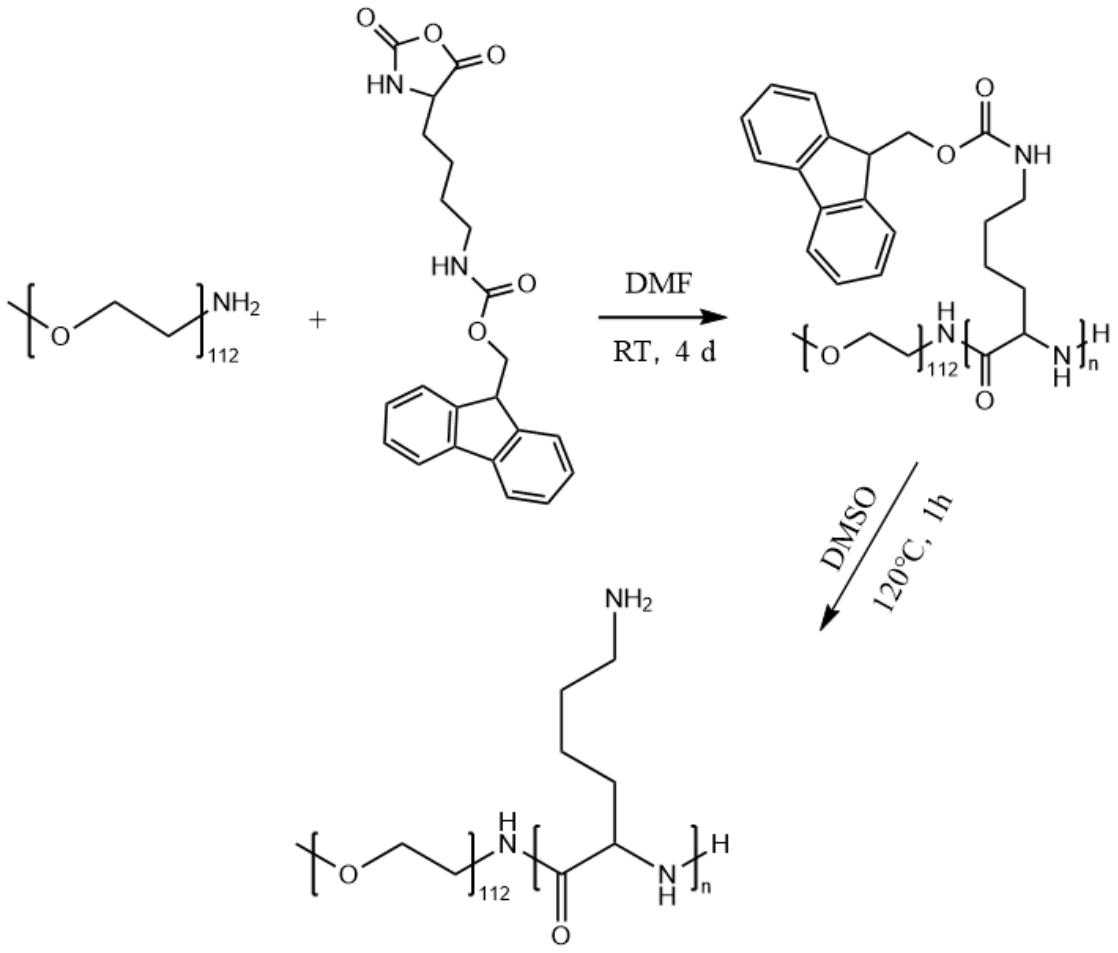

Scheme 3-2 The synthesis of PEG-b-PLys(Fmoc).

FTIR spectroscopy suggested successful block copolymer synthesis owing to the disappearance of the peaks at 1842 cm^{-1} and 1780 cm^{-1} of the NCA that disappear upon complete ring-opening (Figure 3-2). The characteristic band observed at ~1100 cm^{-1} corresponds to the C–O–C stretching vibration of PEG, confirming the presence of PEG segments in the copolymers. The benzyl section of the Fmoc group is represented by peaks at 757 $cm^{-1}$and 735 cm^{-1}.

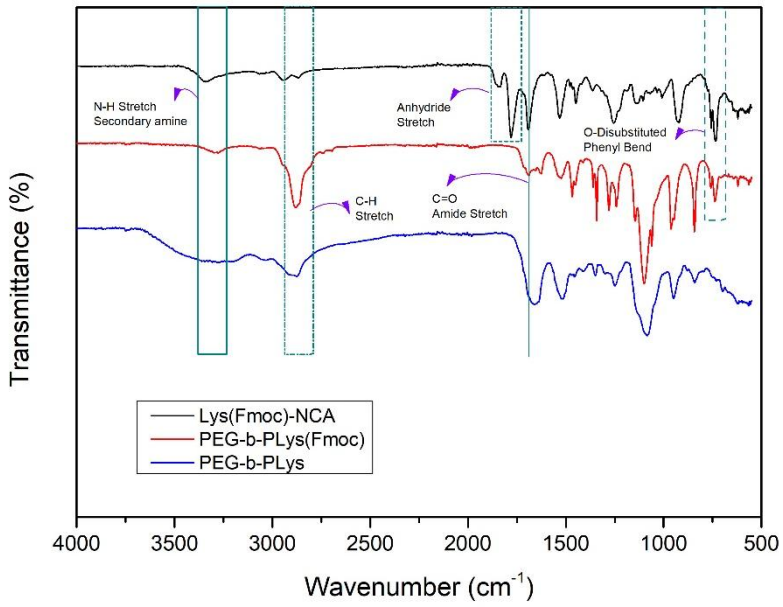

Figure 3-2 FTIR spectra corresponding to Lys(Fmoc)-NCA, PEG-b-PLys(Fmoc), and PEG-b-PLys

^{1}H NMR spectroscopy further confirmed polymer synthesis (Figure S3-4). The peaks representing the four protons of the ethylene glycol repeat units are represented at 3.55 – 3.45 ppm, and the terminal methyl protons of the PEG section are present at 3.24 ppm[158]. Additionally, peaks representative of the PLys(Fmoc) block can be seen; the peaks between 7.00 and 8.00 ppm are attributed to the aromatic protons of the Fmoc group. The protons of the alkyl chain of the lysine R group are shown between 1.00 and 2.00 ppm. NMR analysis was conducted after several washing steps with different organic solvents to ensure that the peaks present are representative of the desired block copolymer. Integration of the peak corresponding to the terminal methyl protons of PEG versus the peak corresponding to the Fmoc aromatic protons revealed that ~67 Lys(Fmoc) were conjugated to PEG, on average. APC analysis revealed that a block copolymer with a number average molecular weight (M_n) of 26,500 Da and a dispersity of 1.06 had been produced.

3.3.2 Thermal Cleavage of Fmoc to yield PLys

The focus of this research is to determine whether the thermally induced cleavage of Fmoc protecting groups can be applied to polymers that possess pendant Fmoc protecting groups. The thermal deprotection of small amino acids is reported to proceed via an $E1_{CB}$ mechanism[152, 159], with DMSO used as the solvent (Figure 3-3). It is envisaged that upon heating, the Fmoc groups will decompose to dibenzofulvene and carbon dioxide, leaving amine groups that may be utilised for metal scavenging. This concept has been proven for Fmoc cleavage from small molecules but not Fmoc cleavage from homopolymers, such as PLys(Fmoc)$_{47}$, and block copolymers, such as PEG$_{112}$-*b*-PLys(Fmoc)$_{67}$.

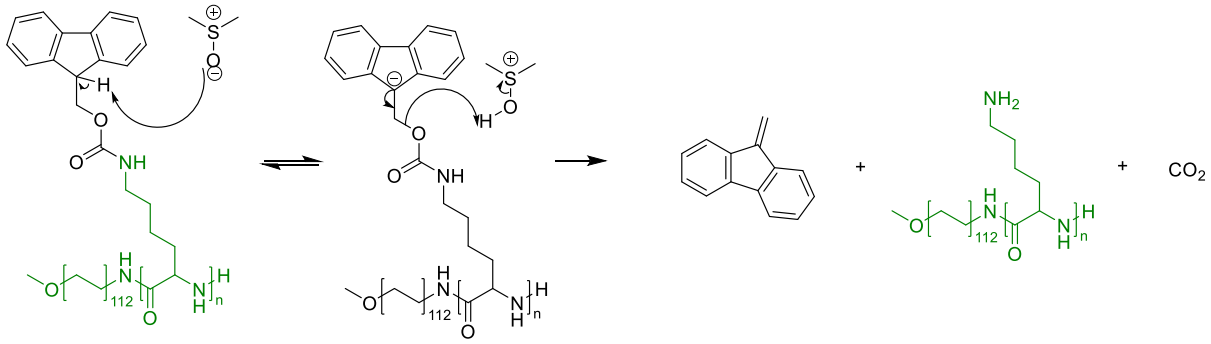

Figure 3-3 Fmoc cleavage from PEG-b-PLys(Fmoc) in DMSO at elevated temperatures.

Studies were conducted by independently heating DMSO solutions containing PEG-*b*-PLys(Fmoc) or PLys(Fmoc), and monitoring Fmoc cleavage as a function of time by ^{1}H NMR spectroscopy. Fmoc cleavage results in the decrease in the integrals of the protons corresponding to the Fmoc units (peaks b and c in Figure 3-4), relative to those of the PLys main chain (peak a in Figure 3-4). For PEG-*b*-PLys(Fmoc), differences in the ^{1}H NMR spectra at 0 minutes and 15 minutes were subtle, but the ratio of peak b: peak a slightly decreased from 0.41 to 0.37 and the ratio of peak c: peak a decreased from 1.63 to 1.54 (Figure 3-4). Values of 0 for peak b:peak a signify complete Fmoc deprotection. After 30 minutes, the peaks corresponding to Fmoc protons became significantly less sharp and a broad peak above 8 ppm gradually appeared, attributed to the protons of a newly formed primary amine group. There was a sharp decrease in the values for the peak b: peak a ratio

(0.10) and the peak c: peak a ratio (0.48), signifying extensive Fmoc removal in both cases. At 60 minutes, the Fmoc groups could not be detected, signifying their complete removal. The broad peak above 8 ppm is retained signifying primary amine liberation.

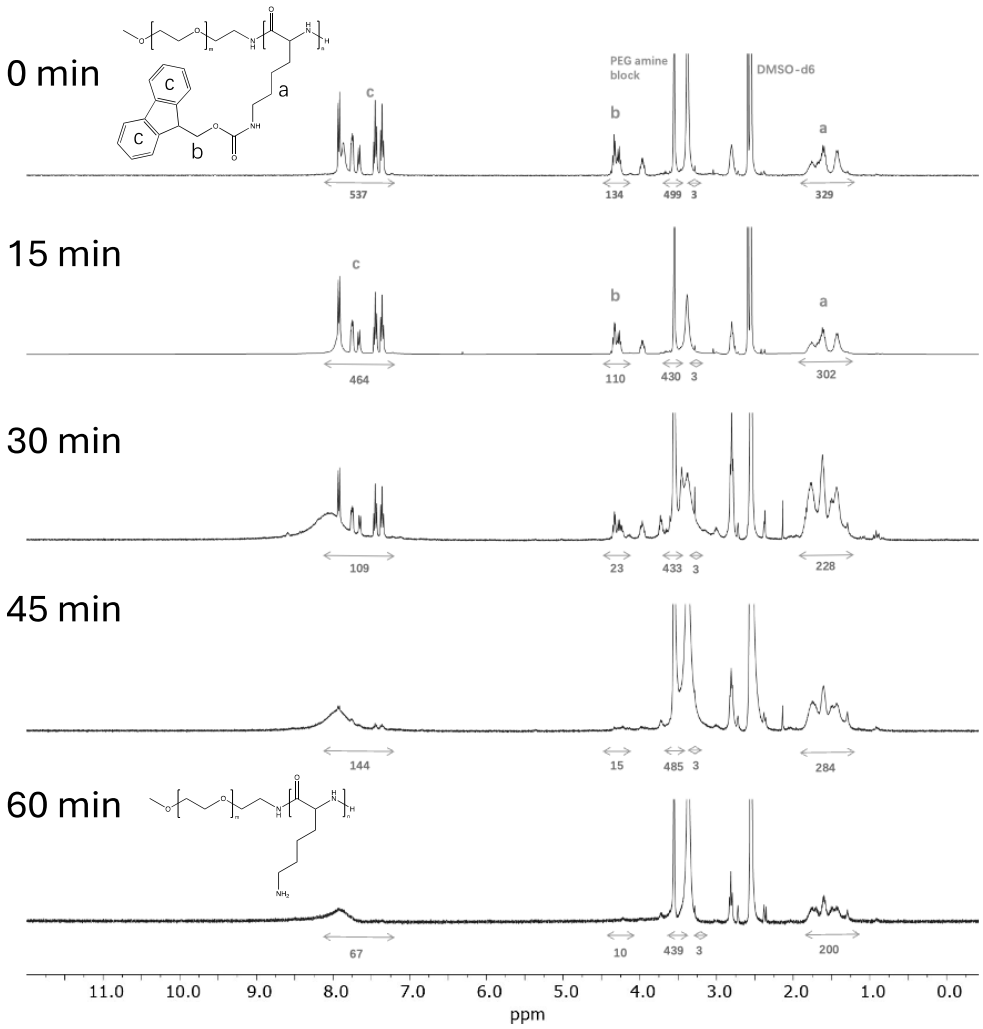

Figure 3-4 Thermal deprotection process of PEG-b-PLys(Fmoc). All spectra were recorded at 400 MHz using DMSO-d_6 as the solvent.

Fmoc cleavage from PLys(Fmoc) homopolymer was somewhat retarded compared to Fmoc cleavage from PEG-*b*-PLys(Fmoc), with significant Fmoc removal not observed until 30 minutes (Figure 3-4 and Figure 3-5). The hydrophilic PEG section may aid block copolymer dispersion, enabling increased access to Fmoc groups in comparison to the homopolymer where intermolecular interactions likely cause tight Fmoc group packing. After 30 minutes

the peaks corresponding to the Fmoc protons became less sharp and a broad peak signifying the presence of a primary amine formed. The peak b: peak a ratio significantly decreased from 0.40 to 0.10 and the peak c: peak a ratio reduced by 50%, signifying the loss of Fmoc groups (Table 3-1). After 60 minutes almost complete Fmoc deprotection was achieved, based on the near complete loss of peaks corresponding to Fmoc protons in the ^{1}H NMR spectrum.

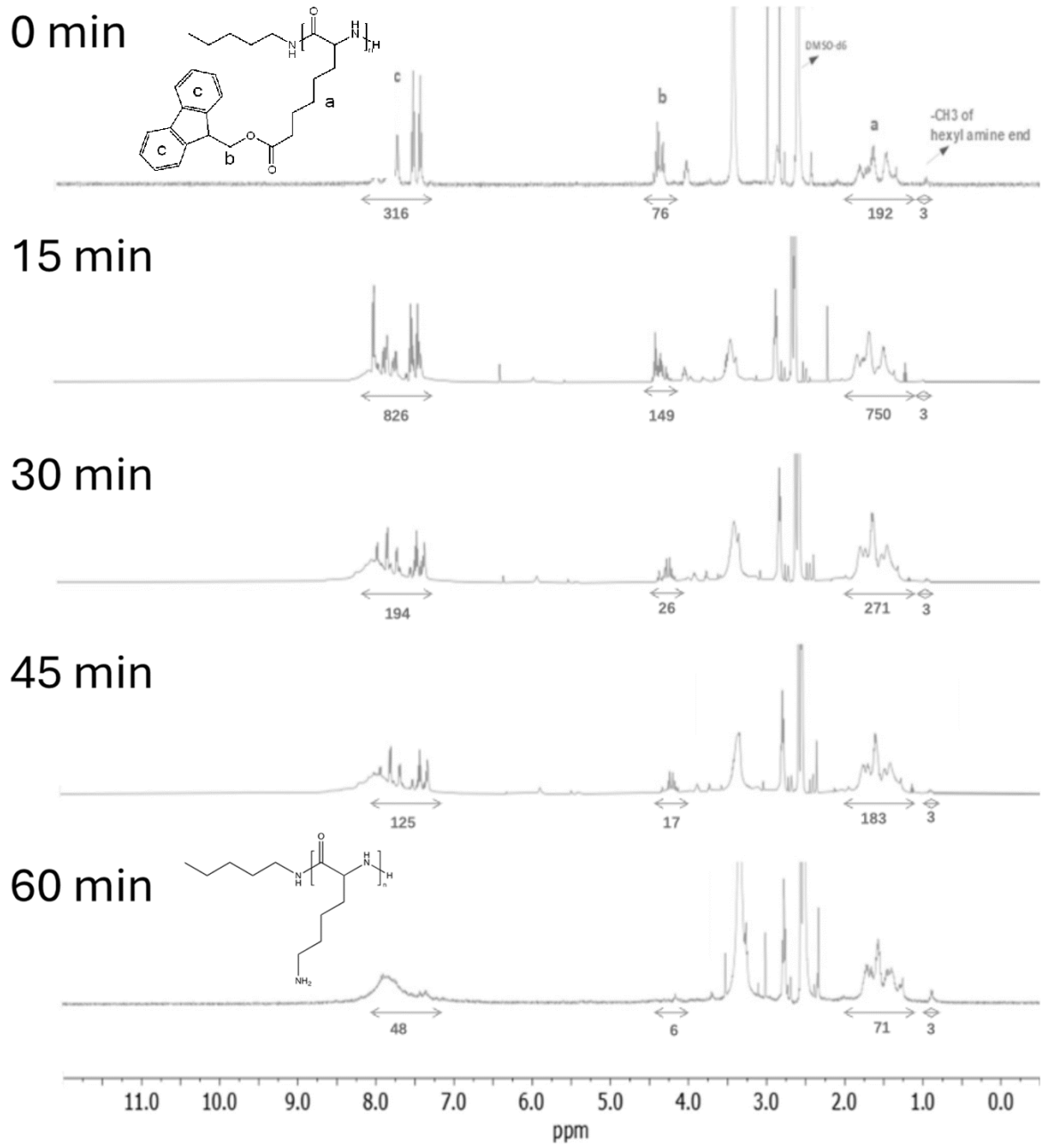

Figure 3-5 Thermal deprotection of PLys(Fmoc). All spectra were recorded at 400 MHz using DMSO-d_6 as the solvent.

APC revealed that the number average molecular weight value (M_n) for PEG-*b*-PLys(Fmoc) was 24,800 Da, signifying that ~ 57 Lys(Fmoc) units were attached to the PEG block (Table 3-1). This value was slightly less than the results provided by ^{1}H NMR spectroscopy (~67 units), although this is not unexpected as the APC value is obtained against PEG homopolymer standards. PLys(Fmoc) exhibited ~ 43 repeat units which aligned closely to the value provided by ^{1}H NMR spectroscopy (~ 40 repeat units). Following thermal deprotection, ~ 52 (PEG-*b*-PLys) and ~43 repeat units (PLys) were found on average for each polymer by APC, confirming that polymer backbone hydrolysis had not occurred. The dispersity values of the polymers produced are close to 1 in most cases, signifying narrow molecular weight distributions.

Table 3-1 Molecular weight of protected and deprotected versions of PEG-b-PLys(Fmoc) and PLys. Mw signifies the weight average molecular weight, Mn signifies the number average molecular weight.

Sample	M_W (Da)	M_n (Da)	Dispersity
PLys(Fmoc)	16,000	15,000	1.06
PLys	6,700	6,000	1.12
PEG-*b*-PLys(Fmoc)	26,500	24,800	1.06
PEG-*b*-PLys	12,000	11,400	1.05

3.3.3 Water solubility of PEG-*b*-PLys and PLys samples with different deprotection degree

The water-solubility of PEG-*b*-PLys and PLys at different stages of thermal deprotection was visually assessed. The water-solubility of PEG-*b*-PLys samples with different deprotection degree is shown in Figure 3-6, revealing that clear and transparent liquids resulted due to seemingly complete block copolymer dissolution. Although Fmoc groups are hydrophobic, PEG amine block worked as hydrophilic layer and assisted PEG-*b*-PLys(Fmoc) to be

dispersed in water, resulting in a visually transparent solution. With deprotection degree increased, the yellow colour of the polymer solutions deepened.

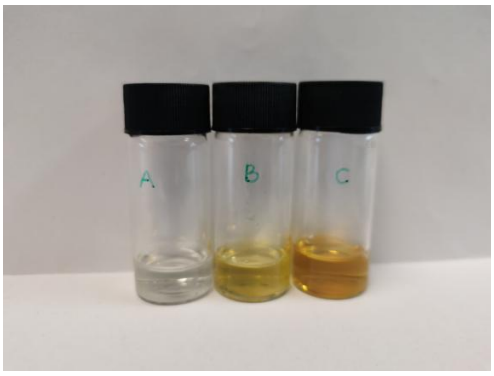

Figure 3-6 Water-solubility of PEG-*b*-PLys samples with different deprotection degree: left-PEG-*b*-PLys(Fmoc), middle-PEG-*b*-PLys after 30 min thermal deprotection, and right- PEG-b-PLys after 60 min thermal deprotection.

As shown in Figure 3-7, PLys(Fmoc) could not be fully dissolved in water and appeared as white turbid dispersion. Upon Fmoc removal the polymer became increasingly water-soluble, with fully deprotected PLys forming a transparent yellow solution in water (60 min).

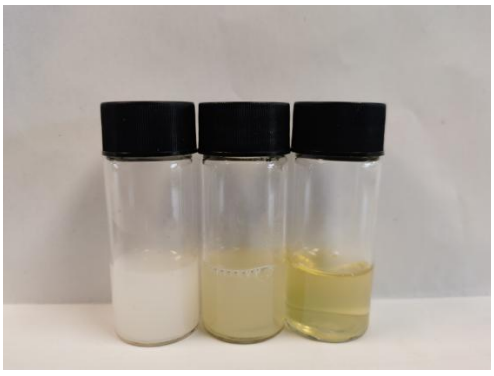

Figure 3-7 Water-solubility of PLys samples with different deprotection degree: left-PLys(Fmoc), middle-PLys after 30 min thermal deprotection, and right-PLys after 60 min thermal deprotection.

3.3.4 Pb^{2+} Removal from Aqueous Solution

Biodegradable and bioderived polymers that are water-soluble have numerous potential applications, including drug delivery systems[160, 161], wound dressing[162], sustainable packaging[163], wastewater treatment[164]. A further key application of such polymers is their use in wastewater purification, particularly for the removal of cytotoxic metals from aqueous environments. Acidic Pb^{2+}-containing wastewater is of great concern owing to its toxicity and the difficulty in its treatment. The removal of Pb^{2+} from the water system is of paramount importance owing to the damage that Pb^{2+} can impart to the heart, kidneys, and reproductive and nervous systems of humans, and in particular children[165]. Polymers that boast pendant primary amine functionality are reported to be effective for Pb^{2+} adsorption owing to chelation between the electron lone pairs of the primary amine nitrogen atom and the metal cation[166]. Although at neutral pH, many primary amine groups become protonated and unable to donate electron lone pairs, it may be hypothesised that the high density of amine groups in PLys ensures that some amine groups remain uncharged and/or favour metal binding over protonation. Consequently, the Pb^{2+} adsorption capabilities of PEG-*b*-PLys and PLys from aqueous solution was assessed.

The effectiveness of the polymers produced to interact with and bind Pb^{2+} was assessed using TGA to quantify Pb^{2+} uptake by the polymers. All TGA experiments were performed in triplicate, and the data shown in Figure 3-8 represent the average values. Following polymer-metal incubation and Pb^{2+} recovery, any remaining matter after heating to 700 °C was assumed to be non-organic and thus correspond to Pb^{2+}. The amount of Pb^{2+} recovered per 1g of PEG-*b*-PLys was found to be 2±0.7 mg (pH=3.5), 71±6 mg (pH=4) and 408±17 mg (pH=4.5) (Figure 3-8). Although the extent of Pb^{2+} uptake from pH 4.5 solution highlighted the potential of the materials for the intended application, the difference in Pb^{2+} uptake as the solution pH changes from pH 3.5 to pH 4.5 was somewhat surprising.

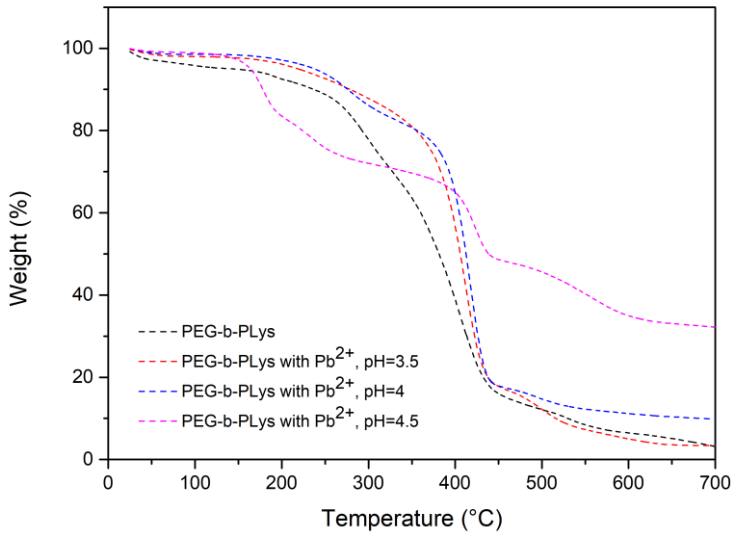

Figure 3-8 Adsorption of Pb^{2+} by PEG-b-PLys from solutions of various pH.

Zeta (ζ) potential measurements were therefore conducted to determine changes in polymer particle stability caused by the amplification or suppression of charge caused by primary amine (de)protonation (Figure 3-9). All ζ potential values of PEG-*b*-PLys are positive in acidic and neutral solutions, but decrease as the solution pH increases. Importantly, the ζ potential value changes from 19.0 mV to 15.9 mV as solution pH changes from pH 3.5 to pH 4, and a relatively modest value of 8.8 mV is recorded in solution of pH 4.5. A large ζ potential value, positive or negative, denotes particle stability which would arise due to electrostatic repulsion between polymer particles in this instance. As the pH increases, cationic charge is supressed rendering polymer aggregation more likely. This suppression of charge due to pendant primary amine deprotonation may feasibly promote Lys-Pb^{2+} chelation rather than Lys-Pb^{2+} repulsion, hence greater Pb^{2+} uptake being recorded in pH 4.5 solution compared to both pH 3.5 and pH 4 solutions[167].

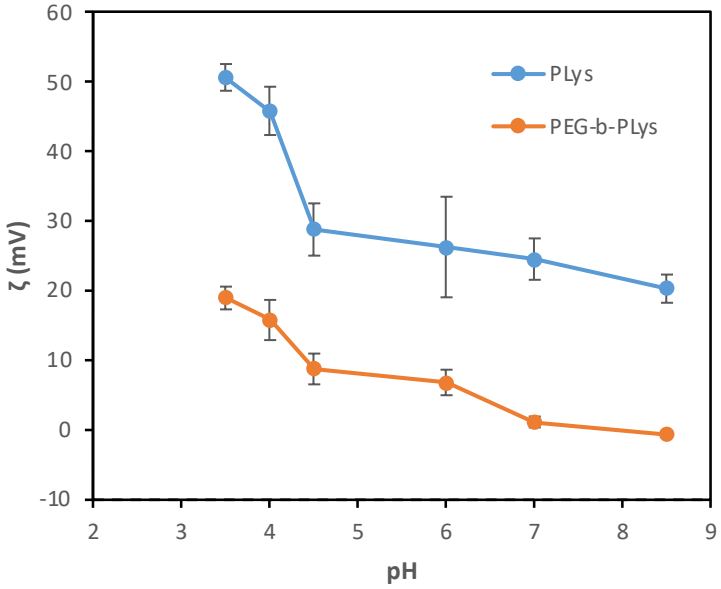

Figure 3-9 ζ potential values for PEG-b-PLys and PLys in various pH solutions

PEG was included in PEG-*b*-PLys formulations as hydrophilic PEG should facilitate metal-polymer dispersion in aqueous solution after the binding event. A water-soluble polymer is converted to a dispersed polymer that can easily be recovered by filtration following metal scavenging. However, the PEG block may be redundant as PLys is water-soluble itself. 1 g of PLys was able to adsorb 538±28 mg of Pb^{2+} at pH 4.5 according to TGA analysis (Figure 3-10). As the extent of adsorption exceeded that of PEG-*b*-PLys (408±17 mg of Pb^{2+} per 1 g of PEG-*b*-PLys), the use of PEG was deemed unnecessary. Enhanced adsorption by PLys compared to PEG-*b*-PLys is not unexpected given the increased primary amine loading of the homopolymer relative to the polymer molecular weight, with this study emphasising the significance of PLys as a very useful material in its own right.

Unlike PEG-*b*-PLys, PLys exhibits a positive ζ potential values at pH levels as high as 8.5 (Figure 3-9). It may be hypothesised that absence of the PEG segment leads to elevated ζ potential values in PLys since the introduction of the PEG block may serve to shield the positive charge originating from amine groups[168, 169]. A significant reduction in ζ

potential values of PLys is observed when pH ranges from 3.5 to 4.5. The value drops to 20.4 mV at pH 4.5, matching the vastly increased amount of adsorbed Pb^{2+} by PLys in aqueous solution of this pH.

A paired t-test comparing PLys and PEG-*b*-PLys across the different pH values showed a t-statistic of 11.01 and a p-value of 0.00011. This very low p-value indicates a highly statistically significant difference between the two groups, with consistently higher Pb^{2+} uptake observed for PLys compared to PEG-*b*-PLys.

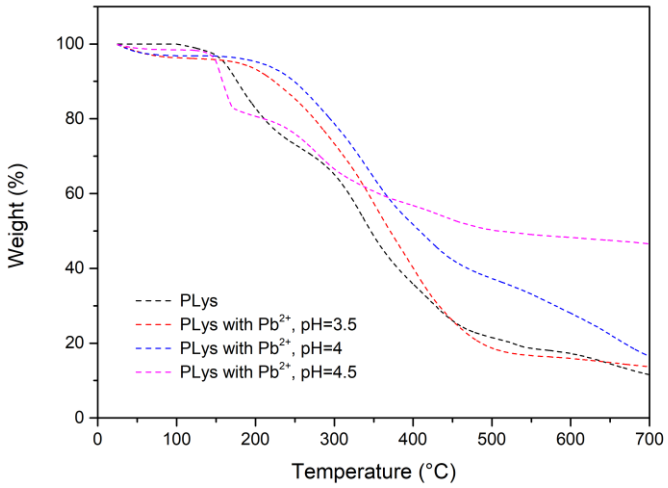

Figure 3-10 TGA data to represent the adsorption of Pb^{2+} by PLys from solutions of various pH.

The maximum Pb^{2+} loading capacities of were compared with those from previous studies by poly(amino acids)-based adsorbents (Table 3-2). However, the preparation of PEG-*b*-PLys and PLys in our studies was done using thermal deprotection as opposed to acid or base deprotection. Besides, PLys can capture more Pb^{2+} from acetic aqueous environment than previous poly(amino acids)-based adsorbents. Therefore, it has the potential to control the accidental Pb^{2+} pollution.

Table 3-2 A comparison of various adsorbents for the removal of Pb^{2+} from the aqueous solution.

No.	Adsorbents	pH	Maximum adsorption capacity (mg/g)	Reference
1	γ-polyglutamic acid grafted lignin	5.5	276	[170]
2	ε-poly-L-lysine grafted lignin	5.5	232	[170]
3	poly-L-glutamic acids/polyethylene-silica complex membranes	5.5	298	[171]
4	poly-L-aspartic acids/polyethylene-silica complex membranes	5.5	121	[171]
5	PEG-*b*-PLys	4.5	408 ± 17	This study
6	PLys	4.5	538 ± 28	This study

3.4 Conclusions

This study presents a groundbreaking approach to the synthesis of linear homopolymer PLys and linear block copolymer PEG-b-PLys via NCA ROP, eliminating the need for toxic deprotection agents for the first time. These water-soluble polymers combine bio-renewability, biodegradability, extensive chemical functionality, and cationic charge, positioning them as valuable candidates for a wide range of industrial and environmental applications. The development of a safe, cost-effective, and efficient thermal deprotection method, achieved within just 1 hour by heating to 120 °C in recyclable DMSO, marks a significant advancement in sustainable polymer production. The demonstrated ability of PLys and PEG-b-PLys to adsorb Pb^{2+} from aqueous solutions at capacities of 538±28 mg/g and 408±17 mg/g, respectively, highlights their potential for addressing urgent environmental challenges, such as heavy metal pollution. Future research should expand the application scope of α-polylysine and PEG-*b*-PLys beyond Pb^{2+} ions to other significant heavy metals

such as cadmium, mercury, and chromium, to fully exploit their potential in diverse environmental remediation scenarios. Additionally, studying these polymers under representative environmental conditions represents an imminent research goal. However, this study not only reduces the environmental footprint and cost of PLys production but also opens new avenues for their widespread application in water purification, biotechnology, and beyond. By enhancing the safety, scalability, and sustainability of PLys production, this work paves the way for the next generation of functional polymers to make a tangible impact in addressing global sustainability challenges.

Chapter 4 Polylysine(PLys)-based Hydrogels for Adsorption of Reactive Black 5 (RB5)

4.1 Introduction

Azo dyes, xenobiotic compounds containing one or more azo bonds (–N=N–) and aromatic rings, are extensively used in the textile industry for dyeing processes[172, 173]. Annually, over 5000 tons of azo dyes are consumed by global textile industries[174, 175]. The washing of tinted or printed textiles generates significant liquid waste containing dyes, posing serious threats to aquatic ecosystems and human health[176, 177]. Therefore, the removal of azo dyes from aquatic environments is essential. Reactive Black 5 (RB5), one of the most commonly used azo dyes, is widely employed in textile dyeing[173, 178], printing processes[179, 180], and as an industrial colouring agent[181, 182]. The widespread use of RB5 can be attributed to its relatively low cost, low energy requirements, vibrant colour, and high stability[183, 184]. However, due to the inefficiency of textile dyeing processes, more than 15% of RB5 remains unbound to fibres and fabrics and is released into wastewater[185]. Even a tiny amount of RB5 can significantly alter the colour of a water body[186], and prolonged exposure to RB5 may lead to allergic reactions and kidney damage[187]. Consequently, RB5 was selected as a representative dye pollutant for removal investigation in this study.

Several methods are available for removing RB5 from sewage effluents, including strong oxidants[178, 188], photocatalysis[189, 190], electrochemistry[191], biodegradation[192-194], and adsorption [194-196]techniques. In the strong oxidant method, the Fenton reagent effectively degraded RB5 by generating hydroxyl radicals[188]. A higher H_2O_2/Fe^{2+} ratio promoted the production of more hydroxyl radicals, enhancing RB5 removal efficiency. Similarly, ozonation can completely degrade RB5 dye solutions within 10 minutes, enabling the treated water to be reused for cotton dyeing with reactive dyes[178]. Although the strong oxidant method is highly efficient, potential toxicity of byproducts and high operating cost limit the development of this method. Photocatalysis and electrochemistry methods also face

challenges related to high costs, hindering their widespread adoption. In the photocatalysis method, photogenerated valence holes are created when the surface catalyst particles are irradiated with UV light. These holes oxidize OH^- or H_2O, generating hydroxyl radicals that can effectively degrade many organic compounds, including RB5[197]. Both TiO_2 and ZnO photocatalysts demonstrated excellent performance in RB5 degradation. For instance, a TiO_2/UV system can completely decolorize 3 L of RB5 solution with a concentration of 20 ppm within 100 minutes[189]. In comparison, a ZnO/UV slurry reactor achieved nearly 100% RB5 removal within 60 minutes when treating 1 L of RB5 solution with a concentration of 75 ppm[190]. Furthermore, the ZnO/UV system showed potential for reuse, enhancing its applicability for wastewater treatment. Electro-oxidation is a promising method for the removal of wastewater with high anionic content[198]. In this method, anodic polarisation of boron-doped diamond (BDD) films generated hydroxyl radicals by oxidising water molecules near the electrode surface and can remove and mineralize 91% of RB5 within 240 minutes at a current density of 100 mA/cm regardless of the initial RB5 concentration[191]. While electro-oxidation is efficient and fast, its application is limited by the high cost of electrodes and significant energy consumption. Different from advanced oxidation processes mentioned above, biodegradation of RB5 using microorganism has gained popularity due to its low cost. The bacterium *Bacillus albus* DD1 exhibited a 95% decolourisation efficiency under the following conditions: an initial dye concentration of 200 ppm, bacterial inoculum at 20% (v/v), and a treatment duration of 5 days at 37 °C[192]. A novel halotolerant yeast has been cultivated from 18 xylose-fermenting yeast species, demonstrating a 92% RB5 removal rate from a solution containing 50 ppm RB5 and 50 g/L NaCl after 24 hours of treatment[193]. This method is green and sustainable; however, its drawbacks include a slow degradation rate and the potential formation of carcinogenic aromatic amine byproducts[199]. Physical adsorption method gathered huge attention in recent years because of its cost-effectiveness and ease of implementation[187]. Biomass, and biomass derivatives have been utilised to adsorb RB5 due to their affinity for dye molecules. For example, Brazilian pine-fruit shells have demonstrated maximum RB5 adsorption capacities of 74.6 mg/g after a 16-hour period, whereas the activated carbon derived from these shells achieved a significantly higher capacity of 446.2 mg/g in just

4 hours[194]. This substantial enhancement is primarily due to the activated carbon's well-developed porous structure and extensive internal surface area, which markedly improves its adsorption capacity and efficiency[200]. 1 g of chitin can only adsorb up to 92 mg of RB5 within 600 minutes at room temperature, primarily due to the non-ionic interaction between hydroxyl groups on chitin and the anionic RB5 molecules[195]. In comparison, chitosan granules crosslinked with Glu exhibit a significantly higher maximum adsorption capacity, reaching 224 mg/g after a treatment process of 1080 minutes[196]. The primary limitation of physical adsorption lies in the need to replace or regenerate the adsorbent, which may lead to secondary pollution. However, with proper control and optimisation, this drawback can be transformed into an advantage. Unlike other methods, physical adsorption preserves the structure of RB5 during the removal process, whereas other techniques degrade, decolourise, or destroy the dye molecule. This characteristic of adsorption offers the opportunity to recover both the adsorbents and RB5 molecules, enhancing sustainability.

Hydrogels formed from amine-rich compounds, such as chitosan-based hydrogels, are ideal materials for anion dye adsorption due to their porous structure and high amine group content, because electrostatic attraction between protonated amine groups and negatively charged dye molecules favours adsorption process[201]. Chitosan-based hydrogels, in particular, have been extensively studied for their effectiveness in dye adsorption applications[202-204]. In addition to chitosan-based hydrogels, PLys-based hydrogels also have great potential as dye adsorbents. Chitosan, with a 100% degree of deacetylation, is a linear homopolymer composed of D-glucosamine[205]. PLys is a linear peptide composed of lysine residues, which provides a higher charge density than chitosan and thus may enhance dye adsorption capacity[81, 206]. However, due to the high cost of PLys preparation, PLys-based hydrogels are typically reserved for advanced biomedical applications, such as drug delivery vehicles[207], gene delivery systems[50], tissue adhesives[208], and wound healing materials[209]. For dye adsorption, PLys is often utilised as an auxiliary material or as a modifying agent for other raw materials[83, 210]. Zhang *et al*. reported a magnetic adsorbent prepared by modifying PLys onto Fe_3O_4 nanoparticles, achieving an adsorption capacity of 318 mg/g for methyl blue within 60 min[83].

Jiang and Zhou modified PLys on oxidised viscose fibres, resulting in a material capable of adsorbing 43 mg of methyl blue per gram while also exhibiting strong antibacterial activity against *E. coli*[210].

Given this background, it is essential to investigate the performance of PLys-based adsorbents where PLys serves as the primary component. In this study, PLys will be made to form a hydrogel to not only enhance adsorption capacity but also facilitate RB5 dye retrieval from aqueous environments. Two common crosslinkers, glutaraldehyde and genipin, were employed in hydrogel preparation, and RB5 was selected as the model dye due to ease of detection via UV spectroscopy at 598 nm. The effects of pH, contact time, and initial dye concentration on the adsorption process will be systematically examined.

4.2 Experimental

4.2.1 Preapration of Lys(cbz)-NCA

16 mmol of H-Lys(cbz)-OH was placed in a three-necked round-bottom flask fitted with a condenser, nitrogen supply, and a dropping funnel. The flask was kept under vacuum for one hour to remove moisture from the system. Next, 70 mL of anhydrous THF and 32 mL (32 mmol) of α-pinene were added to the flask under a continuous nitrogen flow to scavenge the HCl generated during the reaction. A solution of 10 g (33 mmol) of triphosgene in 20 mL anhydrous THF was then added dropwise via the dropping funnel until the heated mixture began to reflux. The reaction was deemed complete when the mixture became clear, indicating the formation of NCAs, which are soluble in THF. The reaction time last 3 hours. If the reaction mixture remained cloudy, the clear liquid containing Lys(cbz)-NCA was separated by filtration. The clear solution was concentrated to ~20 mL via rotary evaporation before being precipitated into hexane (hexane: THF ratio = 8:1, v/v) to obtain the NCA. The product was stored in a freezer overnight to enhance further NCA precipitation. The crude product was collected by vacuum

filtration, washed with cold THF to remove unreacted reagents, and then subjected to at least two rounds of recrystallization under vacuum at room temperature (RT) to yield the final product. ^{1}H NMR (500 MHz, DMSO-d_6, ppm): δ 7.40-7.23 (m, 5H, aromatic), 5.07-4.96 (s, 2H, OCH_2), ,4,46-4.38 (t, 1H, COCH), 3.03-2.93 (dd, 2H, NCH_2), 1.83-1.20 (m, 6H, $CH_2CH_2CH_2$). Yield: 82.6%.

4.2.2 Preparation of PLys

PLys was synthesized via two distinct routes. One approach followed the method outlined in Section 3.3.1 and 3.3.2: briefly, Lyz(Fmoc) was first opened using the initiator hexylamine (HA) to produce PLys(Fmoc). The intermediate product was subsequently heated in DMSO at 120 ℃ to remove the Fmoc protecting groups before PLys were obtained. This batch of PLys were named as PLys 1.

The other method consists of two main steps: (1) adding initiator hexylamine (HA) to react with Lys(cbz)-NCA prepared in 4.2.1 to synthesize PLys(cbz), and (2) fully dissolving PLys(cbz) in Trifluoroacetic acid (TFA), followed by adding 33% HBr/AcOH solutions to the mixture to remove the cbz protecting group.

To specific, Lys(cbz)-NCA were added to an oven-dried Schlenk tube which was purged with nitrogen to remove water from the system. Then, 5 mL of anhydrous dimethylformamide (DMF) and HA (HA/Lys(cbz)-NCA molar ratio = 1:80) were added into reaction system as solvent and initiator, respectively. The reaction was conducted at RT for at least 4 days, with anhydrous conditions maintained through a continuous flow of N_2. After synthesis, the solution was added dropwise to ice-cooled diethyl ether and the precipitated product collected by centrifugation. The homopolymer PLy(cbz) produced was washed several times with diethyl ether and then dried in the vacuum oven at 55 °C overnight. ^{1}H NMR (500 MHz, DMSO-d_6, ppm): δ 7.98-7.69 (s, 1H, NH), 7.42-7.05 (m, 5H, aromatic), 5.06-4.87 (s, 2H, OCH_2), 4.28-4.07 (br, 1H, COCH), 3.00-2.89 (dd, 2H, NCH_2), 1.80-1.05 (m, 6H, $CH_2CH_2CH_2$), 0.87-0.76 (t, 3H, CH_3).

Yield: 82.4%.

0.3 g of PLys(cbz) was dissolved in 8 mL of TFA, followed by the addition of 2 mL of a 33% HBr/AcOH solution to deprotect the carboxybenzyl groups. The reaction proceeded for 1 day. The crude product was then precipitated in ice-cooled diethyl ether, collected by centrifugation, and dissolved in deionized water. This mixture was dialyzed against deionized water for 2 days, after which the solution inside the dialysis tube was frozen using liquid nitrogen. The final product, PLys, was obtained by freeze-drying. ^{1}H NMR (500 MHz, DMSO-d_6, ppm): δ 7.94-7.82 (s, 2H, NH_2), 4.36-4.07 (br, 1H, COCH), 2.84-2.66 (br, 2H, NCH_2), 1.88-1.17 (m, 6H, $CH_2CH_2CH_2$), 0.88-0.80 (t, 3H, CH_3). Yield:80.1%. PLys prepared via above method were named as PLys 2.

4.2.3 Preparation of PLys/Glu hydrogels and PLys/Gen hydrogels

For the preparation of PLys/Glu hydrogels, approximately 100 mg of PLys 1 and the crosslinker Glu were dissolved in 0.2 mL of deionized water. The mixture was then put at 50 °C for 1 day to facilitate gel formation. The weight ratios of PLys to Glu were adjusted to 20:3 and 10:3, resulting in hydrogels designated as PLys/Glu Gel 1 and PLys/Glu Gel 2, respectively, arranged according to an ascending order of crosslinker concentration.

In a similar procedure for PLys/Gen hydrogels, around 100 mg of PLys 2 and the crosslinker genipin were dissolved in 0.2 mL of deionized water. Following the same gelation conditions (50 °C for 1 day), weight ratios of PLys to genipin were set at 5:1, 15:1, and 20:1. The resulting hydrogels were named PLys/Gen Gel (I) through (III) respectively in order of decreasing crosslinker concentration.

4.2.4 Swelling behaviour of PLys/Glu hydrogels and PLys/Gen hydrogels

All hydrogels prepared in step 3.3.3 were immersed in 10 mL of phosphate-buffered saline (PBS) at room temperature (RT). The water absorption capacity of each hydrogel was assessed by measuring their weights at different time intervals. Each measurement was conducted a minimum of three times to ensure data reliability.

4.2.5 RB5 adsorption experiments

In the adsorption experiment, PLys-based hydrogels were added to RB5 dye solutions at room temperature. The experimental parameters, including the oven-dried mass of the hydrogels, volume of RB5 solutions, initial dye concentrations, pH values, and adsorption durations, were adjusted to accommodate different conditions. All experiments were conducted at least 3 times under continuous stirring at 350 ppm.

To investigate the effects of pH on RB5 adsorption, a series of 25 mL RB5 solutions with different pH values were configured by 0.1 M HCl and 0.1 M NaOH. The initial concentration for RB5 solutions was maintained at 100 mg/L. After reaching water adsorption equilibrium, 0.2 g of PLys/Glu Gel 1 and PLys/Gen Gel (III) were respectively introduced into the RB5 solutions. For the experiments involving PLys/Glu Gel 1, the pH values were set to 3, 4, 5.5, 7.5, and 9, while for PLys/Gen Gel (III), the pH levels were adjusted to 3, 4, 5.5, 6.5, and 7.5. The adsorption time was 1 d.

For kinetic adsorption experiments of PLys/Glu Gels on RB5, the adsorption duration was extended up to 9 h. 1 g of PLys/Glu Gels, which had reached their maximum water adsorption capacity were immersed in 400 mL RB5 solutions with an initial concentration of 25 mg/L and a pH of 5.5. During the first 20 min, RB5 concentrations were measured every 5 min; over the subsequent 60 min, measurements were taken at 10-min intervals. Afterward, concentrations were monitored every 20 min until the 5 h mark, and for the final 4 h, concentration readings were taken once per hour.

For kinetic adsorption experiments of PLys/Gen Gels on RB5, experiments were conducted over a period extending up to 8h. 0.5 g of PLys/Gen Gels was submerged in 200 mL RB5 solutions. The initial concentration of RB5 was 30 ppm. pH of RB5 solutions was controlled at 5.5. During the first 2 h of the adsorption process, RB5 concentrations were measured at 10-min intervals. Over the subsequent 2 h, measurements were taken every 20 min. From 4 h until the 6-hour mark, the concentrations were monitored every 30 min. In the final 2 hours of the experiment, concentration assessments were performed once every hour.

For adsorption isotherm experiments, the pH of the RB5 solutions was controlled at 5.5. The adsorption period was set to 6 h for PLys/Glu hydrogels and for PLys/Gen hydrogels. For PLys/Glu hydrogels, the initial RB5 concentrations were adjusted to 25, 50, 100, 150, 200, 300, 400, and 500 ppm, while for PLys/Gen hydrogels, the initial concentrations were set at 30, 50, 100, 200, 300, 400, and 500 ppm.

The concentration of RB5 in the aqueous solution was measured by UV-Vis spectrophotometer (Varian Cary 50, Agilent Technologies, United States). The amount of metal ions adsorbed from the solution was calculated by the following Equation 4-1:

$$q_e = \frac{(C_0 - C_e)V}{m} \tag{4-1}$$

where C_0 and C_e represent the initial metal ion concentration and adsorption equilibrium mental ion concentration (ppm), respectively, while the V represents the volume of the solution (L) and m is the absolute dry mass of the PLys-based hydrogels used (g).

4.2.6 Recovery of RB5 on PLys/Glu hydrogels

Desorption of RB5 from PLys/Glu Gel 1 was carried out as follows. Once PLys/Glu Gel 1 from the kinetic adsorption experiments reached RB5 adsorption equilibrium, the pH of the solution

was adjusted to 12 using 1 M NaOH. The mixtures were stirred at 350 rpm on a magnetic stirrer at RT for 1 day, and Samples were taken from the solution to monitor the amount of RB5 desorbed into the solution. After the desorption test, the pH of RB5 solutions were adjusted to 5.5 again to initiate the next cycle of adsorption. The adsorption–desorption experiments were conducted for four cycles.

4.3 Results and discussion

4.3.1 Characterization of Lys(cbz)-NCA, PLys(cbz) and PLys

The NCA ROP method, known for its high efficiency, was used for the synthesis of PLys. Two synthetic routes were employed for PLys preparation. The first route involved synthesising PLys(Fmoc) by performing NCA-ROP with Lys(Fmoc)-NCA, followed by thermal deprotection in DMSO at 120 °C, as described in Chapter 3. The second route entailed the preparation of PLys(cbz) via NCA-ROP from Lys(cbz)-NCA, followed by acid deprotection using 33% HBr/AcOH (Figure 4-1). Analogous to other protecting groups, the incorporation of a cbz protecting group serves to shield the lysine side-chain amino groups during polymerisation, effectively preventing undesired side reactions such as branching. This HBr/AcOH deprotection method is efficient for removing the cbz group, enabling nearly complete deprotection and yielding highly pure PLys with exposed amino groups[211].

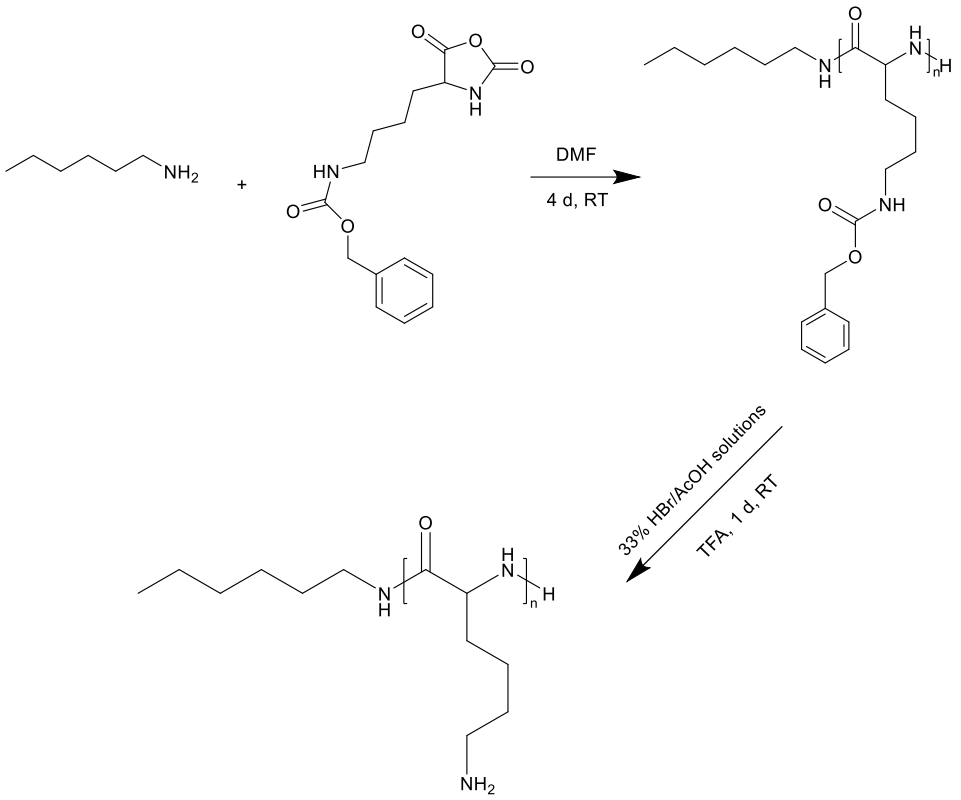

Figure 4-1 Scheme of preparation of PLys from Lys(cbz)-NCA.

Lys(cbz)-NCA was synthesised as a white powder following a widely established protocol. ^{1}H NMR spectroscopy confirmed successful synthesis, as indicated by the presence of aromatic protons from the cbz protecting group, which was detected as a multiplet within chemical shift range of 7.42-7.05 ppm[212]. Additionally, a single at 5.00 ppm attributed to benzylic -CH_2- protons of cbz group[212](Figure S4-1). Further confirmation of successful NCA synthesis was provided by FTIR spectroscopy (Figure 4-2), which displayed characteristic peaks at 1848 cm^{-1} and 1772 cm^{-1}, corresponding to the C=O bonds in the NCA anhydride structure[212]. Additional peaks at around 736 cm^{-1} (phenyl C-H bending vibrations), along with a peak at 1685 cm^{-1} (C=O from acylamino), confirmed the presence of cbz protecting groups[155].

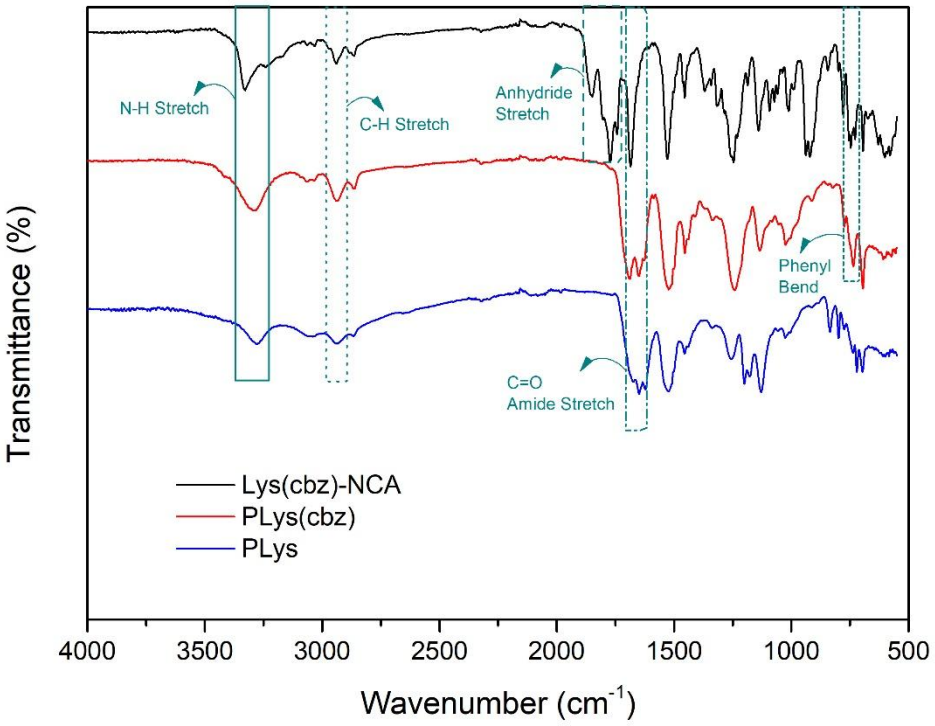

Figure 4-2 FTIR spectrum corresponding to Lys(cbz)-NCA, PLys(cbz), and PLys.

The ^{1}H NMR spectrum of PLys(cbz) (Figure S4-2) revealed not only the identifiable alkyl chain (0.87-0.76 ppm) attributed to the initiator end but also characteristic peaks corresponding to the cbz protecting group (7.42-7.05 ppm belonging to aromatic protons, 5.00 ppm belonging to methylene protons), providing preliminary evidence for the successful synthesis of PLys(cbz). Further confirmation was provided by FTIR spectroscopy (Figure 3-2, red line). The successful NCA ring-opening was indicated by the disappearance of the characteristic anhydride stretching peaks at 1848 cm^{-1} and 1772 cm^{-1}. The absence of these peaks in the FTIR spectrum after polymerisation confirmed that all monomer molecules had undergone complete conversion through ring-opening.

Following a 24-hour acid deprotection process in TFA, precipitation and dialysis steps are important to eliminate residual reagents and byproducts, ensuring a high-purity product with free amine groups suitable for further functionalisation or application. The complete

elimination of the cbz protecting groups was confirmed via ^{1}HNMR spectroscopy (Figure S4-3) and FTIR analysis of PLys (Figure 3-2, blue line). The ^{1}H NMR spectrum showed no detectable signals corresponding to aromatic protons, and the disappearance of the peak at 736 cm^{-1} in the FTIR spectrum, previously associated with aromatic C–H bending vibrations[213], indicated that cbz groups had been successfully deprotected.

MALDI mass spectrometry was used for polymer molecular weight analysis. PLys 1 displayed its molecular weight distribution, with the most prominent peaks ranging from 5480 to 7420 m/z, indicating that the primary molecular weights of PLys 1 fell within this range (5480 g/mol to 7420 g/mol) (Figure 4-3). The central peak, located at 6270 m/z, exhibited the highest signal intensity, suggesting an average molecular weight of approximately 6270 g/mol, which aligned closely with APC results (Table3-1, Mn=6000 g/mol). The MALDI spectrum consisted of multiple smaller peaks, with intervals of around 128 m/z, matching the molecular weight of the PLys repeat unit and further confirming successful polymer synthesis.

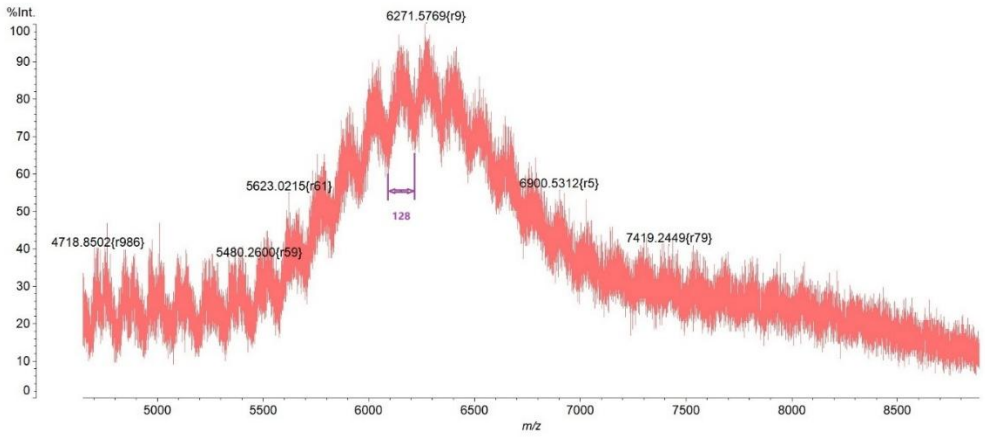

Figure 4-3 MALDI test result of PLys1 (prepared from thermal DMSO deprotection method).

Compared with PLys 1, which was discussed in detail in Chapter 2, PLys 2 synthesised from Lys(cbz)-NCA demonstrated a broader molecular weight distribution, ranging from 5600 g/mol to 8100 g/mol, as illustrated in Figure 4-4. The most prominent signal for PLys 2 was observed at approximately 6520 m/z, suggesting an average molecular weight of around 6520 g/mol,

slightly exceeding that of PLys 1. Additionally, the MALDI spectrum of PLys 2 also featured multiple minor peaks with intervals of 128 m/z. These intervals correspond to the molecular weight of a PLys repeat unit. When exposed to high-energy laser irradiation, these repeat units fragment may detach from the polymer chain, and are subsequently detected by the instrument.

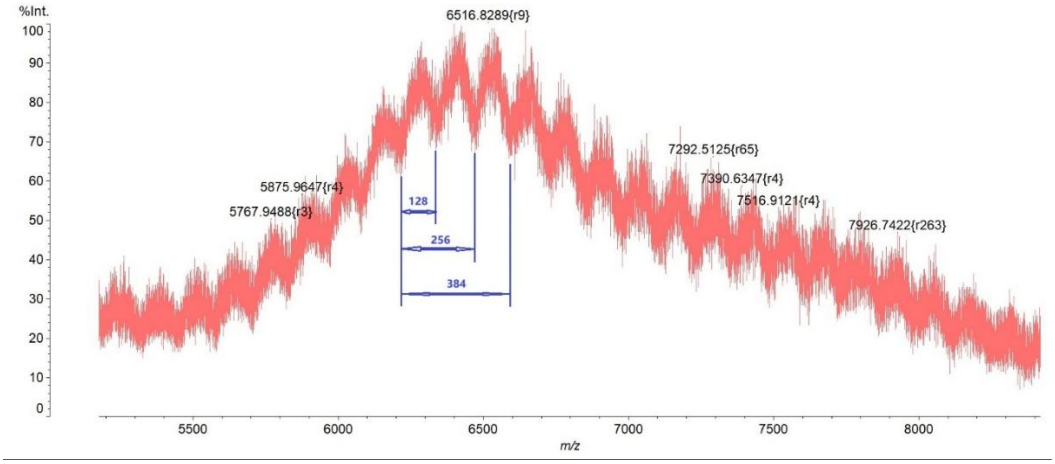

Figure 4-4 MALDI test result of PLys 2 (from HBr/AcOH deprotection method)

The average molecular weights of PLys 1 and PLys 2 were determined to be 6270 g/mol and 6520 g/mol, respectively, based on the most prominent MALDI signals. This suggested that PLys 2 contained approximately two additional repeat units compared to PLys 1. However, this slight difference was not deemed significant to be considered for subsequent adsorption studies.

4.3.2 Mechanism of fabrication of PLys/Glu and PLys/Gen hydrogels.

In the absence of a crosslinker, PLys in pH neutral aqueous solution lacks the ability to form a stable, three-dimensional network, dissolving to form a solution instead. Crosslinkers are therefore essential for converting a liquid polymer solution into a gel structure capable of retaining water, providing mechanical stability, and thus enabling use in a range of applications.

Given that PLys contains abundant amine groups (-NH_2), Glu and genipin were selected as crosslinkers to facilitate hydrogel formation. Glu, a small bifunctional aldehyde, is widely

employed as a crosslinking agent for proteins, polysaccharides, and various polymeric materials. Its crosslinking mechanism involves the formation of covalent bonds with amine groups (-NH_2) in biomolecules, such as lysine residues in proteins, or analogous functional groups in polymers[214]. However, frequent contact with Glu may cause irritation and corrosion to human skin, eyes, and respiratory system[215]. In contrast, genipin is a natural, low-toxicity alternative. It has been shown to effectively crosslink biopolymers including chitosan, gelatin, and collagen, and offers biocompatibility and biodegradability[216]. In both cases, PLys crosslinking can be done in aqueous solution to enable hydrogel formation *in situ* as PLys crosslinking occurs.

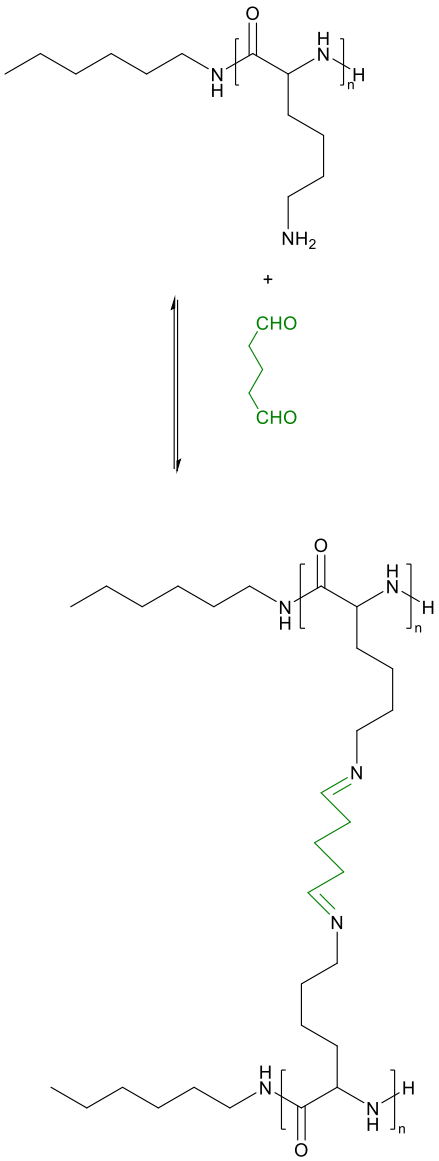

Figure 4-5 Mechanism for crosslinking of HAPLys with Glu.

The crosslinking mechanism between PLys and Glu is driven by a Schiff-base reaction (Figure 4-5)[217]. The nucleophilic addition reaction begins when a lone pair of electrons from the nitrogen atom in the amine group of PLys attacks the positively charged carbon atom of the carbonyl group in Glu. This interaction forms an intermediate α-hydroxyamine compound, which subsequently undergoes dehydration, leading to the formation of PLys/Glu hydrogels. A distinctive yellow/brown coloration appeared, indicating a rapid cross-linking reaction. Following hydrogel formation, a distinctive yellow/brown coloration developed, characteristic of the reaction between Glu and amines. This coloration is likely due to the formation of a Schiff base[218].

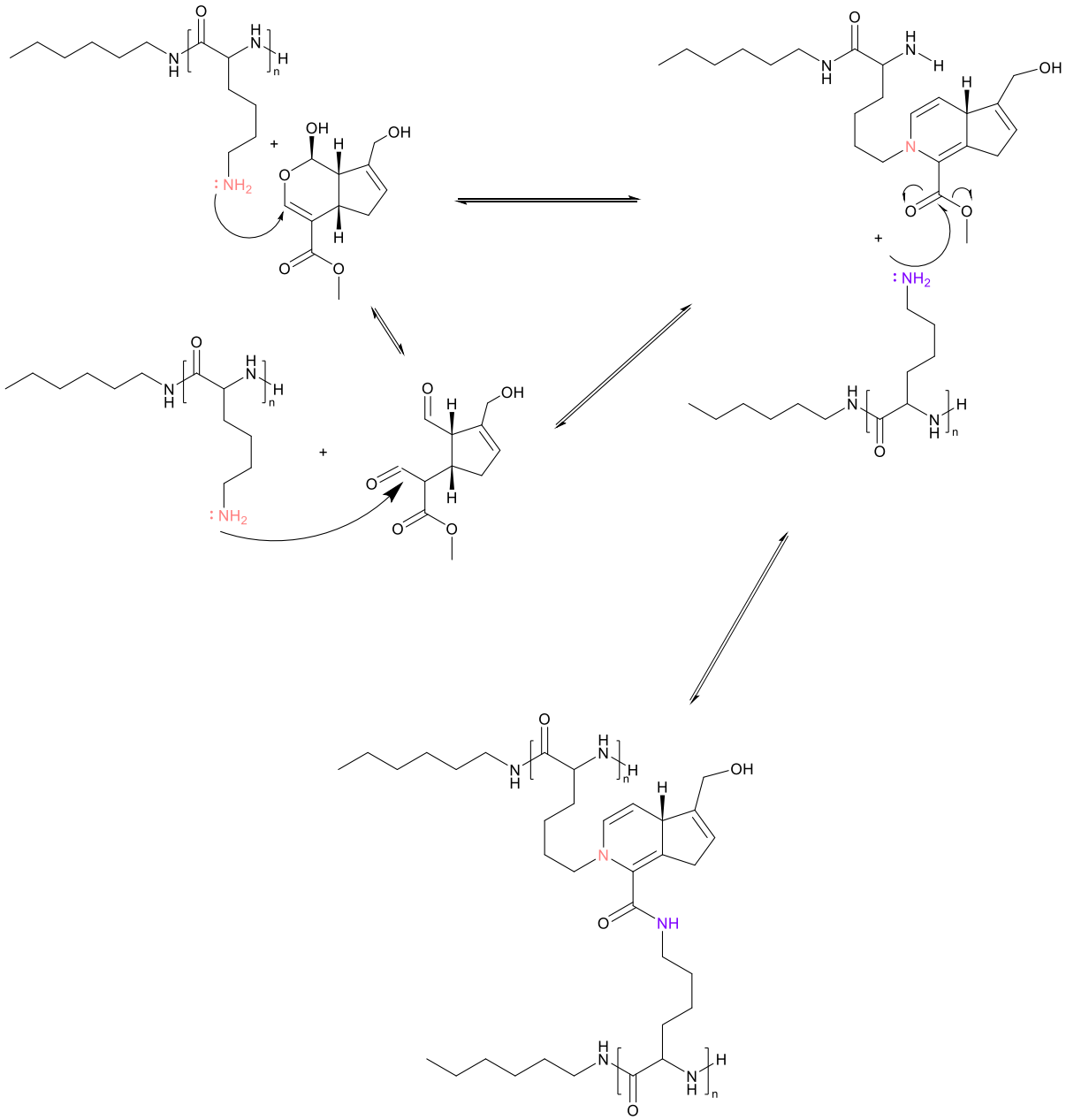

Figure 4-6 Possible mechanism for the crosslinking of HAPLys with genipin.

Since the discovery by Fujikawa et al. of genipin dimer formation in the presence of glycine, covalent crosslinking between genipin and polymers bearing free primary amine groups has been extensively employed to fabricate hydrogels for biomedical applications[94], however, genipin crosslinked PLys has not been reported before. Apart from that, the precise mechanism underlying this crosslinking remains insufficiently explained. A potential mechanism for the crosslinking between PLys and genipin is proposed, inspired by the hypothesised mechanism

of genipin's interaction with chitosan.

As illustrated in Figure 4-6, an amine group from PLys (in pink) initiates a nucleophilic attack on the α, β-unsaturated ester group of genipin, forming the corresponding intermediate[219]. Subsequently, the methoxycarbonyl group undergoes nucleophilic attack by an amine group (in purple) from another PLys chain, resulting in the formation of a secondary amide bond with the release of one methanol molecule. In aqueous solution, genipin exists as individual molecules that remain colourless at low concentrations. The characteristic blue-green colour emerges only when genipin reacts with amines, resulting in the formation of chromophores—light-absorbing structures responsible for the blue coloration.

4.3.3 Swelling behaviour of PLys/Glu and PLys/Gen hydrogels

The composition of various PLys-based hydrogels was detailed in Table 4-1. Following gel formation, the hydrogels' water adsorption capacity and stability were evaluated by immersing them in PBS buffer for seven days. The mass of the hydrogels was recorded daily to determine the extent of water uptake, and the results displayed in Figure 4-7. The round legend denotes PLys/Glu Gels, while the triangle legend represents PLys/Gen Gels.

Table 4-1 Different PLys-based hydrogels for RB5 adsorption.

Hydrogel	Composition
PLys/Glu Gel 1	PLys:Glu (weight ratio)= 20:3
PLys/Glu Gel 2	PLys:Glu (weight ratio)= 10:3
PLys/Gen Gel (I)	PLys:genipin (weight ratio)=5:1
PLys/Gen Gel (II)	PLys:genipin (weight ratio)=15:1
PLys/Gen Gel (III)	PLys:genipin (weight ratio)=20:1

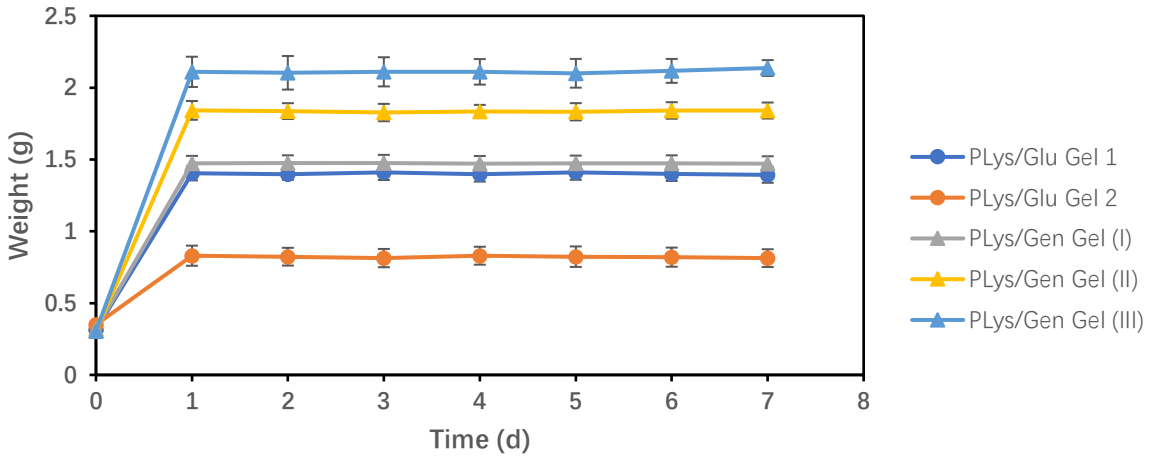

Figure 4-7 Water adsorption capacity of PLys-based hydrogels.

Regardless of the crosslinker used, PLys-based hydrogels achieved maximum water adsorption capacity after one day and remained stable in aqueous solution for at least seven days.

To examine the effect of crosslinker quantity on the swelling ratio of the hydrogels, data from Figure 6 were used to calculate the swelling ratio based on Equation (4-2).

$$Swelling\ ratio = \frac{W_e - W_0}{W_0} \times 100\% \quad (4\text{-}2)$$

In this equation, W_e represents the equilibrium weight of the hydrogels, measured after one day, while W_0 denotes the initial weight of the prepared hydrogels.

The results, displayed as column chart in Figure 4-8, show that for PLys/Glu Gels, a weight ratio of PLys to Glu of 20:3 allowed 0.315 g of PLys/Glu Gel 1 to absorb an additional average 1.085 g of water, yielding a swelling ratio of 346±17%. When this ratio was reduced to 10:3, 0.33 g of PLys/Glu Gel 2 absorbed only average 0.5 g of water, resulting in a swelling ratio of 152±21%, less than half that of PLys/Glu Gel 1. This indicated that the swelling ratio of PLys/Glu Gels decreased as the Glu content increased. The molar ratios of amine to aldehyde functional groups provided additional insight: for PLys/Glu Gels 1 and 2, the ratios were 2.5

and 1.25, respectively. A higher amine/aldehyde molar ratio corresponds to a looser network structure of hydrogel, resulting in increased water adsorption capacity[220].

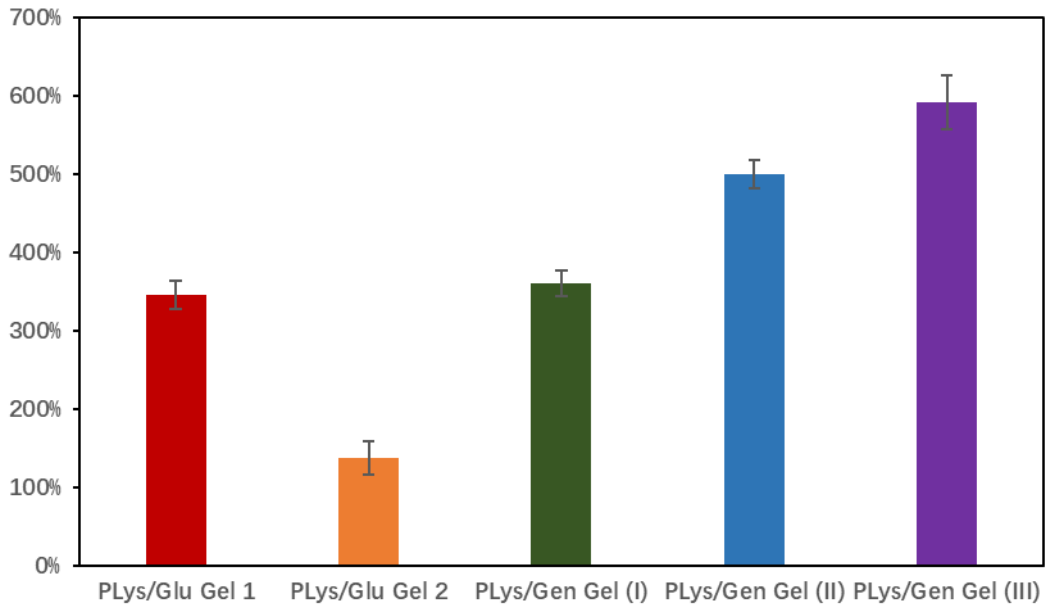

Figure 4-8 Swelling ratio of PLys-based hydrogels

For PLys/Gen Gels, as the genipin content increased from 4 mg to 20 mg per 100 mg of PLys 2, the molar ratio of amine groups in PLys to the two reactive sites in genipin decreased from 17.8 to 4.4, and the swelling ratio decreased correspondingly from 592±35% to 360±16%. This decreasing trend in swelling with higher genipin content aligns with expectations, as increased genipin reduces the number of protonated primary amine groups that contribute to hydrogel swelling via electrostatic repulsion. Additionally, crosslinking restricts PLys chain mobility, resulting a more compact hydrogel structure and diminishing the polymer's capacity to swell in aqueous solution.

Among the chosen PLys/crosslinker weight ratios, PLys/Gen Gels demonstrated a higher water adsorption capacity compared to PLys/Glu Gels. Crosslink density of hydrogels can explain the difference, and it can be numerically represented by molar ratio of amine groups in PLys and reactive sites of crosslinker (for PLys/Glu Gel is two aldehyde groups, for PLys/Gen Gel is two reactive sites shown in Fig. 4-6). For PLys/Glu Gels, these ratios are from 1.25 to 2.5,

while for PLys/Gen Gels, these ratios range from 4.4 to 17.8. The higher molar ratios observed in PLys/Gen Gels contribute to a less compact structure of hydrogel, thereby enhancing their water adsorption capacity. Among those hydrogels, swelling ratio of PLys/Gen Gen (III) is the highest, and can be high up to 592±35%, exhibiting strong potential for materials requiring superior water adsorption.

4.3.4 SEM analysis of PLys-based hydrogels

To visualise the internal structure of the hydrogel, the fully hydrated hydrogel was rapidly frozen in liquid nitrogen, freeze-dried, and subsequently examined by SEM. This approach to visualisation preserves the hydrogel's original microstructure, preventing collapse or deformation during sample preparation and observation.

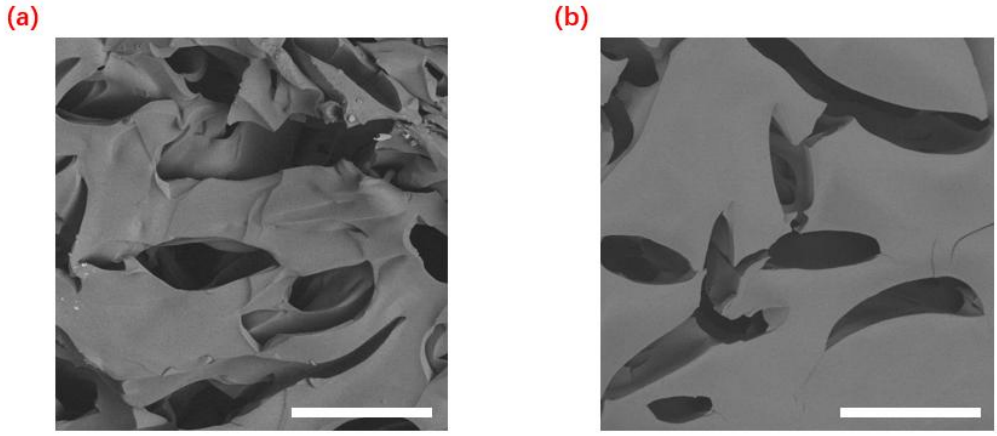

Figure 4-9 SEM images of (a) PLys/Glu Gel 1 and (b) PLys Glu Gel 2 (The white scale bar in the image represents a length of 50 μm).

In Figure 4-9, the dark region represents pore structures of PLys/Glu Gels. Pore sizes of PLys/Glu Gel 1 generally ranged from 10 to 100 μm, with an irregular pore shape that reflected a diverse pore structure (Figure 4-9 (a)).

As seen in Figure 4-9 (b), PLys/Glu 2 also displayed pore sizes typically ranging from 10 to 100 μm. The dark region became less, with pores arranged more sparsely, resulting in a more compact structure due to the higher proportion of Glu[221]. This structural configuration may enhance the mechanical strength of the hydrogel; however, it likely decreases its water content owing to the restricted expansion space.

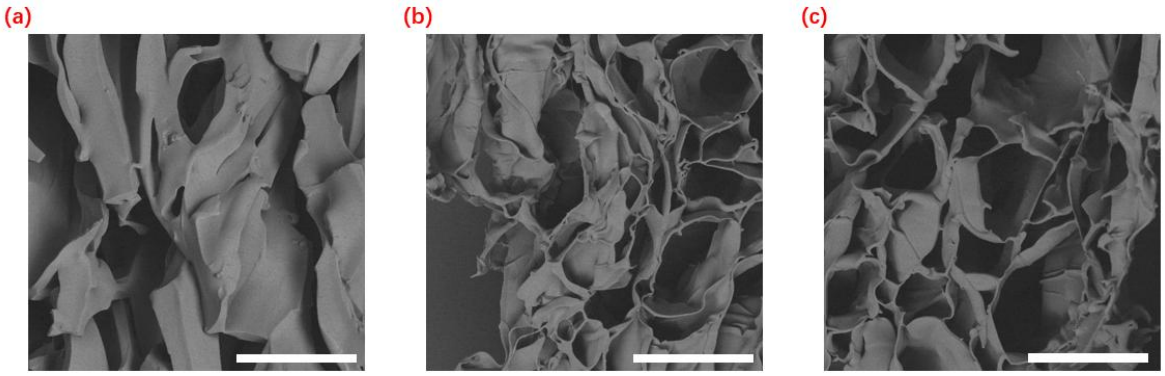

Figure 4-10 SEM of (a) PLys/Gen Gel (I), (b) PLys/Gen Gel (II) and (c) PLys/Gen Gel (III) (The white scale bar in the image represents a length of 50 μm).

All porous structures of PLys/Gen Gels can be proved in the Figure 4-10, confirming hydrogel network formation. The porosity represented by dark areas of these gels increased in such an order (PLys/Gen Gel (I) < PLys/Gen Gel (II) < PLys/Gen Gel (III)), with decreasing content of genipin. PLys/Glu Gels network structures seemed to be fairly closed, while those of PLys/Gen Gels were more open, which correlated to the swelling data obtained in Figure 4-8. Higher porosity facilitates the transfer of water or other substances throughout the gel network, making it suitable for applications that require higher permeability, such as drug release systems or biological scaffolds[222].

In PLys-based hydrogels, high porosity improves the transport of water and other substances. Theoretically, hydrogels with greater porosity and more amine groups are more favourable for RB5 adsorption. This hypothesis will be tested in the subsequent RB5 adsorption experiments.

4.3.5 Rheology tests of PLys-based hydrogels

Rheological analysis was performed to confirm the formation of hydrogels and to evaluate their rheological properties. PLys/Gen hydrogels for rheology testing were prepared according to the method outlined in Section 3.3.3. After preparation, the gels were fully swollen in 1 mL of deionized (DI) water.

In Figure 4-11 (a), the storage and loss modulus of PLys/Glu Gel 1 are presented. No crossover point was observed between the storage modulus (G') and the loss modulus (G'') throughout the tested frequency range, indicating robust solid-like behaviour and the presence of a crosslinked fibrous network within the hydrogels[223]. As the frequency increased from 1 Hz to 100 Hz, the storage modulus of this hydrogel declined from 70 kPa to 44 kPa, while the loss modulus increased gradually from 4400 Pa to 5200 Pa. Relative low cross-linking density in Gel 1 may account for the frequency-dependent changes. Less crosslink points of the hydrogel mean less restriction between the PLys chains, which hinders their ability to return to their original state and promotes greater relaxation of the chain segments under high-frequency conditions[224]. The hydrogel primarily exhibited elastic behaviour, as indicated by its storage modulus being substantially higher than the loss modulus. Similarly, PLys/Glu Gel 2 also demonstrated predominantly elastic characteristics. However, the storage and loss modulus of PLys/Glu Gel 2 remained consistent across varying frequencies, maintaining values of 280 kPa and 26 kPa, respectively, highlighting its strong mechanical stability across a broad frequency range.

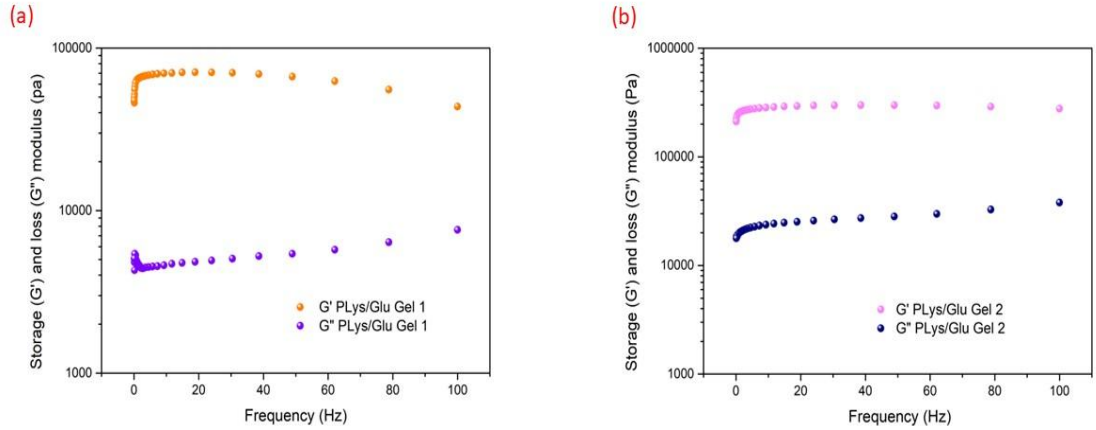

Figure 4-11 Storage (G') and loss (G") modulus of PLys/Glu Gels: (a) PLys/Glu Gel 1 and (b) PLys/Glu Gel 2.

Rheology test of PLys/Gen hydrogels are depicted in Figure 4-12. At a higher mass ratio of PLys/Genipin (20:1 for PLys/Gen Gel (III)), where the lowest genipin content necessary for hydrogel formation, a crossover point between G' and G" was observed across the tested frequency range, indicating limited crosslinking points in the hydrogel, though SEM Figure (Figure 4-10 (c)) proved crosslinked networks of this hydrogel. Hydrogels with low crosslinking degree may be hard to maintain previous G' and G" at low frequency. Conversely, at lower mass ratios (5:1 for PLys/Gen Gel (I) and 15:1 for PLys/Gen Gel (II)), where more genipin was added, no crossover point appeared, suggesting the formation of permanent covalent bonds, characteristic of a chemically crosslinked hydrogel[225]. Besides, for these two hydrogels, the G' consistently remained higher than G" over the entire frequency range, which indicates robust solid-like behaviour and an interwoven network structure in the hydrogels. Increasing the proportion of genipin allows for control over the mechanical strength of the hydrogels.

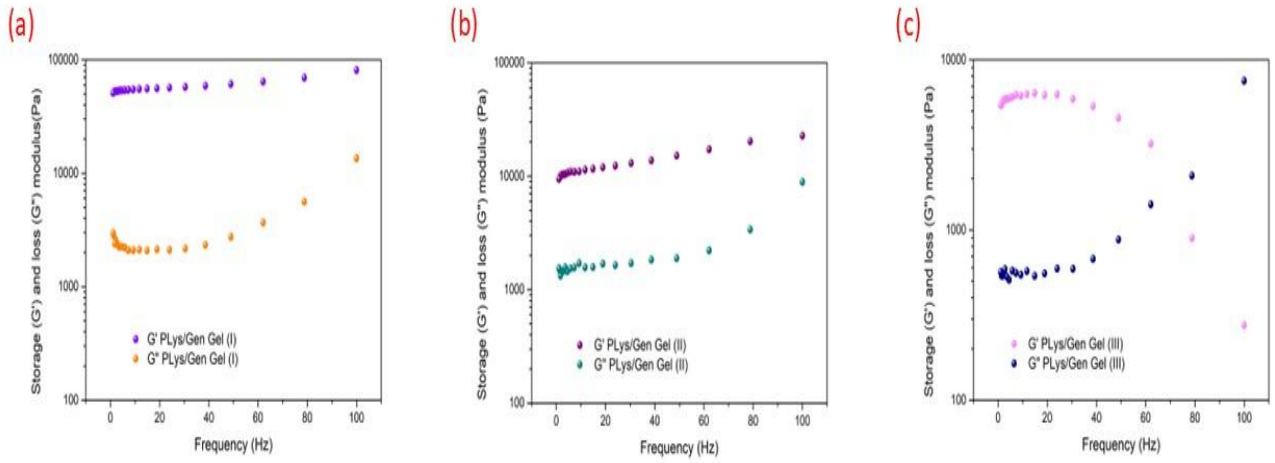

Figure 4-12 Storage (G') and loss (G") modulus of PLys/Gen Gels: (a) PLys/Gen Gel (I), (b) PLys/Gen Gel (II) and (c) PLys/Gen Gel (III).

For PLys/Gen Gels (I)-(III), when the frequency was below 40 Hz, both the storage modulus (G') and the loss modulus (G") remained nearly constant or exhibited minimal changes. This stability indicated that PLys/Gen Gels maintain consistent viscoelastic properties within this frequency range. As genipin/PLys mass ratio increased from 5% (Gel (III)) to 20% (Gel (I)), there was a notable increase in G' from 5.34 kPa to 58.9 kPa and in G" from 680 Pa to 2.33 kPa, revealing that the higher PLys/Gen hydrogel crosslinking density enhanced mechanical strength. This hydrogel with more rigid structure not only demonstrated improved resistance to deformation but also increased intermolecular friction[226], reflected in the concurrent rise of both G' and G".

However, at test frequencies above 60 Hz, the behaviour of the hydrogels varied depending on the proportion genipin included as the crosslinker. For Gel (III), the storage modulus of this hydrogel sharply declined from 5.34 kPa to 280 Pa, while the loss modulus gradually increased from 680 Pa to 7.50 kPa. The lower genipin content in Gel (III) means a lower network density of this hydrogel. The reduced cross-linking density impairs the hydrogel's ability to withstand high-frequency deformation, as fewer cross-linking points provide limited structural rigidity[227]. At high frequencies, this network lacks sufficient restoring force to sustain elastic

deformation, leading to a drop in the elastic modulus. Although the molecular chain of low cross-linking density hydrogel is not highly restricted, it can hardly relax swiftly in response to external high-frequency stress, resulting in greater friction between segments. The increased internal friction between molecular chains converts into thermal energy and non-elastic molecular dissipation, which causes the loss modulus to rise at higher frequencies[228]. For Gel (I) and (II), both G' and G" showed further increases. Specifically, G' and G" of Gel (I) increased to 81.1 kPa and 13.5 kPa, respectively, while those of Gel (II) increased to 22.7kPa and 8.9 kPa. Hydrogels with relatively high cross-linking density exhibit viscoelastic dual characteristics at high frequencies[228]. The short action time at these frequencies limits the ability of molecular chains to rearrange or relax, leading to greater resistance to deformation. Consequently, the elastic network primarily "stores" the high-frequency stress, resulting in an increase in the elastic modulus. Meanwhile, the frequent vibrations of molecular chains generate more friction both between chains and within segments, causing additional energy loss as thermal energy and thereby increasing the loss modulus.

When comparing PLys/Glu Gel 1 with PLys/Gen Gel (III), which share similar polymer/crosslinker mass ratios, it was observed that the G' of PLys/Glu Gel 1 was higher than that of PLys/Gen Gel (III). Although these hydrogels form through different mechanisms, differences cross-linking density likely account for this difference. In both hydrogels, the molecular weights of PLys were similar, as confirmed by MALDI testing, leading to comparable repeating amine groups. Given that genipin (226.23 g/mol) has a higher molecular weight than Glu (100.12 g/mol), and molar amount of crosslinker in PLys/Glu Gel is approximately twice that in PLys/Gen Gel, so PLys/Glu Gel 1 exhibits a denser network structure than PLys/Gen Gel (III), which contributes to the enhanced mechanical strength observed in PLys/Glu Gel 1.

4.3.6 Effect of pH on RB5 adsorption on PLys-based hydrogels

pH plays a critical role in the adsorption of organic dyes. RB5 adsorption on PLys-based hydrogels is driven by electrostatic attraction between the protonated free amine groups in the hydrogels and the anionic sodium sulfonate groups on RB5 molecules (Figure 4-13 and 4-14). The pKa of PLys generally falls between 9.0 and 9.5[94], while RB5 has a pKa of around 3.8, associated with its amine groups[229]. However, the pKa of the dye's sodium sulfonate groups (-SO_3Na) is significantly lower, sometimes even reaching negative values[229]. Therefore, for adsorption experiments with PLys/Glu Gel 1, pH levels varied from 3 to 9, while for PLys/Gen Gel (III), the pH was adjusted from 3 to 7.5.

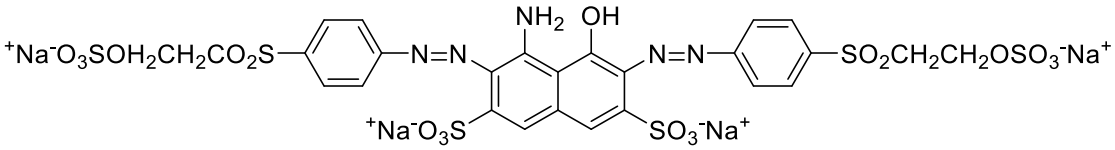

Figure 4-13 Chemical structure of Reactive Black 5.

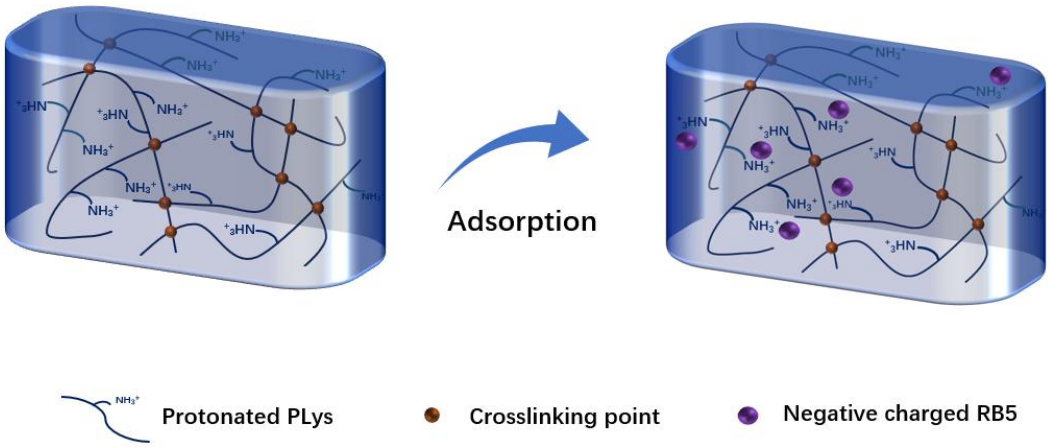

Figure 4-14 Illustrated diagram how PLys/Glu and PLys/Gen Gels adsorbed RB5 ions.

The influence of medium pH on RB5 uptake is presented in Figure 4-15. For PLys/Glu Gels, the highest dye adsorption value was recorded at pH 4. Above pH 4, the RB5 adsorption value gradually decreased from 114±5 mg/g to 85±3 mg/g, based on dry weight of gels. This trend

can be attributed to the reduced protonation of amino groups at higher pH levels, which diminishes their positive charge and thus weakens electrostatic interactions with the negatively charged dye molecules[230]. At pH 3, a slight decrease in adsorption was observed, likely due to the protonation of RB5's amine groups, which reduces the concentration of anionic dye species available to interact with the hydrogel's active sites[230].

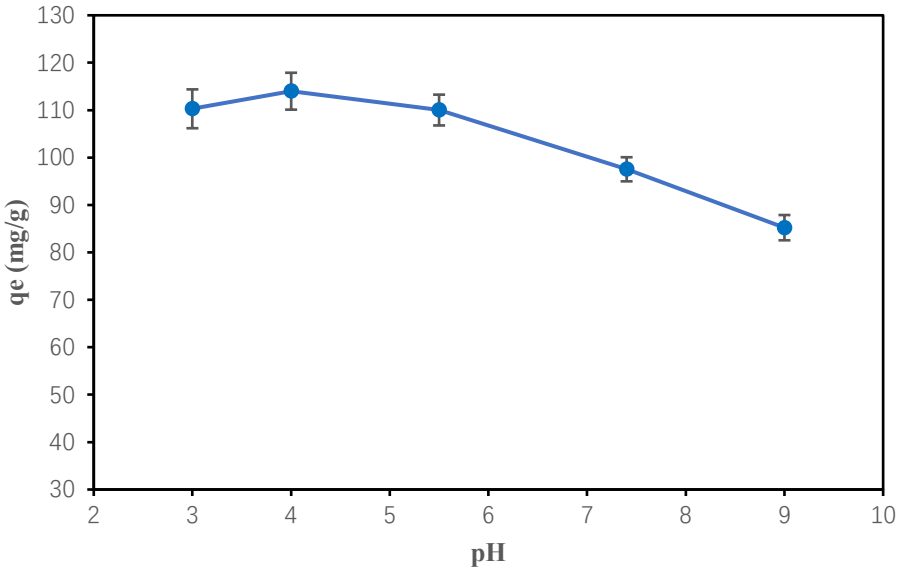

Figure 4-15 The effects of pH on the adsorption of RB5 by PLys/Glu Gel 1 (0.2 g PLys/Glu Gel 1 (swollen equilibrium state) in 25 mL and 100 ppm RB5 solution, contact time 1 d, q_e means RB5 adsorption capacity of oven dried hydrogel after equilibrium).

The effect of pH on RB5 adsorption by PLys/Gen Gel (III) is illustrated in Figure 4-16. As the pH increased from 3 to 5, there was no obvious change as for the adsorbed amount of RB5, ranging from 194±7 mg/g to 199±5 mg/g. When pH value was beyond 5, there was a gradual decline in RB5 uptake to 162±4 mg/g as pH continued to rise. This decrease is likely due to deprotonation of the hydrogel's amine groups, weakening their interaction with the negatively charged RB5 anions[230].

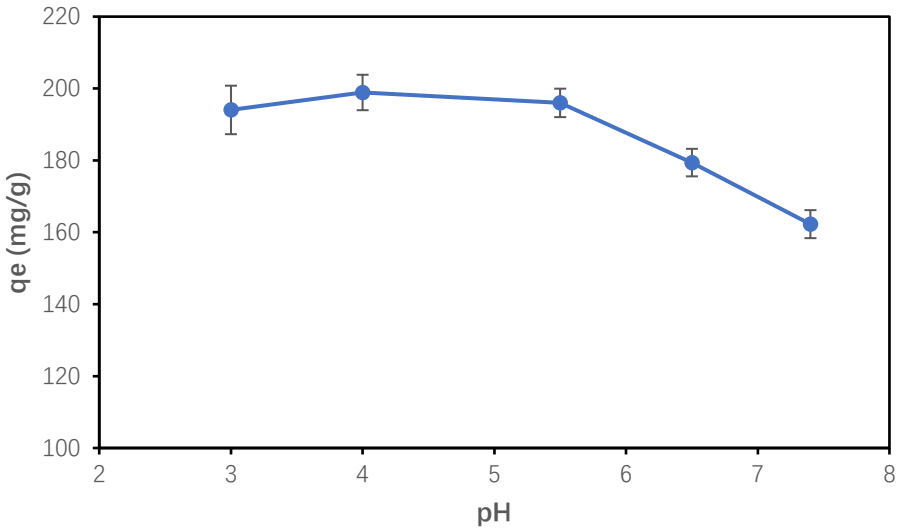

Figure 4-16 The effects of pH on the adsorption of RB5 by PLys/Gen Gel (III) (0.2 g PLys/Gen Gel (III) (swollen equilibrium state) in 25 mL and100 ppm RB5 solution, contact time 1 d, q_e means RB5 adsorption capacity of oven dried hydrogel after equilibrium).

At pH 4, both hydrogels exhibited their maximum RB5 adsorption capacity, with PLys/Gen Gel (III) achieving an adsorption capacity 85 mg/g higher than PLys/Glu Gel 1. This difference can be attributed to the greater number of free amine groups following crosslinking, and the higher swelling ratio of the PLys/Gen Gel (III). As the pH increased to 5.5, though RB5 uptake by both hydrogels slightly decreased, the difference was minimal. Given the practical requirements for organic dye wastewater treatment and the susceptibility of equipment to corrosion in overly acidic or alkaline conditions, the pH of RB5 solutions was set to 5.5 for subsequent adsorption experiments.

4.3.7 Effect of contact time on RB5 adsorption on PLys-based hydrogels

By studying the effects of contact time on the adsorption of RB5 onto PLys-based hydrogels, the equilibrium adsorption capacity can be obtained, which can be used to fit the adsorption kinetic model. Figure 4-17 shows the effects of contact time on the amount of RB5 adsorbed per gram of PLys/Glu Gels at pH 5.5. Adsorption of RB5 by PLys/Glu Gel 1 increased rapidly during the initial 100 minutes, reaching approximately 29.4% of its equilibrium adsorption

capacity. After this phase, the adsorption rate slowed until 200 minutes, followed by an accelerated adsorption stage—exceeding the rate of the first “fast” stage—over the next 60 minutes, during which adsorption increased from ~37.1% to ~93.6% of the equilibrium capacity. The adsorption then gradually reached its maximum value of 109±6 mg/g at 360 minutes. Similarly, PLys/Glu Gel 2, which has fewer active amine groups, adsorbed RB5 rapidly during the first 30 minutes, reaching ~28.6% of its equilibrium adsorption capacity. This was followed by a slower adsorption phase until 200 minutes, after which the adsorption rate increased again over the next 100 minutes, rising from ~34.9% to ~96.2% of the equilibrium capacity. The adsorption gradually plateaued, reaching a maximum RB5 adsorption of 54±6 mg/g at 360 minutes.

RB5 adsorption on PLys/Glu Gels followed a “fast-slow-fast-slow” adsorption pattern before reaching equilibrium. In the initial "fast" phase, RB5 ions were rapidly captured by surface amine groups. Adsorption then slowed due to several possible factors: (1) progressive occupation of active sites on the hydrogel surface, reducing available sites, (2) the diffusion of RB5 molecules into the hydrogel’s interior, and (3) the formation of a negatively charged layer by adsorbed RB5 on the hydrogel surface, which repels additional anionic dye molecules. Following this phase, adsorption accelerated again as amine groups within the hydrogel’s interior absorbed more RB5. During this stage, some hydrogels broke into smaller pieces under stirring, increasing the contact surface area between the gels and RB5 ions. Eventually, adsorption slowed again as equilibrium was approached.

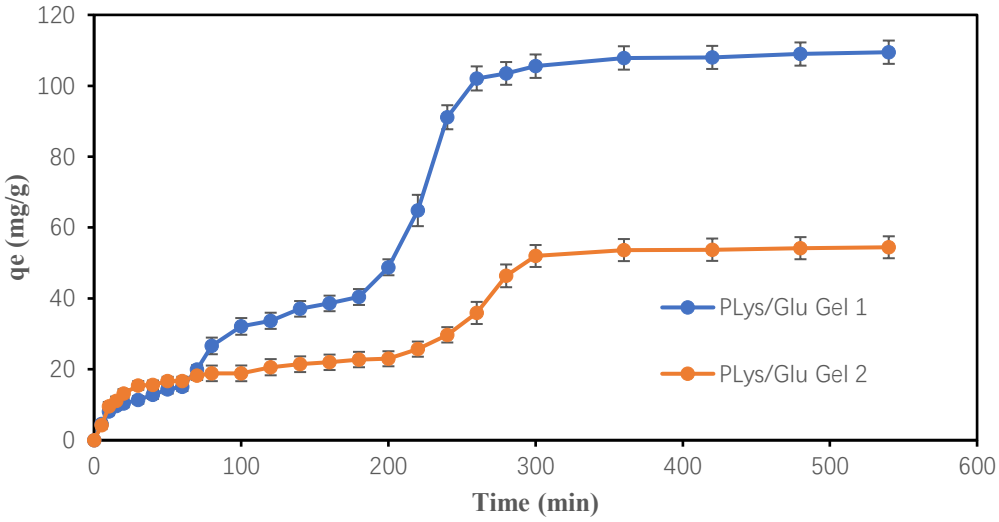

Figure 4-17 The effects of contact time on the adsorption capacity of PLys/Glu Gels for RB5 (initial concentration of RB5 25 ppm, 1g PLys/Glu Gel (in swollen equilibrium state) in 400 mL solutions).

Two common kinetic adsorption models are often applied to fit experimental data in order to identify the controlling mechanism of the adsorption process. One of these is the pseudo-first-order model, primarily governed by a physical adsorption mechanism[231, 232]. Its linear equation is given as Equation (4-3):

$$ln(q_e - q_t) = -K_1 t + lnq_e \tag{4-3}$$

where q_e (mg/g) represents the adsorption amount at equilibrium, while q_t is the adsorption amount at time t, and $K_1(min^{-1})$ is the kinetic adsorption rate constant in the pseudo-first-order model. The parameters K_1 and q_e are determined by linearly fitting $ln(q_e - q_t)$ against t.

The other model is a pseudo-second-order model dominated by a chemical mechanism[97, 232], and is represented by Equation (4-4):

$$\frac{t}{q_t} = \frac{1}{K_2 {q_e}^2} + \frac{t}{q_e} \tag{4-4}$$

where the q_e and q_t are defined as in Eq. (1). K_2 (g/(mg·min)) is the kinetic adsorption rate constant of the pseudo-second-order model. The second-order rate constants K_2 and q_e are determined via the linear fitting of t/q_t to t.

As listed in Table 4-2 and shown in Figure S4-5 to Figure S4-8, for RB5 adsorption on PLys/Glu Gel 1, R_1^2= 0.912 is greater than R_2^2= 0.328; similarly, for PLys/Glu Gel 2, R_1^2= 0.839 exceeds R_2^2= 0.691. This suggests that RB5 adsorption onto PLys/Glu Gels aligns more closely with the first-order kinetic model, indicating that the adsorption is primarily a physical process governed by electrostatic interactions between protonated amine groups and negatively charged RB5 anions. The constant K_1 in the pseudo-first-order model represents the rate constant of adsorption, reflecting the speed at which equilibrium is reached. For PLys/Glu Gel 1, K_1 is 0.0104 min^{-1}, nearly identical to that of PLys/Glu Gel 2, indicating that their equilibrium times are similar, as confirmed by the 6-hour equilibrium time shown in Figure 4-17.

Table 4-2 The key kinetic parameters of first- and second-pseudo-order model for RB5 adsorption on PLys/Glu Gels ($q_{e,exp}$ means adsorbed RB5 at equilibrium in the experiments, $q_{e,cal}$ is predicted RB5 adsorption capacity at equilibrium according to the model fittin

Samples	C_0 (mg/L)	$q_{e,exp}$ (mg/g)	pseudo-first-order model			pseudo-second-order model		
			K_1 (min^{-1})	$q_{e,cal}$ (mg/g)	R_1^2	K_2 [g/(mg*min)]	$q_{e,cal}$ (mg/g)	R_2^2
PLys/Glu Gel 1	25	110.2	0.0104	175.8	0.912	$5.416*10^{-6}$	270.3	0.328
PLys/Glu Gel 2	25	54.5	0.0108	93.9	0.839	$8.132*10^{-5}$	66.7	0.691

From Figure 4-18, PLys/Gen Gel (III) and (II) adsorbed RB5 ions following the previously described “fast-slow-fast-slow” pattern. The adsorbed RB5 amount increased rapidly to 144±

11 mg/g at 80 minutes, reaching 72.7% of the maximum equilibrium value. The adsorption rate then slowed until 220 minutes, after which a relatively fast adsorption phase occurred, with RB5 capacity rising from 159±6 mg/g to 193±6 mg/g. The rate slowed once again, eventually reaching equilibrium at 360 minutes with the highest RB5 adsorption value of 198±4 mg/g. For PLys/Gen Gel (II), maybe due to a lower number of free amine groups on the surface, the initial RB5 adsorption rate was fast in the first 10 minutes, with the adsorbed amount reaching ~16.1% of its equilibrium value (75.7±4 mg/g). The adsorption rate then slowed until 300 minutes, followed by a brief faster stage over the next 60 minutes before reaching equilibrium. While for PLy/Gen (I), the adsorption behaviour differed, which can be described as "slow-fast-slow" mode. It adsorbed RB5 at a relatively slow rate during the initial 50 minutes, followed by a faster adsorption phase over the next 20 minutes and then the adsorption rate slowed again before reaching equilibrium at 100 min with a maximum RB5 adsorption capacity of 29.2±3 mg/g.

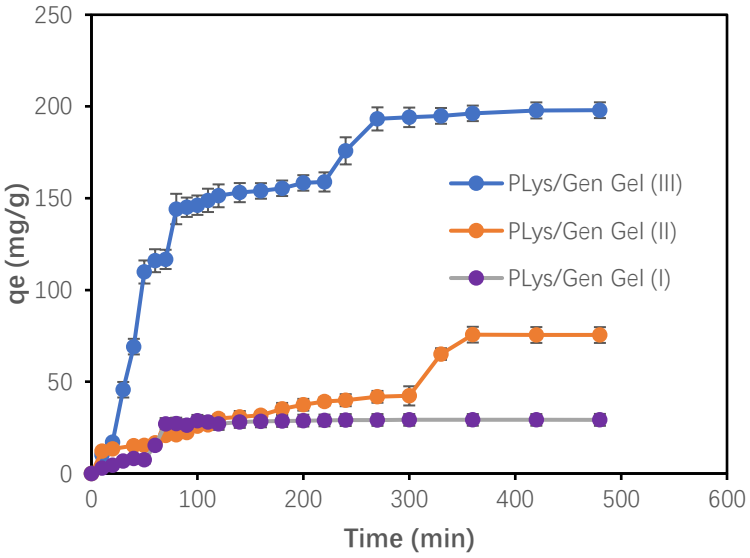

Figure 4-18 The effects of contact time on the adsorption capacity of PLys/Gen Gels for RB5 (initial concentration of RB5 30 ppm, 0.5 g PLys/Glu Gel (in swollen equilibrium state) in 200 mL solutions).

For PLys/Gen Gels with abundant free amine groups, the RB5 adsorption process followed a "fast-slow-fast-slow" pattern, similar to that observed in PLys/Glu Gels. However, as the

genipin content increased—reducing the number of free amine groups—the duration of the initial "fast" phase shortened, accompanied by a decrease in the amount of RB5 adsorbed. With further increases in genipin content, the hydrogel structure became more compact and primary amine sites became occupied, providing fewer active adsorption sites. This led to a reduction in the initial surface adsorption rate and a slower overall adsorption process, causing the initial "fast" adsorption stage to disappear. Despite this, the second "fast" phase remained, representing accelerated adsorption controlled by the interior amine groups of the hydrogel as they continued to capture RB5 ions.

Table 4-3 The key kinetic parameters of first- and second-pseudo-order model for RB5 adsorption on PLys/Gen Gels ($q_{e,exp}$ means adsorbed RB5 at equilibrium in the experiments, $q_{e,cal}$ is predicted RB5 adsorption capacity at equilibrium according to the model fitting).

Samples	C_0 (mg/L)	$q_{e,exp}$ (mg/g)	pseudo-first-order model			pseudo-second-order model		
			K_1 (min^{-1})	$q_{e,cal}$ (mg/g)	R_1^2	K_2 [g/(mg*min)]	$q_{e,cal}$ (mg/g)	R_2^2
PLys/Gen Gen (I)	30	29.2	0.020	21.1	0.929	$3.43*10^{-4}$	36.9	0.890
PLys/Gen Gen (II)	30	75.7	0.012	166.6	0.640	$3.09*10^{-5}$	107.5	0.638
PLys/Gen Gen (III)	30	197.9	0.014	260.1	0.888	$3.10*10^{-5}$	263.2	0.861

As recorded in Table 4-3 and Figure S4-9 to Figure S4-14, for RB5 adsorption on all PLys/Gen Gels the values of R_1^2 are greater than those of R_2^2, indicating that the first-order kinetic model provides a better fit for RB5 adsorption. This suggests that the adsorption process is predominantly physical, driven by electrostatic interactions between protonated amine groups and the negatively charged RB5 ions. For PLys/Gen Gel (I), K_1 in the first-order kinetic model is 0.020 min^{-1}, greater than that of PLys/Gen Gel (II) and (III), which corresponds to the fact that PLys reached equilibrium in 70 min, while the equilibrium times of PLys/Gen Gel (II) and (III) were longer (360 min).

Figure 4-19 illustrates partial PLys-based hydrogels immersed in DI water before and after RB5 adsorption. For PLys/Glu Gels (Figure 3-19 (a)), the hydrogels changed from dark orange to dark blue after adsorbing RB5 molecules. In contrast, PLys/Gen Gels (Figure 3-19 (b)), which initially appeared dark blue due to genipin, showed no significant colour change following RB5 adsorption. The solutions of both hydrogels after adsorption appeared a very pale blue, likely due to trace amounts of RB5 desorbing from the hydrogel surface to the DI water.

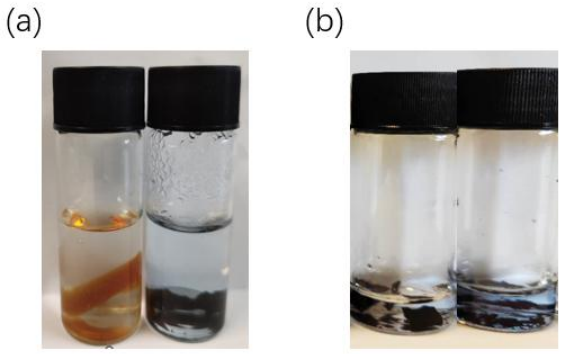

Figure 4-19 PLys-based hydrogels before and after RB5 adsorption ((a): PLys/Glu Gel 1, (b): PLys/Gen Gel (III)).

4.3.8 Effect of RB5 concentration on adsorption on PLys-based hydrogels

To study the effect of initial RB5 concentration on the adsorption behaviour of PLys-based hydrogels, a series of experiments were conducted as described in Section 4.2.5. From a mechanistic perspective, these experiments are the basis for fabrication of adsorption isotherm model which favours deepening understanding of adsorption behaviour. From a programmatic standpoint, to optimise dyes removal process from sewage, figuring out the concentration range at which adsorbents show superior performance is essential. Through analysis of model fit result and parameters, mechanisms underlying RB5 adsorption by two PLys-based hydrogels can be explored and their adsorption performance at low and high concentration can be

compared to determine the optimised conditions corresponding to highest adsorption capacity. In the contact time experiments for RB5 adsorption, most PLys-based hydrogels reached equilibrium within 6 hours. For consistency in subsequent operations, the adsorption time in this section was also set to 6 hours.

Figure 4-20 illustrates the effect of initial RB5 anion concentration on the adsorption capacity of PLys/Glu Gels, with data suitable for fitting to an adsorption isotherm model. For both PLys/Glu Gels, at initial RB5 concentrations below 200 ppm, the saturated adsorption capacity increased almost linearly with the rise in RB5 concentration. However, when the initial ion concentration exceeded 200 ppm, the saturated adsorption capacity plateaued, showing no further increase. The maximum RB5 adsorption of PLys/Glu Gel 1 and 2 was 430±8 mg/g and 190±6 mg/g, respectively.

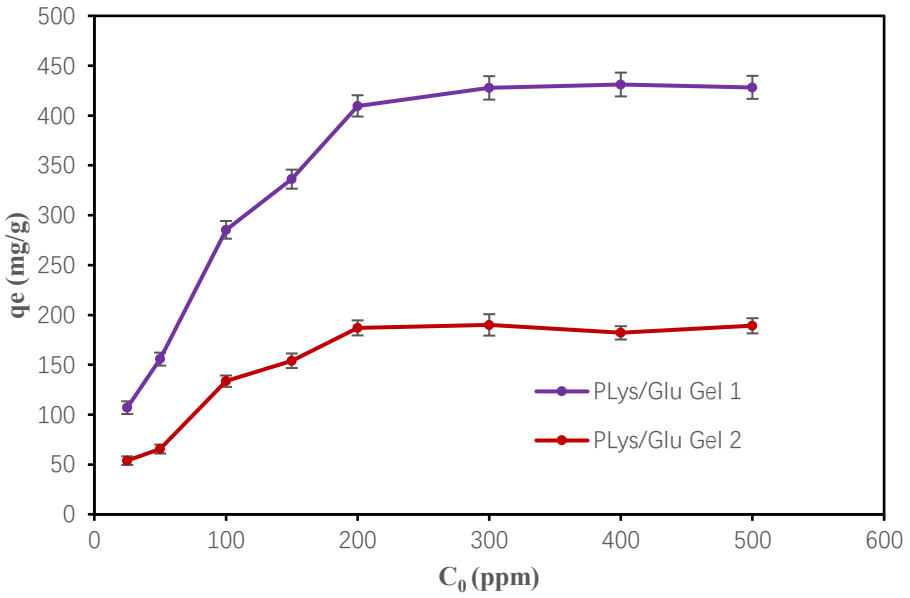

Figure 4-20 The effects of RB5 initial concentration on adsorption capacity of PLys/Glu Gels (pH= 5.5, contact time 6 h, 0.1g adsorbent (in swollen equilibrium) in 40 mL solutions).

At lower RB5 concentrations (<200 ppm), sufficient active adsorption sites are available on the hydrogel to bind with a greater concentration of dye molecules. As the RB5 concentration increases, more of these sites are occupied, resulting in a nearly linear increase in adsorption

capacity. However, once the RB5 concentration surpasses 200 ppm, the majority of active sites on the PLys/Glu Gels become saturated, and the adsorbent reaches its maximum capacity. Beyond this point, adding more dye does not lead to further adsorption, as no additional sites are available for binding, causing the adsorption capacity to plateau. Once the hydrogel structure is established, a lower Glu content, allowing for existence of more free amine functional groups, enhances RB5 adsorption capacity by providing additional active sites for binding.

There are also two typical isotherms to explain the adsorption mechanism. One is the Langmuir isotherm, the other is Freundlich isotherm. The Langmuir isotherm is suitable for the explanation of adsorption mechanism of many adsorbents and the linear equation (Equation 4-5) of it is listed below[233, 234]:

$$\frac{C_e}{q_e} = \frac{C_e}{q_m} + \frac{1}{bq_m} \tag{4-5}$$

where C_e (mg/L) represents the amount of adsorbed substances in the solution at adsorption equilibrium, q_i (mg/g) represents the equilibrium capacity of the adsorbent, q_m (mg/g) is the maximum adsorption capacity of the adsorbent, and b (L/mg) is the Langmuir isotherm constant. q_m and b are calculated by the linear fitting of C_e/q_e to C_e.

In addition, the Freundlich isotherm is frequently applied in heterogeneous adsorption systems and its linear equation (Equation 4-6) is shown as below[105, 106]:

$$logq_e = logk_f + \frac{logC_e}{n} \tag{4-6}$$

where q_e and C_e are equal to Equation (4-5), k_f ($mg^{1-n} \cdot g^{-1} \cdot L^{-n}$) is the constant depicting adsorption capacity and n is the constant describing the adsorption intensity. The value of n generally ranges from 2 to 3, and $n > 1$ is favourable to adsorption, $n = 1$ is linear adsorption,

$n < 1$ is detrimental to adsorption. The k_f and n values are determined by the linear plot of log q_e to log C_e.

Table 4-4 Langmuir and Freundlich isotherm constants and values of R2 for the adsorption of RB5 by PLys/Glu Gels.

Samples	Langmuir parameters			Freundlish parameters		
	b (L/mg)	q_m (mg/g)	R^2	K_f (L/g)	n	R^2
PLys/Glu Gel 1	0.048	454.5	0.997	34.4	3.24	0.929
PLys/Glu Gel 2	0.042	200.0	0.992	78.8	3.27	0.868

Table 4-4 presents Langmuir and Freundlich isotherm constants along with values of R^2. Based on the fitting results, all the R^2 values from the Freundlich model are lower than those from the Langmuir model, so the Langmuir isotherm provides a better fit to the experimental data than the Freundlich isotherm. In addition, most of the q_m values predicted by the Langmuir model are close to the experimental data (Table 4-4 and Figure S4-15 to Figure S4-18). Therefore, adsorption process for RB5 ions on PLys/Glu Gels can be better interpreted by Langmuir isotherm model. Although R^2 values of Freundlich model are slightly lower, the n values of Freundlich model are all larger than 1, showing that these adsorption processes are favourable.

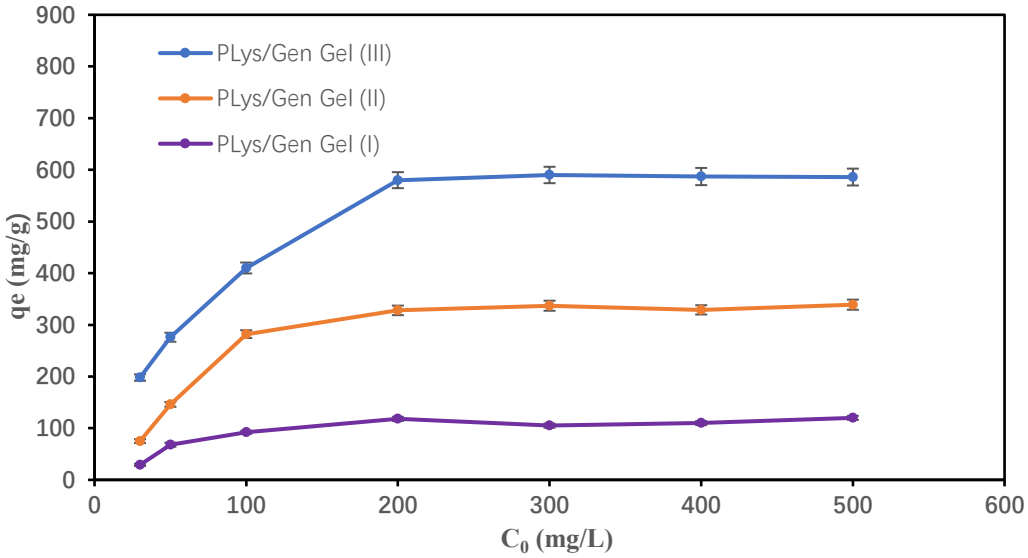

Figure 4-21 The effects of RB5 initial concentration on adsorption capacity of PLys/Gen Gels (pH= 5.5, contact time 6 h, 0.1g adsorbent (in swollen equilibrium) in 40 mL solutions).

As shown in Figure 4-21, the RB5 adsorption capacities of PLys/Gen Gels were ranked consistently across whole range of initial RB5 concentrations as follows: PLys/Gen Gel (III) > Gel (II) > Gel (I), corresponding to the PLys content in each gel. As the initial RB5 concentration increased from 30 to 200 ppm, the amount of RB5 adsorbed per gram of oven-dried hydrogel increased by approximately 193% for Gel (III), 337% for Gel (II), and 307% for Gel (I). However, as the concentration rose further, all three gels reached their maximum adsorption capacities: 590±4 mg/g for Gel (III), 328±2 mg/g for Gel (II), and 118±1 mg/g for Gel (I).

The explanation for how the initial concentration of RB5 affects the RB5 adsorption capacity of PLys/Glu Gels also applies to PLys/Gen Gels. At lower RB5 concentrations, ample active adsorption sites are available on the hydrogel, allowing for increased adsorption as concentration rises. As the RB5 concentration increases, these sites become progressively occupied until saturation is reached, where additional dye does not enhance adsorption capacity. Hence, adsorption capacity levels off at higher concentrations.

Table 4-5 Langmuir and Freundlich isotherm constants and values of R^2 for the adsorption of RB5 by PLys/Gen Gels.

Samples	Langmuir parameters			Freundlish parameters		
	b	q_m		K_f		
	(L/mg)	(mg/g)	R^2	(L/g)	n	R^2
PLys/Gen Gel (I)	0.021	129.9	0.982	13.7	2.68	0.730
PLys/Gen Gel (II)	0.025	370.4	0.987	34.8	2.46	0.763
PLys/Gen Gel (III)	0.066	625.0	0.999	137.8	3.83	0.946

For all PLys/Gen Gels, the fitting results indicate that the Langmuir model better describes the RB5 adsorption process than the Freundlich model, as the Langmuir model fitting results consistently show higher reliability (Table 4-5 and Figure S4-19 to Figure S4-24). This suggests that RB5 molecules form a monolayer rather than multiple layers on the surfaces of PLys/Gen Gels, similar to the adsorption characteristics of RB5 observed in PLys/Glu Gels. In other words, each adsorption site on the PLys-based hydrogels can accommodate only one RB5 molecule, and once a site is occupied, no additional RB5 adsorption can occur at that site.

4.3.9 Recovery of RB5 on PLys/Glu hydrogels

PLys/Glu Gel 1 after RB5 adsorption in the experiment which studied the effect of contact time on the adsorption at pH 5.5 was selected to do four times adsorption-desorption cycles. At pH 12, amine groups ($-NH_3^+$) on the hydrogels become deprotonated to their neutral $-NH_2$ form, decreasing the electrostatic attraction with negatively charged RB5 ions[235]. RB5 are less tightly bound to the adsorbent and can be released back into the solution, facilitating desorption.

The results of the circulation experiments, recorded in Table 4-6, indicate that after the desorption process, the amount of RB5 adsorbed by PLys/Glu Gel 1 decreased to approximately 35 mg/g. Not all RB5 molecules were removed, as some might be firmly embedded within the hydrogel network and could not be easily desorbed, while a small portion

was adsorbed by the hydrogel in solution form. After the pH was readjusted to 5.5, the amount of RB5 adsorbed during re-adsorption accounted for only ~90% of the previous adsorption capacity. Overall, PLys/Glu Gel demonstrated good reusability for RB5 removal and recovery, maintaining relatively stable adsorption performance over multiple cycles.

Table 4-6 Adsorption amounts of RB 5 on PLys/Glu Gel 1 from four adsorption–desorption cycles.

Cycle number	Amount of dyes adsorbed (mg/g)	
	pH=5.5	pH=12
1	109.3	35.4
2	102.6	36.6
3	98.6	34.1
4	93.7	35.5

4.4. Conclusion

Two types of PLys-based hydrogel, PLys/Glu Gels and PLys/Gen Gels were synthesised via mixing varying proportions of crosslinkers, Glu and genipin, into PLys solutions, respectively. Permanently chemically crosslinked hydrogels were observed for PLy/Glu Gels and PLys/Gen Gels. As the crosslinker content increased, the swelling rate of the hydrogels decreased, while both the storage modulus (G') and loss modulus (G") increased. This suggests that a higher concentration of crosslinker creates a more compact network structure, reducing the hydrogel's ability to swell but significantly enhancing its mechanical strength and stability.

The adsorption of RB5 onto the two types of PLys-based hydrogels, PLys/Glu Gels and PLys/Gen Gels, was investigated. Maximum adsorption occurred at pH 4. Protonation of RB5's amine groups below this pH or deprotonation of PLys's amine groups at higher pH values weakened the electrostatic interactions between the hydrogels and RB5 ions.

PLys/Glu Gels exhibited a “fast-slow-fast-slow” adsorption pattern before reaching equilibrium at 6 hours. There are two possible factors for explain the appearance of the second "fast" stage: one is after the first “slow” adsorption phase, during which RB5 solution penetrates the inner parts of the hydrogel, the amine groups within the hydrogel began to rapidly capture RB5 molecules; the other is under mechanical stirring, the hydrogels broke into smaller pieces, increasing the contact area with RB5, leading to accelerated adsorption behaviour.

For PLys/Gen Gels, hydrogels with relatively high PLys content (mass ratio of PLys/genipin = 20:1, Gel (III), and 15:1, Gel (II)) followed a similar adsorption pattern and reached equilibrium at 6 hours. However, as the genipin content increased, the first “fast” stage became shorter (as in Gel (II)) or disappeared entirely (as in Gel (I), with a mass ratio of PLys/genipin = 5:1). The increased genipin content resulted in a more compact hydrogel structure with fewer active adsorption sites. This compaction reduced the adsorption rate on the initial surface of hydrogels.

The RB5 adsorption kinetics on all PLys-based hydrogels were well described by the pseudo-first-order model, while the adsorption isotherm data aligned closely with the Langmuir model. This indicates that the adsorption process was physical and involved monolayer adsorption. A lower crosslinker content, resulting in more free active amine groups in the hydrogels, significantly enhanced RB5 adsorption. Within the tested mass ratio range of PLys to crosslinker, hydrogels with the lowest crosslinker content exhibited the highest RB5 adsorption capacity.

For PLys/Glu Gels, PLys/Glu Gel 1 demonstrated the highest RB5 adsorption capacity at 430 ±8 mg/g, while for PLys/Gen Gels, PLys/Gen Gel (III) achieved the highest capacity at 590± 4 mg/g. Additionally, PLys/Glu Gel could be reused up to four cycles, albeit with some reduction in adsorption capacity. This study highlights the potential of PLys/Glu Gel and PLys/Gen Gel as bioadsorbents for the effective removal of RB5 dye from wastewater, offering

an environmentally friendly solution for dye pollution management.

Chapter 5 Genipin-Crosslinked Polylysine Hydrogels for the Controlled Release of DIC

5.1. Introduction

PLys has a range of chemical properties that give it significant potential for biomedical applications including use in drug delivery[236], gene delivery[50], and biosensing[237]. Because of its hydrophilicity, PLys can effectively interact with cells or biomolecules in biological environments, overcoming extracellular barriers to allow cellular internalisation, which is fundamental for its use as a drug or gene delivery vehicle[238, 239]. Side chain primary amine groups are protonated under physiological conditions and thus interact electrostatically with cells or other negatively charged biomolecules, such as DNA or RNA, facilitating intracellular delivery[240, 241]. The synthesis of PLys by ROP is controlled, enabling a variety of polymer chain lengths and architectures to be created[26]. PLys nanoparticles have been reported that enable extended drug circulation time and improved drug efficacy *in vivo*[242]. PLys can adopt different conformations depending on the solution pH or its concentration in the solution, which is crucial for its use in biosensors and intelligent materials[243].

PLys has shown potential in controlled drug delivery applications[244, 245]. For instance, the direct conjugation between drug and PLys or modified PLys derivatives is a way to employ PLys as a drug carrier[239, 246]. It has been shown that carbodiimide-catalysed conjugation of PLys and human serum albumin or horseradish-paroxidase can effectively promote cellular uptake of both proteins[247]. A liver-targeting conjugate was formed by coupling Ribavirin (l-β-D-Ribofuranosyl-1,2,4-triazole-3-carboxamide) (RIBV) to lactosaminated PLys[248]. This conjugate can be selectively taken up by the liver after intramuscular administration in mice, reducing the risk of anemia and allowing for higher drug concentrations in hepatocytes. The product of the conjugation of PLys-citramide with a pseudopeptide has been shown to exhibit activity against HIV protease[249]. As a raw material for drug carriers, PLys can be modified

to reduce clearance from the circulatory system, thereby prolonging drug circulation time and enhancing its effectiveness[239]. For example, PEG-grafted PLys can improve biodistribution by controlling the size and surface charge, thereby achieving high stability, high accumulation of the complex in targeted organs[17]. PLys also has the ability to prevent the degradation of encapsulated drugs[18]. PLys nanoparticle has been reported to encapsulate a bovine serum albumin (BSA) by mixing Plys and BSA solutions together, and higher PLys content contributes to better encapsulation, protecting BSA from the degradation by protease[250].

PLys therefore has great potential for use within a biomedical context, and possibly beyond. However, PLys synthesis is commonly done via NCA ROP in which the NCA is produced using in the presence of phosgene [251, 252]. The safety of this process may be improved by using triphosgene as a source of phosgene. Triphosgene is a crystalline solid at room temperature and pressure that decomposes at ~150 ℃ to release phosgene. In this way the phosgene generated remains within the fume cupboard at all times, but it remains a potential threat to the health, causing irreparable damage to lungs and respiratory system and so its use is undesirable.[253] Additionally, organic solvents such as THF are conventionally used to produce the NCA in a reaction in which the starting amino acid in insoluble, but the NCA product conveniently is soluble. This enables the end of the reaction to be easily determined. Ideally, PLys synthesis will be done in the absence of toxic reactants and organic solvents during monomer synthesis. Phosgene-free routes to NCA synthesis have been reported recently. Guillaume *et al*. reported a mild, non-acidic process for synthesising α-amino acid NCAs from N-Boc-protected α-amino acid derivatives utilising n-propanephosphonic acid anhydride (T3P) as an activating reagent[30]. A range of NCAs with high yield and purity can be obtained via this method, but limitations exist, for instance the required use of N-Boc protected α-amino acid derivatives which increases the cost of the amino acid starting material, and consequently NCA synthesis overall.

An alternative strategy to PLys synthesis via ROP is to replace the NCA with a different cyclic structure that is formed from amino acid starting materials. DKPs, are rigid six membered

heterocyclic rings that consists of two amide linkages between two amino acids. They feature cis-amide bonds, with the nitrogen atoms and carbonyl groups positioned on opposite sides of the ring[31]. The most common approach for synthesising DKPs involves dipeptide formation followed by intramolecular cyclization[31]. This process typically requires esterification at the carboxyl terminus and substitution at the amino terminus of the dipeptide. Upon deprotection of the amino group, the molecule can spontaneously cyclise to form the DKP ring. To reduce the risk of epimerization during synthesis, careful selection of reagents and reaction conditions is essential[31]. Meanwhile, as an abundant natural material, DKPs may be produced from the degradation of polypeptides or by the direct condensation of two amino acids in solvents that have elevated boiling points such as glycerol or ethylene glycol at 170℃-180℃[254]. This renewable and natural chemical has the potential to replace NCA if it can undergo ROP and is created in the absence of harmful and costly organic solvents and coupling agents. Research on the ROP of DKP is limited, but annular diesters such as glycolide and lactides have both been reported to undergo ROP in different kinds of catalytic system[34, 255-257]. The structural difference between DKPs and glycolide is that the DKP contains a nitrogen atom as part of the amide bond, as opposed to the oxygen atom of the ester bonds that feature in glycolide. Nevertheless, successful glycolide ROP provides optimism for successful DKP ROP. Catalyst stannous octoate ($Sn(Oct)_2$) was reported to facilitate ROP of lactide, but further efforts are required to enhance the reaction rate to improve its efficiency for practical applications. Nonstoichiometric acid−base organocatalyst has been used to promote the ROP of L-lactide[34]. The catalyst was made up of one equivalent of 4-(dimethylamino)-pyridine (DMAP) and two equivalents of MSA, and these two components collaboratively attack the carbonyl groups. Consequently, MSA and another strong, non-nucleophilic base, DIPEA were selected as catalysts to facilitate the ROP of Lys(cbz) DKP.

Crosslinked PLys enables the production of stimuli-responsive PLys-based hydrogels, broadening its applications as a drug delivery platform. This occurs because PLys is water-soluble, PLys dissolution is not possible if the polymer chains are linked either covalently or physically. In both instances the PLys swells, as opposed to dissolving, forming chemical

(covalent crosslinks) or physical (non-covalent crosslinks) hydrogels. An obvious characteristic of PLys-based hydrogels is their pH-dependent swelling behaviour, due to the presence of amine groups. At acidic pH, the gel swells as a result of ionic repulsion between protonated amino groups and increased polymer-water interactions, while at higher pH values it collapses due to the removal of charge from the polymer[246]. Site-specific controlled drug delivery using these hydrogels can enhance therapeutic outcomes while minimising negative side effects[258]. PLys modified with hyaluronic acid (HA) and nogo-66 receptor antibody (antiNgR) has shown promoted recovery from central nervous system injuries[91]. Ionic strength/pH/enzyme triple-responsive hydrogels were prepared through a coupling reaction between carboxyl and amine groups, facilitated by 1-ethyl-3-(3-dimethylaminopropyl) carbodiimide · HCl (EDC · HCl), Hydrogels loaded with two model drugs, doxorubicin hydrochloride (DOX · HCl), a positively charged anti-cancer drug, and DIC, a negatively charged anti-inflammatory drug, exhibited accelerated and complete drug release, along with full enzymatic degradation of PLys in the presence of trypsin[258]. PLys and sodium alginate physically crosslinked by calcium ions can form a hydrogel capable of immobilising maintaining anthocyanin. Increasing the PLys content in the hydrogel made it softer without affecting the drug release efficiency[259]. Chen's group designed a multi-layer, shell-stacked drug delivery carrier[260]. The outer layer consisted of 2,3-dimethylmaleic anhydride (DMMA)-modified PEG-*b*-PLys, the middle layer was a disulfide crosslinked PLys network, and the inner core contained the encapsulated DOX. After intentionally reducing the ratio of outer layer to middle layer, the size of the drug delivery system decreased from 140 nm to 40 nm, and the surface charge shifted from negative to positive, making it more conducive to the aggregation and penetration of target tumour cells. The network structure of the intermediate layer effectively prevents the premature release of drugs, ensuring controlled delivery to the desired site.

5.2 Research Aims

The aim of our research is divided into two parts:

One is using a greener DKP ROP synthesis to prepare PLys from Lys(cbz)-DKP, with MSA and DIPEA serving as catalysts.

The other is using PLys to fabricate PLys-based hydrogels for drug encapsulation, and subsequent controlled release. Genipin was chosen as the crosslinker for this process as it is a natural compound extracted from the fruit gardenia that has reduced toxicity compared to other Schiff-base crosslinkers. Genipin is thus widely used in biomedical applications owing to its favourable biocompatibility[216, 261]. Due to its analgesic, anti-inflammatory, and antipyretic effects, DIC, a well-established nonsteroidal anti-inflammatory drug (NSAID) that is a popular choice for managing acute pain and inflammation effectively[262, 263]. DIC has relatively short half-life in the body and functions by inhibiting prostaglandin synthesis, achieved through the inhibition of cyclooxygenase-1 (COX-1) and cyclooxygenase-2 (COX-2)[262, 263]. DIC was selected as the model drug to be encapsulated within the hydrogels featured in this chapter. The hydrogel system is designed to steadily release DIC in the intestinal environment, thereby extending its therapeutic time in the human body.

5.3 Experimental

5.3.1 Preparation of Lys(cbz)DKP

H-Lys(cbz)-OH (5 g, 24.0 mmol) was combined with glycerol (36 mL) and heated at 175 ℃ for 24 hours. After cooling to room temperature, the reaction mixture was poured into a mixture of acetone and water (30 mL/25 mL), resulting in the formation of a precipitate. The pale-yellow solid was collected by vacuum filtration and washed three times with acetone/water (30 mL/25 mL). The product, referred to as Lys(cbz)DKP, was obtained after drying under vacuum. ^{1}H NMR (400 MHz, DMSO-d_6, ppm): δ 8.33-8.01 (s, 2H, NH), 7.65-7.00 (m, 10H, aromatic), 5.10-4.91 (s, 4H, OCH_2), 3.89-3.70 (br, 2H, COCH), 3.05-2.87 (dd, 4H, NCH_2), 1.79-1.15 (m,

12H, $CH_2CH_2CH_2$). Yield: 65.5%.

5.3.2 Preparation of PLys(cbz)

Lys(cbz)DKP and methanesulfonic acid (MSA) (Molar ratio= 25:1) were added to a round-bottom flask with reflux column under nitrogen atmosphere. N,N-dimethylformamide (DMF) was then added, and the temperature was raised to 140 ℃. Hexylamine (Molar ratio of hexylamine/Lys(cbz)= 1:80) was injected into the solution, and the reaction mixture was stirred for 2 days. The solution was then cooled to room temperature before DIPEA (Molar ratio of Lys(cbz)DKP/DIPEA= 15:1) was added. The temperature was again increased to 140 ℃ and the reaction maintained for an additional 4 days. After cooling the reaction mixture to room temperature, the white solid product was obtained by precipitation in ice-cold diethyl ether. The polymer produced (PLys(cbz)) was washed several times with diethyl ether and then dried in the vacuum oven at 55 °C overnight. ^{1}H NMR (400 MHz, DMSO-d_6, ppm): δ 8.14-8.03 (s, 1H, NH), 7.41-7.07 (m, 5H, aromatic), 5.11-4.85 (s, 2H, OCH_2), 3.89-3.70 (br, 1H, COCH), 3.06-2.87 (dd, 2H, NCH_2), 1.80-1.14 (m, 6H, $CH_2CH_2CH_2$), 0.89-0.79 (t, 3H, CH_3). Yield: 65.0%.

5.3.3 Preparation of PLys

0.4 g of PLys(cbz) was dissolved in 8 mL of trifluoroacetic acid (TFA), and then 2 mL of a 33% HBr/AcOH solution was added to the mixture to remove the carboxybenzyl protecting groups. The reaction was allowed to proceed for 1 day. The crude product was precipitated in ice-cooled diethyl ether, collected by centrifugation and then dissolved in the DI water. The resulting mixture was dialyzed against deionized water for 2 days, after which the liquid inside the dialysis tube was frozen using liquid nitrogen. The product (PLys) was collected by freeze-drying. ^{1}H NMR (400 MHz, DMSO-d_6, ppm): δ, 1.81-1.05 (m, 6H, $CH_2CH_2CH_2$), 0.89-0.79 (t, 3H, CH_3). Yield:78.2%.

5.3.4 Preparation of PLys/Gen hydrogels

Approximately 100 mg of PLys and the crosslinker genipin were dissolved in 0.2 mL of deionized water. Gels were formed by placing the mixture at 50 °C for 1 day. The weight ratios of PLys to genepin were set at 5:1, 10:1, 15:1, 20:1, and 25:1. The resulting gels were named Plys/Gen Gel 1 to 5, respectively, in order of decreasing crosslinker content.

5.3.5 Swelling behaviour of PLys/Gen hydrogels

All the hydrogels prepared in step 4.3.4 were immersed in 10 mL of phosphate buffer solution (PBS) at room temperature (RT). The amount of water absorbed by the hydrogels was determined by weighing them at various time intervals. Each data point was measured at least three times.

5.3.6 Loading and *in vitro* release of diclofenac sodium salt

For the DIC loading experiment, all hydrogels obtained from step 4.3.4 were thoroughly washed multiple times with deionized (DI) water until the washing solution became colourless and transparent. This step was performed to ensure the removal of unreacted genipin, which could interfere with DIC detection by UV spectroscopy. After washing, the hydrogels were placed in liquid nitrogen and freeze-dried. Next, 20 mg of pure PLys/Gen gels were added to 200 mL of DIC solution with a concentration of 5 ppm at room temperature (RT). The types of hydrogels and pH values varied based on different conditions.

To investigate the effect of pH, PLys/Gen Gel 5 was immersed in DIC solutions at pH levels of 1.7, 5.5, and 7.4, respectively. The pH of the DIC solutions was adjusted using 0.1 M HCl, DI water, and PBS buffer. To study the effect of the crosslinker concentration (genipin), PLys/Gen Gels 1, 3, 4, and 5 were selected for the DIC loading experiment at a pH of 1.7 (Table

3.4).

In the DIC release experiment, selected types of PLys/Gen gels from the DIC loading experiment were collected via filtration, sealed in dialysis tubes, and immersed in 200 mL of PBS buffer under magnetic stirring at 37 °C. The experiment continued until the concentration of DIC in the solution outside the dialysis tubes reached equilibrium. The DIC concentration in the external solution was measured using UV-Vis spectroscopy. The stirring speed was maintained at 100 rpm. The selected PLys/Gen gels included PLys/Gen Gel 3 (pH 1.7), PLys/Gen Gel 4 (pH 1.7), PLys/Gen Gel 5 (pH 1.7), PLys/Gen Gel 5 (pH 5.5) and Plys/Gen Gel 5 (pH 7.4).

All DIC loading and release experiments were conducted in triplicate.

5.4 Results and Discussion

5.4.1 The Synthesis and Characterisation of Lys(cbz)DKP

DKP ROP was carried out as an alternative to NCA ROP for PLys synthesis. This avoids the use of triphosgene, which is cost-ineffective and lethal. Such factors likely hinder the everyday application of NCA ROP. DKP ROP may overcome both of these issues, with polymer synthesis possible in three steps: 1) Lys(cbz)DKP synthesis, 2) Lys(cbz)DKP polymerisation, and 3) PLys(cbz) acid deprotection to yield PLys.

Preparation of pure Lys(cbz)DKP is crucial to ensure successful polymerisation of the six-membered ring. Lys(cbz)DKP was obtained as an off-white powder, and its successful synthesis confirmed by ^{1}H NMR spectroscopy (Figure 5-1). The peaks observed in the spectrum, with their chemical shifts and integrals, are consistent with literature value[264]: peak 'a' corresponds to the COC*H* proton in the six-membered ring; peaks 'b', 'c', and 'd'

represent the CH_2 groups of the Lys side chain; peak 'e' is assigned to the CH_2 groups adjacent to the amide group; peak 'f' corresponds to the NH group of the side chain; peak 'g' represents the OCH_2 groups; and peak 'h' is associated with the aromatic groups at the end.

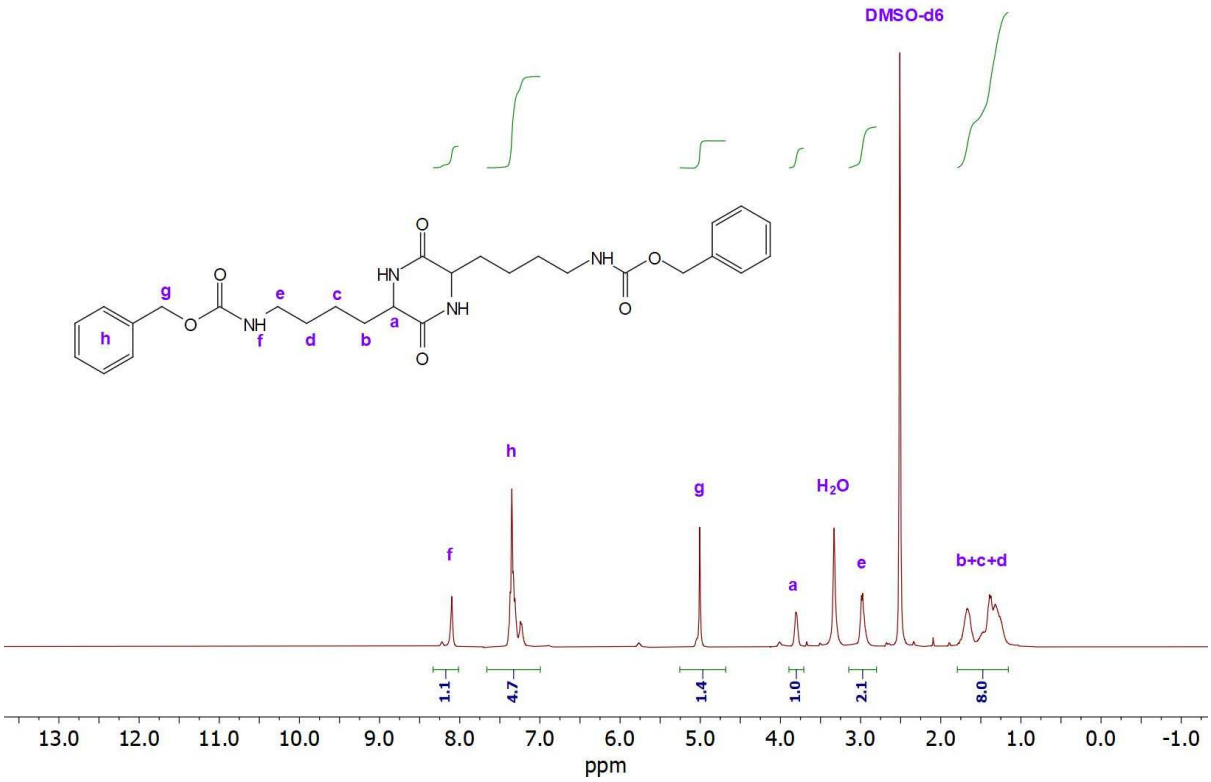

Figure 5-1 ^{1}H NMR spectrum of Lys(cbz)DKP recorded at 400 MHz using DMSO-d_6 as the solvent.

FTIR spectroscopy further confirmed the successful synthesis of Lys(cbz)DKP (Figure 5-2). The spectrum shows a peak at 3328 cm^{-1}, representing a hydrogen-bonded N-H stretch; a peak at 3059 cm^{-1}, corresponding to an aromatic C-H stretch; a peak at 2937 cm^{-1}, indicating an alkyl C-H stretch; and a peak at 1667 cm^{-1}, attributed to a C=O amide stretch, confirming the condensation of two units of Lys(cbz)-OH. This is evident when compared to the FTIR spectrum of Lys(cbz)-OH where no peak was detected at this position, indicating the formation of the amide bond[212]. For PLys(cbz), in addition to the band at 1667 cm^{-1}, another peak is observed at 1603 cm^{-1}, which is assigned to an amide-related vibration of the carbonyl group adjacent to the hexyl amine side chain. A similar feature is also observed in PLys. The peak at

1480 cm^{-1} is attributed to alkyl C-H bending vibrations. The peak at 738 cm^{-1}, associated with a phenyl C-H bend.

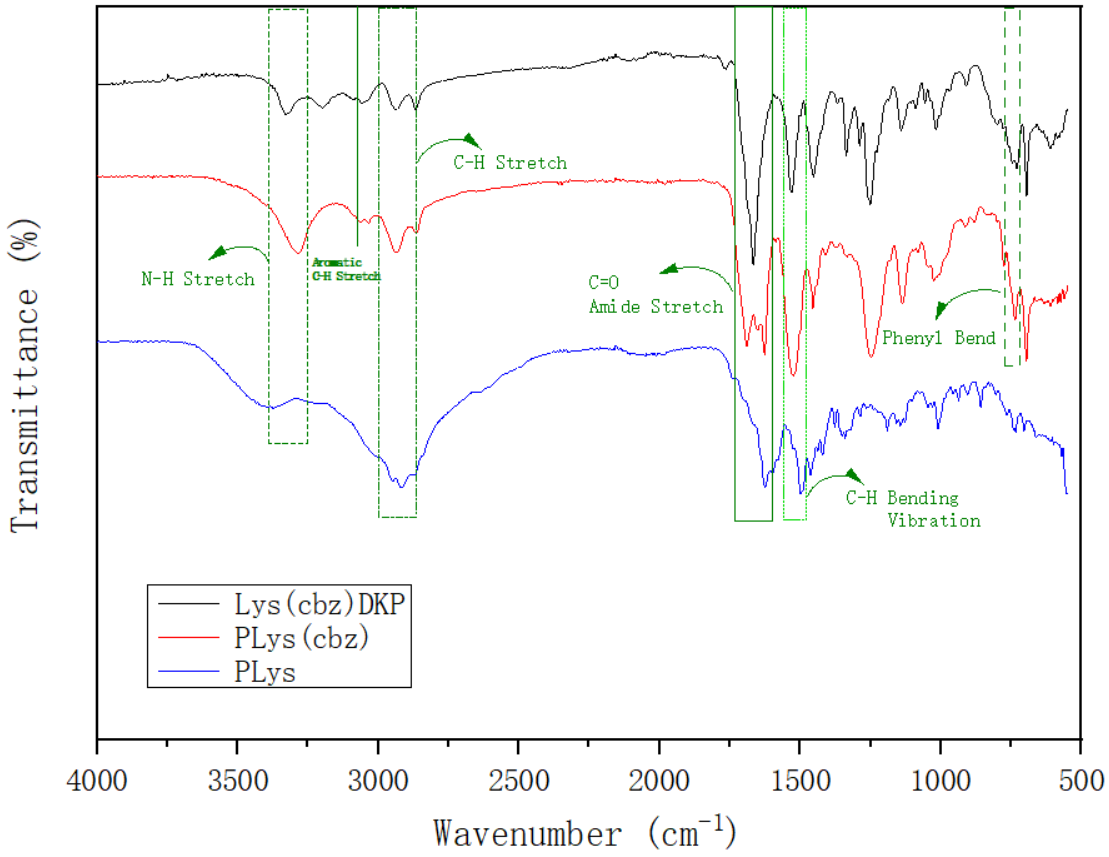

Figure 5-2 FTIR spectra of Lys(cbz)DKP, PLys(cbz) and PLys.

LC-MS is an effective tool to verify the synthesised compounds, as it directly provides the difference in mass, enabling precise identification of the molecular structure. As shown in the LC-MS spectrum (Figure S5-1), the molecular weight (Mw) of compounds 2-6 (retention time between 0.8 and 1.0 minutes) was approximately 524.2 g/mol, which matches the Mw of Lys(cbz)DKP rather than the 542.6 g/mol expected for Lys(cbz)-dipeptide. This indicates that two units of H-Lys(cbz)-OH condensed to form a six-membered ring compound (Lys(cbz)DKP) with the loss of two H_2O molecules, as opposed to the dipeptide forming with the loss of a single water molecule.

Following analysis, it was determined that the other peaks reported were due to impurities present on the LC column, with the exception to the peak corresponding to a molecular weight of 1048.72 g/mol. It is hypothesised that this peak is due to the non-covalent formation and elution of dimers owing to extensive hydrogen bonding between Lys(cbz) DKP groups. This has been observed for the DKPs of alanine, phenylalanine, and glycine[265], and confirmed by accurate mass analysis where the peak corresponding to double the expected molecular weight was not found in each case.

5.4.2 The Synthesis and Characterisation of PLys(cbz) and PLys

The synthesis of PLys(cbz) was then attempted from the Lys(cbz) DKP successfully produced (Scheme 5-1). HA was chosen as the initiator because its alkyl chain is easily distinguishable in ^{1}H NMR spectroscopy spectra. This is not the case for the commonly used benzylamine which possesses an aromatic group with protons that overlap with the protons of the aromatic part of the cbz group. Such overlap prohibits the degree of polymerisation to be determined with confidence by ^{1}H NMR spectroscopy. Since both Lys(cbz)DKP and hexylamine are soluble in DMF, the polymerisation process was straightforward. However, DKP ROP is more challenging compared to NCA ROP. In the latter, the most electrophilic carbonyl, located opposite the nitrogen atom in the ring, can be easily attacked by a nucleophilic initiator[266]. While Lys(cbz)DKP is a highly symmetrical hexagonal ring structure that is more stable than the corresponding NCA, and the electrophilicity of the carbonyl is reduced due to the influence of the symmetric secondary amide group [267]. Hence, the acid-base organocatalyst MSA and DIPEA, along with a high temperature (140 ℃) were used to facilitate DKP ROP. This contrasts to NCA ROP, which can readily be successfully conducted in the absence of catalyst at room temperature and is the primary drawback of DKP ROP.

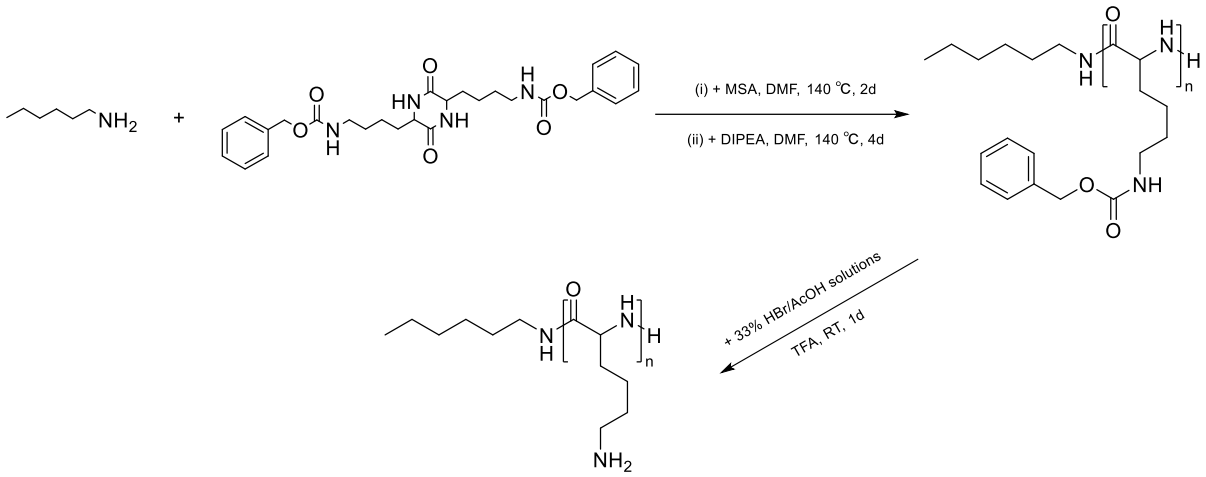

Scheme 5-1 PLys synthesis using DKP ROP.

There was no significant difference between the FTIR spectra of Lys(cbz)DKP and PLys(cbz) as both molecules possess analogous chemical functionality, for instance the presence of amide groups. However, a comparison of initiator and repeat unit integrals using ^{1}H NMR spectroscopy confirmed the successful synthesis of PLys(cbz) (Figure 5-3). Peak 'n' corresponds to the terminal methyl protons and peaks i-m stand for methylene groups of hexylamine end, while the other peaks represent characteristic groups of the repeat units and are clearly labelled with letters a-h. For example, peak 'a' is attributed to the phenyl groups at the end, and peak 'b' corresponds to the OCH_2 group. The repeat unit of PLys(cbz) was calculated as 38, determined by average values of distinct functional groups within the repeat unit. Specifically, after assigning an integral value of 3 to the hexylamine methyl protons, the calculation was proceeded as follows: the integral of peak a (191) divided by five (five protons in aromatic ring), followed by adding the integrals of peaks c (38) and h (38), and then this total was divided by three.

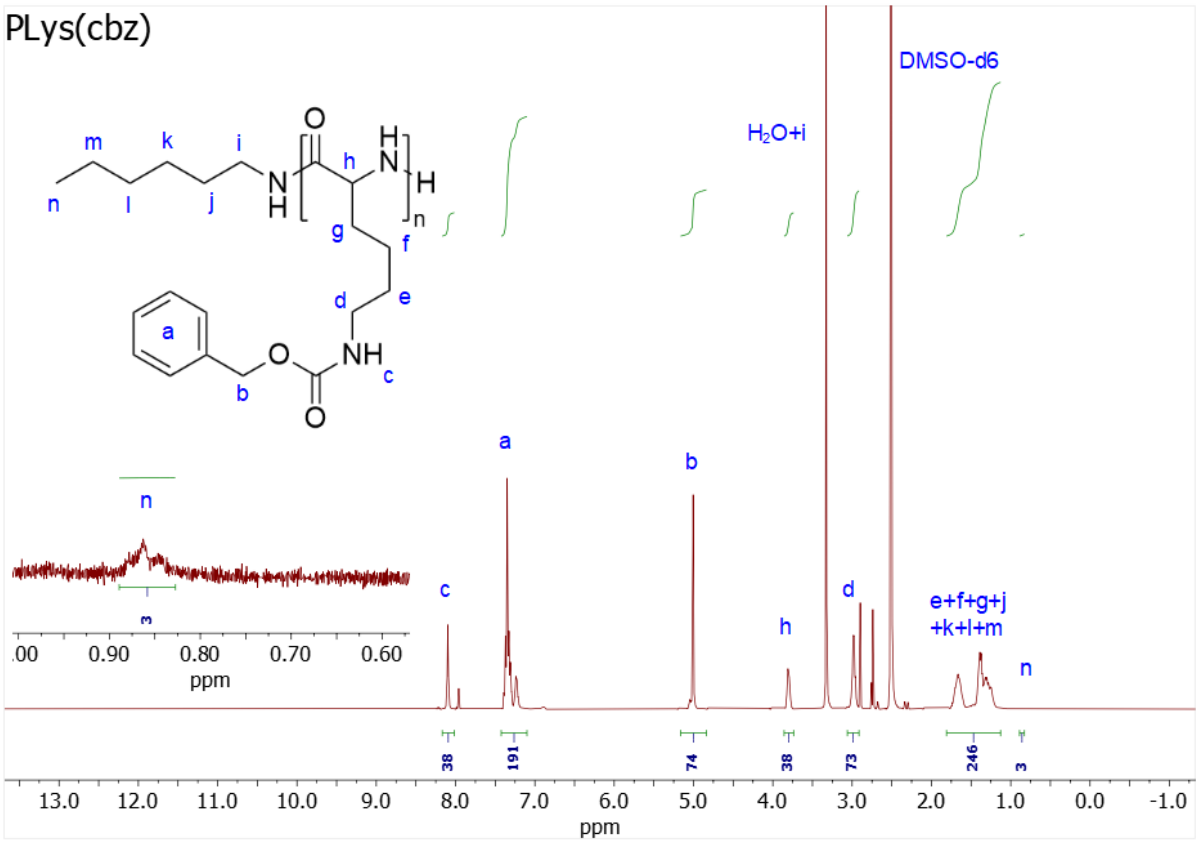

Figure 5-3 ^{1}H NMR of PLys(cbz) recorded at 400 MHz using DMSO-d_6 as the solvent.

To remove the cbz protecting group, a commonly used acid deprotection protocol was employed, where 33% HBr/AcOH solution was added to the polymer dissolved in TFA. To maintain the sustainability credentials of this method of PLys synthesis, a more environmentally acceptable method of side-group deprotection must be sought. However, at this stage emphasis was placed on safe, straightforward, and cost-effective monomer production, successful monomer polymerisation, and then utilising the PLys formed to create useful materials. Complete removal of the cbz groups was confirmed by ^{1}H NMR (Figure 5-4) and FTIR (Figure 5-2) analyses. The ^{1}H NMR spectrum showed that the peaks between 7.43-7.09 ppm, representing the benzyl ring, had disappeared. Additionally, the FTIR spectrum showed that the aromatic C-H stretch at 2937 cm^{-1} and the phenyl C-H bend at 695 cm^{-1} were no longer detectable after the acid deprotection step, showing full deprotection. The repeat unit of PLys was calculated to be 35, based on the average values of distinct functional groups within the polymer's repeat unit, indicating minimal structural changes before and after acid

deprotection. Specifically, after assigning an integral value of 3 to the hexylamine methyl protons, the calculation proceeded as follows: the integral of peak g (32), representing the proton attached to the tertiary carbon, was added to the integral of peak k (63), divided by two (corresponding to the two protons of CH_2 groups bonded to amine groups), and the integral of peak i (80), also divided by two (representing two protons from amine groups). The resulting sum was then divided by three, yielding the calculated repeat unit value.

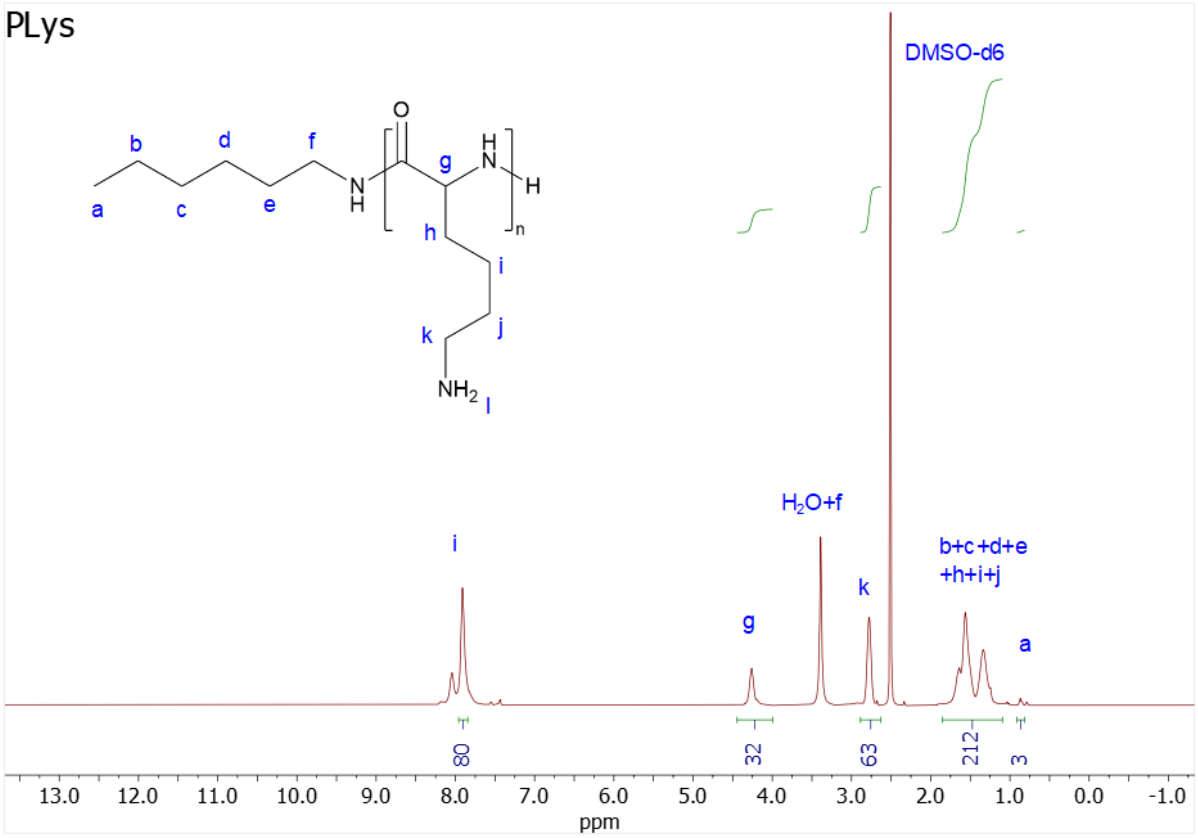

Figure 5-4 ^{1}H NMR of PLys recorded at 400 MHz using DMSO-d_6 as the solvent.

Before characterisation, PLys was dialysed against DI water for at least two days with frequent water changes to remove any water-soluble impurities. During dialysis, low molecular weight PLys, PLys oligomers, deprotected but unreacted DKP, unreacted lysine, and HBr remnant can pass through the dialysis tubing, whilst pure PLys with higher molecular weight remains within the dialysis tubing that has a molecular weight cut-off of 2,000 g/mol. This loss of the materials might explain why the final yield of PLys product was 78.2%. However, such a yield for

poly(amino acid) production is positive when compared to typical NCA ROP yields that are affected by significant atom loss due to the production of carbon dioxide during NCA ROP. Unlike PLys(cbz), PLys was water-soluble, further indicating that the desired product had been successfully made.

The MALDI mass spectroscopy spectrum of PLys revealed a molecular weight distribution ranging from 2,500 g/mol to 6000 g/mol, with the most prominent signal observed at approximately 3,900 m/z (Figure S5-2). This indicated that the majority of PLys synthesised from Lys(cbz)DKP had a molecular weight of around 3,900 g/mol. The curve in the figure consisted of numerous small peaks with intervals of approximately 128 m/z, corresponding to the molecular weight of the PLys repeat unit. Under irradiation, segments of these repeat units detached from the PLys chains and were detected, further confirming the successful synthesis and molecular structure of PLys. The MALDI test results indicated that PLys had approximately 30 repeat units, which was five fewer than the value calculated from the NMR analysis, suggesting a broad molecular weight distribution for PLys synthesized via DKP ROP. The difference can be attributed to MALDI's lower ionization efficiency for polymers with higher molecular weights, making it more likely to detect components in the lower molecular weight range.

5.4.3 The preparation of PLys/Gen hydrogels

Following the preparation of water-soluble PLys by DKP ROP, covalent polymer crosslinking with genipin was attempted in order to produce chemical hydrogels. Unlike many synthetic crosslinkers that are used to produce chemical hydrogels and crosslinked polymers in general, genipin is derived from a natural source, rendering it an attractive option for applications that require biocompatibility and reduced toxicity[268]. Genipin reacts primarily with amino groups, forming stable crosslinked networks (chapter 4)[269]. This property is particularly valuable in the development of biocompatible materials that may be applied within a

biomedical context, for instance as scaffolds for tissue engineering or drug delivery vehicles where both material safety and stability are crucial[94].

During the hydrogel formation stage, excessive water can impede proper gel formation and so the PLys concentration in water was maintained at a minimum of 33%. After gel formation, the water adsorption capacity and stability of the hydrogels formed were assessed by maintaining the hydrogels into PBS buffer (pH 7.4) for seven days. A range of hydrogels were created (Table 5-1) and the weight of each hydrogel measured every day (Figure 5-5). All data points feature error, but the error bars are too insignificant to be visible. The gels were produced limited aqueous solution before being added to excess solution to enable uninhibited hydrogel swelling. After one day, all hydrogels reached a saturation state, with lower crosslinker content leading to greater water absorption. Encouragingly, all of the hydrogels produced remained stable in aqueous PBS solution for at least seven days.

Table 5-1 The composition of the different PLys/Gen hydrogels produced.

Hydrogels	PLys/genipin weight ratio
PLys/Gen Gel 1	5:1
PLys/Gen Gel 2	10:1
PLys/Gen Gel 3	15:1
PLys/Gen Gel 4	20:1
PLys/Gen Gel 5	25:1

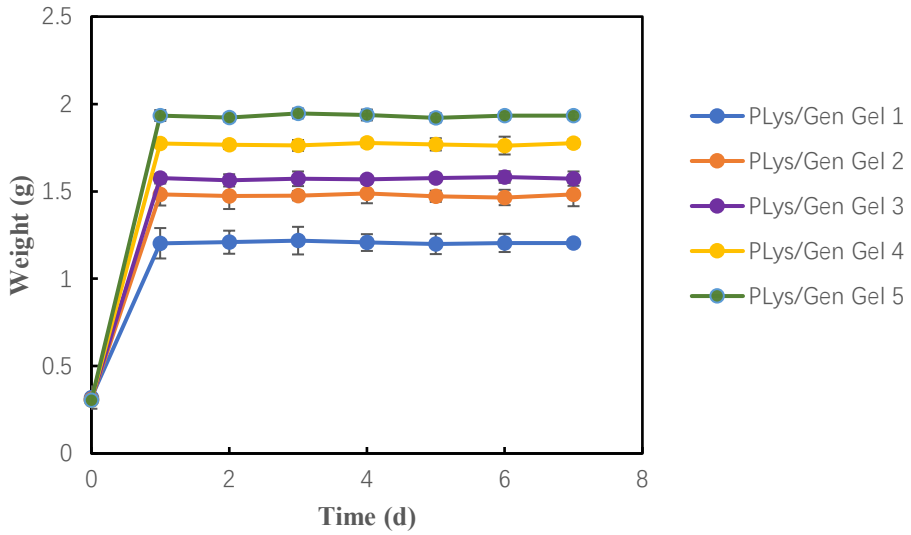

Figure 5-5 Water adsorption capacity of PLys/Gen hydrogels.

To investigate the effect of the amount of genipin included in the hydrogel composition on the swelling ratio of the hydrogel, the data collected from Figure.5-5 was used to calculate the swelling ratio according to Equation (5-1) [94].

$$Swelling\ ratio = \frac{w_e - w_0}{w_0} \times 100\% \quad (5\text{-}1)$$

In this equation, W_e represents the weight of the hydrogels at equilibrium which was the weight of hydrogels after 1d, while W_0 represents the initial weight of the prepared hydrogels.

These results are recorded in Figure 5-6. When the weight ratio of PLys to genipin was 5:1, 0.32 g of PLys/Gen Gel 1 could absorb an additional average 0.88 g of water, resulting in a swelling ratio of 281%. However, when this ratio increased to 25:1, 0.304 g of PLys/Gen Gel 5 could absorb an additional average 1.63 g of water, leading to a swelling ratio of 535±20%, more than double the swelling ratio of PLys/Gen Gel 1. As the amount of genipin added increased from 4 mg to 6.7 mg per 100 mg of hydrogel, the swelling ratio of PLys/Gen Gels decreased from 535±20% to 410±14%. When the genipin amount exceeded 6.7 mg (up to 20 mg), the swelling ratio further decreased to 281±20%. This trend of reduced hydrogel swelling

with increased crosslink density is not unexpected as crosslinking reduces the amount of protonated primary amine groups that cause hydrogel swelling through electrostatic repulsion. Polymer crosslinking also reduces PLys chain mobility, further reducing the capability of the polymer to swell in aqueous solution. The three-dimensional structure of the hydrogel is relatively loose at low crosslink density, providing more space for expansion and allowing it to absorb more water. As the content of genipin increased, the three-dimensional structure of the hydrogel became more compact, which limited the expansion space and led to a rapid decrease in the swelling rate of the hydrogel. When the amount of genipin added exceeded 6.7 mg, the effect in hydrogel swelling became marginal. At this point, the increase in the compactness of the hydrogel's three-dimensional structure became limited, leading to a slower decrease in the swelling ratio. Such swelling behaviour has been observed in the previously[270, 271]. Moreover, in the six days following the PLys/Gen Gels reaching their equilibrium state, the weight of the hydrogels remained unchanged, confirming the stability of the PLys/Gen Gels in PBS buffer. This is an important feature of the hydrogels, suggesting that they may remain intact *in vivo* for extended periods of time, providing early evidence for their potential applicability as scaffolds that promote tissue growth. However, further studies in simulated tissue environments are required to confirm this.

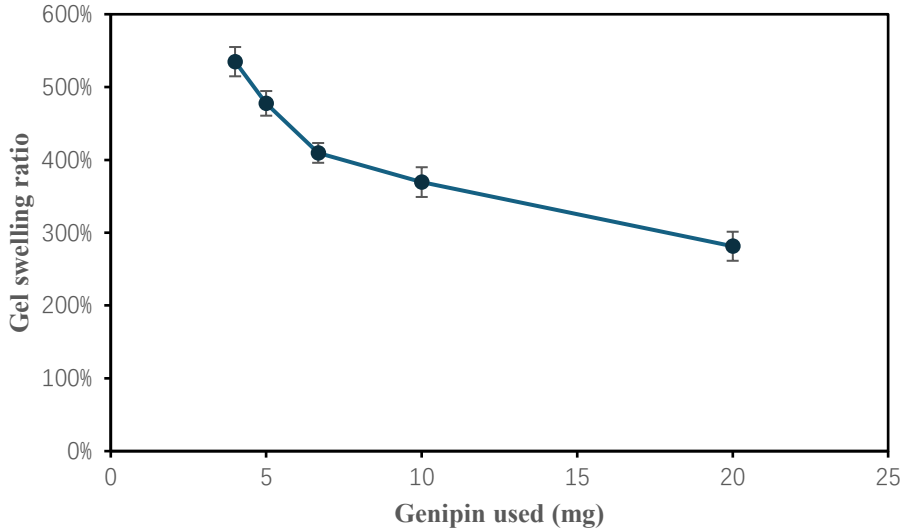

Figure 5-6 The effect of genipin used on swelling ratio of PLys/Gen Gels. 100 mg of PLys was used in each instance.

5.4.4 Rheological characterisation

To confirm that hydrogels had been produced, and to assess the rheological characteristics of these potential gels, rheology was conducted. PLys/Gen hydrogels used for rheology tests were prepared following the method described in Section 5.3.4. After preparation, the gels were fully swollen in 1 mL of DI water until they reached the appropriate volume necessary for testing. As shown in Figure 5-7, hydrogels with a higher mass ratio of PLys/Genipin (20:1 for Gel 4 and 25:1 for Gel 5), where the amount of added crosslinker genipin was limited, exhibited a crossover point between the storage modulus (G') and loss modulus (G") across the tested frequency range. In contrast, for hydrogels with a lower mass ratio of PLys/Genipin (5:1 for Gel 1, 10:1 for Gel 2, and 15:1 for Gel 3), where the genipin content was proportionally higher, no crossover point was observed, suggesting permanent chemical crosslinking[225]. Additionally, for these three gels, G' was significantly higher than G" over the entire frequency range, indicating strong solid-like behaviour and the presence of an entangled fibrous network in the hydrogels[223]. These results demonstrate that hydrogel characteristics such as strength formation may be controlled by the genipin-to-PLys ratio.

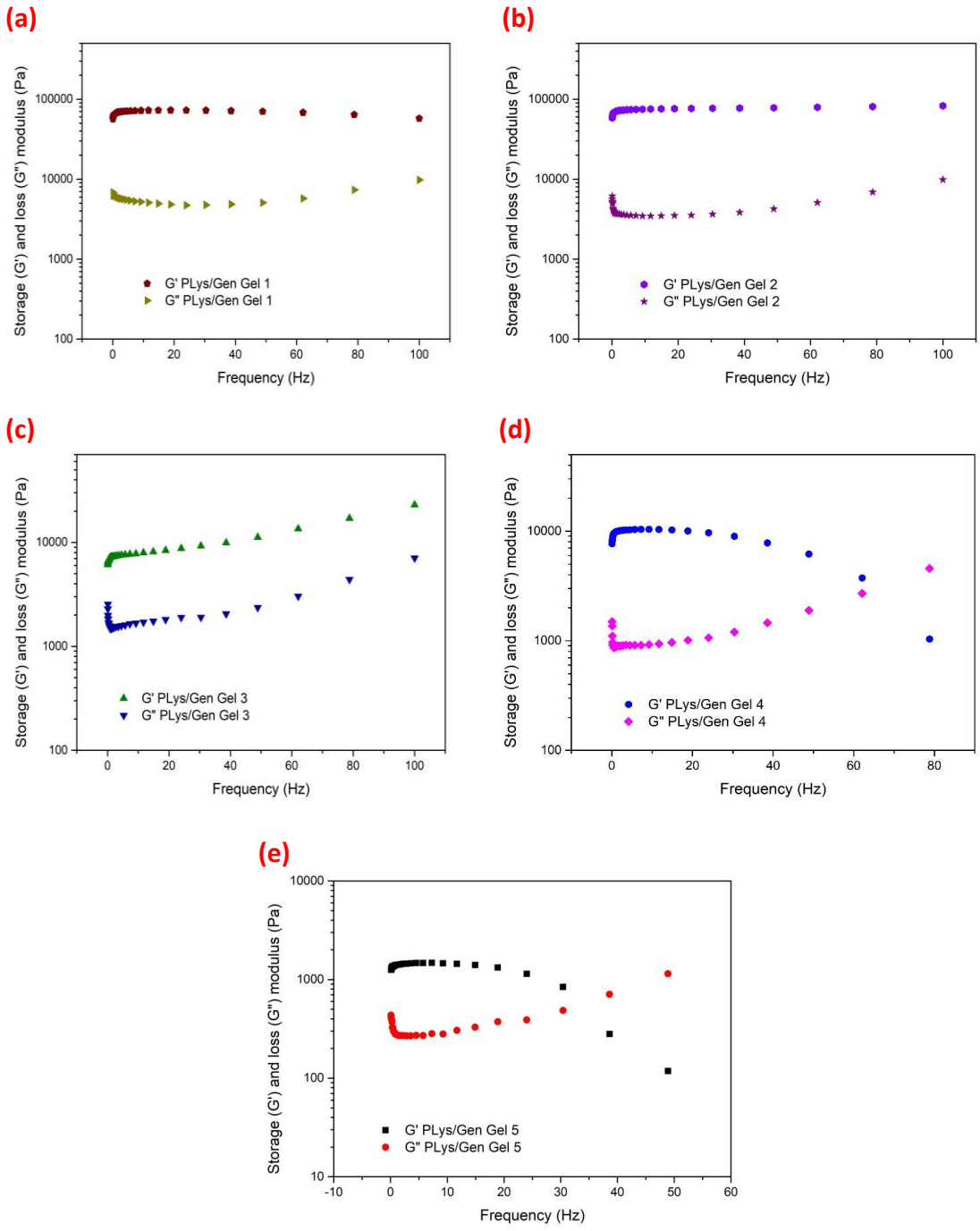

Figure 5-7 Storage and loss modulus of PLys/Gen Gels: (a) PLys/Gen Gels 1, (b) PLys/Gen Gel 2, (c) PLys/Gen Gel 3, (d) PLys/Gen Gel 4 and (e) PLys/Gen Gel 5.

For PLys/Gen Gels 2-5, as the genipin content increased, both the storage modulus (G') and

loss modulus (G") of the hydrogels increased. Specifically, G' increased from 1,800 Pa (Gel 5) to 77,400 Pa (Gel 2), and G" rose from 1,140 Pa (Gel 5) to 9,860 Pa (Gel 2). This can be attributed to the higher crosslinker concentration, which results in a denser hydrogel network. A denser network allows the hydrogel to store more mechanical energy during deformation, making it more resistant to deformation and thus enhancing its elastic behaviour (higher G')[224]. For the loss modulus, representing the viscous or energy-dissipative characteristics, a similar increase occurs, though to a lesser extent than G'. The increased network density offers greater resistance to flow, causing a moderate rise in energy dissipation during deformation[272]. As the genipin content further increased, comparing Gel 2 with Gel 1, the G' value for the hydrogel slightly decreased while G" remained nearly unchanged. This may be due to the excessive crosslinker concentration, which makes the hydrogel structure too rigid and reduces the flexibility of the polymer chains. This reduced chain mobility limits the hydrogel's ability to efficiently store mechanical energy (G') or dissipate it as heat (G"), leading to the observed slight decrease in G' and the stabilisation of G"[273].

5.4.5 SEM characterisation of PLys/Gen Gels 1 and 5

To study the influence of cross-linking agent content on the internal structure of the hydrogel, Gel 1 and Gel 5 prepared in step 5.3.4 were fully swollen in DI water and then freeze-dried for SEM observation. In Figure 5-8a, Gel 1 shows oval pores with diameters predominantly in the range of 1–10 μm. In comparison, Gel 5 has a similar number of small-sized pores (1–10 μm) but also features many larger pores measuring 30–50 μm, with improved connectivity between the pores (Figure.5-8b). These results visually demonstrate that as genipin content increases, the hydrogel structure becomes more compact and interconnected.

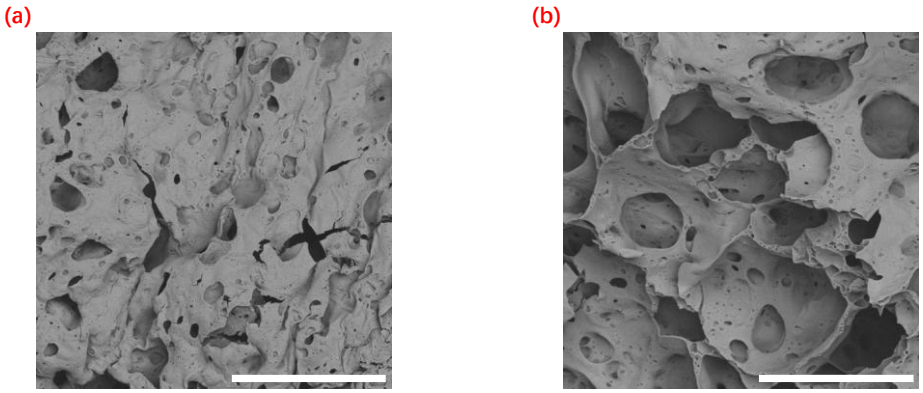

Figure 5-8 SEM of PLys/Gen Gel 1 and Gel5 (The white scale bar in the image represents a length of 50 μm).

5.4.6 Loading and in vitro release of diclofenac sodium salt

Following successful hydrogel creation, their capability to uptake, withhold, and release a therapeutic payload was then assessed. DIC is a NSAID widely used to alleviate inflammation, pain, and swelling associated with conditions such as arthritis, muscle pain, and migraines. Its sodium salt form enhances its solubility in water, making it an ideal choice as a model drug for various formulations. The amount of DIC loaded into PLys/Gen Gel 5 is shown in Figure.5-9. The highest loading, 32.9±1.5 mg/g, was observed at pH 1.7, which decreased to 20.2±2.8 mg/g at pH 5.5, and further dropped to 12.4±3.1 mg/g at pH 7.4. The trend shows that as the pH increases, the amount of loaded DIC decreases. This can be explained by the behaviour of the free amine groups in PLys. Under acidic conditions, close to the pH of gastric acid, these amino groups become protonated and repel each other, expanding the hydrogel's internal structure. This increased swelling allows for greater DIC loading. As the pH rises, the amino groups gradually deprotonate, reducing repulsion and causing the hydrogel to shrink. DIC precipitation was not observed under the experimental conditions of a 5 ppm 200 mL DIC solution, despite DIC existing in its protonated form at pH 1.7. At pH 1.7, the lack of charge on DIC presumably makes DIC-PLys interactions less favourable, potentially causing DIC to diffuse out of the gel without binding. However, the strongly positive charge of the PLys gel

probably induces dissociation of DIC near the gel's surface, which may eliminate previously mentioned limitation and thereby facilitating additional loading. At pH 5.5, DIC exists in its anionic form, enabling electrostatic attraction to the positively charged surface of the PLys gel. However, as the pH increases, the amine groups in PLys undergo deprotonation, reducing the gel's positive charge density. This reduction weakens the electrostatic attraction between the gel surface and DIC, leading to a lower DIC loading capacity. At pH 7.4, the deprotonation becomes more extensive, further diminishing the attraction and causing an additional decrease in DIC loading. DIC PLys/Gen Gel 5 expanded to a larger volume compared to the dark blue colour of the initially prepared PLys/Gen Gel and remained stable in HCl solutions at pH 1.7 (Figure.5-10). Therefore, in the subsequent experiments, the pH value for loading DIC onto PLys/Gen gels was set at 1.7 to maximize the drug loading capacity.

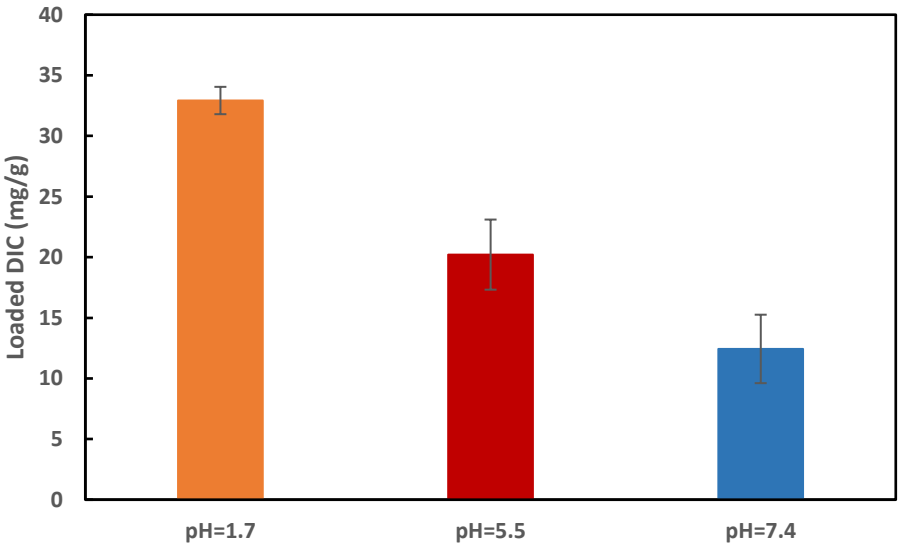

Figure 5-9 DIC loading within PLys/Gen Gel 5 at different pH levels.

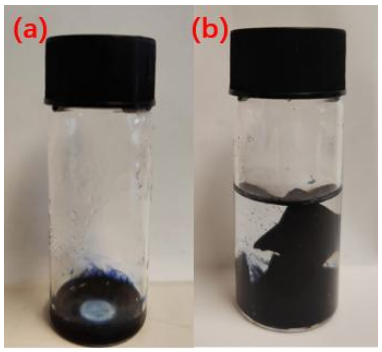

Figure 5-10 (a) Initially prepared PLys/Gen Gel 5 and (b) PLys/Gen Gel 5 at pH 1.7.

The DIC loading results for PLys/Gen gels with different PLys/Gen weight ratios are presented in Figure.5-11. The amount of DIC loaded was determined using the following equation (5-2):

$$DIC\ loaded\ (mg/g) = \frac{(5-C_u)\times 0.2}{m} \quad (5\text{-}2)$$

Where 5 is the initial concentration of DIC (5 ppm) before loading. C_u is the concentration of DIC in the solution after loading. 0.2 refers to the volume of the DIC solution, which is 0.2 L (200 mL), and m represents the mass of the completely dry PLys/Gen Gel used in grams (g).

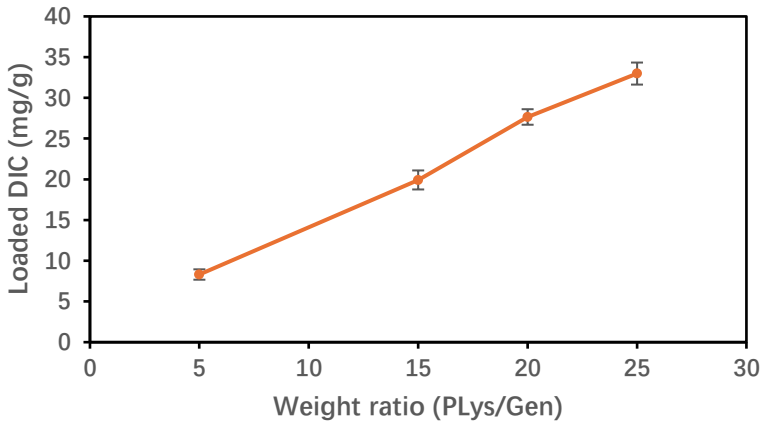

Figure 5-11 The effect of the PLys/Gen weight ratio of hydrogels on the amount of DIC loaded at pH 1.7.

As the weight ratio of PLys/Gen in the hydrogel increased gradually from 5 to 25, the amount of DIC loaded into the hydrogel increased from 8.3±0.7 mg/g to 32.9±1.5 mg/g. This suggests that a lower genipin content in the hydrogel improves its capacity for DIC loading, likely due to the reduced crosslinking density allowing for more available space within the hydrogel network for DIC to be absorbed.

For drug release experiment, the hydrogels containing DIC were sealed in a dialysis tube which was then maintained in PBS buffer at 37 ℃. DIC that is released and passes through the dialysis tubing can then be measured. This simulates the scenario where a DIC-loaded hydrogel, after fully swelling in gastric acid, enters the intestinal tract for DIC release. The hydrogels with relatively high loading amount of DIC were selected to conduct DIC release experiment (Figure.5-12). All data features standard error bars; however, some were so small that they are not visible in the figure. All the DIC-loaded PLys/Gen gels incubated at pH 1.7 reached drug release equilibrium at 8 hours. The PLys/Genipin weight ratios for PLys/Gen Gel 3, 4, and 5 were 15:1, 20:1, and 25:1, respectively. After drug loading at pH 1.7 and subsequent release at pH 7.4, the final DIC release percentages were 92.2±2.8%, 85.7±1.1%, and 84.0±3.9% within 8 hours, respectively. As the genipin content increased, the final percentage of DIC release also increased. Since DIC is a water-soluble anionic drug, it can interact with the amine groups in PLys. Increasing the amount of genipin in the hydrogels reduces the number of free amine groups available to interact with DIC, thereby restricting electrostatic interactions and leading to a higher DIC release percentage.

The DIC release behaviour of these three gels can be summarised as follows (Figure 5-12):
At pH 1.7, the hydrogel initially exhibited an expanded state, containing a significant amount of uncharged or locally negatively charged DIC molecules. This is consistent with the pKa of DIC being approximately 4.0, as reported in previous research[274]. Upon contact with the PBS buffer, the hydrogel began to shrink, and a large amount of DIC was squeezed out during

the first 90 minutes. At this stage, the interaction between DIC molecules and the amine groups in the hydrogel was relatively weak, facilitating rapid release. As the pH within the hydrogel structure increased to approximately 4, DIC molecules underwent deprotonation, adopting an anionic form. The resulting electrostatic attraction between the anionic DIC and the positively charged amine groups slowed the release of DIC, despite the continued shrinkage of the hydrogel. This phase marked the transition to a slower release rate. Eventually, after 8 hours, the DIC release from the hydrogel reached its maximum value, leaving only a small fraction of DIC retained within the hydrogel structure.

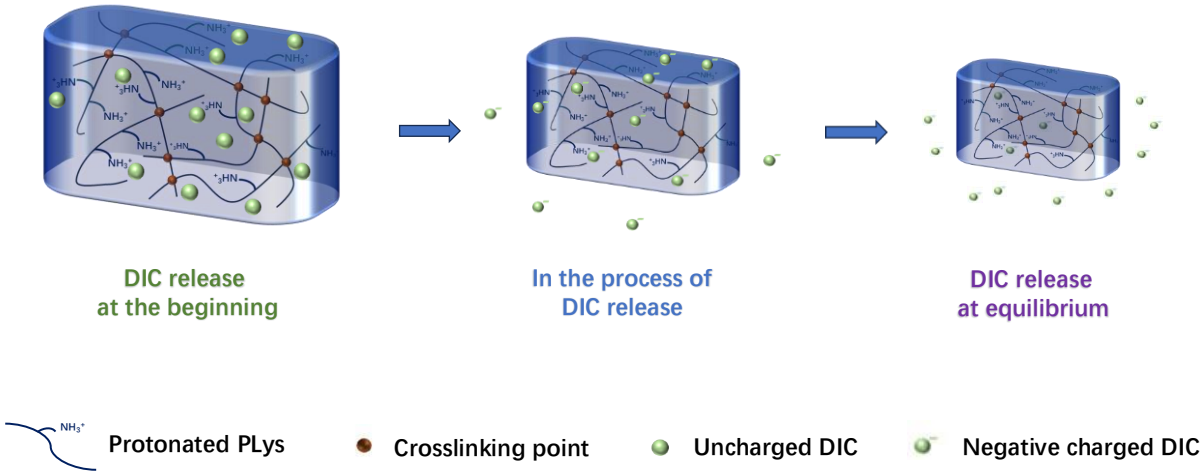

Figure 5-12 Illustration of DIC release process for PLys/Gen Gels loaded drug at pH= 1.7.

Based on Figure 5-13, the DIC release profiles for PLys/Gen Gel 5, loaded at different pH levels (pH 1.7, pH 5.5, and pH 7.4), exhibited variations in both the equilibrium time and the final release percentages of DIC. For the hydrogel loaded at pH 1.7, the maximum release of DIC occurred after 8 hours, accounting for 84.0±3.9% of the loaded drug; the hydrogel loaded at pH 5.5 reached equilibrium in 6 hours, releasing 72.3±2.9% of the loaded DIC; and the hydrogel loaded at pH 7.4 released 65.3±3.1% of the DIC at equilibrium after 3 hours. Given

that the pKa value of DIC is 4.0 [274], more DIC exhibited negative charge when pH was above 4. Ignoring the transitional behaviour DIC in Gel 5 loaded at pH 1.7 encountered, as the pH of the loading solution decreased, the positive intensity of the PLys/Gen Gel 5 surface also declined, resulting in weaker electrostatic attraction between the DIC anions and the protonated amine groups. Consequently, the DIC release equilibrium time for Gel 5 loaded at different pH levels followed the trend: pH 1.7 > pH 5.5 > pH 7.4. The discrepancy of DIC release percentage occurred because pH not only affected the anionic state of DIC but also controlled the swelling behaviour of the hydrogels. The larger pH differential (ΔpH) between loading and release solutions created a stronger driving force for the hydrogel to transition from a stretched to a shrunken state. More DIC in the hydrogels were squeezed out under the influence of the transition and dispersed in the solutions outside the dialysis tube. As a result, the DIC release percentages for Gel 5 loaded at different pH values also followed the trend: pH 1.7 > pH 5.5 > pH 7.4.

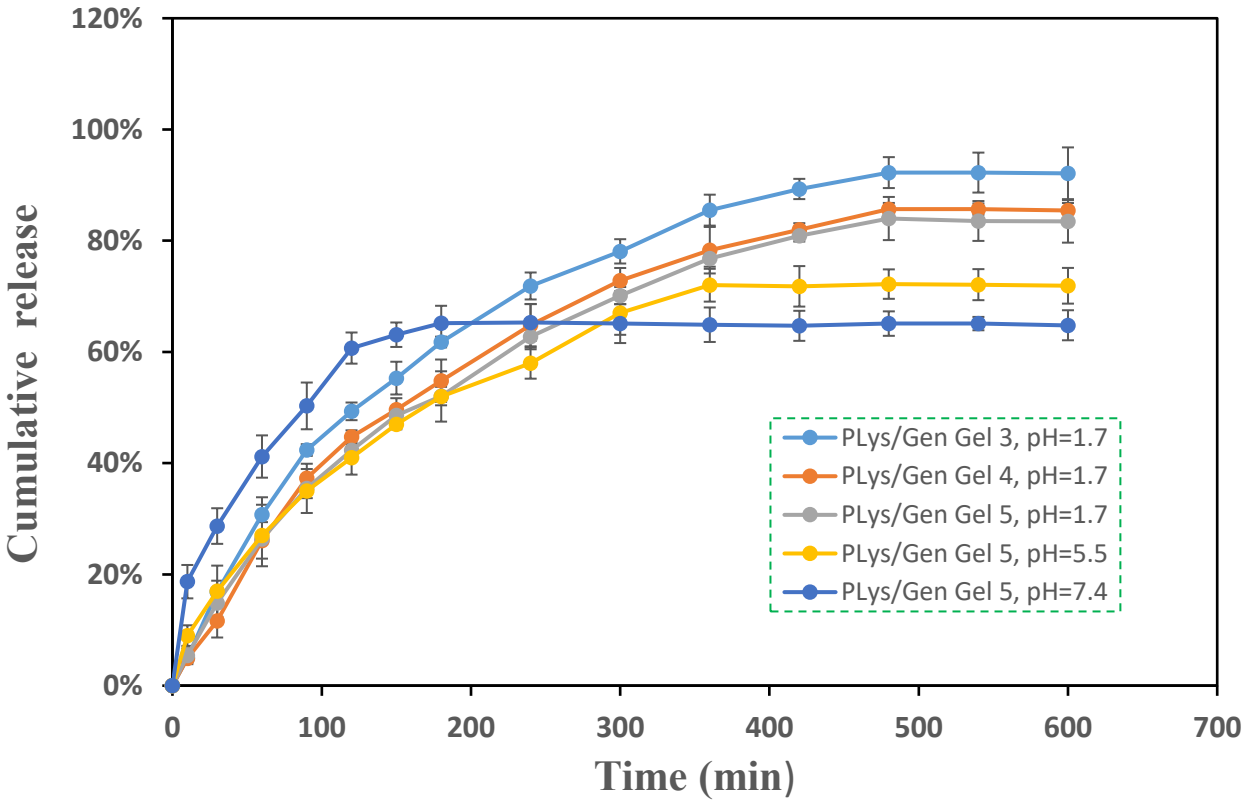

Figure 5-13 DIC release observation of different PLys/Gen Gels.

Table 5-2 summarises the amounts of DIC loaded within and released from PLys/Gen gels which act as potential drug delivery vehicles. The highest amount of released DIC (27.6±1.3 mg/g) was observed when PLys/Gen Gel 5 was used to load DIC at pH 1.7 and release it at pH 7.4. To gain a deeper understanding of the DIC release process, the simple yet comprehensive Korsmeyer-Peppas model was employed to analyse the release of DIC from the polymeric matrix. This model is particularly useful for studying drug release mechanisms in hydrogels, providing insight into the relationship between diffusion and polymer relaxation during the release process.

To investigate the mechanism and kinetics of DIC release, the results from Figure.5-13 were fitted to the semi-empirical equation.5-3 of the Korsmeyer-Peppas mathematical model. [275].

$$\frac{M_t}{M_e} = kt^n \tag{5-3}$$

Where M_t represents the amount of DIC released at time t, M_e is the amount of DIC released at equilibrium, k is the release velocity constant and n is the release diffusion coefficient, which is related to the drug release mechanism. According to the value of n, and for cylindrical tablets, the release of the drug can be classified as either Fickian or non-Fickian. When $n<0.45$, the drug release follows a Fickian model, where the process is primarily governed by diffusion; in contrast, when $0.45<n<1$, the drug release follows an anomalous non-Fickian transport mechanism[121]. In this case, the release is governed not only by diffusion but also by the swelling of the polymeric matrix, meaning that both molecular diffusion and polymer relaxation contribute to the overall drug release process. The data fitting results, summarised in Table 4-3 and Figure S5-3 to Figure S5-7, revealed that the n-values for all PLys/Gen gels fell within the range of 0.45–1, except for Gel 5, where both DIC loading and release occurred at pH 7.4. The n-value for this hydrogel was 0.456, closely aligning with the drug release mechanism dominated purely by diffusion. This finding corresponds well with the experimental observation that no shrinking behaviour occurred under this condition. For

PLys/Gen gels loaded at lower pH values, a non-Fickian diffusion mechanism better describes the DIC release process at pH 7.4, as the release is influenced not only by diffusion but also by the structural changes in the hydrogel, such as the transition from stretched to shrunken states.

Table 5-2 Loaded DIC, released DIC and fitting results of DIC release model.

Hydrogels	Loaded DIC (mg/g)	Released DIC (mg/g)	Maximum release percentage	*n* release diffusion coefficient	R^2
PLys/Gen Gel 3, pH= 1.7	19.9±2.1	18.4±0.6	92.2±2.8%	0.722	0.953
PLys/Gen Gel 4, pH= 1.7	27.6±1.6	23.6±0.3	85.7±1.1%	0.743	0.955
PLys/Gen Gel 5, pH= 1.7	32.9±1.5	27.6±1.3	84.0±3.9%	0.693	0.975
PLys/Gen Gel 5, pH= 5.5	20.2±2.8	14.6±0.6	72.3±2.9%	0.561	0.984
PLys/Gen Gel 5, pH= 7.4	12.4±3.1	8.1±0.4	65.3±3.1%	0.456	0.986

Hence, among all kind of PLys/Gen Gels, PLys/Gen Gel 5 exhibits the biggest potential for DIC loading and releasing. With lowest amount addition of genipin (weight ratio of PLys/Gen= 25:1, 1g hydrogels can withhold the maximum amount of DIC (32.9±1.5 mg) and release the maximum amount of DIC (27.6±1.3 mg) of all the gels tested. After DIC loading, the hydrogel can plausibly swell in the simulated acidic environment of gastric juice and then shrink in the intestinal fluid environment, releasing approximately 35% of the loaded DIC within the first 90 minutes. Under the combined influence of drug diffusion and hydrogel volume changes, DIC release reaches equilibrium after 8 hours. This characteristic of PLys/Gen gels, featuring an initial rapid release followed by a prolonged slow release, highlights their potential as carrier

materials for enteric-coated DIC tablets, potentially enhancing the drug's sustained release and therapeutic efficacy.

5.4.7 Injectable PLys/Gen Gels

Hydrogels that can pass through a syringe are advantageous as they may be used as injectable payload delivery vehicles. Consequently, the capability of the PLys/Gen gels to be injected was assessed. After complete swelling in PBS solutions, PLys/Gen gels were placed into a syringe, subjected to thrust, and successfully injected into a glass bottle (Figure.5-14). This demonstrates that PLys/Gen gels are injectable and opens-up the possibility for new therapeutic applications for the biomaterial. After DIC loading, the hydrogel could be directly injected into the joint, where DIC release to the joint fluid would then occur. This method may offer a simple but effective approach for treating inflammation, providing localised drug delivery and potentially enhancing treatment outcomes.

Figure 5-14 Injectable PLys/Gen gels.

5.5. Conclusions

Chemical hydrogels were created from a DKP starting material that underwent ROP, for the first time. This route to poly(amino acid)-based hydrogels aimed to minimise the use of toxic chemicals during monomer synthesis. PLys with 30 repeating units was successfully

synthesised via Lys(cbz)DKP, which was then reacted with hexylamine in the presence of MSA and DIPEA catalysts to yield PLys(cbz) Finally, PLys was created following successful cbz deprotection. Whilst monomer synthesis is environmentally favourable in comparison to conventional NCA synthesis, research must be undertaken to improve the environmental credentials of the polymerisation and the final cbz deprotection step, which is analogous to the deprotection step of PLys produced by NCA ROP.

PLys/Gen gels were prepared by mixing PLys with varying proportions of the crosslinker genipin in DI water. As the genipin content increased, the swelling rate of the hydrogels decreased, while both the storage modulus (G') and loss modulus (G'') increased. Additionally, a transition from limited crosslinked to permanently chemically crosslinked hydrogels was observed. This suggests that a higher concentration of genipin creates a denser network structure, reducing the hydrogel's swelling capacity but significantly enhancing its mechanical strength and stability.

Furthermore, in the DIC loading experiment, a lower pH value (pH = 1.7) and a lower proportion of genipin (PLys/Genipin mass ratio of 25:1) were favourable for enhancing the DIC loading amount. These conditions promote a more flexible hydrogel network and increase the available space for drug absorption, leading to higher DIC loading capacity. In the DIC release experiments, PLys/Gen Gel can rapidly release 35% of loaded DIC and then the maximum release amount of DIC (27.6±1.3 mg/g) from PLys/Gen Gel 5 were detected after 8 hours in a stimulated intestinal environment (pH 7.4). The drug release followed an anomalous non-Fickian transport mechanism, meaning that the release was governed by both diffusion and the swelling of the polymeric matrix.

PLys/Gen Gel 5 is an ideal candidate for drug delivery with properties of an initial rapid release followed by a prolonged slow release. Additionally, the hydrogel's injectability offers the potential for localized drug delivery, expanding its versatility as a drug delivery system.

Chapter 6 Summary of Research

This thesis reports novel ways to create PLys, and applications for which PLys may be exploited.

Chapter three details the synthesis of linear PLys using thermal deprotection in the final, post-polymerisation, deprotection step. Using heat eliminates the use of toxic reactants such as HBr and piperidine that are conventional used for PLys side-chain deprotection. PLys and PEG-*b*-PLys were successfully synthesised following the cleavage of Fmoc groups over 1 h through in DMSO at 120 °C. Both polymers exhibited remarkable Pb(II) ion adsorption capacities, with PLys achieving a maximum capacity of 538±28 mg/g and PEG-b-PLys reaching 408±17 mg/g. These findings emphasise the environmental and practical benefits of producing PLys through thermally induced side-chain deprotection, offering potential application in wastewater treatment and related fields.

The versatility of PLys as a material was demonstrated in **Chapter Four**, in which covalently crosslinked PLys hydrogels were reported as adsorbents for RB5. Glutaraldehyde (PLys/Glu) and the more environmentally positive genipin (PLys/Gen) were used as crosslinkers to maintain hydrogel morphology. PLys/Glu hydrogels demonstrated a maximum RB5 adsorption capacity of 430±8 mg/g, while PLys/Gen Gel achieved a higher capacity of 590±4 mg/g at pH 5.5. This latter result is particularly notable owing to both the novelty and the particular application of PLys/Gen hydrogels. The adsorption kinetics followed the pseudo-first-order model and the adsorption isotherm data were well-fitted by the Langmuir model, indicating physically-induced monolayer adsorption. These findings can provide valuable theoretical guidance for practical organic dye adsorption applications.

Greater crosslinking density enhanced the mechanical strength of PLys-based hydrogels but simultaneously reduced their dye adsorption capacity. This was also observed for the uptake of

DIC by PLys/Gen hydrogels, reported in **Chapter Five**. In this case, increased crosslinking density led to a reduction in the number of free amine groups available for DIC uptake. Therefore, achieving an optimal balance between mechanical stability and adsorption/drug uptake performance is essential for the practical application of PLys-based hydrogels. However, manipulating covalent crosslinker density allows these factors to be controlled. In **Chapter Five**, a triphosgene-free approach was adopted to prepare a potential drug carrier for oral administration, focusing on the synthesis of Lys(cbz)-DKP as a precursor for further PLys polymerisation. This method aimed to minimise the use of toxic reactants, most notably triphosgene. MSA and DIPEA were employed as catalysts for Lys(cbz)-DKP ROP, and were essential owing to the resistance of the DKP to undergo ROP in their absence. Under acidic conditions (pH = 1.7), PLys/Gen Gel demonstrated effective DIC uptake. Regarding drug release, approximately 35% of the loaded DIC was released rapidly in the initial stage. After eight hours in a simulated intestinal environment (pH 7.4), the maximum DIC release from PLys/Gen Gel 5 reached 27.6±1.3 mg/g, indicating its potential for controlled and sustained drug delivery. The observed release followed an anomalous non-Fickian transport mechanism, indicating that both diffusion processes and polymeric matrix swelling influenced the release dynamics. PLys/Gen Gel 5 demonstrates strong potential as an oral drug delivery system, providing an initial burst release followed by a sustained and controlled release over an extended period.

Chapter 7 Future Plans

Based on **Chapter Three**, thermal deprotection has been proved an effective and piperidine free method to remove Fmoc protecting group from linear PEG-*b*-PLys(Fmoc) and PLys(Fmoc). The deprotection degree of the two polymers increased progressively with time, reaching its maximum after 1 hour. DLS analysis would allow a study to be undertaken to determine whether the extent of Fmoc removal impacts nanoparticle size and stability. Fmoc groups remaining may drive polymer self-assembly via hydrophobic interactions and π-π stacking between adjacent polymer chains. The presence of residual Fmoc groups facilitates π-π stacking, and thus it has the potential to prepare self-assembly nanoscale amphiphilic polymers and be employed as drug delivery tools, such as carriers for amphiphilic anti-cancer drug, DOX. DOX can be encapsulated and distributed within hydrophobic part of amphiphilic nanoparticles[158, 276].

The control of nanoparticle size for PEG-*b*-PLys(Fmoc) can be addressed from two approaches. One is to adjust the molar ratio of PEG amine to Lys(Fmoc)-NCA and PEG-*b*-PLys(Fmoc) with fewer repeat units can be prepared through this way without deprotection. The other, for PEG-*b*-PLys(Fmoc) synthesised with a larger number of repeat units, is to optimise the deprotection time in DMSO to reducing the retention of hydrophobic Fmoc groups.

The recyclability of the PEG-*b*-PLys and PLys discussed in **Chapter three** can be investigated in future work. Ethylenediaminetetraacetic acid disodium salt (EDTA-Na), known for its strong chelating ability with metal ions, and could be used as a metal ion desorption agent[277]. Studies could be undertaken in which EDTA-Na is added to the aqueous solution to facilitate the release of captured metal ions, liberating free PLys, carboxymethyl cellulose and chitosan. After filtration to remove metal contaminants, the polymers may then be re-used in aqueous solution or recovered by lyophilisation or water evaporation for re-use. This procedure could be assessed to determine efficient routes to polymer recovery and re-use.

The RB5 adsorption and desorption recycling experiments in **Chapter Four** only featured the PLys/Glu hydrogels. This is because the PLys/Gen Gels decomposed at pH 12, leaving no gel-like material in the solution. The underlying reason for this instability remains unclear and requires further investigation in future work. A potential explanation is that the crosslinking structure of PLys/Gen Gels may not be stable in highly alkaline environments. A possible crosslinking structure is illustrated in Figure 7-1, based on references to crosslinked collagen protein/genipin structures[278]. At high pH, OH^- may attack the N^+ position in the six-membered ring, leading to the breakdown of the crosslinking structure and subsequent gel decomposition. However, the existence of this proposed structure requires further verification through detailed experimental and analytical studies. Other sustainable crosslinkers could be evaluated to produce PLys-based chemical hydrogels that may remain stable for extended periods in an alkaline environment, such as citric acid

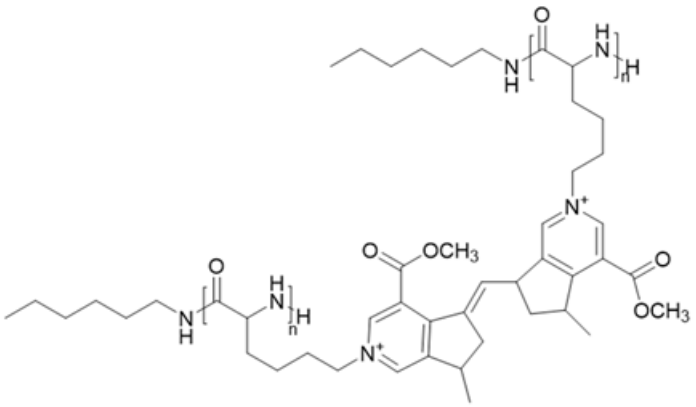

Figure 7-1 Another structure of PLys/Gen crosslinking structure.

In **Chapter Five**, the non-toxic nature of the drug delivery vehicle is crucial for its biomedical applications. To satisfy this requirement, a triphosgene-free synthesis method for PLys production from DKP was employed. Additionally, the biocompatible crosslinker genipin was

used to fabricate the hydrogel matrix. However, HBr/AcOH solutions were utilised in the deprotection process, raising concerns about potential toxicity. For future work, an alternative synthetic route involving Lys(Fmoc)-DKP synthesis could be explored. This approach will be combined with the thermal deprotection method described in **Chapter Three** to develop a more environmentally sustainable pathway for PLys preparation, ensuring enhanced biocompatibility and safety for biomedical applications.

The small, negatively charged drug DIC was selected for the release study. For future research, the release behaviour of larger molecular weight anionic proteins, such as albumin using the same delivery vector PLys/Gen hydrogels, could be explored, potentially expanding the applicability of the system for protein-based therapy. Albumin is frequently employed for volume replacement or the correction of hypoalbuminemia[279]. It also has potential applications in targeted therapy due to its ability to interact with secreted protein acidic and rich in cysteine (SPARC), an albumin receptor that is overexpressed in many types of tumour cells[280]. Proteins like albumin absorb UV light at 280 nm due to the presence of aromatic amino acids, allowing the concentration of albumin in solutions to be measured, provided interference from genipin is properly excluded. Besides, chondroitin sulphate, an anionic polymeric drug for treatment of osteoarthritis, can be also selected as the loaded drug.

The Proposed DKP ROP mechanism by MSA/DIPEA catalyst is provided in Figure 7-2. However, further experimental validation and detailed mechanistic studies are needed to confirm this proposed pathway in the future. Density functional theory (DFT) calculations can assist verification of this possible mechanism. Dissociation energy can be calculated to evaluate the stability of each complex mentioned in the Figure 7-2.

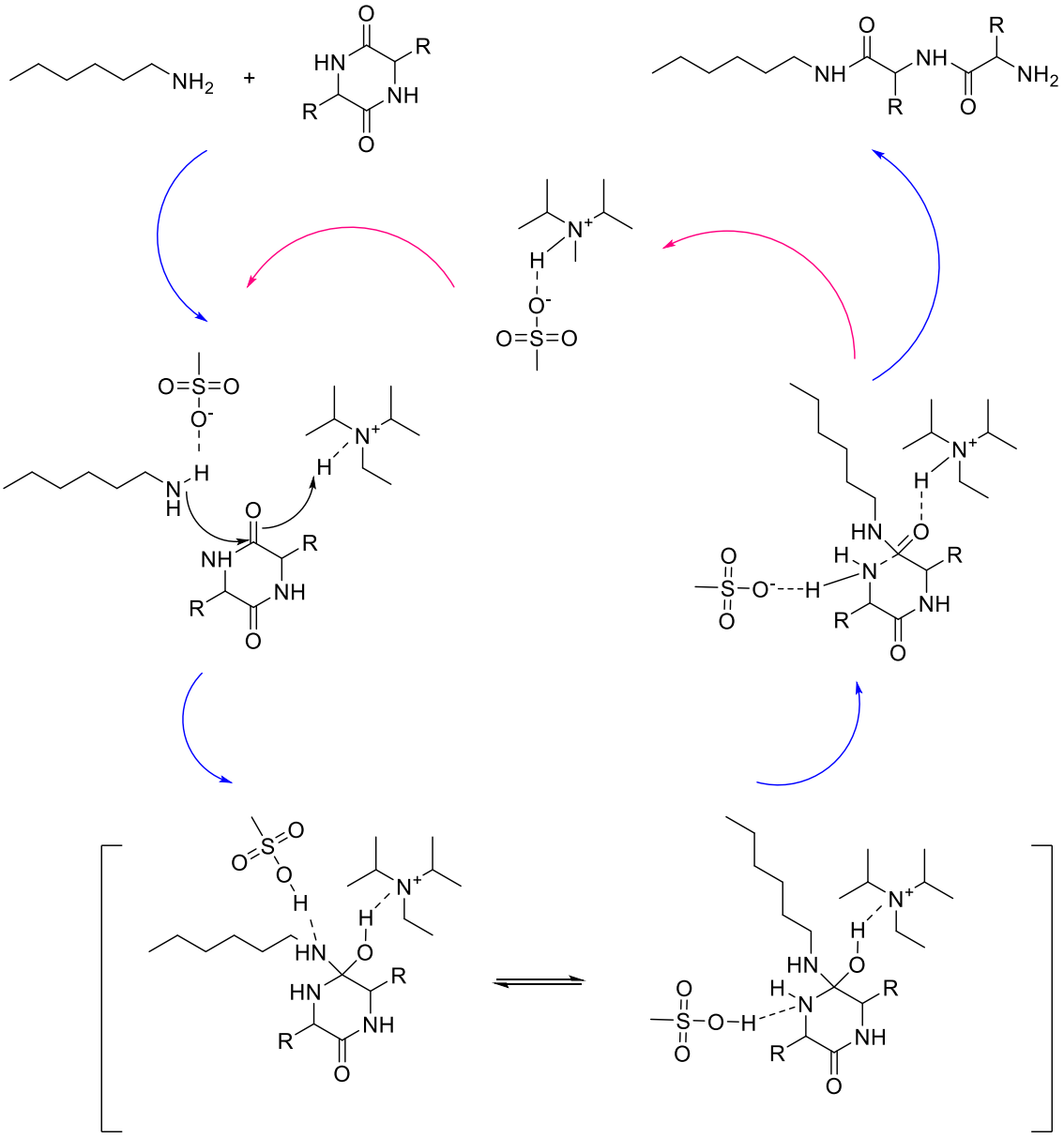

Figure 7-2 Possible DKP ROP mechanism by MSA/DIPEA catalyst.

The application of α-PLys in the biomedical field remains limited due to its physiological toxicity, primarily caused by its high positive charge density[15]. However, many physiological toxicity studies have been conducted using α-PLys with a large molecular weight (above 30,000 g/mol), often compared to natural ε-polylysine, which typically has 25-30 repeat units (~3840 g/mol). Conducting toxicity tests on α-PLys with a molecular weight comparable to that of ε-polylysine could provide more accurate toxicity assessments and potentially expand its applicability in biomedical research and therapeutic development. L929 mouse fibroblasts can

be used as target cells to evaluate the cytotoxicity of PLys using the MTT (3-(4,5-dimethylthiazol-2-yl)-2,5-diphenyl tetrazolium bromide) assay. The cells will be incubated with PLys solutions of varying concentrations and molecular weights, with a blank sample served as the control. Cell viability will be assessed spectrophotometrically since yellow-coloured MTT can be reduced to deep purple formazan crystals by metabolically active cells[281].

In addition, the morphology of the cells after incubation can be observed through microscope to provide supplementary insights into the cytotoxic effects of PLys on cellular structure.

List of References

1. Sela, M. and E. Katchalski, *Biological properties of poly-α-amino acids*, in *Advances in protein chemistry*. 1959, Elsevier. p. 391-478.
2. Patil, N.A. and B.J.E.P.J. Kandasubramanian, *Functionalized polylysine biomaterials for advanced medical applications: A review.* 2021. **146**: p. 110248.
3. Lee, K.W., et al., *α-Poly-l-lysine functions as an adipogenic inducer in 3T3-L1 preadipocytes.* 2021. **53**: p. 587-596.
4. Shima, S. and H. Sakai, *Polylysine Produced by Streptomyces.* Agricultural and Biological Chemistry, 1977. **41**(9): p. 1807-1809.
5. Shima, S. and H. Sakai, *Poly-l-lysine Produced by Streptomyces. Part II. Taxonomy and Fermentation Studies.* Agricultural and Biological Chemistry, 1981. **45**(11): p. 2497-2502.
6. Gurtovenko, A.A., *Molecular-Level Insight into the Interactions of DNA/Polycation Complexes with Model Cell Membranes.* The Journal of Physical Chemistry B, 2019. **123**(30): p. 6505-6514.
7. Damodaran, S.J.F.s.f.c., *Amino acids, peptides and proteins.* 2008. **4**: p. 425-439.
8. Manouchehri, S., et al., *Advanced delivery systems based on lysine or lysine polymers.* 2021. **18**(10): p. 3652-3670.
9. Mirtič, A. and J. Grdadolnik, *The structure of poly-l-lysine in different solvents.* Biophysical Chemistry, 2013. **175-176**: p. 47-53.
10. Athanasiou, V., et al., *Synthesis and Characterization of the Novel N(ε)-9-Fluorenylmethoxycarbonyl-l-Lysine N-Carboxy Anhydride. Synthesis of Well-Defined Linear and Branched Polypeptides.* Polymers (Basel), 2020. **12**(12).
11. Ge, Y., et al., *Hyperbranched polylysine: Synthesis, mechanism and preparation for NIR-absorbing gold nanoparticles.* Chinese Chemical Letters, 2019. **30**(7): p. 1428-1431.
12. Benoit, F., et al., *Exploring the Conformational Landscape of Poly(l-lysine) Dendrimers Using Ion Mobility Mass Spectrometry.* Analytical Chemistry, 2024. **96**(23): p. 9390-9398.
13. Stover, T.C., et al., *Thermoresponsive and biodegradable linear-dendritic nanoparticles for targeted and sustained release of a pro-apoptotic drug.* 2008. **29**(3): p. 359-369.
14. Kadlecova, Z., et al., *Comparative Study on the In Vitro Cytotoxicity of Linear, Dendritic, and Hyperbranched Polylysine Analogues.* Biomacromolecules, 2012. **13**(10): p. 3127-3137.
15. Fischer, D., et al., *In vitro cytotoxicity testing of polycations: influence of polymer structure on cell viability and hemolysis.* 2003. **24**(7): p. 1121-1131.
16. Ham, R.G. and W.L.J.M.i.e. McKeehan, *[5] Media and growth requirements.* 1979. **58**: p. 44-93.
17. Kurihara, R., et al., *Biodistribution and tumor localization of PEG-modified dendritic poly (L-lysine) oligonucleotide complexes.* 2012. **23**(18): p. 2369-2380.
18. Okuda, T., et al., *Biodistribution characteristics of amino acid dendrimers and their PEGylated derivatives after intravenous administration.* 2006. **114**(1): p. 69-77.
19. Ryser, H.J.-P. and W.-C.J.P.o.t.N.A.o.S. Shen, *Conjugation of methotrexate to poly (L-*

lysine) increases drug transport and overcomes drug resistance in cultured cells. 1978. **75**(8): p. 3867-3870.
20. Meyer, M., et al., *Breathing life into polycations: functionalization with pH-responsive endosomolytic peptides and polyethylene glycol enables siRNA delivery.* 2008. **130**(11): p. 3272-3273.
21. Meyer, M., et al., *A dimethylmaleic acid–melittin-polylysine conjugate with reduced toxicity, pH-triggered endosomolytic activity and enhanced gene transfer potential.* 2007. **9**(9): p. 797-805.
22. Bakeev, K.N., et al., *Kinetics and mechanism of interpolyelectrolyte exchange and addition reactions.* 1992. **25**(17): p. 4249-4254.
23. Kadlecova, Z., et al., *Comparative study on the in vitro cytotoxicity of linear, dendritic, and hyperbranched polylysine analogues.* 2012. **13**(10): p. 3127-3137.
24. Stamou, A., H. Iatrou, and C. Tsitsilianis, *NIPAm-Based Modification of Poly(L-lysine): A pH-Dependent LCST-Type Thermo-Responsive Biodegradable Polymer*. Polymers, 2022. **14**(4): p. 802.
25. Kricheldorf, H.R.J.A.C.I.E., *Polypeptides and 100 years of chemistry of α-amino acid N-carboxyanhydrides.* 2006. **45**(35): p. 5752-5784.
26. Huang, J. and A.J.C.S.R. Heise, *Stimuli responsive synthetic polypeptides derived from N-carboxyanhydride (NCA) polymerisation.* 2013. **42**(17): p. 7373-7390.
27. Zheng, B., et al., *An inspection into multifarious ways to synthesize poly (amino acid) s.* 2021. **42**(22): p. 2100453.
28. Hadjichristidis, N., et al., *Synthesis of well-defined polypeptide-based materials via the ring-opening polymerization of α-amino acid N-carboxyanhydrides.* 2009. **109**(11): p. 5528-5578.
29. Johnson, R.P., J.V. John, and I.J.E.p.j. Kim, *Recent developments in polymer–block–polypeptide and protein–polymer bioconjugate hybrid materials.* 2013. **49**(10): p. 2925-2948.
30. Laconde, G., M. Amblard, and J.J.O.L. Martinez, *Synthesis of α-Amino Acid N-Carboxyanhydrides.* 2021. **23**(16): p. 6412-6416.
31. Borthwick, A.D.J.C.r., *2, 5-Diketopiperazines: synthesis, reactions, medicinal chemistry, and bioactive natural products.* 2012. **112**(7): p. 3641-3716.
32. Mezzasalma, L., A.P. Dove, and O.J.E.P.J. Coulembier, *Organocatalytic ring-opening polymerization of L-lactide in bulk: A long standing challenge.* 2017. **95**: p. 628-634.
33. Katiyar, V. and H.J.P.C. Nanavati, *Ring-opening polymerization of L-lactide using N-heterocyclic molecules: mechanistic, kinetics and DFT studies.* 2010. **1**(9): p. 1491-1500.
34. Basterretxea, A., et al., *Stereoretention in the bulk ROP of L-lactide guided by a thermally stable organocatalyst*. 2021. **54**(13): p. 6214-6225.
35. Stewart, W.E. and T.H.J.C.R. Siddall, *Nuclear magnetic resonance studies of amides.* 1970. **70**(5): p. 517-551.
36. Isidro-Llobet, A., M. Alvarez, and F.J.C.r. Albericio, *Amino acid-protecting groups.* 2009. **109**(6): p. 2455-2504.
37. Gibson, F.S., S.C. Bergmeier, and H.J.T.J.o.O.C. Rapoport, *Selective removal of an N-BOC protecting group in the presence of a tert-butyl ester and other acid-sensitive groups.*

1994. **59**(11): p. 3216-3218.
38. Tsuda, Y., et al., *Solution-Phase Peptide Synthesis.* 2010. **3**: p. 201-251.
39. Dias, L.C. and P.L.J.J.o.t.B.C.S. Campano, *Conjugate Reduction of a, b-Unsaturated Carbonyl Compounds. Selective Inhibition of Benzyl Ether Hydrogenolysis by NH4OH/MeOH.* 1998. **9**: p. 97-99.
40. Fields, G.B.J.P.s.p., *Methods for removing the Fmoc group.* 1995: p. 17-27.
41. Fernández-Forner, D., et al., *Solid-phase synthesis of 4-aminopiperidine analogues using the Alloc protecting group: an investigation of Alloc removal from secondary amines.* 2001. **42**(27): p. 4471-4474.
42. Barlos, K., D. Gatos, and S.J.T.J.o.p.r. Koutsogianni, *Fmoc/Trt-amino acids: comparison to Fmoc/tBu-amino acids in peptide synthesis.* 1998. **51**(3): p. 194-200.
43. Mintzer, M.A. and E.E.J.C.r. Simanek, *Nonviral vectors for gene delivery.* 2009. **109**(2): p. 259-302.
44. Hong, S., et al., *Interaction of polycationic polymers with supported lipid bilayers and cells: nanoscale hole formation and enhanced membrane permeability.* 2006. **17**(3): p. 728-734.
45. Cho, K.C., et al., *Folate receptor-mediated gene delivery using folate-poly (ethylene glycol)-poly (l-lysine) conjugate.* 2005. **5**(6): p. 512-519.
46. Fernandez, C.A., et al., *Discovery of metabolically stabilized electronegative polyacridine-PEG peptide DNA open polyplexes.* 2010. **21**(4): p. 723-730.
47. Abbasi, M., et al., *Further investigation of lipid-substituted poly (L-Lysine) polymers for transfection of human skin fibroblasts.* 2008. **9**(6): p. 1618-1630.
48. Thiersch, M., et al., *The angiogenic response to PLL-g-PEG-mediated HIF-1α plasmid DNA delivery in healthy and diabetic rats.* 2013. **34**(16): p. 4173-4182.
49. von Erlach, T., et al., *Formation and characterization of DNA-polymer-condensates based on poly (2-methyl-2-oxazoline) grafted poly (L-lysine) for non-viral delivery of therapeutic DNA.* 2011. **32**(22): p. 5291-5303.
50. Hartono, S.B., et al., *Poly-L-lysine functionalized large pore cubic mesostructured silica nanoparticles as biocompatible carriers for gene delivery.* 2012. **6**(3): p. 2104-2117.
51. Prokopovic, V.Z., et al., *Binding mechanism of the model charged dye carboxyfluorescein to hyaluronan/polylysine multilayers.* 2017. **9**(44): p. 38908-38918.
52. Wang, C., et al., *A pH-responsive superamphiphile based on dynamic covalent bonds.* 2011. **12**(17): p. 3322-3325.
53. Johnson, R.P., et al., *Poly (PEGA)-b-poly (L-lysine)-b-poly (L-histidine) hybrid vesicles for tumoral pH-triggered intracellular delivery of doxorubicin hydrochloride.* 2015. **7**(39): p. 21770-21779.
54. Li, J., et al., *Stimuli-responsive zwitterionic block copolypeptides: poly (N-isopropylacrylamide)-block-poly (lysine-co-glutamic acid).* 2008. **9**(10): p. 2670-2676.
55. Huang, C.-J. and F.-C.J.M. Chang, *Polypeptide diblock copolymers: syntheses and properties of poly (N-isopropylacrylamide)-b-polylysine.* 2008. **41**(19): p. 7041-7052.
56. Ansari, M.J., et al., *Poly(N-isopropylacrylamide)-Based Hydrogels for Biomedical Applications: A Review of the State-of-the-Art.* Gels, 2022. **8**(7).
57. Siow, W.X., et al., *Interaction of poly-l-lysine coating and heparan sulfate proteoglycan*

on magnetic nanoparticle uptake by tumor cells. Int J Nanomedicine, 2018. **13**: p. 1693-1706.
58. Liu, G., et al., *Biological properties of poly-L-lysine-DNA complexes generated by cooperative binding of the polycation.* J Biol Chem, 2001. **276**(37): p. 34379-87.
59. Guo, C., et al., *Synthesis and characterization of polycation block copolymer Poly (l-lysine)-b-poly [N-(N ' , N ' -diisopropyl-aminoethyl) aspartamide] as potential pH responsive gene delivery system.* 2012. **53**(2): p. 342-349.
60. Rao, S.S. and J. Winter, *Adhesion molecule-modified biomaterials for neural tissue engineering.* Frontiers in Neuroengineering, 2009. **Volume 2 - 2009**.
61. Miranda, A., et al., *Poly-L-Lysine and Human Plasmatic Fibronectin Films as Proactive Coatings to Improve Implant Biointegration.* Front Bioeng Biotechnol, 2021. **9**: p. 807697.
62. Smith, R.J., Jr., et al., *Capture of endothelial cells under flow using immobilized vascular endothelial growth factor.* Biomaterials, 2015. **51**: p. 303-312.
63. Niepel, M.S., et al., *Cross-linking multilayers of poly-l-lysine and hyaluronic acid: Effect on mesenchymal stem cell behavior.* 2018. **41**(4): p. 223-235.
64. Richert, L., et al., *pH dependent growth of poly (L-lysine)/poly (L-glutamic) acid multilayer films and their cell adhesion properties.* 2004. **570**(1-2): p. 13-29.
65. Zarrintaj, P., et al., *Polylysine for skin regeneration: A review of recent advances and future perspectives*. 2022. **7**(1): p. e10261.
66. Deepak, A., et al., *Polylysine in biomedical applications: from composites to breakthroughs*. 2024. **19**(6): p. 062002.
67. Singh, N., et al., *Water purification by using adsorbents: a review.* 2018. **11**: p. 187-240.
68. Jaishankar, M., et al., *Toxicity, mechanism and health effects of some heavy metals.* Interdiscip Toxicol, 2014. **7**(2): p. 60-72.
69. Singh, N.B., et al., *Water purification by using Adsorbents: A Review.* Environmental Technology & Innovation, 2018. **11**: p. 187-240.
70. Roslan, N.N., et al., *Recent Advances in Advanced Oxidation Processes for Degrading Pharmaceuticals in Wastewater—A Review.* Catalysts, 2024. **14**(3): p. 189.
71. Kato, S. and Y. Kansha, *Comprehensive review of industrial wastewater treatment techniques.* Environ Sci Pollut Res Int, 2024. **31**(39): p. 51064-51097.
72. Zhu, R., et al., *Adsorbents based on montmorillonite for contaminant removal from water: A review.* 2016. **123**: p. 239-258.
73. Raval, N.P., P.U. Shah, and N.K. Shah, *Adsorptive removal of nickel(II) ions from aqueous environment: A review.* Journal of Environmental Management, 2016. **179**: p. 1-20.
74. Amalina, F., et al., *The effects of chemical modification on adsorbent performance on water and wastewater treatment - A review.* Bioresource Technology Reports, 2022. **20**: p. 101259.
75. *adsorbate*. 2025, International Union of Pure and Applied Chemistry (IUPAC).
76. Costa, T.B.d., M.G.C.d. Silva, and M.G.A. Vieira, *Recovery of rare-earth metals from aqueous solutions by bio/adsorption using non-conventional materials: a review with recent studies and promising approaches in column applications.* Journal of Rare Earths, 2020. **38**(4): p. 339-355.
77. Gupta, A., et al., *A Review of Adsorbents for Heavy Metal Decontamination: Growing*

Approach to Wastewater Treatment. Materials (Basel), 2021. **14**(16).
78. Worch, E., *Adsorption technology in water treatment*. Vol. 10. 2012: de Gruyter Berlin.
79. Gautam, R.K., et al., *Biomass-derived biosorbents for metal ions sequestration: Adsorbent modification and activation methods and adsorbent regeneration.* 2014. **2**(1): p. 239-259.
80. Rinaudo, M.J.P.i.p.s., *Chitin and chitosan: Properties and applications.* 2006. **31**(7): p. 603-632.
81. Ren, Y., et al., *Comparative investigation of the binding characteristics of poly-l-lysine and chitosan on alginate hydrogel.* 2016. **84**: p. 135-141.
82. Chakraborti, A., *α-POLY-L-LYSINE AS A POTENTIAL BIOSORBENT FOR REMOVAL OF HEXAVALENT CHROMIUM FROM INDUSTRIAL WASTE WATER A THESIS*. 2009, Worcester Polytechnic Institute.
83. Zhang, Y.-R., et al., *A magnetic nanomaterial modified with poly-lysine for efficient removal of anionic dyes from water.* 2015. **262**: p. 313-318.
84. Hu, D., et al., *Synthesis of water-dispersible poly-L-lysine-functionalized magnetic Fe_3O_4-(GO-MWCNTs) nanocomposite hybrid with a large surface area for high-efficiency removal of tartrazine and Pb (II).* 2017. **105**: p. 1611-1621.
85. Wichterle, O. and D.J.N. Lim, *Hydrophilic gels for biological use.* 1960. **185**(4706): p. 117-118.
86. Bahram, M., N. Mohseni, and M. Moghtader, *An introduction to hydrogels and some recent applications*, in *Emerging concepts in analysis and applications of hydrogels*. 2016, IntechOpen.
87. Yang, J.-A., et al., *In situ-forming injectable hydrogels for regenerative medicine.* 2014. **39**(12): p. 1973-1986.
88. Sun, J.-Y., et al., *Highly stretchable and tough hydrogels*. 2012. **489**(7414): p. 133-136.
89. Zheng, M., et al., *Poly(α-l-lysine)-based nanomaterials for versatile biomedical applications: Current advances and perspectives.* Bioact Mater, 2021. **6**(7): p. 1878-1909.
90. Zarrintaj, P., et al., *Polylysine for skin regeneration: A review of recent advances and future perspectives.* Bioeng Transl Med, 2022. **7**(1): p. e10261.
91. Wei, Y.T., et al., *Hyaluronic acid hydrogel modified with nogo-66 receptor antibody and poly-L-lysine to promote axon regrowth after spinal cord injury.* 2010. **95**(1): p. 110-117.
92. Karimi-Soflou, R., I. Shabani, and A.J.I.J.o.B.M. Karkhaneh, *Enhanced neural differentiation by applying electrical stimulation utilizing conductive and antioxidant alginate-polypyrrole/poly-l-lysine hydrogels.* 2023. **237**: p. 124063.
93. Wang, R., et al., *Forward wound closure with regenerated silk fibroin and polylysine-modified chitosan composite bioadhesives as dressings.* 2020. **3**(11): p. 7941-7951.
94. Wang, S.S., et al., *Genipin-cross-linked poly (L-lysine)-based hydrogels: synthesis, characterization, and drug encapsulation.* 2013. **111**: p. 423-431.
95. Lagergren, S., *Zur theorie der sogenannten adsorption geloster stoffe.* 1898.
96. Blanchard, G., M. Maunaye, and G.J.W.r. Martin, *Removal of heavy metals from waters by means of natural zeolites.* 1984. **18**(12): p. 1501-1507.
97. Ho, Y.-S. and G.J.P.b. McKay, *Pseudo-second order model for sorption processes.* 1999. **34**(5): p. 451-465.
98. Simonin, J.-P.J.C.E.J., *On the comparison of pseudo-first order and pseudo-second order*

rate laws in the modeling of adsorption kinetics. 2016. **300**: p. 254-263.
99. Ho, Y.-S.J.J.o.h.m., *Review of second-order models for adsorption systems.* 2006. **136**(3): p. 681-689.
100. Qiu, H., et al., *Critical review in adsorption kinetic models.* 2009. **10**(5): p. 716-724.
101. Knezevic, Z., et al., *Palm oil hydrolysis by lipase from Candida cylindracea immobilized on zeolite type Y.* 1998. **22**(4): p. 275-280.
102. George, R. and S.J.J.o.M.C.B.E. Sugunan, *Kinetics of adsorption of lipase onto different mesoporous materials: Evaluation of Avrami model and leaching studies.* 2014. **105**: p. 26-32.
103. Swenson, H. and N.P.J.L. Stadie, *Langmuir's theory of adsorption: A centennial review.* 2019. **35**(16): p. 5409-5426.
104. Alafnan, S., et al., *Langmuir adsorption isotherm in unconventional resources: Applicability and limitations.* 2021. **207**: p. 109172.
105. Proctor, A. and J.J.J.o.t.A.O.C.S. Toro-Vazquez, *The Freundlich isotherm in studying adsorption in oil processing.* 1996. **73**: p. 1627-1633.
106. Vigdorowitsch, M., et al., *Freundlich isotherm: An adsorption model complete framework.* 2021. **11**(17): p. 8078.
107. Ali, S.A., O.C.S. Al Hamouz, and N.M.J.J.o.h.m. Hassan, *Novel cross-linked polymers having pH-responsive amino acid residues for the removal of Cu2+ from aqueous solution at low concentrations.* 2013. **248**: p. 47-58.
108. Celebi, O., et al., *A radiotracer study of the adsorption behavior of aqueous Ba2+ ions on nanoparticles of zero-valent iron.* 2007. **148**(3): p. 761-767.
109. Al-Ghouti, M.A. and D.A.J.J.o.h.m. Da'ana, *Guidelines for the use and interpretation of adsorption isotherm models: A review.* 2020. **393**: p. 122383.
110. Hu, Q. and Z.J.J.o.M.L. Zhang, *Application of Dubinin–Radushkevich isotherm model at the solid/solution interface: A theoretical analysis.* 2019. **277**: p. 646-648.
111. Geszke-Moritz, M. and M.J.A.S.S. Moritz, *APTES-modified mesoporous silicas as the carriers for poorly water-soluble drug. Modeling of diflunisal adsorption and release.* 2016. **368**: p. 348-359.
112. Tran, H.N., et al., *Mistakes and inconsistencies regarding adsorption of contaminants from aqueous solutions: a critical review.* 2017. **120**: p. 88-116.
113. Koopal, L., et al., *Analytical isotherm equations for multicomponent adsorption to heterogeneous surfaces.* 1994. **166**(1): p. 51-60.
114. Peppas, N.A. and B.J.J.o.C.R. Narasimhan, *Mathematical models in drug delivery: How modeling has shaped the way we design new drug delivery systems.* 2014. **190**: p. 75-81.
115. Siepmann, J. and N.A.J.A.d.d.r. Peppas, *Modeling of drug release from delivery systems based on hydroxypropyl methylcellulose (HPMC).* 2012. **64**: p. 163-174.
116. Walters, K.A. and K.R. Brain, *Dermatological formulation and transdermal systems*, in *Dermatological and transdermal formulations*. 2002, CRC Press. p. 337-418.
117. Singhvi, G. and M.J.I.J.P.S.R. Singh, *In-vitro drug release characterization models.* 2011. **2**(1): p. 77-84.
118. Nikolić, L., Z. Djurić, and M.J.J.o.p.s. Jovanović, *Influence of in vitro test conditions on release of aspirin from commercial tablets.* 1992. **81**(4): p. 386-391.

119. Higuchi, T.J.J.o.p.s., *Rate of release of medicaments from ointment bases containing drugs in suspension.* 1961. **50**(10): p. 874-875.
120. Omidian, H. and K.J.B.a.o.h.h. Park, *Introduction to hydrogels.* 2010: p. 1-16.
121. Elmas, A., et al., *Mathematical modelling of drug release.* 2020. **6**(4).
122. Khuphe, M. and P.D. Thornton, *7 - Poly(amino acids)*. 2018, Elsevier Ltd. p. 199-228.
123. Habraken, G.J.M., A. Heise, and P.D. Thornton, *Block Copolypeptides Prepared by N-Carboxyanhydride Ring-Opening Polymerization.* Macromolecular rapid communications., 2012. **33**(4): p. 272-286.
124. Kordasht, H.K., et al., *Poly (amino acids) towards sensing: Recent progress and challenges.* TrAC, Trends in analytical chemistry (Regular ed.), 2021. **140**: p. 116279.
125. Meister, A., *Biochemistry of the amino acids*. 2012: Elsevier.
126. Brown, M., et al., *Preliminary characterization of novel amino acid based polymeric vesicles as gene and drug delivery agents.* 2000. **11**(6): p. 880-891.
127. Boddu, S.H., et al., *Polyamide/poly (amino acid) polymers for drug delivery.* 2021. **12**(4): p. 58.
128. Hu, W., et al., *Poly (amino acid)-based carrier for drug delivery systems.* 2018. **14**(8): p. 1359-1374.
129. Karimi, P., A.S. Rizkalla, and K.J.M. Mequanint, *Versatile biodegradable poly (ester amide) s derived from α-amino acids for vascular tissue engineering.* 2010. **3**(4): p. 2346-2368.
130. Hwang, J.J. and S.I.J.J.o.B.S. Stupp, Polymer Edition, *Poly (amino acid) bioadhesives for tissue repair.* 2000. **11**(10): p. 1023-1038.
131. Datta, S., et al., *Alginate-poly (amino acid) extrusion printed scaffolds for tissue engineering applications.* 2020. **69**(2): p. 65-72.
132. Er, S., et al., *Amino acids, peptides, and proteins: implications for nanotechnological applications in biosensing and drug/gene delivery.* 2021. **11**(11): p. 3002.
133. Wu, J., et al., *Enzyme-Free Amplification Strategy for Biosensing Using Fe3+–Poly(glutamic acid) Coordination Chemistry.* Analytical Chemistry, 2018. **90**(7): p. 4725-4732.
134. Yuan, Y., et al., *Self-enhanced PEI-Ru (II) complex with polyamino acid as booster to construct ultrasensitive electrochemiluminescence immunosensor for carcinoembryonic antigen detection.* 2018. **1001**: p. 112-118.
135. Quadir, M.A., M. Martin, and P.T. Hammond, *Clickable Synthetic Polypeptides Routes to New Highly Adaptive Biomaterials.* Chemistry of materials, 2014. **26**(1): p. 461-476.
136. McAvan, B.S., M. Khuphe, and P.D.J.E.P.J. Thornton, *Polymer hydrogels for glutathione-mediated protein release.* 2017. **87**: p. 468-477.
137. Zhou, X. and Z.J.A.h.m. Li, *Advances and biomedical applications of polypeptide hydrogels derived from α-amino acid N-carboxyanhydride (NCA) polymerizations.* 2018. **7**(15): p. 1800020.
138. Byrne, M., et al., *Molecular weight and architectural dependence of well-defined star-shaped poly (lysine) as a gene delivery vector.* 2013. **1**(12): p. 1223-1234.
139. Kosuri, S., *Study of polylysine and chitosan nanoparticles synthesized using various cross-linkers and their applications for heavy metal ion recovery*. 2016: Rutgers The State University of New Jersey, School of Graduate Studies.

140. Carolin, C.F., et al., *Efficient techniques for the removal of toxic heavy metals from aquatic environment: A review.* Journal of environmental chemical engineering, 2017. **5**(3): p. 2782-2799.
141. Abdullah, N., et al., *Recent trends of heavy metal removal from water/wastewater by membrane technologies.* 2019. **76**: p. 17-38.
142. Qu, X., P.J.J. Alvarez, and Q. Li, *Applications of nanotechnology in water and wastewater treatment.* Water research (Oxford), 2013. **47**(12): p. 3931-3946.
143. Collin, M.S., et al., *Bioaccumulation of lead (Pb) and its effects on human: A review.* 2022. **7**: p. 100094.
144. Hama Aziz, K.H., et al., *Heavy metal pollution in the aquatic environment: efficient and low-cost removal approaches to eliminate their toxicity: a review.* RSC advances, 2023. **13**(26): p. 17595-1761.
145. Chakraborty, R., et al., *Adsorption of heavy metal ions by various low-cost adsorbents: a review.* International journal of environmental analytical chemistry, 2022. **102**(2): p. 342-379.
146. Chowdhury, I.R., et al., *Removal of lead ions (Pb2+) from water and wastewater: a review on the low-cost adsorbents.* 2022. **12**(8): p. 185.
147. Wu, Y., et al., *Recent Advances and Future Developments in the Preparation of Polypeptides via N-Carboxyanhydride (NCA) Ring-Opening Polymerization.* 2024. **146**(35): p. 24189-24208.
148. Piyachaturawat, P., T. Glinsukon, and C. Toskulkao, *Acute and subacute toxicity of piperine in mice, rats and hamsters.* Toxicology letters, 1983. **16**(3): p. 351-359.
149. Ralhan, K., V.G. KrishnaKumar, and S. Gupta, *Piperazine and DBU: a safer alternative for rapid and efficient Fmoc deprotection in solid phase peptide synthesis.* RSC advances, 2015. **5**(126): p. 104417-104425.
150. Hernández, J.R. and H.A.J.J.o.P.S.P.A.P.C. Klok, *Synthesis and ring - opening (co) polymerization of L-lysine N-carboxyanhydrides containing labile side-chain protective groups.* 2003. **41**(9): p. 1167-1187.
151. Podlech, J., et al., *Protection of the α-Amino Group*. 2002, Georg Thieme Verlag: Stuttgart and New York. p. 41-165.
152. Höck, S., et al., *Thermal Cleavage of the Fmoc Protection Group: FH–HES.* 2010. **64**(3): p. 200-200.
153. Deming, T.J., *Polypeptide and Polypeptide Hybrid Copolymer Synthesis via NCA Polymerization*, in *Peptide Hybrid Polymers*, H.-A. Klok and H. Schlaad, Editors. 2006, Springer Berlin Heidelberg: Berlin, Heidelberg. p. 1-18.
154. Ding, H.-H., et al., *Cholesteroled polymer (Chol-b-Lys)-based nanoparticles (CL-NPs) confer antibacterial efficacy without resistance.* 2021. **45**(44): p. 20743-20750.
155. Stukenkemper, T., et al., *Block copolypeptide nanoparticles for the delivery of ocular therapeutics.* 2015. **15**(1): p. 138-145.
156. Peeters, A., R. Ameloot, and D.E.J.G.c. De Vos, *Carbon dioxide as a reversible amine-protecting agent in selective Michael additions and acylations.* 2013. **15**(6): p. 1550-1557.
157. Deng, C., et al., *Functional polypeptide and hybrid materials: Precision synthesis via α-amino acid N-carboxyanhydride polymerization and emerging biomedical applications.*

Progress in polymer science, 2014. **39**(2): p. 330-364.
158. Yu, H., et al., *Meticulous Doxorubicin Release from pH-Responsive Nanoparticles Entrapped within an Injectable Thermoresponsive Depot.* 2020. **26**(59): p. 13352-13358.
159. Arimitsu, K. and K. Ichimura, *Nonlinear organic reaction of 9-fluorenylmethyl carbamates as base amplifiers to proliferate aliphatic amines and their application to a novel photopolymer system.* Journal of materials chemistry, 2004. **14**(3): p. 336-343.
160. Kalia, S. and L. Avérous, *Biodegradable and biobased polymers for environmental and biomedical applications*. 2016: John Wiley & Sons.
161. Aoki, K. and N.J.P. Saito, *Biodegradable polymers as drug delivery systems for bone regeneration.* 2020. **12**(2): p. 95.
162. Farasati Far, B., et al., *Combinational system of lipid-based nanocarriers and biodegradable polymers for wound healing: an updated review.* 2023. **14**(2): p. 115.
163. Helanto, K., et al., *Bio-based polymers for sustainable packaging and biobarriers: A critical review.* 2019. **14**(2): p. 4902-4951.
164. Priya, A., M. Muruganandam, and S.J.C. Suresh, *Bio-derived carbon-based materials for sustainable environmental remediation and wastewater treatment.* 2024: p. 142731.
165. Zhang, K., et al., *Removal of lead from acidic wastewater by bio-mineralized bacteria with pH self-regulation.* Chemosphere (Oxford), 2020. **241**: p. 125041-125041.
166. Jin, L., *Mechanisms of Lead Adsorption on Chitosan/PVA Hydrogel Beads.* Langmuir, 2002. **18**(25): p. 9765-9770.
167. Jin, X., et al., *Polyethyleneimine-bacterial cellulose bioadsorbent for effective removal of copper and lead ions from aqueous solution.* Bioresource technology, 2017. **244**(Pt 1): p. 844-849.
168. Zaichik, S., et al., *Zeta potential changing nanoemulsions: Impact of PEG-corona on phosphate cleavage.* International journal of pharmaceutics, 2020. **581**: p. 119299.
169. Chibowski, S. and M. Paszkiewicz, *Studies of Some Properties and the Structure of Polyethylene Glycol (PEG) Macromolecules Adsorbed on a TiO 2 Surface.* Adsorption science & technology, 2001. **19**(5): p. 397-407.
170. Lin, X., et al., *Synthesis, characterization, and utilization of poly-amino acid-functionalized lignin for efficient and selective removal of lead ion from aqueous solution.* Journal of cleaner production, 2022. **347**: p. 131219.
171. Ritchie, S.M.C., et al., *Polycysteine and Other Polyamino Acid Functionalized Microfiltration Membranes for Heavy Metal Capture.* Environmental science & technology, 2001. **35**(15): p. 3252-3258.
172. Dias, A.A., et al., *In vivo and laccase-catalysed decolourization of xenobiotic azo dyes by a basidiomycetous fungus: characterization of its ligninolytic system.* 2003. **19**: p. 969-975.
173. Lucas, M.S., J.A.J.D. Peres, and Pigments, *Decolorization of the azo dye Reactive Black 5 by Fenton and photo-Fenton oxidation.* 2006. **71**(3): p. 236-244.
174. Chandanshive, V., et al., *In situ textile wastewater treatment in high rate transpiration system furrows planted with aquatic macrophytes and floating phytobeds.* 2020. **252**: p. 126513.
175. Zafar, S., D.A. Bukhari, and A.J.S.J.o.B.S. Rehman, *Azo dyes degradation by*

microorganisms–An efficient and sustainable approach. 2022. **29**(12): p. 103437.
176. Mechichi, T., N. Mhiri, and S.J.C. Sayadi, *Remazol Brilliant Blue R decolourization by the laccase from Trametes trogii.* 2006. **64**(6): p. 998-1005.
177. Roriz, M.S., et al., *Application of response surface methodological approach to optimise Reactive Black 5 decolouration by crude laccase from Trametes pubescens.* 2009. **169**(1-3): p. 691-696.
178. Colindres, P., H. Yee-Madeira, and E.J.D. Reguera, *Removal of Reactive Black 5 from aqueous solution by ozone for water reuse in textile dyeing processes.* 2010. **258**(1-3): p. 154-158.
179. Petrinić, I., et al., *The removal of reactive dye printing compounds using nanofiltration.* 2007. **74**(3): p. 512-518.
180. Murugesan, K., et al., *Decolourization of reactive black 5 by laccase: optimization by response surface methodology.* 2007. **75**(1): p. 176-184.
181. Nabil, G.M., et al., *Enhanced decolorization of reactive black 5 dye by active carbon sorbent-immobilized-cationic surfactant (AC-CS).* 2014. **20**(3): p. 994-1002.
182. Mahmood, S., et al., *Potential of newly isolated bacterial strains for simultaneous removal of hexavalent chromium and reactive black-5 azo dye from tannery effluent.* 2013. **88**(8): p. 1506-1513.
183. Ranjusha, V., et al., *Biosorption of Remazol Black B dye (Azo dye) by the growing Aspergillus flavus.* 2010. **45**(10): p. 1256-1263.
184. Thi Thanh, M., et al., *Synthesis of iron doped zeolite imidazolate framework-8 and its remazol deep black RGB dye adsorption ability.* 2017. **2017**(1): p. 5045973.
185. Park, H., W.J.J.o.P. Choi, and P.A. Chemistry, *Visible light and Fe (III)-mediated degradation of Acid Orange 7 in the absence of H2O2.* 2003. **159**(3): p. 241-247.
186. Sheshmani, S., B. Falahat, and F.R.J.I.j.o.b.m. Nikmaram, *Preparation of magnetic graphene oxide-ferrite nanocomposites for oxidative decomposition of Remazol Black B.* 2017. **97**: p. 671-678.
187. Jalali Sarvestani, M.R., Z.J.J.o.W. Doroudi, and E. Nanotechnology, *Removal of reactive black 5 from waste waters by adsorption: a comprehensive review.* 2020. **5**(2): p. 180-190.
188. Asghar, A., et al., *Effect of Fenton's Reagent Concentration for COD Removal of Reactive Black 5 Dye.* 2014: p. 955-967.
189. Yu, C.-H., et al., *Decolorization of CI Reactive Black 5 in UV/TiO2, UV/oxidant and UV/TiO2/oxidant systems: A comparative study.* 2010. **158**(3): p. 578-583.
190. Laohaprapanon, S., et al., *Photodegradation of reactive black 5 in a ZnO/UV slurry membrane reactor.* 2015. **49**: p. 136-141.
191. Vasconcelos, V.M., et al., *Electrochemical removal of Reactive Black 5 azo dye using non-commercial boron-doped diamond film anodes.* 2015. **178**: p. 484-493.
192. Srivastava, A., et al., *Optimization, kinetics, and thermodynamics aspects in the biodegradation of reactive black 5 (RB5) dye from textile wastewater using isolated bacterial strain, Bacillus albus DD1.* 2022. **86**(3): p. 610-624.
193. Al-Tohamy, R., et al., *Ecofriendly biodegradation of Reactive Black 5 by newly isolated Sterigmatomyces halophilus SSA1575, valued for textile azo dye wastewater processing and detoxification.* 2020. **10**(1): p. 12370.

194. Cardoso, N.F., et al., *Removal of remazol black B textile dye from aqueous solution by adsorption.* 2011. **269**(1-3): p. 92-103.
195. González, J.A., et al., *Development of a chitin/graphene oxide hybrid composite for the removal of pollutant dyes: adsorption and desorption study.* 2015. **280**: p. 41-48.
196. Travlou, N.A., et al., *Graphite oxide/chitosan composite for reactive dye removal.* 2013. **217**: p. 256-265.
197. Kansal, S.K., N. Kaur, and S.J.N.r.l. Singh, *Photocatalytic degradation of two commercial reactive dyes in aqueous phase using nanophotocatalysts.* 2009. **4**: p. 709-716.
198. Guzmán-Duque, F.L., et al., *Relationship between anode material, supporting electrolyte and current density during electrochemical degradation of organic compounds in water.* 2014. **278**: p. 221-226.
199. Singh, K., S.J.C.r.i.e.s. Arora, and technology, *Removal of synthetic textile dyes from wastewaters: a critical review on present treatment technologies.* 2011. **41**(9): p. 807-878.
200. Olivares-Marín, M., et al., *The development of an activated carbon from cherry stones and its use in the removal of ochratoxin A from red wine.* 2009. **20**(3): p. 298-303.
201. Chatterjee, S., M.W. Lee, and S.H.J.B.t. Woo, *Adsorption of congo red by chitosan hydrogel beads impregnated with carbon nanotubes.* 2010. **101**(6): p. 1800-1806.
202. Yang, J., et al., *Role of chitosan-based hydrogels in pollutants adsorption and freshwater harvesting: A critical review.* 2021. **189**: p. 53-64.
203. Crini, G., et al., *Cross-linked chitosan-based hydrogels for dye removal.* 2019: p. 381-425.
204. Crini, G., et al., *Dye removal by biosorption using cross-linked chitosan-based hydrogels.* 2019. **17**(4): p. 1645-1666.
205. Kou, S.G., L.M. Peters, and M.R.J.I.J.o.B.M. Mucalo, *Chitosan: A review of sources and preparation methods.* 2021. **169**: p. 85-94.
206. De, S. and D.J.J.o.C.R. Robinson, *Polymer relationships during preparation of chitosan–alginate and poly-l-lysine–alginate nanospheres.* 2003. **89**(1): p. 101-112.
207. Nguyen, C.T., et al., *Bifunctional succinylated ε-polylysine-coated mesoporous silica nanoparticles for pH-responsive and intracellular drug delivery targeting the colon.* 2017. **9**(11): p. 9470-9483.
208. Zhou, Y., et al., *Rapid gelling chitosan/polylysine hydrogel with enhanced bulk cohesive and interfacial adhesive force: mimicking features of epineurial matrix for peripheral nerve anastomosis.* 2016. **17**(2): p. 622-630.
209. Wang, R., et al., *Fast in situ generated ε-polylysine-poly (ethylene glycol) hydrogels as tissue adhesives and hemostatic materials using an enzyme-catalyzed method.* 2015. **29**(8): p. 1167-1179.
210. Jiang, W. and X.J.I.J.o.B.M. Zhou, *Enzymatic preparation of oxidized viscose fibers-based biosorbent modified with ε-polylysine for dyes removal and microbial inactivation.* 2021. **166**: p. 509-520.
211. Goodman, M., C. Zapf, and Y.J.P.S.O.R.o.B. Rew, *New reagents, reactions, and peptidomimetics for drug design.* 2001. **60**(3): p. 229-245.
212. Li, C., et al., *Fabrication of photosensitive multilayered films via layer-by-layer assembly with well controlled porous structure.* 2012. **22**(5): p. 2045-2050.
213. Olsztyńska-Janus, S. and M.J.S.C. Komorowska, *Conformational changes of L-*

phenylalanine induced by near infrared radiation. ATR-FTIR studies. 2012. **23**: p. 1399-1407.
214. Yamamoto, H., H.J.M.S. Tanisho, and E. C, *Gel formation and its properties as hydrogel of cross-linked lysine polypeptides using organic cross-linking agents.* 1993. **1**(1): p. 45-51.
215. Takigawa, T. and Y. Endo, *Effects of glutaraldehyde exposure on human health.* Journal of occupational health, 2006. **48**(2): p. 75-87.
216. Muzzarelli, R.A.J.C.P., *Genipin-crosslinked chitosan hydrogels as biomedical and pharmaceutical aids.* 2009. **77**(1): p. 1-9.
217. Jia, Y. and J.J.C.r. Li, *Molecular assembly of Schiff base interactions: construction and application.* 2015. **115**(3): p. 1597-1621.
218. Hense, D., O.I.J.A.B.S. Strube, and Engineering, *Glutaraldehyde Cross-Linking of Salt-Induced Fibrinogen Hydrogels.* 2024.
219. Tacias-Pascacio, V.G., et al., *Genipin as an emergent tool in the design of biocatalysts: mechanism of reaction and applications.* 2019. **9**(12): p. 1035.
220. Iftime, M.M., G.L. Ailiesei, and D.J.G. Ailincai, *Tuning Antioxidant Function through Dynamic Design of Chitosan-Based Hydrogels.* 2024. **10**(10): p. 655.
221. Wen, P., et al., *Fabrication of chitosan scaffolds with tunable porous orientation structure for tissue engineering.* 2011. **22**(1-3): p. 19-40.
222. Fujiyabu, T., et al., *Permeation of water through hydrogels with controlled network structure.* 2017. **50**(23): p. 9411-9416.
223. Dong, H., et al., *Cation-induced hydrogels of cellulose nanofibrils with tunable moduli.* 2013. **14**(9): p. 3338-3345.
224. Wu, S., et al., *Poly (vinyl alcohol) hydrogels with broad-range tunable mechanical properties via the Hofmeister effect.* 2021. **33**(11): p. 2007829.
225. Stojkov, G., et al., *Relationship between structure and rheology of hydrogels for various applications.* 2021. **7**(4): p. 255.
226. Xu, C., et al., *Mechanical Regulation of Polymer Gels.* 2024. **124**(18): p. 10435-10508.
227. Lu, X., et al., *In situ synthesis of mechanically robust, transparent nanofiber-reinforced hydrogels for highly sensitive multiple sensing.* 2021. **31**(30): p. 2103117.
228. Baby, D., *Rheology of Polymer Blends and Nanocomposites*. 2020, Elsevier Amsterdam, The Netherlands:.
229. Saroyan, H., et al., *Reactive black 5 degradation on manganese oxides supported on sodium hydroxide modified graphene oxide.* 2019. **9**(10): p. 2167.
230. Elwakeel, K.Z., et al., *Enhanced remediation of Reactive Black 5 from aqueous media using new chitosan ion exchangers.* 2013. **34**(7): p. 1008-1019.
231. Chowdhury, S. and P.J.C.E.J. Saha, *Sea shell powder as a new adsorbent to remove Basic Green 4 (Malachite Green) from aqueous solutions: Equilibrium, kinetic and thermodynamic studies.* 2010. **164**(1): p. 168-177.
232. Revellame, E.D., et al., *Adsorption kinetic modeling using pseudo-first order and pseudo-second order rate laws: A review.* 2020. **1**: p. 100032.
233. Liu, Y.J.C., S.A. Physicochemical, and E. Aspects, *Some consideration on the Langmuir isotherm equation.* 2006. **274**(1-3): p. 34-36.
234. Choy, K.K., et al., *Langmuir isotherm models applied to the multicomponent sorption of*

acid dyes from effluent onto activated carbon. 2000. **45**(4): p. 575-584.
235. Chen, A.-H. and Y.-Y.J.J.o.H.M. Huang, *Adsorption of Remazol Black 5 from aqueous solution by the templated crosslinked-chitosans.* 2010. **177**(1-3): p. 668-675.
236. Skwarczynski, M., et al., *Poly (amino acids) as a potent self-adjuvanting delivery system for peptide-based nanovaccines.* 2020. **6**(5): p. eaax2285.
237. Kordasht, H.K., et al., *Poly (amino acids) towards sensing: Recent progress and challenges.* 2021. **140**: p. 116279.
238. Zarrintaj, P., et al., *Polylysine for skin regeneration: A review of recent advances and future perspectives*. Bioengineering & translational medicine, 2022. **7**(1): p. e10261-n/a.
239. Manouchehri, S., et al., *Advanced Delivery Systems Based on Lysine or Lysine Polymers.* Molecular pharmaceutics, 2021. **18**(10): p. 3652-3670.
240. Thomas, T.J., H.A. Tajmir-Riahi, and T. Thomas, *Polyamine–DNA interactions and development of gene delivery vehicles.* Amino Acids, 2016. **48**(10): p. 2423-2431.
241. Gurtovenko, A.A., *Molecular-Level Insight into the Interactions of DNA/Polycation Complexes with Model Cell Membranes.* The journal of physical chemistry. B, 2019. **123**(30): p. 6505-6514.
242. Shen, Y., et al., *Drug delivery systems*. 2020: Springer Berlin.
243. Mirsharghi, S., *Design, synthesis and characterization of polylysine dendrones for biomedical applications*. 2016.
244. Byrne, M., et al., *Star-Shaped Polypeptides: Synthesis and Opportunities for Delivery of Therapeutics.* 2015. **36**(21): p. 1862-1876.
245. Zhu, H., et al., *Polylysine complexes and their biomedical applications.* 2023. **4**(1): p. 20-27.
246. Shukla, S.C., et al., *Review on production and medical applications of ε-polylysine.* 2012. **65**: p. 70-81.
247. Shen, W.-C. and H.J.P.o.t.N.A.o.S. Ryser, *Conjugation of poly-L-lysine to albumin and horseradish peroxidase: a novel method of enhancing the cellular uptake of proteins.* 1978. **75**(4): p. 1872-1876.
248. Brillanti, S., et al., *A pilot study of combination therapy with ribavirin plus interferon alfa for interferon alfa-resistant chronic hepatitis C.* 1994. **107**(3): p. 812-817.
249. Couffin-Hoarau, A.-C., et al., *Peptide− Poly (l-lysine citramide) Conjugates and their In Vitro Anti-HIV Behavior.* 2009. **10**(4): p. 865-876.
250. Flynn, N., et al., *Effect of cationic grafted copolymer structure on the encapsulation of bovine serum albumin.* 2016. **62**: p. 524-531.
251. Wilder, R. and S.J.T.J.o.O.C. Mobashery, *The use of triphosgene in preparation of N-carboxy. alpha.-amino acid anhydrides.* 1992. **57**(9): p. 2755-2756.
252. Lv, W., M. Li, and Y.J.C.J.o.C. Tao, *Scale-up Efficient Synthesis of α-Poly (L-lysine).* 2023. **41**(19): p. 2488-2492.
253. Borak, J., W.F.J.J.o.o. Diller, and e. medicine, *Phosgene exposure: mechanisms of injury and treatment strategies.* 2001. **43**(2): p. 110-119.
254. Pokorna, A., et al., *Investigation of permeation of theophylline through skin using selected piperazine-2, 5-diones.* 2019. **24**(3): p. 566.
255. Sun, H., et al., *α-Amino acid containing degradable polymers as functional biomaterials:*

rational design, synthetic pathway, and biomedical applications. 2011. **12**(6): p. 1937-1955.
256. Feng, Y., et al., *Synthesis of Poly [(lactic acid)-alt-or co-((S)-aspartic acid)] from (3S, 6R, S)-3-[(Benzyloxycarbonyl) methyl]-6-methylmorpholine-2, 5-dione.* 2002. **203**(5-6): p. 819-824.
257. Dechy-Cabaret, O., B. Martin-Vaca, and D.J.C.r. Bourissou, *Controlled ring-opening polymerization of lactide and glycolide.* 2004. **104**(12): p. 6147-6176.
258. Ma, G., et al., *Development of ionic strength/pH/enzyme triple-responsive zwitterionic hydrogel of the mixed l-glutamic acid and l-lysine polypeptide for site-specific drug delivery.* 2017. **5**(5): p. 935-943.
259. Leick, S., A. Kemper, and H.J.S.M. Rehage, *Alginate/poly-l-lysine capsules: mechanical properties and drug release characteristics*. 2011. **7**(14): p. 6684-6694.
260. Chen, J., et al., *Sequentially responsive shell-stacked nanoparticles for deep penetration into solid tumors*. 2017. **29**(32): p. 1701170.
261. Chiono, V., et al., *Genipin-crosslinked chitosan/gelatin blends for biomedical applications.* 2008. **19**: p. 889-898.
262. Gan, T.J.J.C.m.r. and opinion, *Diclofenac: an update on its mechanism of action and safety profile.* 2010. **26**(7): p. 1715-1731.
263. Zacher, J., et al., *Topical diclofenac and its role in pain and inflammation: an evidence-based review.* 2008. **24**(4): p. 925-950.
264. Fenton, O.S., et al., *Customizable lipid nanoparticle materials for the delivery of siRNAs and mRNAs.* 2018. **57**(41): p. 13582-13586.
265. Wall, P.A., *Invention and Development of the Controlled Ring-Opening Polymerisation of 2, 5-Diketopiperazines to Produce Poly (amino acids)*. 2023, University of Leeds.
266. Habraken, G.J., et al., *Optimization of N-carboxyanhydride (NCA) polymerization by variation of reaction temperature and pressure.* 2011. **2**(6): p. 1322-1330.
267. Clayden, J., N. Greeves, and S. Warren, *Organic chemistry*. 2012: Oxford University Press, USA.
268. Manickam, B., R. Sreedharan, and M.J.C.d.d. Elumalai, *'Genipin'–the natural water soluble cross-linking agent and its importance in the modified drug delivery systems: An overview.* 2014. **11**(1): p. 139-145.
269. Yu, Y., et al., *Genipin-cross-linked hydrogels based on biomaterials for drug delivery: A review.* 2021. **9**(5): p. 1583-1597.
270. Moshayedi, S., et al., *Fabrication, swelling behavior, and water absorption kinetics of genipin-crosslinked gelatin–chitosan hydrogels.* 2021. **61**(12): p. 3094-3103.
271. Li, L., et al., *In situ forming biodegradable electroactive hydrogels*. 2014. **5**(8): p. 2880-2890.
272. Hartquist, C., et al., *A Universal Scaling Law for Intrinsic Fracture Energy of Networks.* 2024.
273. Liang, X., et al., *Anisotropically fatigue-resistant hydrogels.* 2021. **33**(30): p. 2102011.
274. Lara-Pérez, C., et al., *Photocatalytic degradation of diclofenac sodium salt: adsorption and reaction kinetic studies.* 2020. **79**(11): p. 277.
275. Korsmeyer, R.W., et al., *Mechanisms of solute release from porous hydrophilic polymers.* 1983. **15**(1): p. 25-35.

276. Li, W., et al., *Microparticle templating as a route to nanoscale polymer vesicles with controlled size distribution for anticancer drug delivery.* 2017. **508**: p. 145-153.
277. Liu, C. and R.J.J.o.M.S. Bai, *Adsorptive removal of copper ions with highly porous chitosan/cellulose acetate blend hollow fiber membranes.* 2006. **284**(1-2): p. 313-322.
278. Jayachandran, B., et al., *Insights on Chemical Crosslinking Strategies for Proteins.* Molecules, 2022. **27**: p. 8124.
279. Boldt, J.J.B.j.o.a., *Use of albumin: an update.* 2010. **104**(3): p. 276-284.
280. Ji, Q., et al., *GP60 and SPARC as albumin receptors: key targeted sites for the delivery of antitumor drugs.* 2024. **15**: p. 1329636.
281. Hanelt, M., M. Gareis, and B.J.M. Kollarczik, *Cytotoxicity of mycotoxins evaluated by the MTT-cell culture assay.* 1994. **128**: p. 167-174.

Appendix A Supplementary Figures

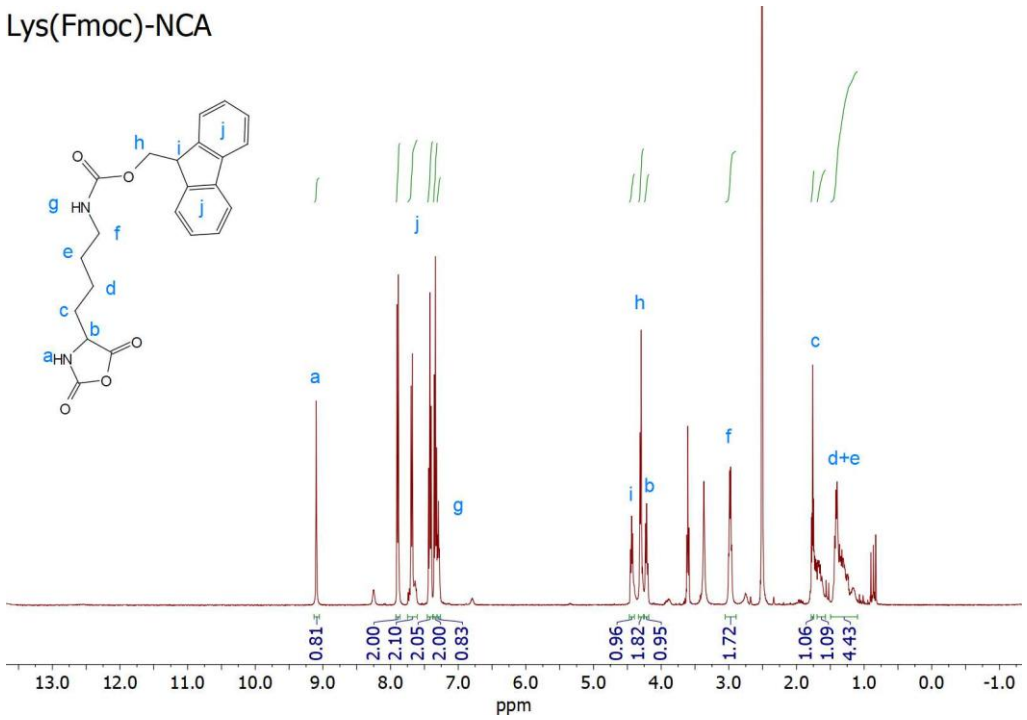

Figure S3-1 ^{1}HNMR spectrum of Lys(Fmoc)-NCA recorded at 400 MHz. DMSO-d_6 was used as the solvent.

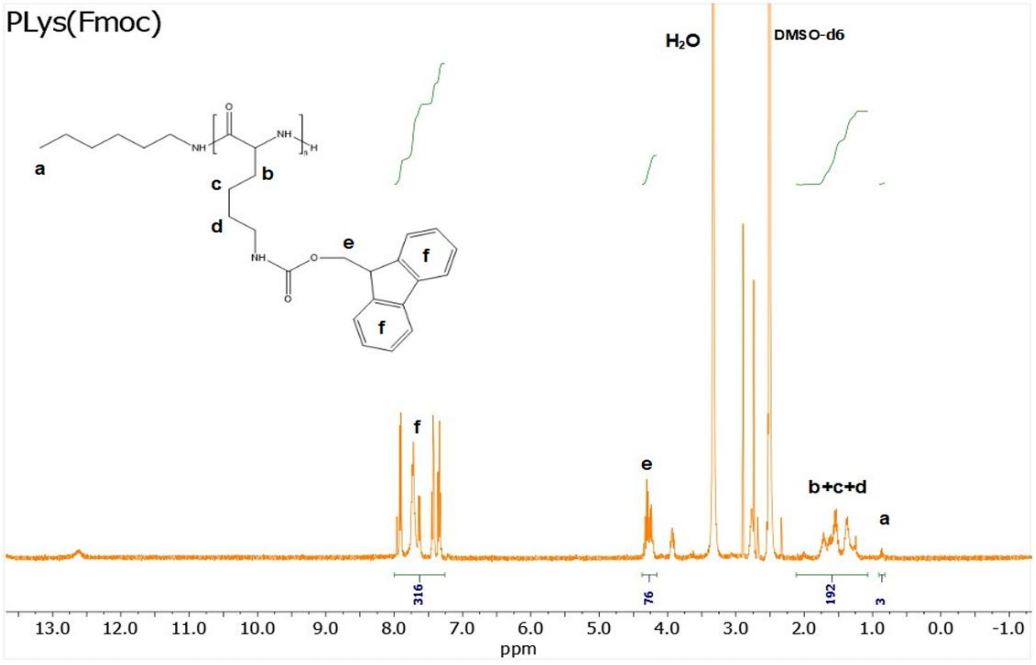

Figure S3-2 ^{1}HNMR spectrum of PLys(Fmoc) recorded at 400 MHz. DMSO-d_6 was used as the solvent.

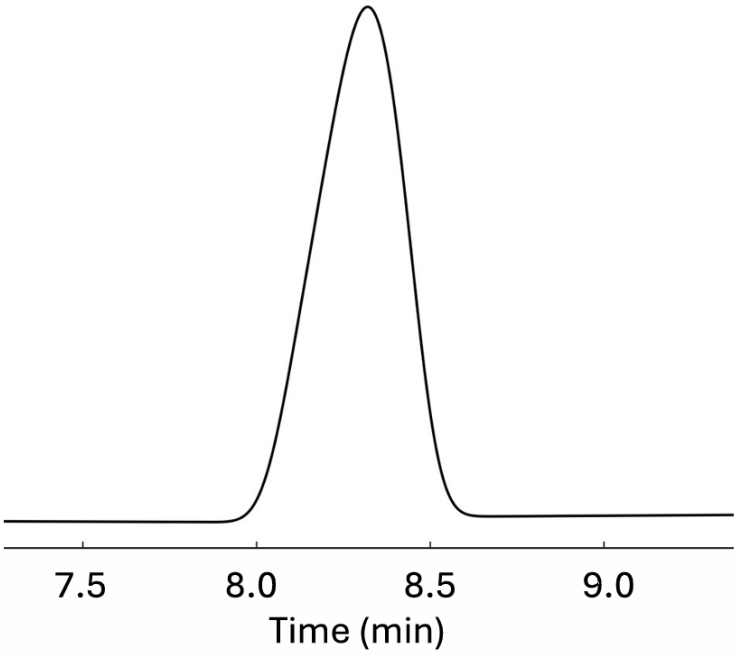

Figure S3-3 APC chromatogram curve corresponding to the elution of PLys(Fmoc).

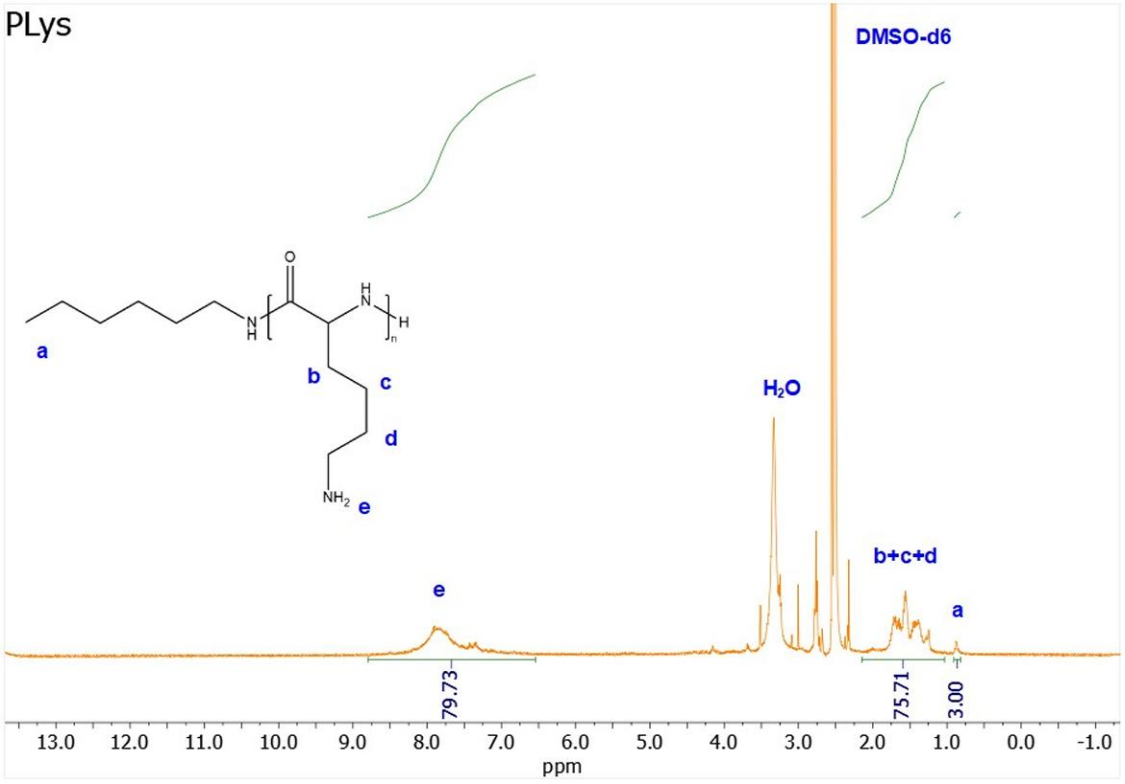

Figure S3-4 ^{1}HNMR spectrum of PLys recorded at 400 MHz. DMSO-d_6 was used as the solvent.

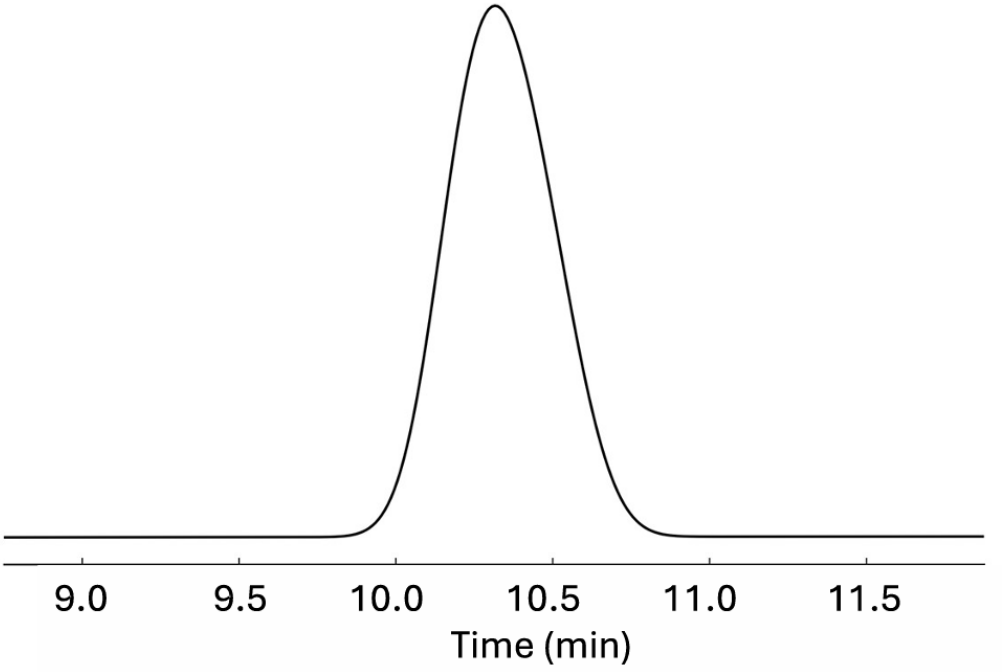

Figure S3-5. APC chromatogram curve corresponding to the elution of PLys.

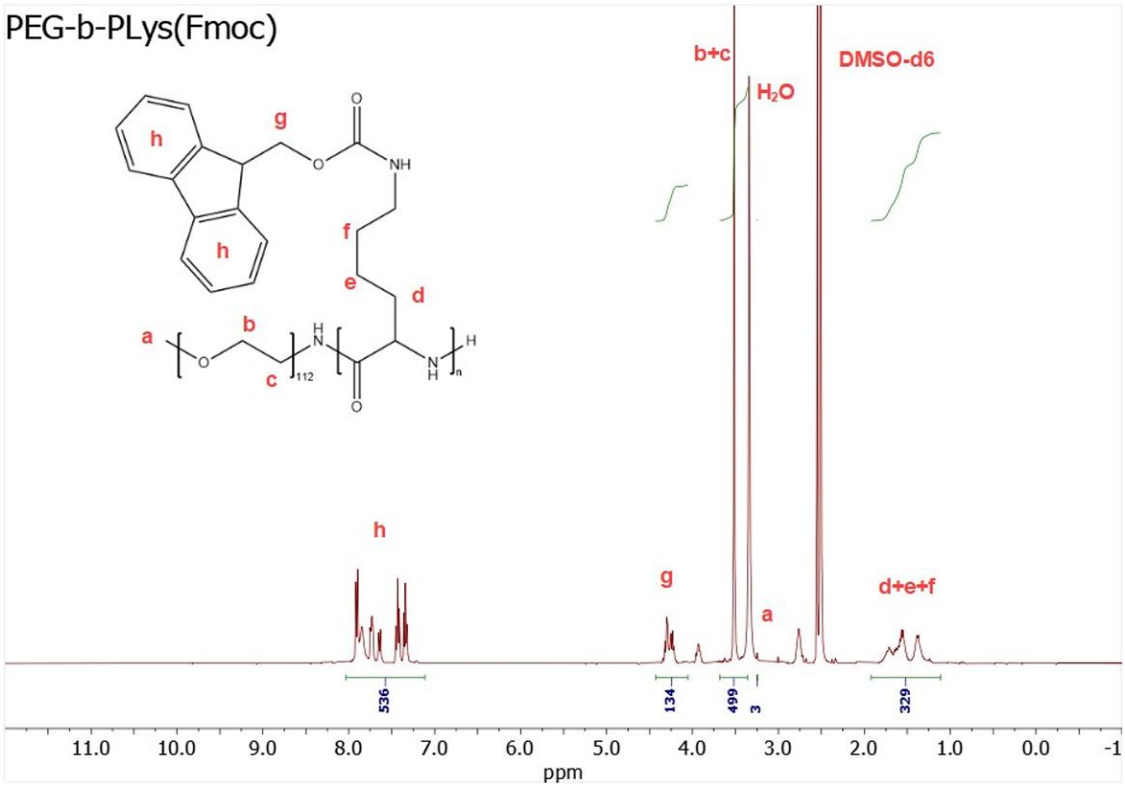

Figure S3-6. ^{1}HNMR spectrum of PEG-*b*-PLys(Fmoc) recorded at 400 MHz. DMSO-d_6 was used as the solvent.

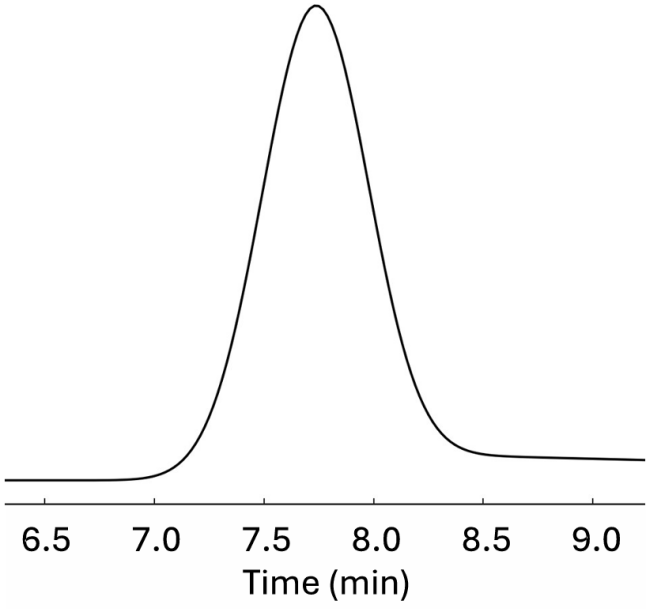

Figure S3-7. APC chromatogram curve corresponding to the elution of PEG-*b*-PLys(Fmoc).

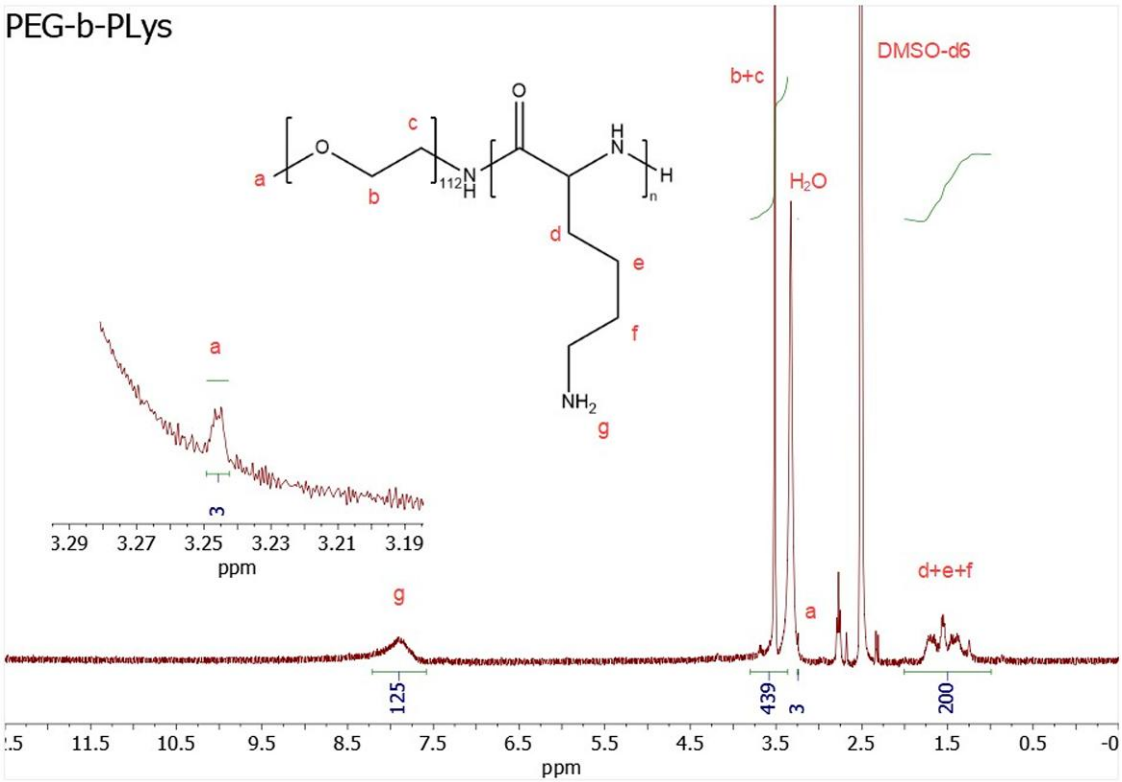

Figure S3-8. ^{1}HNMR spectrum of PEG-*b*-PLys recorded at 400 MHz. DMSO-d_6 was used as the solvent.

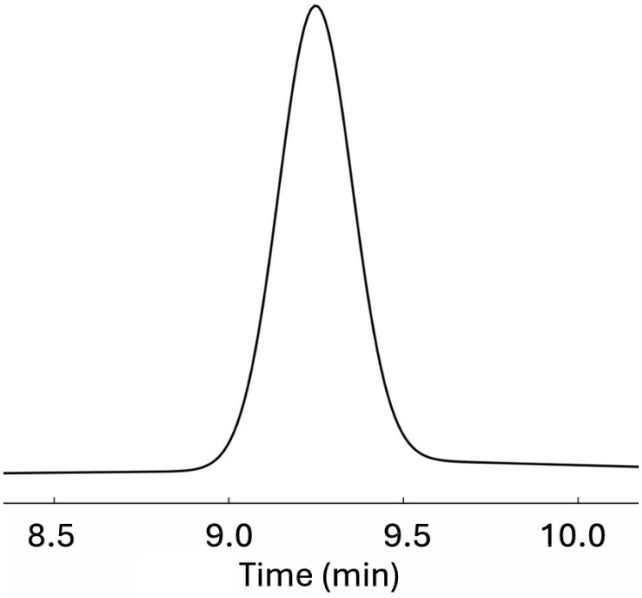

Figure S3-9. APC chromatogram curve corresponding to the elution of PEG-*b*-PLys(Fmoc).

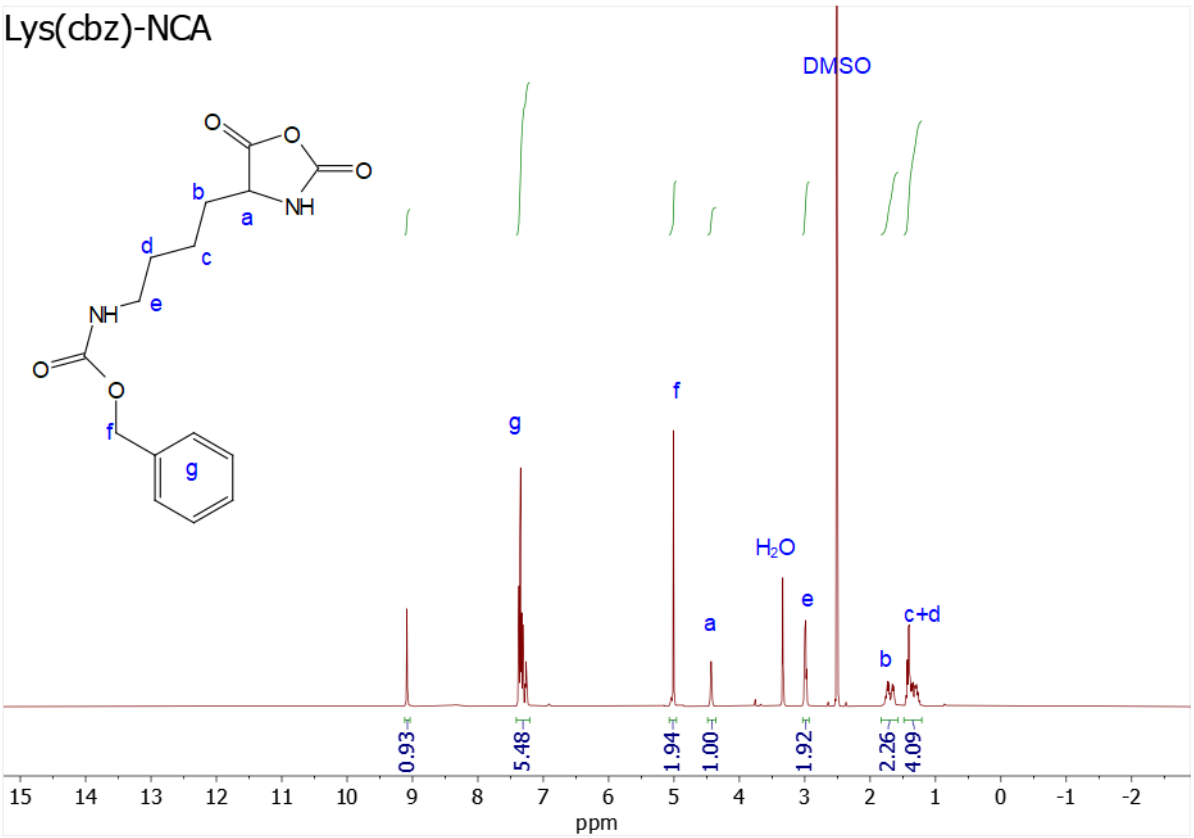

Figure S4-1. [1]HNMR of Lys(cbz)-NCA recorded at 500 MHz using DMSO-d_6 as the solvent.

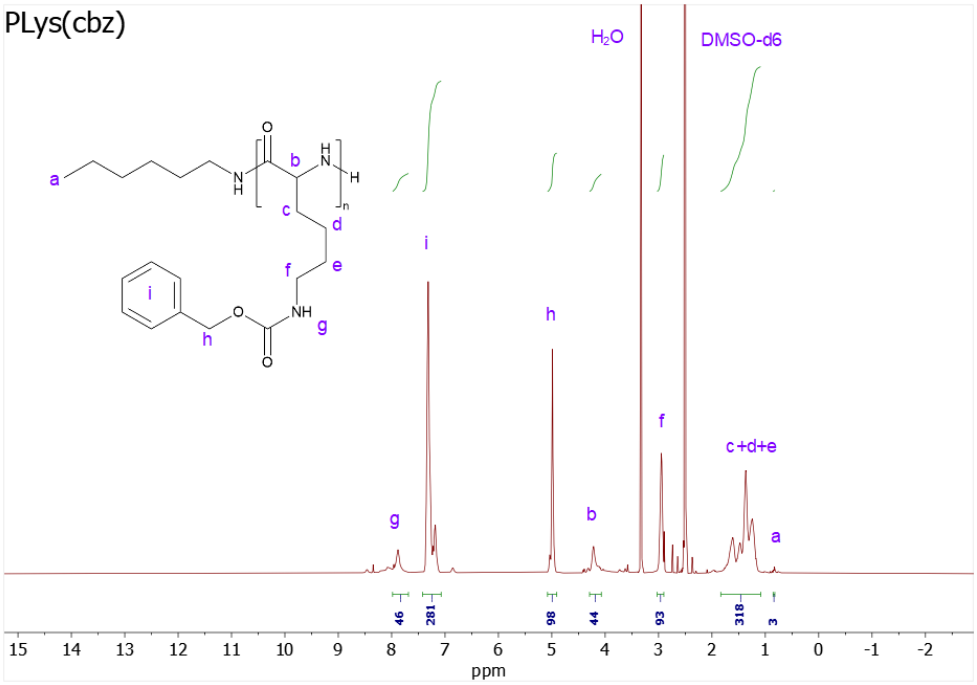

Figure S4-2. [1]HNMR of PLys(cbz) (synthesised from Lys(cbz)-NCA) recorded at 500 MHz using DMSO-d_6 as the solvent.

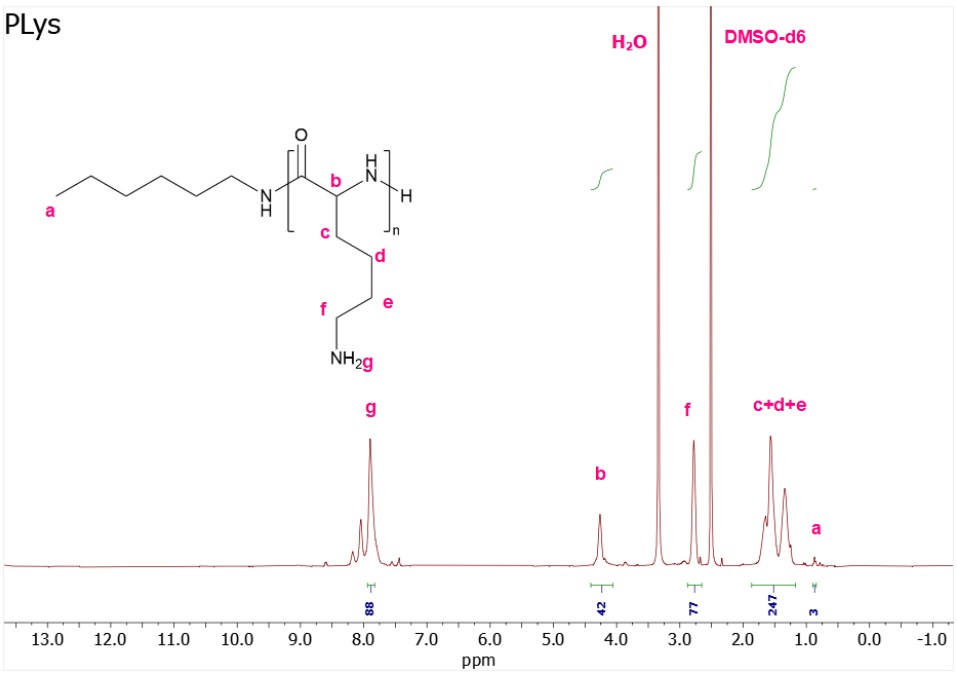

Figure S4-3. [1]HNMR of PLys 2 (deprotected by 33%HBr/AcOH solutions) recorded at 500 MHz using DMSO-d_6 as the solvent.

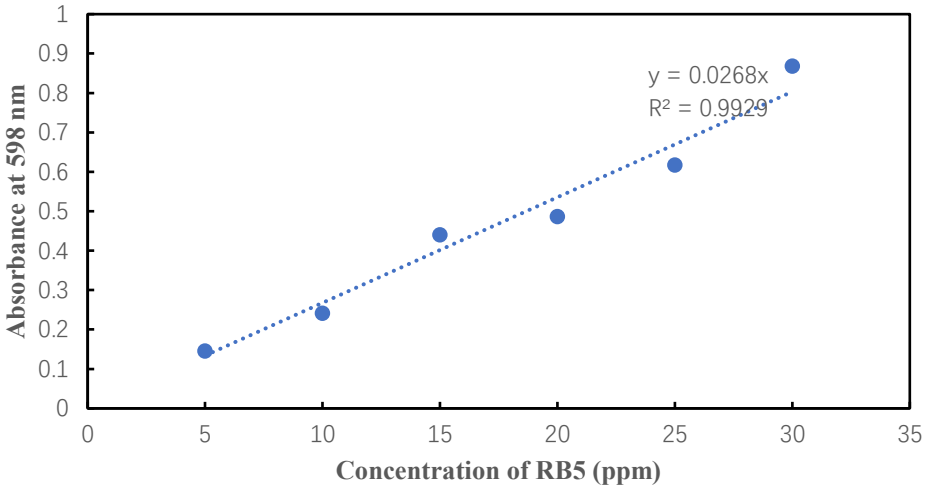

Figure S4-4. Standard Curve of RB5 (5-30ppm).

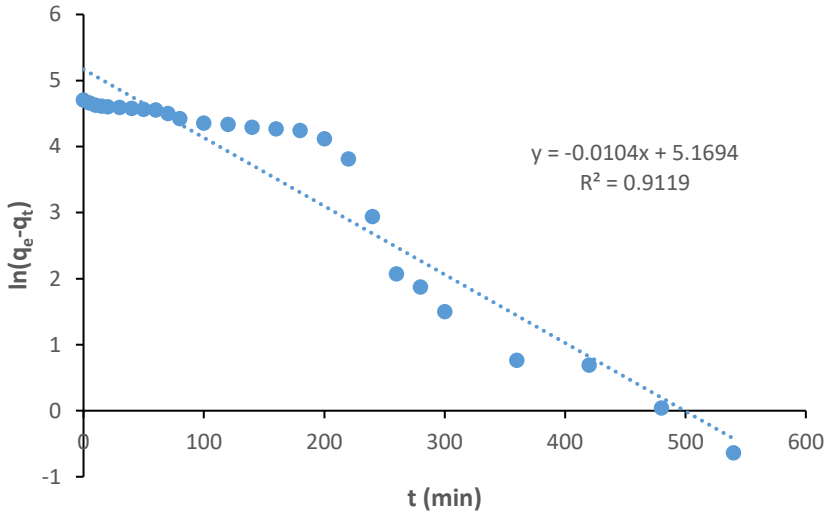

Figure S4-5. Pseudo-first-order model fitting for PLys/Glu Gel 1.

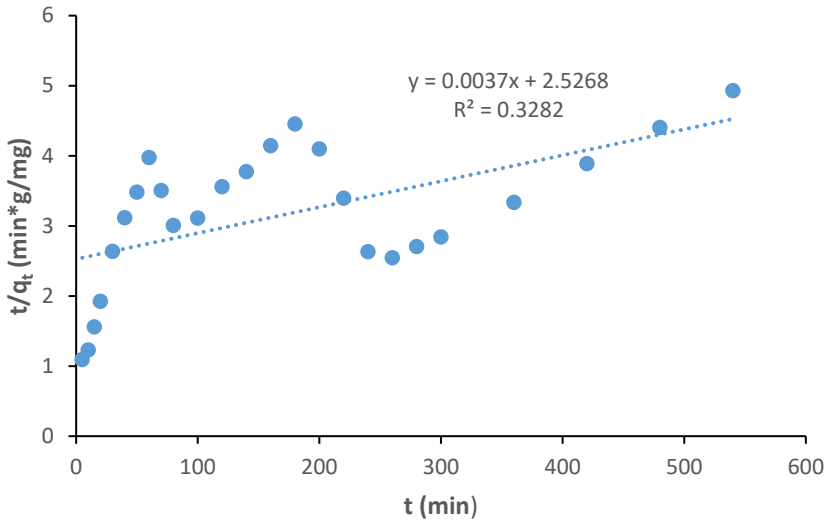

Figure S4-6. Pseudo-second-order model fitting for PLys/Glu Gel 1.

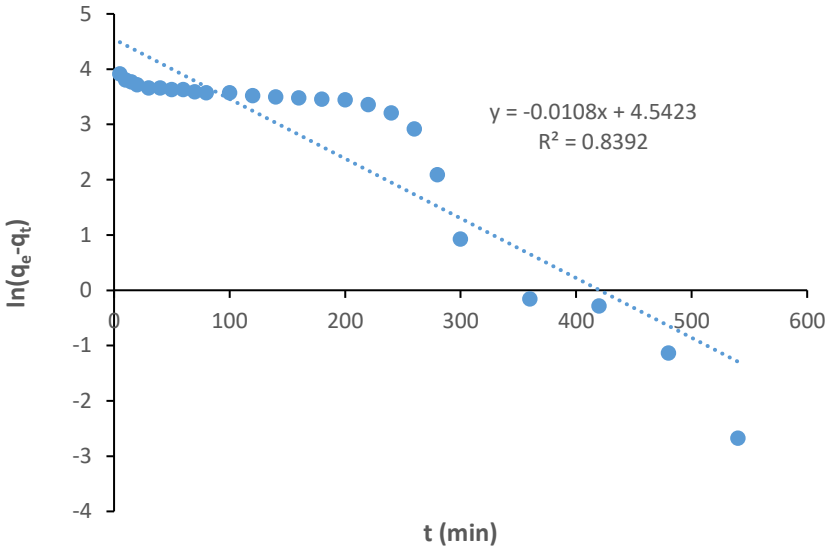

Figure S4-7. Pseudo-first-order model fitting for PLys/Glu Gel 2.

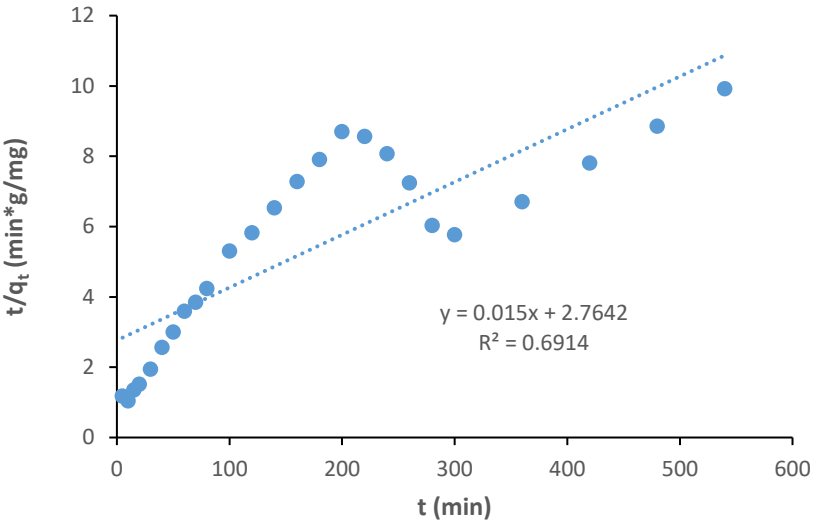

Figure S4-8. Pseudo-second-order model fitting for PLys/Glu Gel 2.

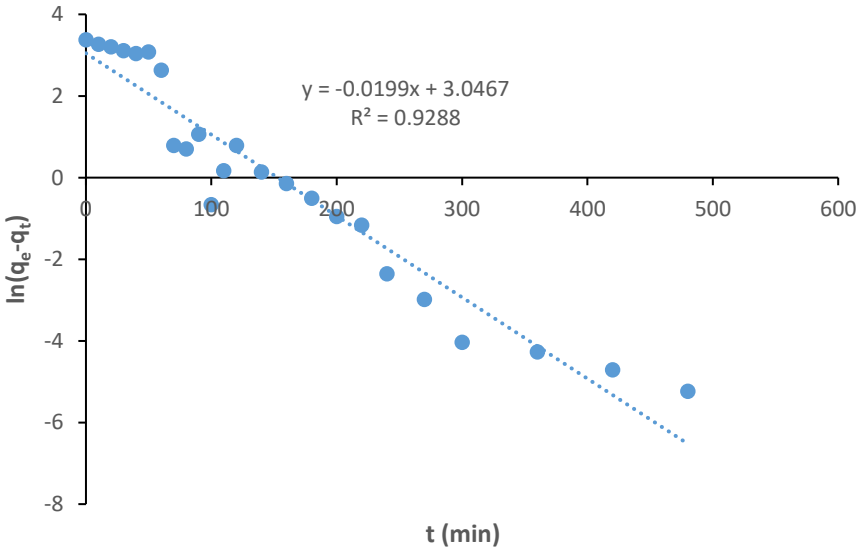

Figure S4-9. Pseudo-first-order model fitting for PLys/Gen Gel (I).

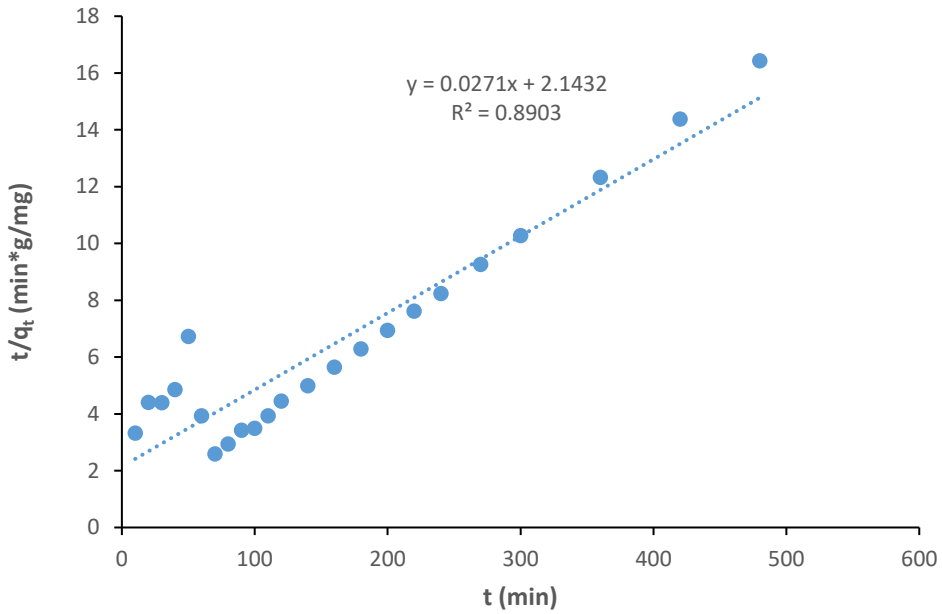

Figure S4-10. Pseudo-second-order model fitting for PLys/Gen Gel (I).

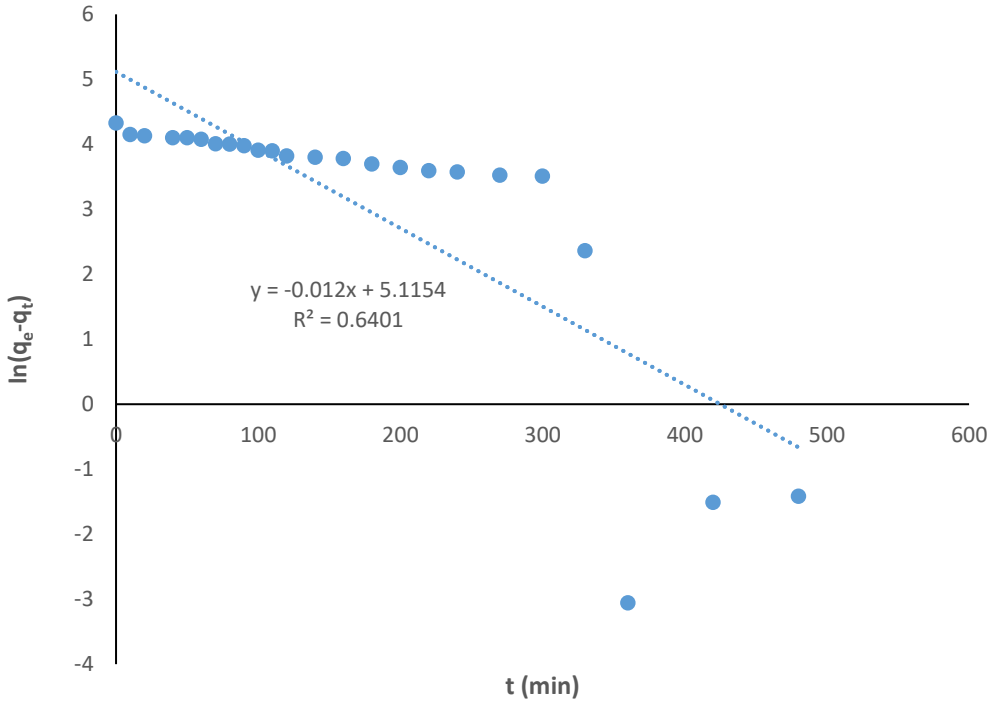

Figure S4-11. Pseudo-first-order model fitting for PLys/Gen Gel (II).

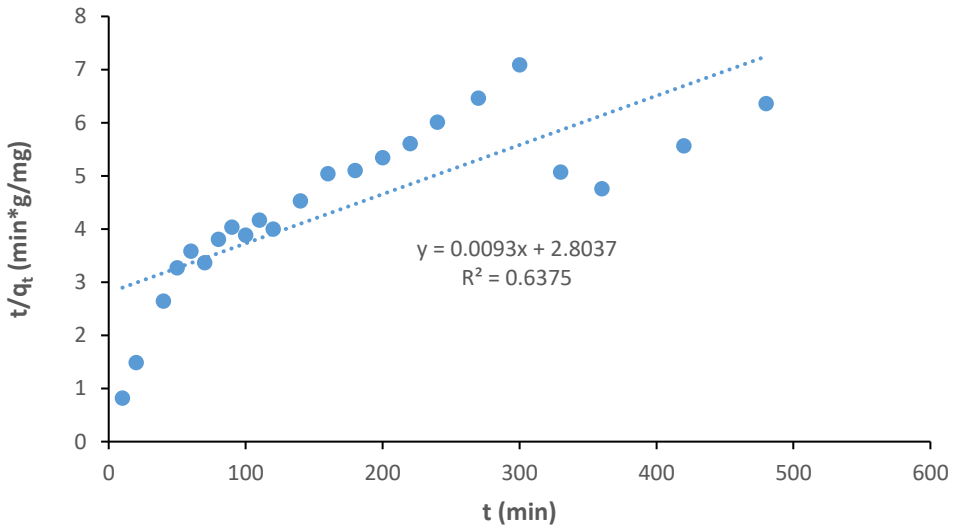

Figure S4-12. Pseudo-second-order model fitting for PLys/Gen Gel (II).

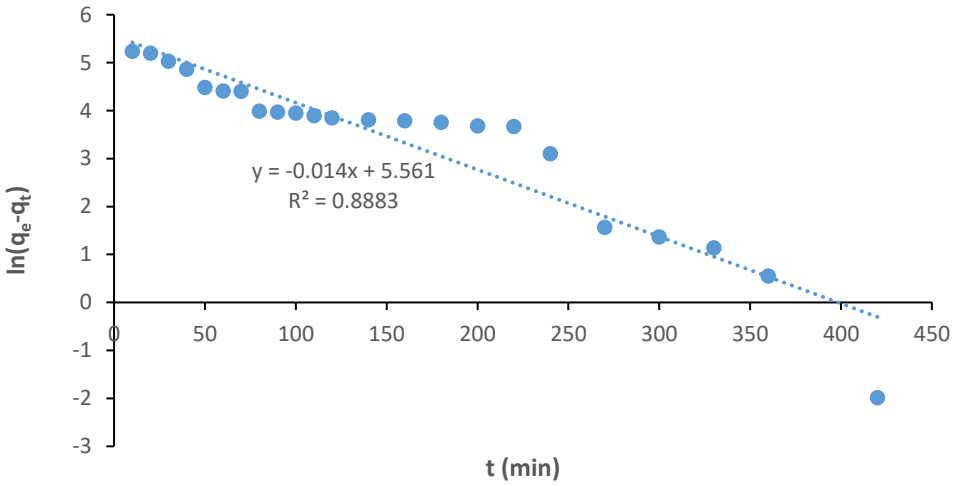

Figure S4-13. Pseudo-first-order model fitting for PLys/Gen Gel (III).

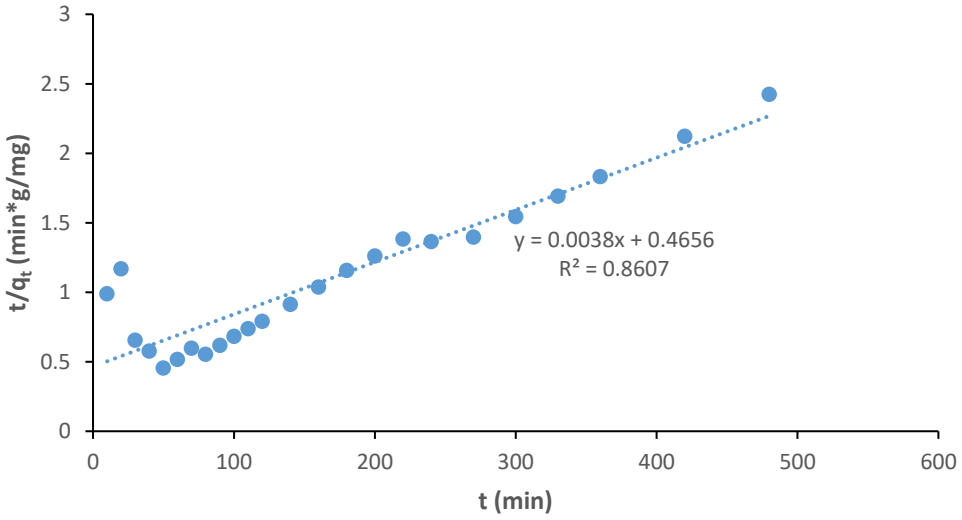

Figure S4-14. Pseudo-second-order model fitting for PLys/Gen Gel (III).

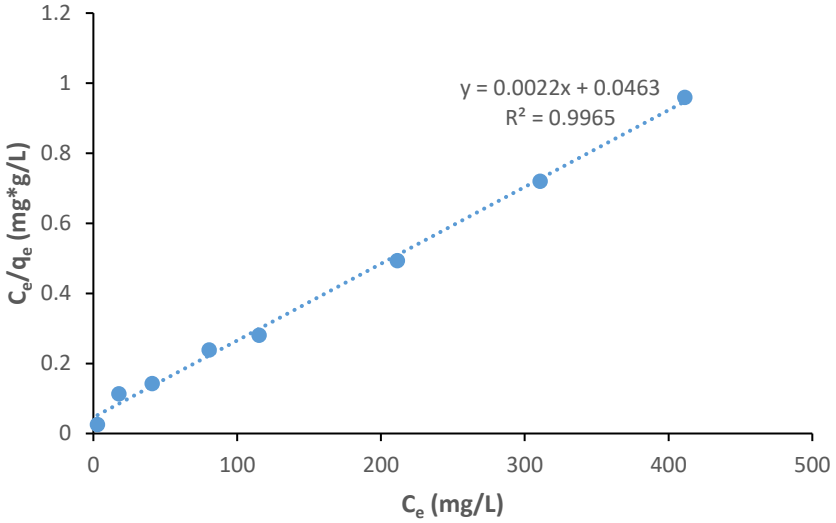

Figure S4-15. Langmuir isotherm fitting for PLys/Glu Gel 1.

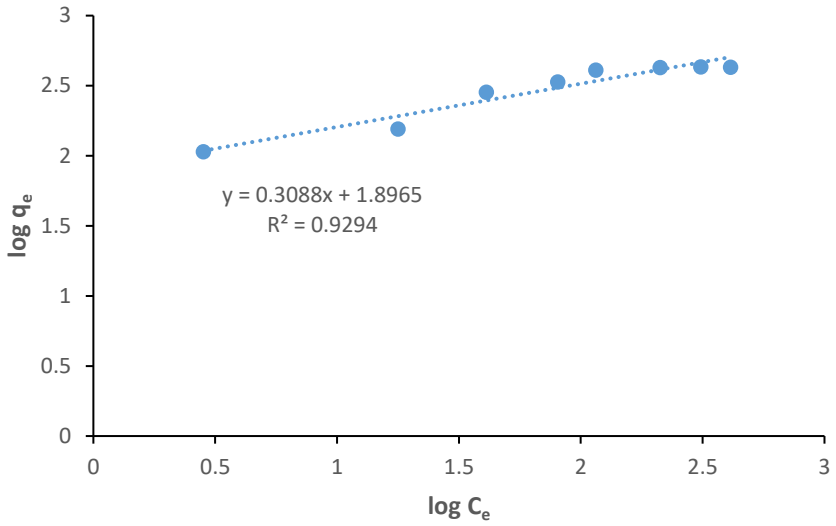

Figure S4-16. Freundlich isotherm fitting for PLys/Glu Gel 1.

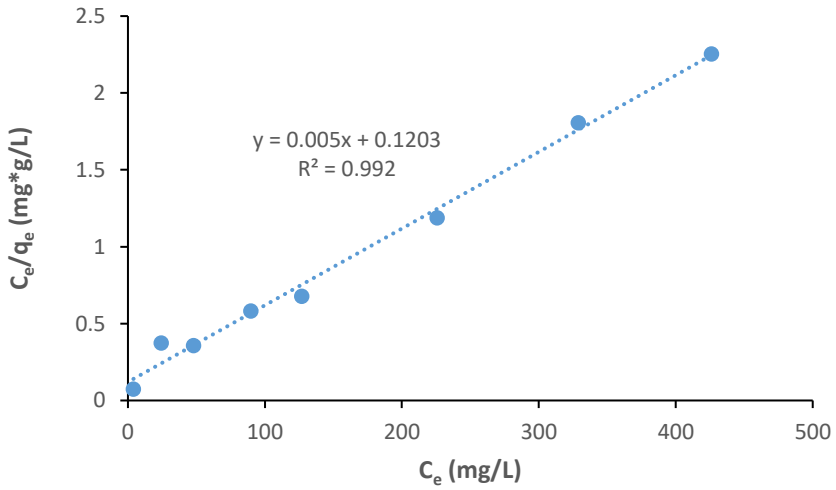

Figure S4-17. Langmuir isotherm fitting for PLys/Glu Gel 2.

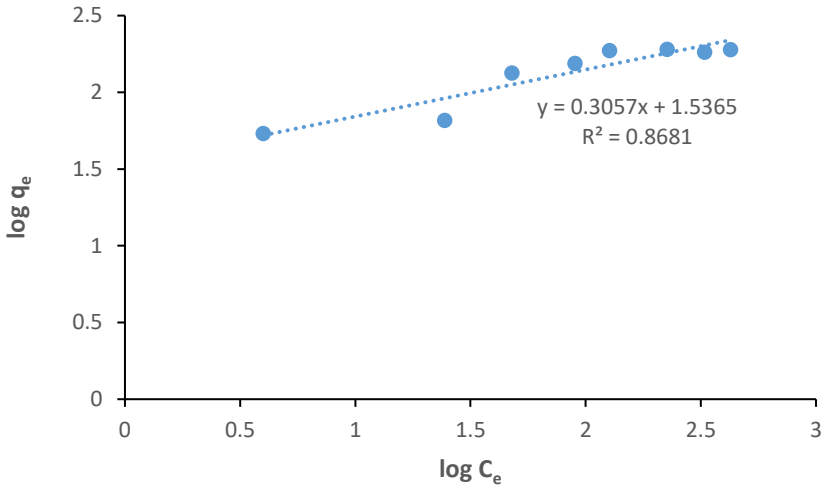

Figure S4-18. Freundlich isotherm fitting for PLys/Glu Gel 2.

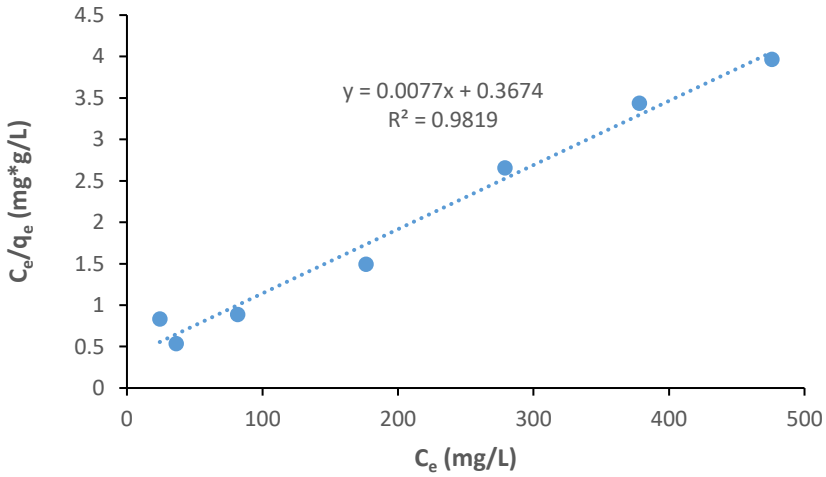

Figure S4-19. Langmuir isotherm fitting for PLys/Gen Gel (I).

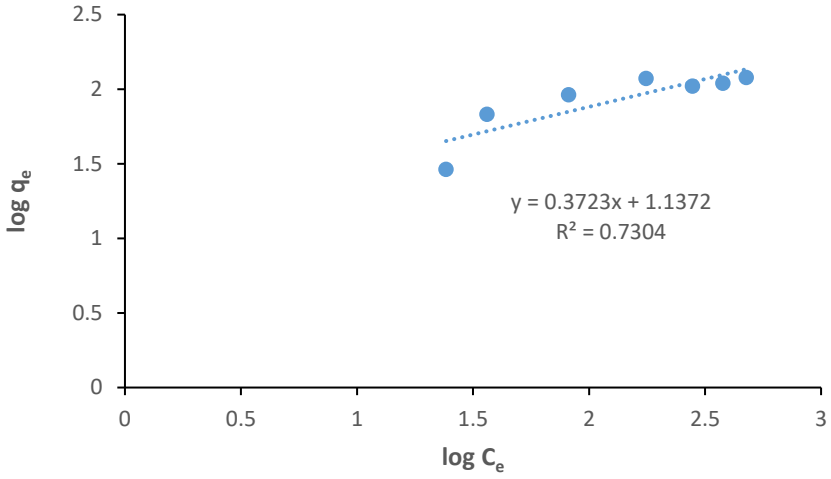

Figure S4-20. Freundlich isotherm fitting for PLys/Gen Gel (I).

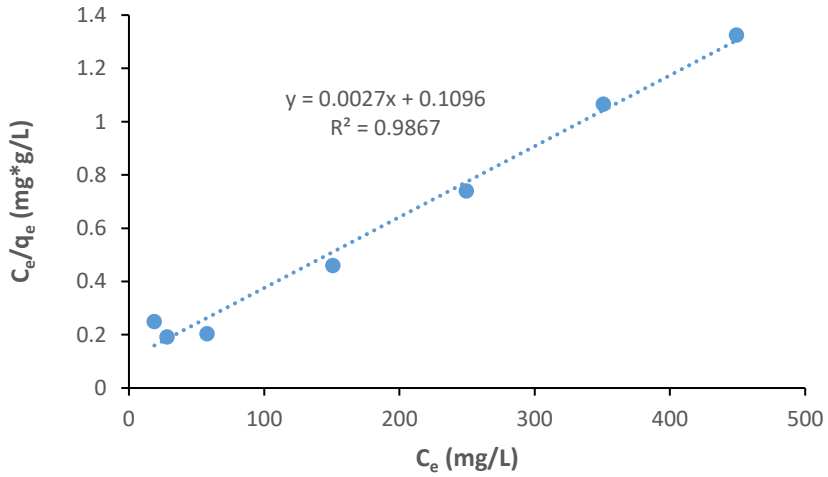

Figure S4-21. Langmuir isotherm fitting for PLys/Gen Gel (II).

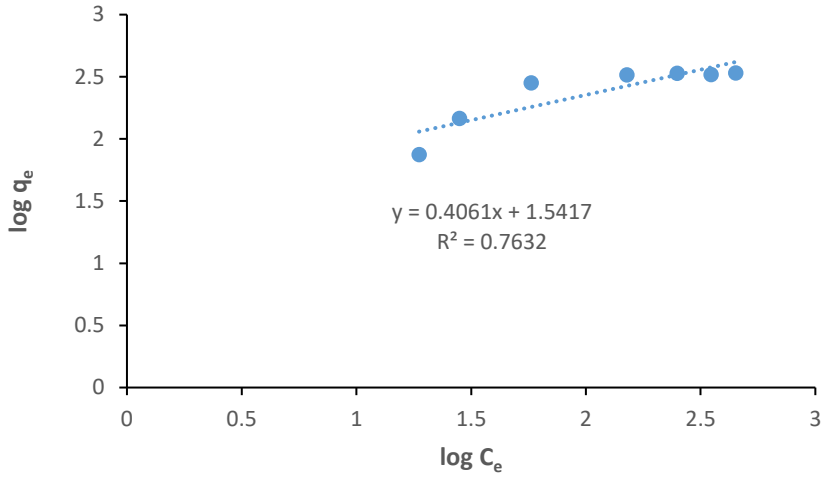

Figure S4-22. Freundlich isotherm fitting for PLys/Gen Gel (II).

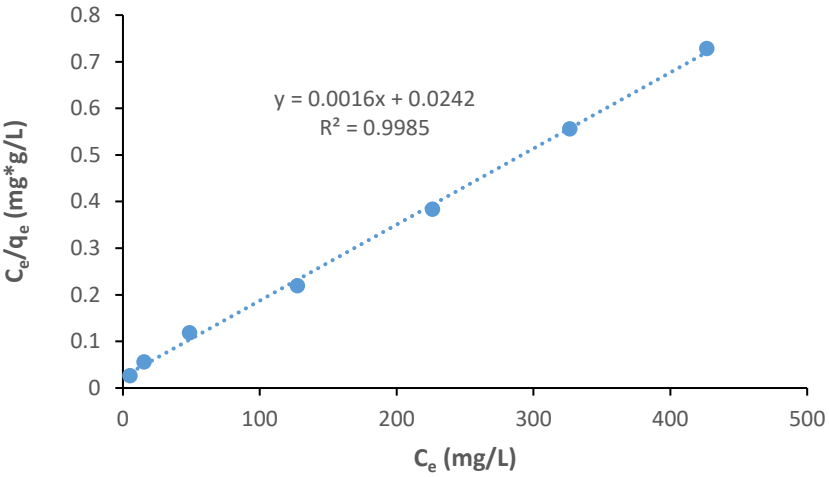

Figure S4-23. Langmuir isotherm fitting for PLys/Gen Gel (III).

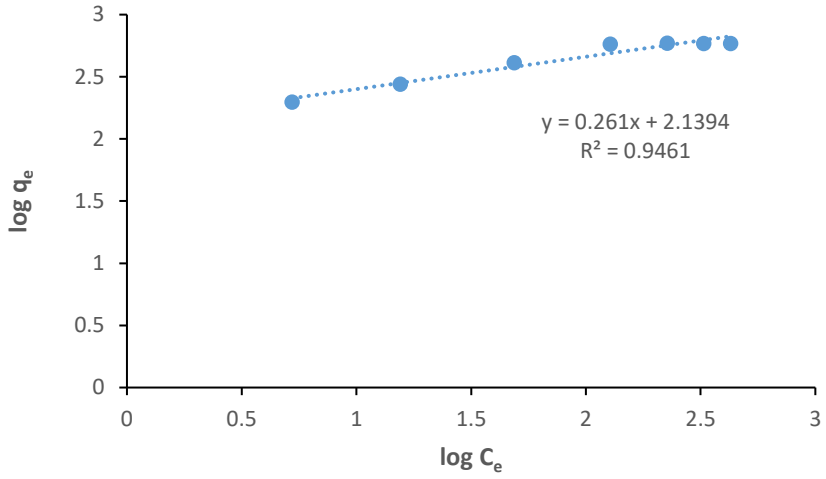

Figure S4-24. Freundlich isotherm fitting for PLys/Gen Gel (III).

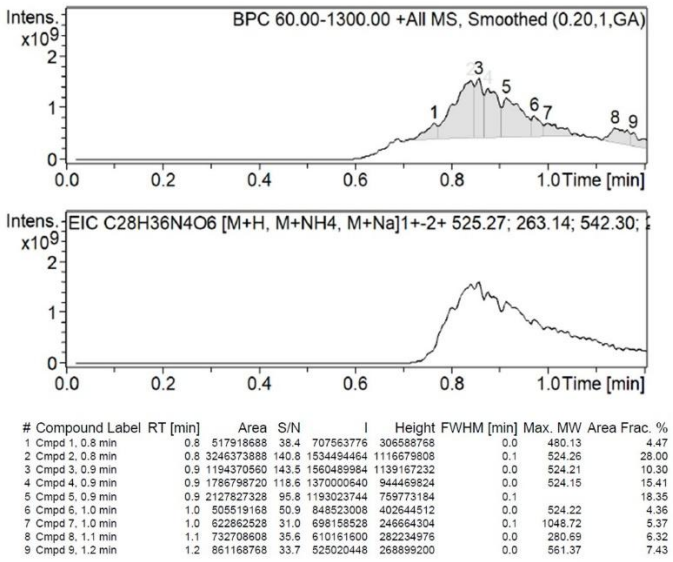

#	Compound Label	RT [min]	Area	S/N	I	Height	FWHM [min]	Max. MW	Area Frac. %
1	Cmpd 1, 0.8 min	0.8	517918688	38.4	707563776	306588768	0.0	480.13	4.47
2	Cmpd 2, 0.8 min	0.8	3246373888	140.8	1534494464	1116679808	0.1	524.26	28.00
3	Cmpd 3, 0.9 min	0.9	1194370560	143.5	1560489984	1139167232	0.0	524.21	10.30
4	Cmpd 4, 0.9 min	0.9	1786798720	118.6	1370000640	944469824	0.0	524.15	15.41
5	Cmpd 5, 0.9 min	0.9	2127827328	95.8	1193023744	759773184	0.1		18.35
6	Cmpd 6, 1.0 min	1.0	505519168	50.9	848523008	402644512	0.0	524.22	4.36
7	Cmpd 7, 1.0 min	1.0	622862528	31.0	698158528	246664304	0.1	1048.72	5.37
8	Cmpd 8, 1.1 min	1.1	732708608	35.6	610161600	282234976	0.0	280.69	6.32
9	Cmpd 9, 1.2 min	1.2	861168768	33.7	525020448	268899200	0.0	561.37	7.43

Figure S5-1. LC-MS of Lys(cbz)DKP (in the appendix)

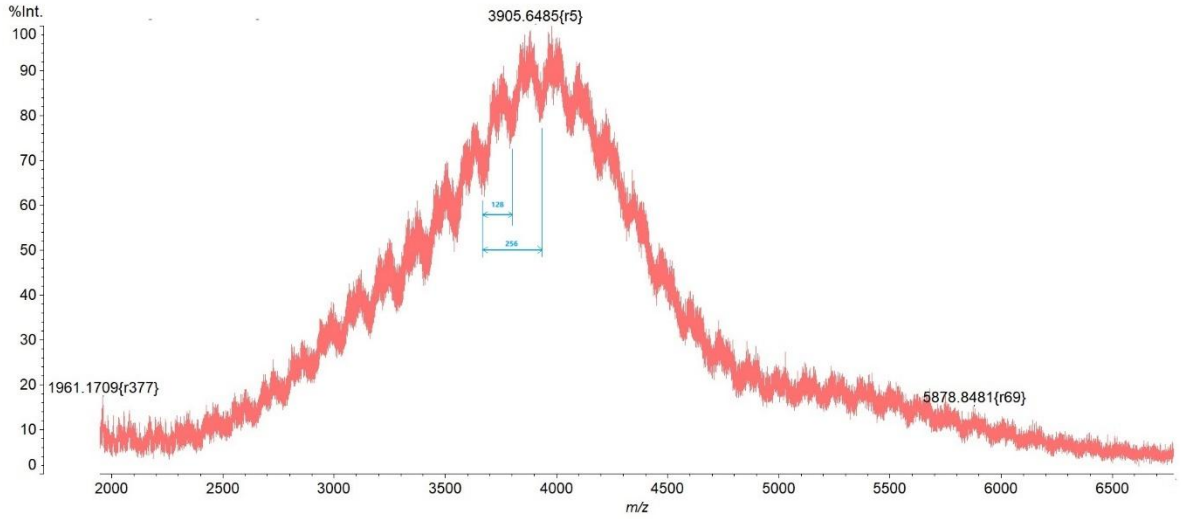

Figure S5-2. MALDI test of PLys (synthesised from DKP method).

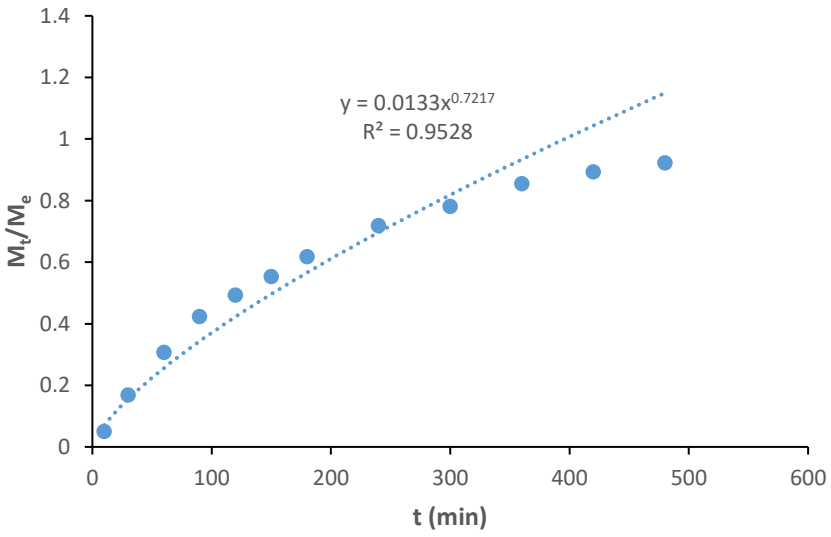

Figure S5-3. Korsmeyer-Peppas mathematical model fitting of PLys/Gen Gel 3, pH= 1.7.

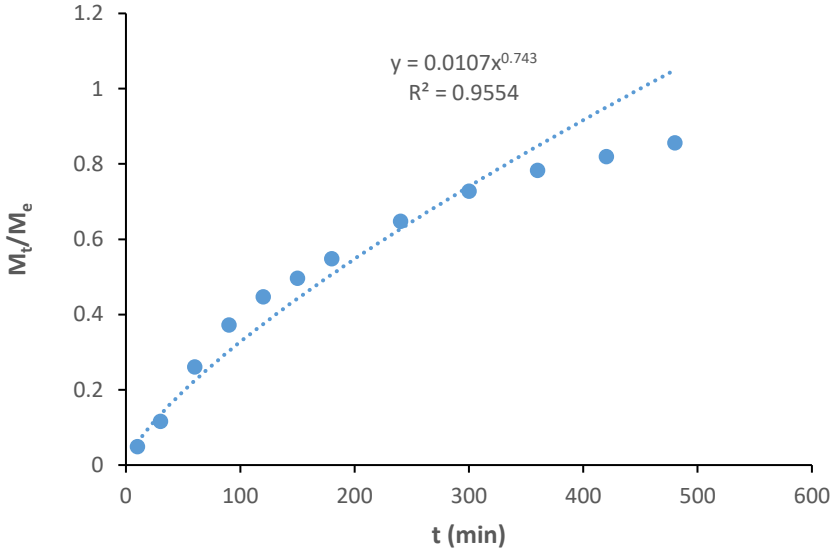

Figure S5-4. Korsmeyer-Peppas mathematical model fitting of PLys/Gen Gel 4, pH= 1.7.

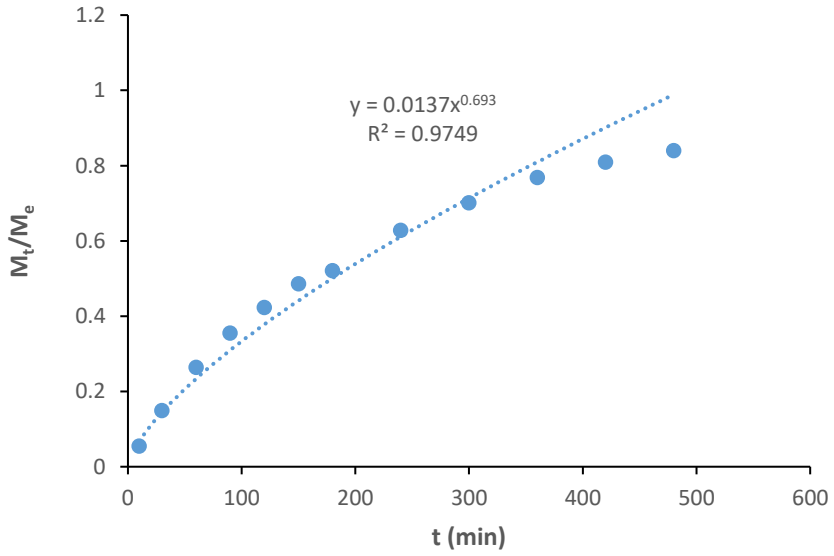

Figure S5-5. Korsmeyer-Peppas mathematical model fitting of PLys/Gen Gel 5, pH= 1.7.

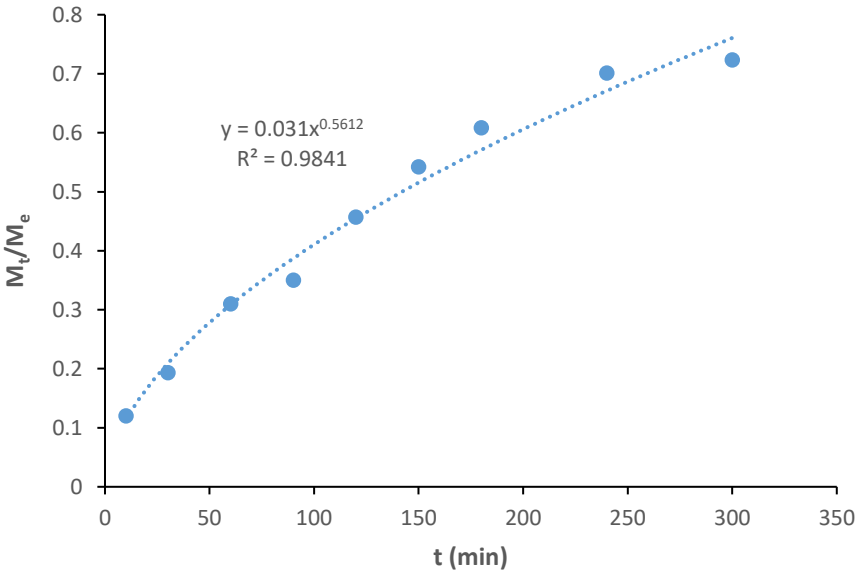

Figure S5-6. Korsmeyer-Peppas mathematical model fitting of PLys/Gen Gel 5, pH= 5.5.

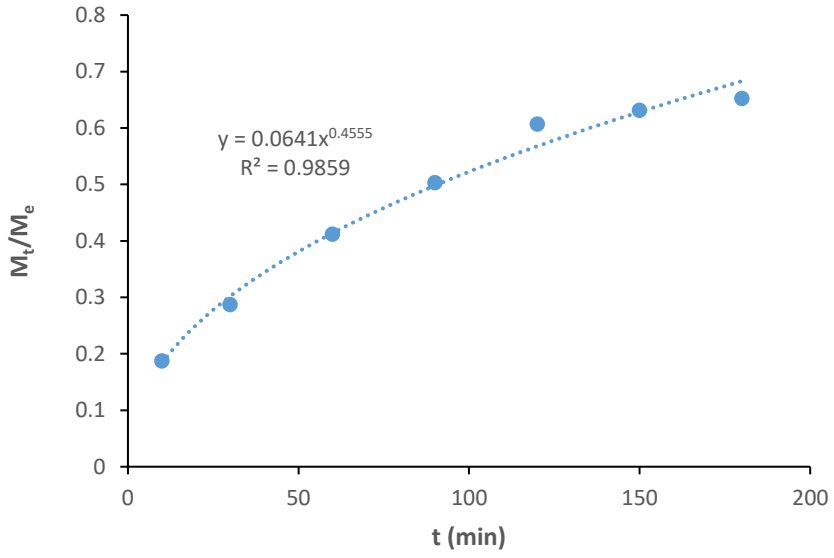

Figure S5-7. Korsmeyer-Peppas mathematical model fitting of PLys/Gen Gel 5, pH= 7.4.

Appendix B Related Publications during PhD Projects

B.1 From Chapter 3

Jin, Xuchen, and Paul D. Thornton. "Thermal deprotection: a sustainable and efficient strategy for synthesising α-polylysine adsorbents." *RSC advances* 15.22 (2025): 17397-17404.